U.S. Department of Transportation
Federal Highway Administration

Errata

Date:	November 21, 2016
Issuing Office:	Federal Highway Administration—Office of Research, Development, and Technology: Insert Office R&D
Address:	Turner-Fairbank Highway Research Center, 6300 Georgetown Pike, McLean, VA 22101
Name of Document:	Insert Document Title
FHWA Publication No.:	FHWA-HRT- 15-074

The following changes were made to the document after publication on the Federal Highway Administration website:

Location	**Incorrect Values**	**Corrected Values**
Page number 215, Figure 217	$T_c = 19.791e^{-0.043T_f} - 19.791e^{-0.043T_r}$	$T_c = 19.791e^{-0.043T_r} - 19.791e^{-0.043T_f}$
Section 508 Caption for Figure 217	**Figure 217. Equation. Temperature correction factor.** T subscript c equals 19.791 times exponential raised to the power of -0.043 times T subscript f minus the quantity 19.791 times exponential raised to the power of -0.043 times T subscript r.	**Figure 217. Equation. Temperature correction factor.** T subscript c equals 19.791 times exponential raised to the power of -0.043 times T subscript r minus the quantity 19.791 times exponential raised to the power of -0.043 times T subscript f.

Pavement Structural Evaluation at the Network Level: Final Report

PUBLICATION NO. FHWA-HRT-15-074

SEPTEMBER 2016

U.S. Department of Transportation
Federal Highway Administration

Research, Development, and Technology
Turner-Fairbank Highway Research Center
6300 Georgetown Pike
McLean, VA 22101-2296

FOREWORD

As State transportation departments begin to consider structural adequacy as part of their routine pavement management system (PMS) activities by incorporating deflection testing, it is important to advance their practices from deflection testing using falling weight deflectometers, which involves a slow, stop-and-go operation and requires lane closures, to a more viable alternative for network-level pavement management applications. The development of moving deflection testing devices that can measure pavement responses at traffic speeds is a more viable alternative.

The goal of this project was to establish a reliable measure of the structural condition of bound pavement layers above the unbound base layer as it deteriorates over time under traffic and environmental loading by measuring pavement deflection at traffic speeds. As part of the project, a literature review was conducted, and questionnaires were developed and followed up by interviews to device manufacturers, owners, and users. Two devices were found to be potentially viable: the Traffic Speed Deflectometer and Rolling Wheel Deflectometer. A work plan was developed and implemented to evaluate if the two devices met a minimum set of specifications related to the structural evaluation of pavements at the network level. Field evaluations and validation analyses were completed in accordance with the work plan. Finally, analysis methodologies and processes were developed for incorporating pavement structural information within PMS applications. This report is intended for use by pavement management engineers and pavement investment decision makers across the United States.

Mayela Sosa
Acting Director, Office of Infrastructure
Research and Development

TECHNICAL DOCUMENTATION PAGE

1. Report No. FHWA-HRT-15-074	2. Government Accession No.	3. Recipient's Catalog No.
4. Title and Subtitle Pavement Structural Evaluation at the Network Level: Final Report		5. Report Date September 2016
		6. Performing Organization Code None
7. Author(s) Gonzalo R. Rada, Soheil Nazarian, Beth A. Visintine, Raj Siddharthan, and Senthil Thyagarajan		8. Performing Organization Report No.
9. Performing Organization Name and Address Amec Foster Wheeler Environment & Infrastructure, Inc. 12000 Indian Creek Court, Suite F, Beltsville, MD 20705 The University of Texas at El Paso Center for Transportation Infrastructure Systems 500 West University Avenue, El Paso, TX 79968 University of Nevada Reno Department of Civil and Environmental Engineering 1664 N. Virginia St., Reno, NV 89557		10. Work Unit No. (TRAIS)
		11. Contract or Grant No. DTFH61-12-C-00031
12. Sponsoring Agency Name and Address Office of Infrastructure Research and Development Federal Highway Administration 6300 Georgetown Pike McLean, VA 22101-2296		13. Type of Report and Period Covered Final Report, September 2012–April 2015
		14. Sponsoring Agency Code

15. Supplementary Notes
The Contracting Officer's Representative was Nadarajah Sivaneswaran, HRDI-20.

16. Abstract
As State transportation departments consider structural adequacy as part of their routine pavement management system (PMS) activities by incorporating deflection testing, it is important to advance their practices from measuring deflection using falling weight deflectometers, which involves a slow, stop-and-go operation and requires lane closures, to a more viable alternative for network-level pavement management applications. The development of moving deflection testing devices that can measure pavement responses at traffic speeds represents this more viable alternative. The modern versions of the moving deflection testing devices that are actively used today include the Traffic Speed Deflectometer (TSD) and a Rolling Wheel Deflectometer (RWD).

The goal of this project was to establish a reliable measure of the structural condition of bound pavement layers above the unbound base layer as it deteriorates over time under traffic and environmental loading based on moving pavement deflection technology measuring at traffic speeds. Moreover, this measure needed to be robust enough in capturing the structural condition or deterioration of the pavement layer notwithstanding the seasonal and spatial variation in base and subgrade layers. As part of the project, a literature review was conducted, and questionnaires were developed for device manufacturers, owners, and users, which were then followed up by interviews. Both the TSD and RWD were found to be potentially viable devices. Based on this finding, a work plan was developed and implemented to evaluate if the two devices met a minimum set of specifications related to the structural evaluation of pavements at the network level including accuracy and precision of deflection measurements, monitoring applied load, operating speed, and distance between deflection measurements. Field evaluations and validation analyses were completed in accordance with the work plan. Ultimately, analysis methodologies and processes were developed for incorporating pavement structural information within highway agencies' PMS applications.

17. Key Words Network-level, Structural evaluation, Rolling wheel deflectometer, Traffic speed deflectometer, Deflection indices	18. Distribution Statement No restrictions. This document is available to the public through the National Technical Information Service, Springfield, VA 22161. http://www.ntis.gov

19. Security Classif. (of this report) Unclassified	20. Security Classif. (of this page) Unclassified	21. No. of Pages 282	22. Price

Form DOT F 1700.7 (8-72) Reproduction of completed page authorized.

SI* (MODERN METRIC) CONVERSION FACTORS

APPROXIMATE CONVERSIONS TO SI UNITS

Symbol	When You Know	Multiply By	To Find	Symbol
		LENGTH		
in	inches	25.4	millimeters	mm
ft	feet	0.305	meters	m
yd	yards	0.914	meters	m
mi	miles	1.61	kilometers	km
		AREA		
in^2	square inches	645.2	square millimeters	mm^2
ft^2	square feet	0.093	square meters	m^2
yd^2	square yard	0.836	square meters	m^2
ac	acres	0.405	hectares	ha
mi^2	square miles	2.59	square kilometers	km^2
		VOLUME		
fl oz	fluid ounces	29.57	milliliters	mL
gal	gallons	3.785	liters	L
ft^3	cubic feet	0.028	cubic meters	m^3
yd^3	cubic yards	0.765	cubic meters	m^3
		NOTE: volumes greater than 1000 L shall be shown in m^3		
		MASS		
oz	ounces	28.35	grams	g
lb	pounds	0.454	kilograms	kg
T	short tons (2000 lb)	0.907	megagrams (or "metric ton")	Mg (or "t")
		TEMPERATURE (exact degrees)		
°F	Fahrenheit	5 (F-32)/9 or (F-32)/1.8	Celsius	°C
		ILLUMINATION		
fc	foot-candles	10.76	lux	lx
fl	foot-Lamberts	3.426	$candela/m^2$	cd/m^2
		FORCE and PRESSURE or STRESS		
lbf	poundforce	4.45	newtons	N
lbf/in^2	poundforce per square inch	6.89	kilopascals	kPa

APPROXIMATE CONVERSIONS FROM SI UNITS

Symbol	When You Know	Multiply By	To Find	Symbol
		LENGTH		
mm	millimeters	0.039	inches	in
m	meters	3.28	feet	ft
m	meters	1.09	yards	yd
km	kilometers	0.621	miles	mi
		AREA		
mm^2	square millimeters	0.0016	square inches	in^2
m^2	square meters	10.764	square feet	ft^2
m^2	square meters	1.195	square yards	yd^2
ha	hectares	2.47	acres	ac
km^2	square kilometers	0.386	square miles	mi^2
		VOLUME		
mL	milliliters	0.034	fluid ounces	fl oz
L	liters	0.264	gallons	gal
m^3	cubic meters	35.314	cubic feet	ft^3
m^3	cubic meters	1.307	cubic yards	yd^3
		MASS		
g	grams	0.035	ounces	oz
kg	kilograms	2.202	pounds	lb
Mg (or "t")	megagrams (or "metric ton")	1.103	short tons (2000 lb)	T
		TEMPERATURE (exact degrees)		
°C	Celsius	1.8C+32	Fahrenheit	°F
		ILLUMINATION		
lx	lux	0.0929	foot-candles	fc
cd/m^2	$candela/m^2$	0.2919	foot-Lamberts	fl
		FORCE and PRESSURE or STRESS		
N	newtons	0.225	poundforce	lbf
kPa	kilopascals	0.145	poundforce per square inch	lbf/in^2

*SI is the symbol for the International System of Units. Appropriate rounding should be made to comply with Section 4 of ASTM E380.
(Revised March 2003)

TABLE OF CONTENTS

CHAPTER 1. INTRODUCTION 1

CHAPTER 2. LITERATURE REVIEW 5
2.1 REFERENCES REVIEWED 5
2.2 LITERATURE REVIEW FINDINGS 6
2.3 SUMMARY 12

CHAPTER 3. MANUFACTURERS', OWNERS', AND USERS' QUESTIONNAIRES 13
3.1 DEVICE MANUFACTURERS' PERSPECTIVES 13
3.2 TSD OWNERS'/USERS' PERSPECTIVES 14
3.3 RWD USERS' PERSPECTIVES 15
3.4 SUMMARY 15

CHAPTER 4. DATA COLLECTION AND ANALYSIS WORK PLAN 17
4.1 ANALYSIS METHODOLOGIES 17
Activity 1: Establish Pavement Structural Condition Threshold Values 21
Activity 2: Relate Structural-Related Responses to Deflection Parameters Measured with TSDDs 25
Activity 3: Establish Ideal Measurement Characteristics for TSDDs 31
Activity 4: Field Evaluation of Devices 32
Activity 5: Best Strategies for Implementing TSDDs in Network-level Evaluation 38
4.2 FIELD TRIALS LOCATION 39
4.3 SUMMARY 40

CHAPTER 5. PROCESS OF EVALUATION AND VALIDATION OF DEVICES 41
5.1 INTRODUCTION 41
5.2 SITE SELECTION 41
5.3 SITE INSTRUMENTATION 43
5.4 DATA COLLECTION 51
5.5 DATA REDUCTION 51
5.6 DATA ANALYSIS 58
Accuracy 58
Precision 64
5.7 PROJECT DATABASE AND WEB SITE 69
5.8 SUMMARY 70

CHAPTER 6. PERFORMANCE EVALUATION OF DEVICES 71
6.1 INTRODUCTION 71
6.2 ACCURACY 71
Overall Accuracy of Reported Deflection Parameters 71
6.3 PRECISION 82
Overall Results 82
Correlation to Pavement Structure 93
Operating Speed 96
Temperature Variation 98
Vertical and Horizontal Curves 99
6.4 SUMMARY 104

CHAPTER 7. 3D-MOVE CALIBRATION 105
7.1 INTRODUCTION 105
Purpose and Overview of Calibration Effort 105
7.2 3D-MOVE PROGRAM OVERVIEW AND CALIBRATION 106
7.3 MATERIALS CHARACTERIZATION OF MNROAD ACCURACY CELLS 107
MnROAD Accuracy Cells 107
Material Characterization 107
Summary 119
7.4 LOADING CHARACTERISTICS OF TSDDS 120
Axle Configurations and Contact Pressure Distribution 121
7.5 3D-MOVE CALIBRATION USING PROJECT SENSOR DATA 123
Project Sensors 123
Case Scenarios for 3D-Move to Bracket the Project Sensor Results 124
3D-Move Results for Accuracy Runs 126
Summary 135
7.6 3D-MOVE CALIBRATION USING MNROAD SENSOR DATA 137
MnROAD Sensors 137
3D-Move Results for Accuracy Runs 138
Summary 147

CHAPTER 8. DEFLECTION BASIN INDICES 149
8.1. INTRODUCTION 149
8.2 STEP 1: USING EXISTING 3D-MOVE SIMULATION RESULTS 150
Defining Response Points in 3D-Move Runs 150
Pavement Properties and Loading in 3D-Move Runs 152
Selection of Deflection Basin Indices 153
Summary of Evaluation of Indices 167
Evaluating Indices Using MnROAD Measured Data 171
Evaluation of RWD Sensor Location from Project Sensor Measurements 173
8.3 STEP 2: CORRELATING DEFLECTION BASIN INDICES USING 3D-MOVE ANALYSIS OF SIMULATED PAVEMENT SECTIONS 174
Simulated Pavements for 3D-Move Based Correlations 174
3D-Move Results and Sensitivity Analysis 177
Most Appropriate Indices for Correlations with Maximum AC Horizontal Strain Using Available Data 196
Summary and Conclusions from 3D-Move Analyses 197
8.4 STEP 3: DETERMINING RELATIONSHIP BETWEEN INDEX AND CRITICAL RESPONSES FROM JULEA ANALYSIS 202
Sensitivity Analysis 203
Sensitivity of Pavement Properties on Fatigue Strain 204
Sensitivity of Indices to Critical Pavement Design Responses 204
Relationship between Indices and Critical Response 206
Effect of TSDD Loading Configuration 207
8.5 FIELD EVALUATION OF INDICES 209
Accuracy 209
Precision 210
Overall Field Results 211

8.6 SUMMARY 213
8.7 TEMPERATURE CORRECTION PROCEDURE 215

CHAPTER 9. SUMMARY AND CONCLUSIONS 217

CHAPTER 10. RECOMMENDATIONS 225
10.1 EQUIPMENT RECOMMENDATIONS 226
10.2 DATA COLLECTION RECOMMENDATIONS 228
10.3 RECOMMENDED DATA ANALYSIS FOR NETWORK-LEVEL PMS APPLICATIONS 229
10.4 RECOMMENDED FUTURE RESEARCH 231

APPENDIX A. DEVICE MANUFACTURERS' QUESTIONNAIRES AND INTERVIEWS 235

APPENDIX B. SENSOR INSTALLATION AND FIELD TRIALS 247
SENSOR INSTALLATION 247
FIELD TRIALS 249

ACKNOWLEDGEMENTS 257

REFERENCES 259

LIST OF FIGURES

Figure 1. Illustration. Treatment matrix for RWD and pavement condition 8
Figure 2. Illustration. Five-sensor triangulation configuration 11
Figure 3. Equation. Deflection under wheel 11
Figure 4. Equation. h_D 11
Figure 5. Flowchart. Idealized approach to successful accomplishment of project's objectives 20
Figure 6. Equation. AI fatigue prediction 22
Figure 7. Equation. AI rutting prediction 22
Figure 8. Equation. Definition of radius of curvature $R1$ 23
Figure 9. Equation. Definition of radius of curvature $R2$ 23
Figure 10. Equation. Definition of deflection basin area (A) 24
Figure 11. Equation. Definition of shape factor $F1$ 24
Figure 12. Equation. Definition of shape factor $F2$ 24
Figure 13. Equation. Definition of SCI 24
Figure 14. Equation. Definition of Base Curvature Index (BCI) 24
Figure 15. Equation. Definition of Base Damage Index (BDI) 24
Figure 16. Equation. Definition of slope of deflection (SD) 24
Figure 17. Equation. Definition of area under pavement profile (AUPP) 24
Figure 18. Equation. Definition of tangent slope (TS) 24
Figure 19. Illustration. RWD sensor locations 28
Figure 20. Illustration. MnROAD mainline test cell map 41
Figure 21. Illustration. MnROAD LVR test cell map 41
Figure 22. Map. Testing loop in Wright County, MN 42
Figure 23. Illustration. Pavement structure cross section of accuracy cells 44
Figure 24. Illustration. Typical test section of MnROAD cell 45
Figure 25. Photo. Pavement coring for sensor installation 46
Figure 26. Photo. Smoothing of holes for sensor installation 46
Figure 27. Photo. Grooving of pavement for sensor installation 46
Figure 28. Photo. Partial grouting of the sensors 47
Figure 29. Photo. Alignment of project sensor with FWD sensor 47
Figure 30. Photo. Sensor verification with FWD 47
Figure 31. Graph. Evaluation of performance of embedded sensors with FWD 48
Figure 32. Graph. Comparison of deflections for embedded geophones 1 and 3 under FWD loading 48
Figure 33. Graph. Comparison of deflections for FWD geophones 3 and 10 49
Figure 34. Photo. Final grouting of sensors 49
Figure 35. Photo. Verifying the embedded sensor alignment 49
Figure 36. Illustration. Test section layout with positioning sensors placement 50
Figure 37. Photo. Sample video snapshot showing wheel location from TSD pass 51
Figure 38. Photo. Sample video snapshot showing wheel location from RWD pass 51
Figure 39. Graph. MnROAD strain gauge data 52
Figure 40. Graph. MnROAD strain gauge reduced data 52
Figure 41. Graph. MnROAD soil compression gauge data 53
Figure 42. Graph. MnROAD soil compression gauge reduced data 53

Figure 43. Graph. Embedded sensor full time history with the peaks created by rear and front axles 54
Figure 44. Graph. Geophone and accelerometer time histories 54
Figure 45. Graph. Typical geophone calibration curve 55
Figure 46. Graph. Geophone velocity before and after calibration 55
Figure 47. Graph. Geophone velocity before and after calibration in the time domain 56
Figure 48. Graph. Deflection velocity in spatial domain 56
Figure 49. Graph. Geophone 3 and accelerometer velocity comparison 57
Figure 50. Graph. Geophone 3 and accelerometer deflection comparison 57
Figure 51. Graph. Velocity comparison of geophones 1 and 3 58
Figure 52. Graph. Deflection comparison of geophones 1 and 3 58
Figure 53. Graph. Comparison between embedded sensor deflection velocity results and TSD measurement 59
Figure 54. Graph. Comparison between embedded sensor deflection results and RWD measurement 59
Figure 55. Graph. Time lag calculation example 60
Figure 56. Graph. Comparison of geophone and TSD measurements 61
Figure 57. Graph. Comparison of geophone and RWD measurements 61
Figure 58. Equation. Absolute difference between the deflection measured by the embedded sensor and the deflection reported by TSDD 61
Figure 59. Graph. Typical algorithm deflection comparison 63
Figure 60. Map. Color-coded statistic map 65
Figure 61. Graph. Precision comparison of passes 66
Figure 62. Graph. Precision linear comparison of passes 66
Figure 63. Graph. Typical slope box plot for precision analysis 67
Figure 64. Graph. Typical R^2 box plot for precision analysis 67
Figure 65. Graph. Typical SEE box plot for precision analysis 67
Figure 66 . Graph. Typical range box plot for precision analysis 68
Figure 67. Graph. Typical deflection for a particular sensor 69
Figure 68. Screenshot. Database Web site homepage 70
Figure 69. Graph. Overall comparison of deflections measured with RWD and embedded sensors 73
Figure 70. Graph. Median sensor difference for RWD with varying speeds 74
Figure 71. Graph. Distributions of deflection difference measured with RWD for each cell 75
Figure 72. Graph. Overall comparison of deflection velocities measured with TSD and embedded sensors 79
Figure 73. Graph. Overall comparison of TSD deflection method 1 and embedded sensors 80
Figure 74. Graph. Overall comparison of TSD deflection method 2 and embedded sensors 80
Figure 75. Graph. Median sensor difference for TSD sensors with varying speeds 81
Figure 76. Graph. Distribution of differences measured with TSD for each cell 81
Figure 77. Graph. RWD overall precision slope in the LVR 82
Figure 78. Graph. RWD overall precision R^2 in the LVR 83
Figure 79. Graph. RWD overall precision SEE in the LVR 83
Figure 80. Graph. RWD overall precision range in the LVR 83
Figure 81. Graph. RWD overall precision slope in the mainline 84
Figure 82. Graph. RWD overall precision R^2 in the mainline 84

Figure 83. Graph. RWD overall precision SEE in the mainline 84
Figure 84. Graph. RWD overall precision range in the mainline 85
Figure 85. Graph. RWD overall precision slope in the 18-mi (29-km) loop 86
Figure 86. Graph. RWD overall precision R^2 in the 18-mi (29-km) loop 86
Figure 87. Graph. RWD overall precision SEE in the 18-mi (29-km) loop 86
Figure 88. Graph. RWD overall precision range in the 18-mi (29-km) loop 87
Figure 89. Graph. TSD overall precision slope in the LVR 87
Figure 90. Graph. TSD overall precision R^2 in the LVR 88
Figure 91. Graph. TSD overall precision SEE in the LVR 88
Figure 92. Graph. TSD overall precision range in the LVR 88
Figure 93. Graph. TSD overall precision slope in the mainline 89
Figure 94. Graph. TSD overall precision R^2 in the mainline 89
Figure 95. Graph. TSD overall precision SEE in the mainline 89
Figure 96. Graph. TSD overall precision range in the mainline 90
Figure 97. Graph. TSD overall precision slope in the 18-mi (29-km) loop 91
Figure 98. Graph. TSD overall precision R^2 in the 18-mi (29-km) loop 92
Figure 99. Graph. TSD overall precision SEE in the 18-mi (29-km) loop 92
Figure 100. Graph. TSD overall precision range in the 18-mi (29-km) loop 92
Figure 101. Graph. Comparison of RWD COV with pavement stiffness over flexible pavement 93
Figure 102. Graph. Comparison of RWD COV with pavement stiffness over rigid pavement 94
Figure 103. Graph. Comparison of RWD COV with IRI over flexible pavement 94
Figure 104. Graph. Comparison of RWD COV with IRI over rigid pavement 94
Figure 105. Graph. Precision TSD COV with pavement stiffness over flexible pavement 95
Figure 106. Graph. Precision TSD COV with pavement stiffness over rigid pavement 95
Figure 107. Graph. Precision TSD COV with IRI over flexible pavement 96
Figure 108. Graph. Precision TSD COV with IRI over rigid pavement 96
Figure 109. Graph. Comparison of RWD COV at different speeds in the LVR 97
Figure 110. Graph. Comparison of RWD COV at different speeds in the mainline 97
Figure 111. Graph. Comparison of TSD COV at different speeds in the LVR 98
Figure 112. Graph. Comparison of TSD COV at different speeds in the mainline 98
Figure 113. Graph. Comparison of RWD COV at different afternoon temperatures 99
Figure 114. Graph. Comparison of TSD COV at different afternoon temperatures 99
Figure 115. Graph. Precision TSD COV with vertical gradients for the closer sensors 100
Figure 116. Graph. Precision TSD COV with vertical gradients for the further sensors 100
Figure 117. Map. Wright County 18-mi (29-km) loop TSD 36-inch (914.4-mm) sensor COV 101
Figure 118. Map. Wright County 18-mi (29-km) loop TSD 24-inch (609.6-mm) sensor COV 102
Figure 119. Map. Wright County 18-mi (29-km) loop TSD 12-inch (304.8-mm) sensor COV 102
Figure 120. Map. Wright County 18-mi (29-km) loop TSD 8-inch (203.2-mm) sensor COV 103
Figure 121. Map. Wright County 18-mi (29-km) loop TSD 4-inch (101.6-mm) sensor COV 103
Figure 122. Graph. precision TSD COV with horizontal curves for the closer sensors 104

Figure 123. Graph. Precision TSD COV with horizontal curves for the further sensors 104
Figure 124. Illustration. Pavement structure of MnROAD accuracy cells 108
Figure 125. Equation. BELLS equation 111
Figure 126. Graph. September 2013 temperature variations in Monticello, MN 111
Figure 127. Equation. Complex dynamic modulus 113
Figure 128. Equation. Modified modulus equation 113
Figure 129. Equation. Rewritten modulus equation 113
Figure 130. Equation. Witczak equation 115
Figure 131. Equation. Temperature-viscosity relationship 115
Figure 132. Graph. Development of existing AC modulus master curves from undamaged AC moduli 116
Figure 133. Equation. Existing modulus equation 116
Figure 134. Graph. Master curves for cell 3 in TSDD field trials 117
Figure 135. Graph. Master curves for cell 19 in TSDD field trials 118
Figure 136. Graph. Master curves for cell 34 in TSDD field trials 119
Figure 137. Graph. Variation of five-axle truck semitrailer 121
Figure 138. Illustration. TSD axle configuration and loads 122
Figure 139. Illustration. RWD axle configuration and loads 122
Figure 140. Illustration. Configuration and spacing of embedded project sensors 123
Figure 141. Illustration. Sketch of pavement structures used for cells 3, 19, and 34 124
Figure 142. Graph. 3D-Move predictions and measured deflections for cell 34 in TSD trials (device velocity = 30 mi/h (48.3 km/h)) 127
Figure 143. Graph. 3D-Move predictions and measured velocities for cell 34 in TSD trials (device velocity = 30 mi/h (48.3 km/h)) 128
Figure 144. Graph. Normalized basins of 3D-Move predictions and measured deflections for cell 34 in TSD trials (device velocity = 30 mi/h (48.3 km/h)) 129
Figure 145. Graph. Definition of percentage of maximum displacement 130
Figure 146. Graph. Comparison of normalized deflection basins at various levels for cell 34 in TSD trials (device velocity = 30 mi/h (48.3 km/h)) 130
Figure 147. Graph. 3D-Move predictions and measured deflections for cell 19 in TSD trials (device velocity = 30 mi/h (48.3 km/h)) 131
Figure 148. Graph. 3D-Move predictions and measured velocities for cell 19 in TSD trials (device velocity = 30 mi/h (48.3 km/h)) 132
Figure 149. Graph. Normalized basins of 3D-Move predictions and measured deflections for cell 19 in TSD trials (device velocity = 30 mi/h (48.3 km/h)) 132
Figure 150. Graph. Comparison of normalized deflection basins at various levels for cell 19 in TSD trials (device velocity = 30 mi/h (48.3 km/h)) 133
Figure 151. Graph. 3D-Move predictions and measured deflections for cell 34 for RWD trials (device velocity = 30 mi/h (48.3 km/h)) 134
Figure 152. Graph. Normalized basins of 3D-Move predictions and measured deflections for cell 34 in RWD trials (device velocity = 30 mi/h (48.3 km/h)) 134
Figure 153. Graph. Comparison of normalized deflection basins at various levels for cell 34 in RWD trials (device velocity = 30 mi/h (48.3 km/h)) 135
Figure 154. Graph. 3D-Move computed maximum displacement versus measured displacement for all cells and vehicle velocities during RWD and TSD trials 136

Figure 155. Graph. 3D-Move computed pulse width versus measured pulse for all cells and velocities in RWD and TSD trials 137
Figure 156. Illustration. Response points for normal pressure in 3D-Move 139
Figure 157. Illustration. Response points for strain gauges in 3D-Move 140
Figure 158. Graph. 3D-Move versus WESLEA predictions and MnROAD pressure cell for cell 34 in TSD trials (device velocity = 30 mi/h (48.3 km/h)) 142
Figure 159. Graph. Normalized basins of 3D-Move predictions and MnROAD pressure cell measurement for cell 34 in TSD trials (device velocity = 30 mi/h (48.3 km/h)) 143
Figure 160. Graph. 3D-Move versus MnROAD strain gauge measurement for cell 34 in TSD trials (device velocity = 30 mi/h (48.3 km/h)) 144
Figure 161. Graph. 3D-Move versus WESLEA predictions and MnROAD pressure cell for cell 3 in RWD trials (device velocity = 30 mi/h (48.3 km/h)) 145
Figure 162. Graph. Normalized basins of 3D-Move predictions and MnROAD pressure cell measurement for cell 3 in RWD trials (device velocity = 30 mi/h (48.3 km/h)) 146
Figure 163. Graph. 3D-Move versus MnROAD strain gauge measurement from cell 3 in RWD trials (device velocity = 30 mi/h (48.3 km/h)) 147
Figure 164. Graph. Computed normal pressure for 3D-Move versus WESLEA 148
Figure 165. Graph. Maximum longitudinal strains from MnROAD sensors and 3D-Move computations 148
Figure 166. Illustration. Predetermined locations for estimation of vertical surface deflections in TSDDs 151
Figure 167. Illustration. Surface displacement from 3D-Move displacement time history 151
Figure 168. Illustration. Selection of response points when using 3D-Move 152
Figure 169. Graph. Relationship between $R1_{12}$ and horizontal strains at bottom of AC with TSD loading data 157
Figure 170. Graph. Relationship between $R1_{12}$ and horizontal strains at bottom of AC with all loading data 157
Figure 171. Graph. Relationship between SCI_{12} and horizontal strains at bottom of AC with TSD loading data 159
Figure 172. Graph. Relationship between SCI_{12} and horizontal strains at bottom of AC with all loading data 159
Figure 173. Graph. Relationship between $SCIm_{12}$ and horizontal strains at bottom of AC with TSD loading data 161
Figure 174. Graph. Relationship between $SCIm_{12}$ and horizontal strains at bottom of AC with all loading data 161
Figure 175. Graph. Relationship between DSI_{4-8} and horizontal strains at bottom of AC with TSD loading data 163
Figure 176. Graph. Relationship between DSI_{4-8} and horizontal strains at bottom of AC with all loading data 163
Figure 177. Graph. Relationship between SCI_{60} and maximum vertical strain on top of the subgrade with TSD loading data 165
Figure 178. Graph. Relationship between SCI_{60} and maximum vertical strain on top of the subgrade with all loading data 165
Figure 179. Graph. Relationship between DSI_{24-36} and maximum vertical strain on top of the subgrade with TSD loading data 166

Figure 180. Graph. Relationship between DSI_{24-36} and maximum vertical strain on top of the subgrade with all loading data 167
Figure 181. Illustration. Pavement structures used with 3D-Move analyses 175
Figure 182. Graph. Variation of SCI_{12} calculated with 3D-Move in simulated pavement combinations 178
Figure 183. Graph. Variation of TS_{60} calculated with 3D-Move in simulated pavement combinations 178
Figure 184. Graph. Variation of R_{60} calculated with 3D-Move in simulated pavement combinations 179
Figure 185. Graph. Variation of D_{60} calculated with 3D-Move in simulated pavement combinations 180
Figure 186. Graph. Variation of maximum horizontal strain at bottom of AC layer in simulated pavement combinations 181
Figure 187. Graph. Variability of relationships of *R*1 with maximum horizontal strain at bottom of AC layer for various AC thicknesses 182
Figure 188. Graph. Variability of relationships of *R*1 with maximum horizontal strain at bottom of AC layer for various subgrade moduli 182
Figure 189. Graph. Variability of relationships of *R*1 with maximum horizontal strain at bottom of AC layer for various AC moduli 183
Figure 190. Graph. Variability of relationships of *R*1 with maximum horizontal strain at bottom of AC layer for various vehicle speeds 183
Figure 191. Graph. Variability of relationships of *R*2 with maximum horizontal strain at bottom of AC layer for various AC thicknesses 184
Figure 192. Graph. Variability of relationships of *R*2 with maximum horizontal strain at bottom of AC layer for various subgrade moduli 184
Figure 193. Graph. Variability of relationships of *R*2 with maximum horizontal strain at bottom of AC layer for various AC moduli 185
Figure 194. Graph. Variability of relationships of *R*2 with maximum horizontal strain at bottom of AC layer for various vehicle speeds 185
Figure 195. Graph. Variability of relationships of *SCI* with maximum horizontal strain at bottom of AC layer for various AC thicknesses 186
Figure 196. Graph. Variability of relationships of *SCI* with maximum horizontal strain at bottom of AC layer for various subgrade moduli 186
Figure 197. Graph. Variability of relationships of *SCI* with maximum horizontal strain at bottom of AC layer for various AC moduli 187
Figure 198. Graph. Variability of relationships of *SCI* with maximum horizontal strain at bottom of AC layer for various vehicle speeds 187
Figure 199. Graph. Variability of relationships of *SCIm* with maximum horizontal strain at bottom of AC layer for various AC thicknesses 188
Figure 200. Graph. Variability of relationships of *SCIm* with maximum horizontal strain at bottom of AC layer for various subgrade moduli 188
Figure 201. Graph. Variability of relationships of *SCIm* with maximum horizontal strain at bottom of AC layer for various AC moduli 189
Figure 202. Graph. Variability of relationships of *SCIm* with maximum horizontal strain at bottom of AC layer for various vehicle speeds 189

Figure 203. Graph. Variability of relationships of DSI_{4-r} with maximum horizontal strain at bottom of AC layer for various AC thicknesses 190
Figure 204. Graph. Variability of relationships of DSI_{4-r} with maximum horizontal strain at bottom of AC layer for various subgrade moduli 190
Figure 205. Graph. Variability of relationships of DSI_{4-r} with maximum horizontal strain at bottom of AC layer for various AC moduli 191
Figure 206. Graph. Variability of relationships of DSI_{4-r} with maximum horizontal strain at bottom of AC layer for various vehicle speeds 191
Figure 207. Equation. Rank order correlation coefficient 203
Figure 208. Graph. Sensitivity of pavement properties on maximum fatigue strain 204
Figure 209. Graph. Sensitivity of curvature index on maximum fatigue strain in thin pavements 205
Figure 210. Graph. Sensitivity of curvature index on maximum fatigue strain in thick pavements 206
Figure 211. Graph. General relationship between maximum fatigue strain and SCI for RWD loading 208
Figure 212. Graph. General relationship between maximum fatigue strain and SCI for TSD loading 208
Figure 213. Graph. Accuracy evaluation of indices 210
Figure 214. Graph. Precision evaluation of indices 211
Figure 215. Graph. Overall field performance of indices 212
Figure 216. Graph. Precision of modeled indices in different pavement thicknesses 212
Figure 217. Equation. Temperature correction factor 215
Figure 218. Equation. Dynamic modulus at reference temperature 216
Figure 219. Flowchart. Idealized PMS containing TSDD structural evaluation component 225
Figure 220. Photo. MnROAD field testing devices (September 22 to 27, 2013) 251

LIST OF TABLES

Table 1. Distribution by references source 5
Table 2. Distribution by type of equipment 5
Table 3. Distribution of references by subject matter 5
Table 4. Summary sheet: device comparison 16
Table 5. Proposed traffic levels for network-level study 21
Table 6. Proposed ranges of structural parameters for flexible pavements 22
Table 7. Evaluation of ideal measurement locations 29
Table 8. Evaluation of test vehicle speed 29
Table 9. Evaluation of seasonal changes 30
Table 10. Evaluation of accuracy of deflection measurements 33
Table 11. Alternative sensors for measuring surface deflection parameters 34
Table 12. Evaluation of instantaneous applied load 35
Table 13. Evaluation of precision of deflection measurements 36
Table 14. Pavement structure of MnROAD test sections 42
Table 15. Pavement Structures corresponding to nine sections of the 18-mi (29-km) loop shown in figure 22 43
Table 16. Pavement response lag results 60
Table 17. TSDD average difference and standard deviation of difference 62
Table 18. TSD and RWD accuracy passes 63
Table 19. Precision testing summary 64
Table 20. Color-coded legend for statistic map in figure 60 65
Table 21. Semi-triangular comparison table 68
Table 22. RWD overall accuracy statistics 72
Table 23. RWD accuracy statistics for individual sensors 73
Table 24. TSD overall accuracy statistics 76
Table 25. TSD accuracy statistics for individual sensors 78
Table 26. Overall precision results for the close sensors 90
Table 27. Overall precision results for far sensors 91
Table 28. Average pavement temperature during precision testing 98
Table 29. Date and time of FWD and TSDD testing 108
Table 30. Backcalculated moduli of pavement layers for accuracy cells 109
Table 31. Depths of TC sensors in accuracy cells 110
Table 32. Measured temperature within AC at the time of FWD test 110
Table 33. Temperature within AC from BELLS equation in cell 19 during FWD test 112
Table 34. Temperature within AC from BELLS equation in cell 34 during FWD test 112
Table 35. Average temperatures within AC layer 113
Table 36. Phase angle and damping for accuracy cells for TSD field trials 114
Table 37. Phase angle and damping for accuracy cells for RWD field trials 114
Table 38. Unbound layer properties used in 3D-Move 120
Table 39. AC modulus at the time of TSDD trials for frequency of 30 Hz 120
Table 40. TSDD accuracy runs at MnROAD 124
Table 41. Available sensor data in cells 3, 19, and 34 (used in 3D-Move calibration) 138
Table 42. 3D-Move versus WESLEA predictions at various offsets for cell 34 during TSD trials (device velocity = 30 mi/h (48.3 km/h)) 141

Table 43. 3D-Move versus WESLEA predictions in various offsets for cell 3 RWD trials (device velocity = 30 mi/h (48.3 km/h)) 144
Table 44. Deflection basin indices used in the evaluation 154
Table 45. Relationships between *R*1 and horizontal strains at bottom of AC with TSD loading data 156
Table 46. Relationship between *R*1 and horizontal strains at bottom of AC with all loading data 157
Table 47. Relationship between SCI and horizontal strains at bottom of AC with TSD loading data 158
Table 48. Relationship between SCI and horizontal strains at bottom of AC with all loading data 158
Table 49. Relationship between *SCIm* and horizontal strains at bottom of AC with TSD loading data 160
Table 50. Relationship between *SCIm* and horizontal strains at bottom of AC with all loading data 160
Table 51. Relationship between DSI_{4-r} and horizontal strains at bottom of AC with TSD loading data 162
Table 52. Relationship between DSI_{4-r} and horizontal strains at bottom of AC with all loading data 162
Table 53. Relationship between SCI and maximum vertical strains on top of the subgrade with TSD loading data 164
Table 54. Relationship between SCI and maximum vertical strains on top of the subgrade with all loading data 164
Table 55. Relationship between DSI_{24-r} and maximum vertical strain on top of the subgrade with TSD loading data 166
Table 56. Relationship between DSI_{24-r} and maximum vertical strain on top of the subgrade with all loading data 166
Table 57. Most appropriate indices using TSD data related to maximum horizontal strain at bottom of AC layer 168
Table 58. Most appropriate indices using all data related to maximum horizontal strain at bottom of AC layer 169
Table 59. Most appropriate indices using TSD data related to maximum vertical strain at top of subgrade 170
Table 60. Most appropriate indices using all data related to maximum vertical strain at top of subgrade 171
Table 61. Comparison of most appropriate indices with respect to maximum horizontal strain: 3D-Move results and MnROAD measured data 172
Table 62. Effect of RWD laser position on deflection and computed index 174
Table 63. Pavement considered in 3D-Move analyses and corresponding identification key 176
Table 64. AC mix properties used with 3D-Move analysis 177
Table 65. Effects of an increase in selected pavement parameters on maximum horizontal strain at bottom of AC layer 181
Table 66. Variability of the relationships of the indices with maximum horizontal strain at bottom of AC with respect to AC thickness, subgrade modulus, AC modulus, and vehicle speed 193

Table 67. Most appropriate correlated indices with maximum horizontal AC strain with total database (79 cases) 197
Table 68. Most appropriate indices for MnROAD accuracy runs (43 cases) with respect to maximum horizontal strain at bottom of AC 198
Table 69. Most appropriate indices for sensitivity analyses (36 cases) with respect to maximum horizontal strain at bottom of AC 199
Table 70. Most appropriate indices for combined MnROAD accuracy and sensitivity analysis data (79 cases) with respect to maximum horizontal strain at bottom of AC 200
Table 71. Best indices correlating maximum fatigue strain chosen from 3D-Move analyses ... 202
Table 72. Pavement property range used in generating database 203
Table 73. Relationship between curvature indices and maximum fatigue strain 207
Table 74. Relationship between curvature indices and critical pavement responses with known AC thickness 207
Table 75. Loading configuration of TSDD used in the field test 208
Table 76. Summary of performances of different indices 213
Table 77. Ranking of different indices 214
Table 78. Relationship between robust TSD index DSI_{4-12} and critical pavement responses with unknown and known AC thickness 215
Table 79. Relationship between maximum fatigue strain (ε) and AC modulus for temperature correction 216
Table 80. Recommended deflection indices 223

LIST OF ACRONYMS

AASHTO	American Association of State Highway and Transportation Officials
AC	asphalt concrete
AI	Asphalt Institute
AUPP	area under pavement profile
BCI	Base Curvature Index
BDI	Base Damage Index
COV	coefficient of variation
DAQ	data acquisition
DMI	distant measuring instrument
DSI	Deflection Slope Index
ESAL	equivalent single-axle load
FDR	full-depth reclamation
FFT	fast Fourier transform
FHWA	Federal Highway Administration
FWD	falling weight deflectometer
GPR	ground penetrating radar
GPS	Global Positioning System
HMA	hot mix asphalt
IRI	International Roughness Index
LE	linear elastic
LED	light-emitting diode
LTPP	Long-Term Pavement Performance
LVDT	linear variable differential transformer
LVR	low-volume road
M&R	maintenance and rehabilitation
MA	member agency
MEPDG	*Mechanistic-Empirical Pavement Design Guide*
MnDOT	Minnesota Department of Transportation
MSI	Modified Structural Index
PCC	portland cement concrete
PG	performance grade

PMS	pavement management system
RWD	Rolling Wheel Deflectometer
SCI	Surface Curvature Index
SD	slope of deflection
SEE	standard error of estimate
SHRP2	Second Strategic Highway Research Program
SN	structural number
TC	thermocouple
TS	tangent slope
TSD	Traffic Speed Deflectometer
TSDD	traffic speed deflection device
UNR	University of Nevada-Reno
UTEP	University of Texas-El Paso
VTS	viscosity temperature susceptibility
WESLEA	Waterways Experiment Station Linear Elastic Analysis

CHAPTER 1. INTRODUCTION

State transportation departments invest billions of dollars each year on providing and managing the transportation infrastructure assets to meet legislative, agency, and public expectations. Pavements are a major component of those transportation assets, with pavement rehabilitation being one of the most critical, costly, and complex elements. This is especially true at present, since a large percentage of pavement networks are reaching the end of their serviceable life, and pavement rehabilitation has become even more daunting given the funding constraints faced by State transportation departments.

At the heart of rehabilitation decisions is the pavement management system (PMS), which provides network-level condition indices or scores for each pavement segment in the system. Earlier generations of PMSs were driven by ride quality and distress as a direct result of the American Association of State Highway Officials Road Test, which introduced the concept of the Present Serviceability Rating and Present Serviceability Index.[(1)] With advances in technology, pavement engineers started to use distress (i.e., cracking, rutting, etc.) and longitudinal roughness, typically in the form of the International Roughness Index (IRI), as key pavement performance indicators in the pavement management decisionmaking process.

Both distress and roughness are important indicators that merit emphasis within the PMS process. However, another important indicator necessary to make rational pavement investment decisions is structural adequacy. A few State transportation departments are beginning to consider structural adequacy as part of their routine PMS activities by incorporating deflection testing.

At present, there is a large array of equipment that can be used to measure the deflection basin resulting from an applied load. The most commonly used device in the United States since the 1980s is the falling weight deflectometer (FWD). FWDs rely on impact loads to produce a pavement response similar to that produced by actual traffic loadings, which is then measured by deflection sensors located at varying distances from the load.

While FWDs represent the state-of-the-practice, they are not without shortcomings. Since FWDs are a stop-and-go operation, lane closures are required, which cause traffic disruptions and, in turn, create a safety hazard to personnel involved in the operation as well as the traveling public. Their frequency of testing is also significantly less than a continuous operation, which affects operational costs. These shortcomings are especially important in terms of network-level pavement management applications, which by their nature require information on a large pavement network measuring in the thousands of miles.

To overcome these shortcomings, several organizations in the United States and Europe have developed devices over the past several decades that can continuously measure pavement deflections at posted traffic speeds (up to 50–60 mi/h (80.5–96.6 km/h)). The modern versions of these moving deflection testing devices that are actively used today include the following:

- Traffic Speed Deflectometer (TSD).
- Rolling Wheel Deflectometer (RWD).

Much work has been done over the past decade toward advancing the state of the technology of moving pavement deflection testing. However, one main question is whether the TSD and/or RWD are ready for immediate implementation in the structural evaluation of pavements for network-level PMS applications. If so, how should the measurements from one or more of these devices be used within the context of network-level PMS? These questions are at the heart of the project presented in this report, whose stated objectives were to perform the following:

1. Assess, evaluate, and validate the capability of traffic speed deflection devices (TSDDs) (including both RWDs and TSDs) that measure deflection or other pavement responses for pavement structural evaluation at the network level for use in pavement management application and decisionmaking.

2. Develop analysis methodologies for enabling the use of the device(s) capable of meeting the first objective or alternatively develop recommendations to further advance promising device(s) and/or technologies if the devices do not meet the first objective.

The ultimate goal of the project was to establish a reliable measure of the structural condition of all bound pavement layers above the unbound base layer as it deteriorates over time under traffic and environmental loading based on moving pavement deflection technology and measured at posted traffic speeds (up to 50–60 mi/h (80.5–96.6 km/h)). Moreover, this measure needed to be robust enough in capturing the structural condition or deterioration of the pavement layer notwithstanding the seasonal and spatial variation in base and subgrade layers.

To accomplish the above stated goal and objectives, the following 2 phases and 10 tasks were carried out as part of the project:

- **Phase 1**: Identification and assessment of capable devices.
    - **Task 1**: Kick-off meeting/detailed project management plan.
    - **Task 2**: Identification and assessment of capable devices.
    - **Task 3**: Access to and documentation of technical, data processing, and analysis details of each capable device.
    - **Task 4**: Work plan for field trials.
    - **Task 5**: Interim report.
    - **Task 6**: Presentation and finalization of the interim report.
- **Phase 2**: Execution of work plan—field evaluation and validation.
    - **Task 7**: Field data collection.
    - **Task 8**: Evaluation and validation of devices.

- **Task 9**: Analysis methodologies and processes for incorporating pavement structural information with State transportation department PMS applications.

- **Task 10**: Final report and deliverables.

This report presents the findings, conclusions, and recommendations from the referenced phases and tasks and is organized as follows:

- **Chapter 1. Introduction**: Presents the study objectives, goal, phases and tasks, and report organization.

- **Chapter 2. Literature Review**: Summarizes the literature review and it findings.

- **Chapter 3. Manufacturers, Owners, and Users Questionnaires**: Presents the various questionnaires and interviews with device manufacturers, owners and users and documents the commitment by the device manufacturers to participate in the field trials.

- **Chapter 4. Data Collection and Analysis Work Plan**: Details the work plan for the field trials and analysis methodologies.

- **Chapter 5. Process of Evaluation and Validation of Devices**: Summarizes the field trials and discusses the project database assembled (based mostly on the field trial results but also other relevant data) in support of the remaining project activities.

- **Chapter 6. Performance Evaluation of Devices**: Details the evaluation and validation of the two devices identified as potentially viable as a result of the phase 1 effort (i.e., the TSD and RWD).

- **Chapter 7. 3D-Move Calibration**: Discusses the calibration and validation of the 3D-Move software in support of the identification and selection of the best indices for incorporating pavement structural information into State transportation departments' PMS applications.[(2)]

- **Chapter 8. Structural Capacity Evaluation Indices and Processes**: Summarizes the identification of candidate indices, the selection of the best indices, and the development of the structural evaluation analysis methodologies and processes.

- **Chapter 9. Summary and Conclusions**: Presents the major findings and conclusions that resulted from the project.

- **Chapter 10. Recommendations**: Presents recommendations for TSDD equipment, data collection, data analysis for network-level PMS applications, and future TSDD research.

CHAPTER 2. LITERATURE REVIEW

The objectives of the literature review were to investigate and evaluate previous, ongoing, and proposed research projects relating to available TSDDs that have the potential to meet the project objectives. Publications by the National Cooperative Highway Research Program, State transportation departments, and the Federal Highway Administration (FHWA) as well as publications discussing overseas agency practices and others related to the topic were reviewed.

During the literature review process, the technology presented was assessed for consideration under task 2, "Identification and Assessment of Capable Devices." Detailed records of each reference were kept including information on the location of the materials, relevance to the topic, and significant findings from the work. Each record contained an index, date completed, author, title, source, source document, and abstract. The relevance of each document was used to prioritize the reports to undergo further detailed review.

2.1 REFERENCES REVIEWED

A total of 22 references were reviewed as part of the project, most of which were recent (i.e., from the last 4 years). (See references 1 and 3–23.) Two of these references contain comprehensive literature reviews on TSDDs until 2011.[3,19] Table 1 shows the distribution of references by reference source, and table 2 shows the distribution of references by type of equipment. Some of the references covered more than one type of equipment, while a few were non-equipment-related references covering analysis methodologies. Table 3 shows the distribution of references by subject matter; some of the references covered more than one subject matter.

Table 1. Distribution by references source.

Source	Number of References
Report	13
Article	11
Total	24

Table 2. Distribution by type of equipment.

Equipment	Number of References
RWD	11
TSD	12

Table 3. Distribution of references by subject matter.

Subject Matter	Number of References
Equipment information/specifications	6
Equipment assessments/field studies	13
Data collection, processing, and quality control/quality assurance	11
Data analysis methodologies	11

2.2 LITERATURE REVIEW FINDINGS

Arora et al. summarized the state of the art of continuous deflection devices by investigating an Airfield RWD, a Swedish road deflection tester, a Texas rolling dynamic deflectometer, a Danish high-speed deflectograph, and the RWD from this study.[3] The research also investigated new methods for structural evaluation, including modulus, deflection ratios, modified modulus and deflection ratios, a method using structural numbers (SNs), an alternative method for determining SN from FWD data, and a simple approach to estimate the SN of pavements. The key findings from Arora et al. are as follows:[3]

- The best return on investment in acquiring and operating a rapid continuous deflection device is realized when measurements can be used to delineate pavement sections that are structurally marginal. This would allow the agencies to program the maintenance or rehabilitation of the sections in subsequent fiscal years.

- A high-speed device with more than one deflection sensor is desirable. Devices with one deflection sensor can delineate the pavement sections that are structurally in poor condition, but the uncertainty in delineating structurally marginal pavement sections may be high.

- The uncertainty in delineating structurally marginal pavements is related to the precision and accuracy of the measured deflections. The greater the uncertainty in measured deflections and load, the greater the risk of not properly identifying structurally marginal sections will be.

- A concerted effort is needed to quantify the variability associated with measured deflections from these devices beyond the spatial variability in deflection measurements due to changes in the natural properties of the subgrade soil and construction-related variability.

- Institutionally, the current FWD-based evaluation and scoring schemes incorporated in the Texas Department of Transportation pavement management information system should be gradually changed if a high-speed deflection device is used.

Rada and Nazarian published a report entitled *The State-of-the-Technology of Moving Pavement Deflection Testing*.[19] Some of the major conclusions from their report are as follows:

- Despite the need for further improvements, the TSD investigated in this study can be used for two of the pavement applications identified: identification of pavement changes/anomalies for use at the network level and the project level and determination of overall pavement structural capacity indicators/indices at the network level. With some modifications, the TSD and RWD can be used for multiple applications within the next 5 years.

- An area of concern with the RWD and TSD seems to be the compromise between the repeatability and loss of details with spatial averaging. Depending on the application, an optimized level of repeatability should be achieved over a reasonable spatial averaging. The threshold values for the repeatability and spatial averaging should be defined.

Rada and Nazarian also provided a comprehensive list of future research needs to improve the accuracy and repeatability of the moving pavement deflection testing devices evaluated.[19] Those needs were grouped into three major categories: equipment-related, measurement-related, and application-related issues.

Flintsch et al., as part of the Second Strategic Highway Research Program (SHRP2) Project R06(F), evaluated continuous deflection devices to support pavement management decisions.[13] The study identified both the TSD and RWD as capable of meeting the criteria for speed, load, and data collection and being close to production mode. Field verification for the TSD showed that it could be used for network-level data collection with adequate repeatability and that although there was significant variation and bias between deflection measurements and surface indices computed using TSD and FWD measurements, the results were broadly comparable.[13] The study recommended several improvements to the devices such as adding additional sensors to provide a more complete deflection bowl, measuring pavement layer thickness with adding a ground penetrating radar (GPR) device, and measuring the dynamic load on the loading wheel assembly.[13] As is discussed in section 3.1, Device Manufacturers' Perspectives, improvements have been made to both the TSD and RWD, including increased number of sensors and ability to measure the dynamic load on the wheel assembly since the assessment was conducted during the SHRP2 study.

Many other studies have investigated TSDDs. Several studies showed consistently repeatable results for the TSD and RWD investigated in this study. (See references 5, 10, 11, 13, and 16.) Hausman and Steele evaluated the use of deflection measurements from the RWD to classify roadways structurally for inclusion in a pavement management matrix of treatment selection.[15] They showed that the RWD could result in higher reliability and lower costs, with savings of 5 percent when used to support pavement preservation practices. For example, figure 1 illustrates a complete treatment matrix based on RWD deflections, pavement condition, and traffic levels. It should be noted that the RWD-based treatment matrix proposed relies on one single vertical deflection at the mid-point between the dual tires. This mid-point deflection represents the vertical response contribution from all pavement layers. The utilization of figure 1 requires the Pavement Condition Index rating of the pavement be known a priori.

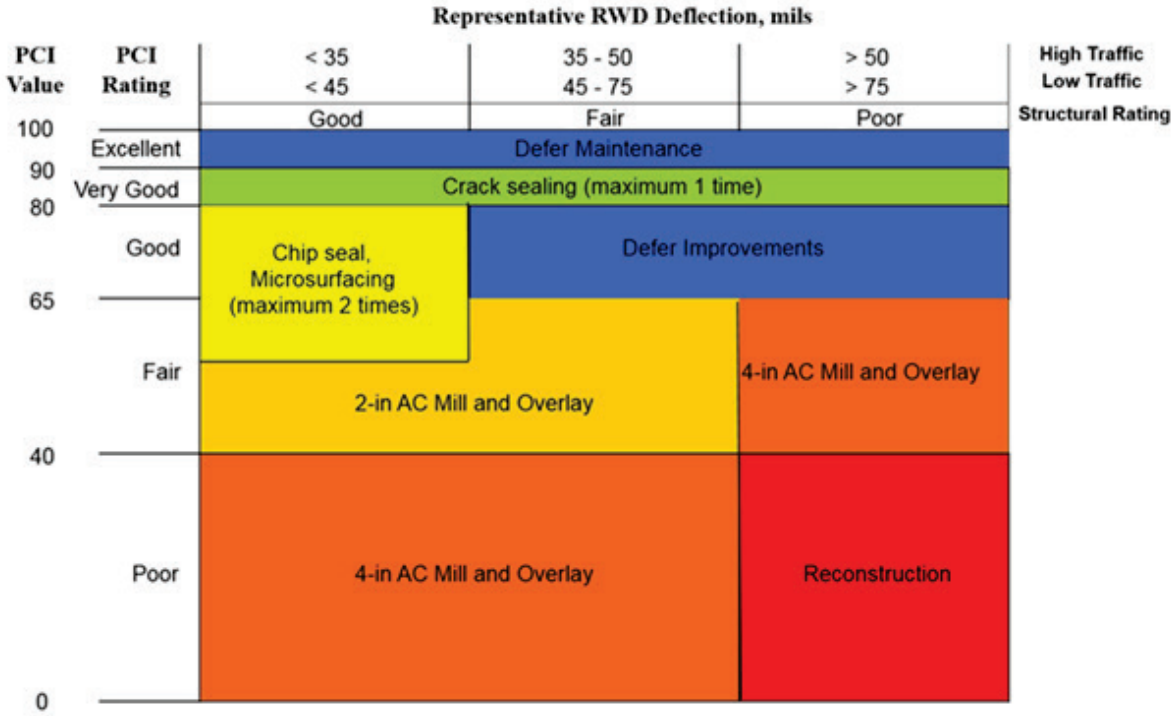

Source: David Hein

1 mil = 0.0254 mm

Figure 1. Illustration. Treatment matrix for RWD and pavement condition.

Ferne et al. chronicled the evaluation and implementation of the TSD for network-level structural evaluation in the United Kingdom, including acceptance testing as well as assessing the effects of testing speed, road surface type, and temperature on TSD measurements.(11) The study showed that the TSD had good short-term repeatability with relatively low standard deviation and that it was capable of differentiating structural strengths equally as well as the deflectograph and FWD.(11)

Thyagarajan et al. developed relationships between curvature indices (based on deflection measurements) and tensile strain at bottom of the asphalt concrete (AC) layer as indicators for progressive deterioration of pavement.(21) They showed deflection measurements can be used to determine tensile strain at bottom of AC layer and used to form structural performance curves for use in PMS.

Gedafa et al. conducted a study comparing deflections measured by the RWD and FWD in Kansas and showed that the center deflections as well as the SNs computed using the devices were statistically similar.(14) As a result of that study, they recommended network-level deflection survey using the RWD on a 4-year cycle. Elseifi et al. conducted a similar comparison between the RWD and FWD in Louisiana.(10) The study showed that the repeatability of the RWD measurements was acceptable with a coefficient of variance of 15 percent and that both the RWD and FWD data properly reflected the pavement condition. Although the RWD measurements were in general agreement with the FWD measurements, the deflections from the two devices were statistically different at 15 out of 16 sites.(10) The study concluded that calculating SN (independent of pavement thickness and layer properties) based on RWD

measurements could be used as a screening tool to identify structurally deficient pavements at the network level.[10] A similar comparison between RWD and FWD measurements in Virginia showed that RWD and FWD results were not well correlated, that repeated RWD measurements were not statistically similar for 8 of the 15 runs, and that RWD standard deviation measurements fluctuated with changes in surface mix type.[7] Based on those findings, it was recommended that the RWD not be pursued for network-level analysis for interstate type facilities in Virginia. It was also suggested that a comprehensive review of the Virginia study is required since it is not known whether the roles of parameters, such as pavement temperature, vehicle speed, and moisture, have been appropriately included in the pavement maintenance and rehabilitation (M&R) and reconstruction decisionmaking. In addition, as previously noted, the RWD measurement of vertical displacement between the tires has a known limitation that it may not fully represent the characteristics of the bound layers alone.

Zhang et al. introduced the use of the Structural Condition Index as a screening tool to discriminate pavements that need structural reinforcement from those that do not.[22] Structural Condition Index is based on the SN of the pavement as determined using FWD data. The study recommended criteria of Structural Condition Index for M&R activities. Stubstad et al. described the use of deflection data to predict pavement performance for certain distresses based on FWD deflection data.[20] Bryce et al. developed a structural index for use in network-level pavement evaluation known as the Modified Structural Index (MSI).[6] MSI is a modified Structural Condition Index for use in the Virginia Department of Transportation's PMS. MSI was selected as a result of the network-level predictions using MSI as the most promising index to predict project-level activities.[6] MSI can be used as a network-level screening tool, for deterioration modeling, or to develop structural performance measures.[6] However, MSI can only be used for flexible pavements. It is based on FWD data, and it is empirical in nature.

Austroads published a study in 2012 that evaluated the use of the TSD in Australia.[4] Although results had shown consistently repeatable results in Europe, the roads in Australia are often quite different, consisting of a considerable amount of granular (unpaved) pavements. Consideration was also given to the harsher climate experienced in Australia compared to Europe. The TSD was evaluated during the Australian summer (December 2009–March 2010) by surveying around 11,185 mi (18,000 km) of the New South Wales and Queensland road networks. The assessments of the technology based on that study were that the TSD could be an effective screening tool at the network level and that it showed considerable promise for design of overlays of granular pavements.[4]

As a follow up to that evaluation study of the TSD, Austroads conducted a survey of eight member agencies (MAs) to determine their interests in network-level strength assessment based on deflection measurement.[17] Seven of the eight MAs expressed interest in having network-level strength assessments and that they would use a TSD for screening out weak and vulnerable pavement sections for further evaluation. Six MAs would use a TSD to estimate pavement rehabilitation and reconstruction budgets, and three MAs would use it to evaluate the performance of maintenance management arrangements.[17] The main concerns expressed by respondents for using the TSD for network-level evaluation were the ability to relate TSD deflection data to FWD deflection data as well as developing robust models based on TSD deflection data.[17]

Using the field data from the 2012 Austroads study, a revised approach for analyzing TSD data to predict the full deflection bowl was performed by Muller and Roberts.[4,18] The study proposed a new methodology for fitting curves based on surface deflection velocities measured by the TSD versus the wheel offset and determining the deflected pavement profile as the cumulative area under the plot of V_V/V_H versus wheel offset, where V_V and V_H represent the vertical and horizontal velocities, respectively.[18] Comparisons were made between the predictions of deflection under the center of the load, D_0 and Surface Curvature Index, SCI_{300} (defined as the difference between D_0 and D_{300} (i.e., 12 inches (300 mm) from the center of the load ($D_0 - D_{300}$) from the proposed methodology, the original Danish analysis, and FWD measurements.[23] The results showed a clear correlation with the shape and magnitude for the deflection bowls of the FWD measurements and the proposed TSD methodology deflection bowls, resulting in d_0 and SCI_{300} predictions from the TSD being on average 6.4 and 16.6 percent higher than the corresponding FWD measurements, respectively.[18]

Dynatest® began redeveloping its version of the RWD based on a former Airfield RWD that was noted in the report by Rada and Nazarian to have been surplused once funding was discontinued.[19] Based on information obtained from the manufacturer in 2011, this new RWD is supposed to utilize the process of triangulation to determine the deflection caused by a moving wheel load. Moreover, it builds on Harr's algorithm, which was developed in the 1970s for a fast-moving heavy wheel load utilizing four sensors where the sensors are equidistant apart and the measurement locations are separated by the same sensor spacing distance.[9]

However, Harr's algorithm only holds true if the sensor nearest the wheel load is the only sensor within the deflection basin, which is not always a correct assumption.[9] Deflections calculated using Harr's algorithm were compared to simulated deflections using the layered elastic program *Waterways Experiment Station Linear Elastic Analysis* (WESLEA) for 27 different pavement sections with various layer thicknesses and layer moduli.[24] Results showed that the Harr algorithm underestimated the deflection.[9] By using more than four sensors, one can correct the influence of the deflection basin on the outer sensors provided that the sensor spacing is greater than the equivalent thickness of the pavement layers.[9] Figure 2 shows a five-sensor configuration and two measurement locations at a distance equal to the sensor spacing as the load travels down the pavement, as designated by the prime and double prime labels.

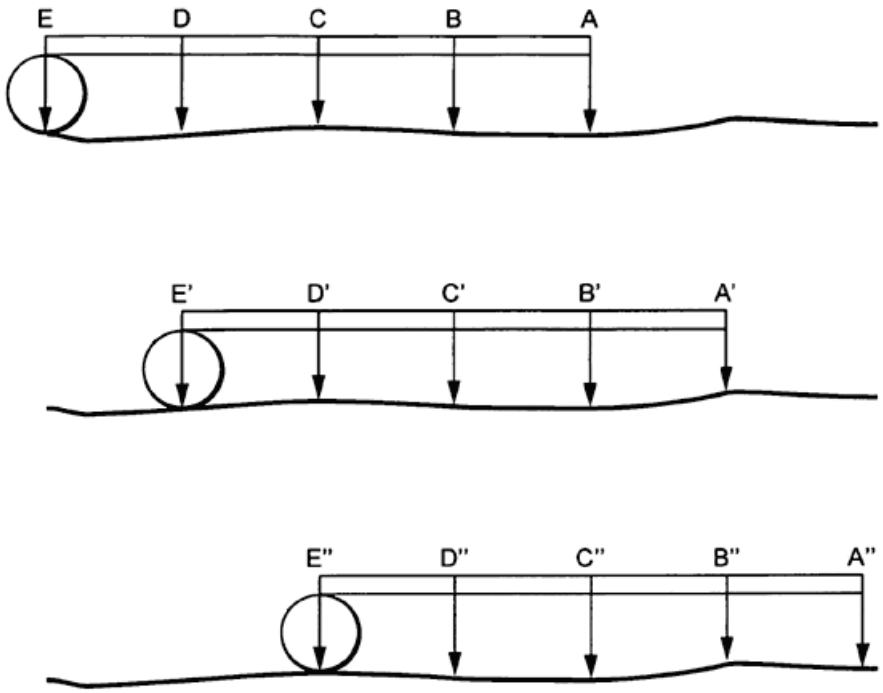

Figure 2. Illustration. Five-sensor triangulation configuration.[9]

The deflection under the wheel, *d*, at sensor E" is calculated using the equation in figure 3, where *k* represents the constant and h_D represents Harr's algorithm. Figure 4 contains an equation to calculate h_D from figure 3. The constant *k* is based on the equivalent thickness. Comparing the deflections calculated using the equation in figure 3 to the model computed theoretical deflections for the 27 pavement sections evaluated previously results in a coefficient of determination (R^2) of 0.9952.[9]

$$d = \left(C'' - \frac{k \times h_D}{2}\right) - 2 \times (D'' - k \times h_D) + E'' - \left(B' - \frac{k \times h_D}{3}\right) + 2 \times \left(C' - \frac{k \times h_D}{2}\right) - (D' - k \times h_D)$$

Figure 3. Equation. Deflection under wheel.

$$h_D = B' - 2 \times C' + D' - A + 2 \times B - C$$

Figure 4. Equation. h_D.

By increasing the number of sensors up to nine, the deflection under the wheel, the deflection measured at a distance one sensor from the wheel load, the deflection measured at a distance of two sensors from the wheel load, and the subgrade modulus can be determined. Utilizing all three deflections and subgrade modulus, the vertical strain at the top of the subgrade layer and the horizontal strain at the bottom of the asphalt layer can be calculated. Comparing the vertical and horizontal strains to the theoretical stain measured based on the 27 pavement sections resulted in R^2 values of 0.99 and 0.91, respectively.[8]

2.3 SUMMARY

As a result of the literature reviewed and the findings summarized in this chapter, it was concluded the both the RWD and the TSD are potentially viable devices, which merit further evaluation. Although the Dynatest® RWD device also appears to be promising, until it is actually functional, it is premature to label it as a potentially viable device. It was anticipated that a functional Dynatest® RWD would be available early in the project; however, that was not the case, and the device was dropped from further consideration in this project. Dynatest® subsequently indicated that they expect to have a functional device by late 2017.

CHAPTER 3. MANUFACTURERS', OWNERS', AND USERS' QUESTIONNAIRES

To augment the literature review findings, questionnaires were developed and sent to the device manufacturers as well as owners and users of the devices. Interviews were also conducted to follow up with specific questions or to pursue clarification. The completed questionnaires and highlights from the interviews conducted are presented in appendix A.

3.1 DEVICE MANUFACTURERS' PERSPECTIVES

The purpose of this questionnaire was to gather information from the manufacturers for analysis, operation, and evaluation. Follow-up interviews were conducted with additional questions to clarify the responses in the questionnaires. The highlights of these interviews are also presented in appendix A.

The RWD utilizes laser sensors to estimate or measure the maximum deflection between the dual tires of an 18-kip (80-kN) single-axle load trailer. The deflection is estimated by comparing the measured undeflected road profile to the deflected road profile at the same location. The TSD utilizes Doppler lasers to estimate the so-called deflection velocity of the road profile that is the velocity the pavement deflects due to the moving load.

The RWD was equipped with four laser sensors, with the first three sensors used to measure the undeflected road profile and the fourth sensor used to measure the deflection 7.25 inches (184.15 mm) behind the center of dual tires at the same location that the undeflected road profile was measured. The laser sensors were spaced 8.5 ft (2.6 m) apart for this spatially coincident approach. Two additional sensors were added to measure a second deflection point at a distance of 15 inches (381 mm) in front of the maximum deflection point to estimate the radius of curvature (R) of the deflection basin. The TSD provided deflection velocities between three and nine points, with the model that was tested in the United States in September 2013 measuring six. Similar to an FWD, the offsets from the load to the measurement points on the TSD could be adjusted. The load applied to the pavement could be varied from 13.2 to 28.7 kip (58.7 to 127.6 kN) for the TSD by using sealed lead loads. Currently, only the TSD estimates the instantaneous dynamic wheel load, but the RWD can be equipped if desired. Both devices are equipped with Global Positioning System (GPS) units and temperature gauges. The TSD was also equipped with a front camera and an inertial profiler with the addition of a GPR under consideration. Although the RWD was not equipped with GPR or video/laser profiling capabilities, these options have been considered.

The recommended speed for data collection with the TSD ranges from 20–55 mi/h (32.2–88.55 km/h). For the RWD, valid measurements can be acquired up to the maximum speed the vehicle is capable of. The minimum speed in which the RWD can acquire valid measurements is 5 mi/h (8.05 km/h).

The fixed factory setting of the Doppler laser limits the reported sampling frequency to a maximum of 1 kHz for the TSD. The recommended distance between successive readings for the RWD is 0.6 inch (15.2 mm) but can be changed by the user to 0.2–0.6 inch (5.1–15.2 mm). The recommended spatial averaging is 32.8 ft (10 m) for the TSD and 528 ft (161.04 m) for the RWD.

To date, owners have mostly only used the TSD on flexible and semi-rigid pavements. The TSD has been used to detect load transfer efficiency issues on rigid pavements to group locations as having or not having significant structural problems. The RWD is capable of working on flexible pavements with AC layers or surface treatments as well as most rigid and composite (AC over portland cement concrete (PCC)) pavements. However, field evaluations of the RWD conducted during this project showed limited application on PCC pavements. The main concern with rigid pavements is the texture as longitudinal tining can distort the data.

Calibration of the TSD includes the proper aligning of the Doppler laser angle to the pavement. RWD users should calibrate the laser sensors annually and should adjust the mounting height of each sensor relative to a flat surface beneath the device prior to each project.

Because both devices utilize a form of a laser sensor, measurements on wet pavements are problematic. Pavement texture can also magnify the random laser measurement error due to the spatially coincident method utilized by the RWD, but spatial averaging reduces this error.

Interviews conducted with manufacturers of both the TSD and RWD provided additional technical information about the devices. Both manufacturers were also open to providing the project team with the processed data for all segments tested and a limited amount of pre-processed/raw data if adequate justification for use of the data is provided and subject to execution of a nondisclosure agreement by the project team with the manufacturers.

3.2 TSD OWNERS'/USERS' PERSPECTIVES

A questionnaire was also developed for owners and users of the TSD, including those in Italy, Poland, South Africa, Australia, and the United Kingdom. The purpose of the questionnaire was to gather information regarding how long each agency has had the device and the main objectives for using the device.

All agencies that purchased the TSD cited that the specific reason was to identify segments of a pavement network for more detailed follow-on structural evaluation using FWDs or other methods. They also indicated that they purchased the TSD to help with the planning and budgeting of major rehabilitation/reconstruction of a pavement network. One responding agency uses the structural indices (SCI_{300} and SCI_{sub} (i.e., SCI subgrade)) to evaluate the bearing capacity of the upper and bottom layers to establish rehabilitation and reconstruction needs. TSD owners expressed that the TSD met their expectations for the intended purpose in terms of operation and data collection. Owners of the TSD also felt that network-level data collection using the TSD should occur every 2–3 years.

Although the system does not currently allow for user calibration, agencies suggested storing angle and odometer calibration values for use in verification during post-processing. Pavement and air temperature are also recorded during measurements, which can be used during analysis such as adjusting SCI_{300} with air temperature.

Overall, owners of the TSD are satisfied. Several suggested improvements include the potential addition of more sensors, faster exporting of data with more custom options, and more details on the built-in analytical model with options for calibration. As a result, the TSD manufacturer will include more details on the analytical model and also output in standard F25 file format that can

be used as input to backcalculation software as with traditional pavement analysis in a future software release.

3.3 RWD USERS' PERSPECTIVES

A questionnaire was developed for users of the RWD including agencies in Virginia, Kansas, Connecticut, and Louisiana. Since the RWD is not currently commercially available, it has mostly been limited to pilot projects and device evaluation projects. Therefore, the purpose of the questionnaire was to gather information regarding how agencies view the RWD and potential applications for it within their agencies. Interviews were conducted to follow up with additional questions.

All agencies participating in the evaluation of the RWD cited the specific reasons were to assess the general network-level structural capacity of the pavements in terms of delineating weak and strong pavement structures within the network. Identifying segments of the pavement network for more detailed structural evaluation using FWDs or other methods was also reported by most agencies.

Operationally, the RWD met the expectations of its intended purpose for all agencies. However, one of the concerns regarding data collection includes loss of accuracy along roadway segments with sharp curves. Another concern expressed is that the lasers are triggered temporally (in time domain) instead of spatially (at set distances), which can increase the likelihood of the successive lasers not measuring the exact same pavement location and also results in varying number of data points per unit length as vehicle speed changes. The data analysis/interpretation currently performed by the manufacturer's staff provides temperature corrected deflection data at 0.1-mi (0.161-km) increments.

The suggested improvements to the RWD included improving data collection and reducing data variability. In terms of data collection, a quicker processing rate of deflection data was preferred. It was also desired to build correlations with FWD data and existing PMS data in order to use RWD data to describe pavement condition by some agencies. Several agencies do not believe that RWD data should be compared to FWD data but instead used to screen locations where pavement structure is changing significantly which can then be followed by other means of structural data collection, such as FWD.

Pavement texture is believed to impact the deflection measurements of the RWD, with one agency noting that the standard deviation of deflection measurements changed significantly with pavement surface type. Wet pavements have also posed problems during data collection as it masks the reflections from the lasers. In addition to pavement texture, it is believed that pavement condition, especially roughness and cracking, also impacts the deflection measurements.

3.4 SUMMARY

Table 4 provides a summary of the RWD and TSD. This represents the initial information provided by the manufacturers and was the basis for the decision of moving forward with the evaluation of the RWD and TSD. Since this time, some updates have been made, including the RWD having two sensors and the TSD having six sensors.

Table 4. Summary sheet: device comparison.

Device Parameter	RWD	TSD
Measurement type (vertical)	Deflection	Deflection velocity
Measurement location of interest	Behind the centerline of load axle at 7.25 inches	Ahead the centerline of the load axle (three locations)
Operation speed (mi/h)	5–60	20–55
Sampling frequency (inches)	0.6	0.8
Deflection accuracy (mil)	2.5	4
Applied load (kip)	18	11
Number of measurements	1	3
Capability of computing SCI	No[a]	Yes (interpolation necessary

1 mi/h = 1.61 km/h
1 inch = 25.4 mm
1 mil = 0.0254 mm
1 kip = 80 kN
[a]If the manufacturer has added the second sensor, this would be possible.

CHAPTER 4. DATA COLLECTION AND ANALYSIS WORK PLAN

Based on a literature review and a survey of device manufacturers, owners, and users, the TSD and the RWD were identified as potentially being capable of meeting the project objectives. The term "TSDD" is used to collectively refer to the two devices.

This chapter details the work plan that was developed and implemented for the field trials and subsequent analyses that were carried out over the remainder of the project to accomplish the following objectives:

- To confirm that the TSDDs met a minimum set of specifications related to the structural evaluation of pavements at the network level.
- To propose processes to incorporate pavement structural information from the successful TSDDs into network-level PMS applications

These objectives and hence the work plan were driven by the analyses that were conducted over the remainder of the project. The work plan was organized into the following sections: analysis methodologies, field trial locations, testing sequence, schedule, and summary.

4.1 ANALYSIS METHODOLOGIES

Rada and Nazarian developed manufacturer-independent specifications required for a number of pavement applications using TSDDs.[19] The authors also provided a comprehensive list of future research needs geared at improving the accuracy and repeatability of the moving pavement deflection testing devices. Those needs were grouped into three major categories: equipment-related, measurement-related, and application-related issues.

The pavement application from the Rada and Nazarian study most relevant to this project is the determination of overall pavement structural capacity indicators/indices. This application serves to assess the overall pavement structural capacity in terms of index values or structural remaining life, and ultimately to support the development of M&R decisions and cost estimates based on structural indicators (comparable to approach used within MicroPAVER™ and other PMSs).[25] However, only the assessment of pavement structural capacity was considered in this work plan, as the development of M&R decisions and costs estimates was beyond the scope of this project. To accomplish the goal of this project, a TSDD must meet the following minimum specifications:

- **Accuracy of deflection measurements**: The absolute values of deflection parameters are important. As such, the device should be able to make accurate measurements. *Accuracy* is defined as the closeness of measured deflections to their actual values.
- **Precision (repeatability) of deflection measurements**: The relative differences in deflection parameters between different points, and as such, the precision of the measurements is also important. *Precision of measurements* is defined as obtaining similar results on a given section with multiple surveys within a short period. The more precise the reported deflections are, the more certain the conclusions drawn with respect

to the assessment of the uniformity of the pavement and the identification of problem spots and anomalous locations will be.

- **Monitoring of applied load**: The magnitude of the load applied by the tire to the pavement as well as the area of the instantaneous contact between the tire and pavement impact the measured deflection parameters. The magnitude of load may change due to a change in parameters such as the roughness of the road, and the contact area may change due to change in tire pressure (e.g., with temperature). Rada and Nazarian recommend that in the short-term, the tire pressure should be monitored during the operation, and in the long-term, appropriate instrumentation that monitors the magnitude of applied load should be added to the devices.[19]

- **Operating speed**: One of the benefits of TSDDs for network-level operations is that traffic control is not necessary. The device should preferably operate at the posted speed limit on a given road without sacrificing the quality of the data collected. The optimal speed of the operation as a function of the road characteristics should be evaluated.

- **Distance between deflection measurements**: One of the major advantages of TSDDs is the denseness of the data collected. A point-to-point density of the measurements of 1 ft (0.305 m) or less is desirable. The feasibility of achieving this density with acceptable quality should also be evaluated.

- **Reporting of measured deflections**: Independent of the denseness of the data collection, the use of statistical methods to report a representative deflection over a representative distance is desirable. Ideally, the reported representative deflections should also include the standard deviation for each representative distance in addition to the mean value. The representative distance should ideally be adjustable based on the length of the survey and variability in the representative deflections reported. The collected data should be segmented and compared with the structural and functional condition of the roads using modern techniques.

- **Collection of additional information**: Additional information about pavement structure from other rapid field testing data is desirable. For example, the moving device can be fitted with a GPR to estimate the pavement layer thicknesses and changes in the pavement structure along the survey. A high-speed video camera is also valuable for visual inspection of the condition of the pavement sections with anomalous deflection readings.

For practicality, a compromise among the precision, accuracy, loss of details with spatial averaging, and speed (and cost) of operation should be made. An optimized level of accuracy and precision should be achieved over a reasonable spatial averaging. The practical threshold values for the accuracy and spatial averaging should be defined based on the pavement structure, pavement responses of interest, and modes of failure associated with these responses.

Figure 5 is an idealized flowchart for accomplishment of the goal and objectives of this project as related to the determination of overall pavement structural condition indicators. Five major activities are identified in the flowchart. Activities 1–3 are desktop studies/analyses that set up the framework for the fieldwork to be done under activity 4. Activity 5 is another desktop study/analysis subtask where the results from the first four subtasks are integrated to recommend an appropriate network-level pavement structural condition assessment algorithm and procedure.

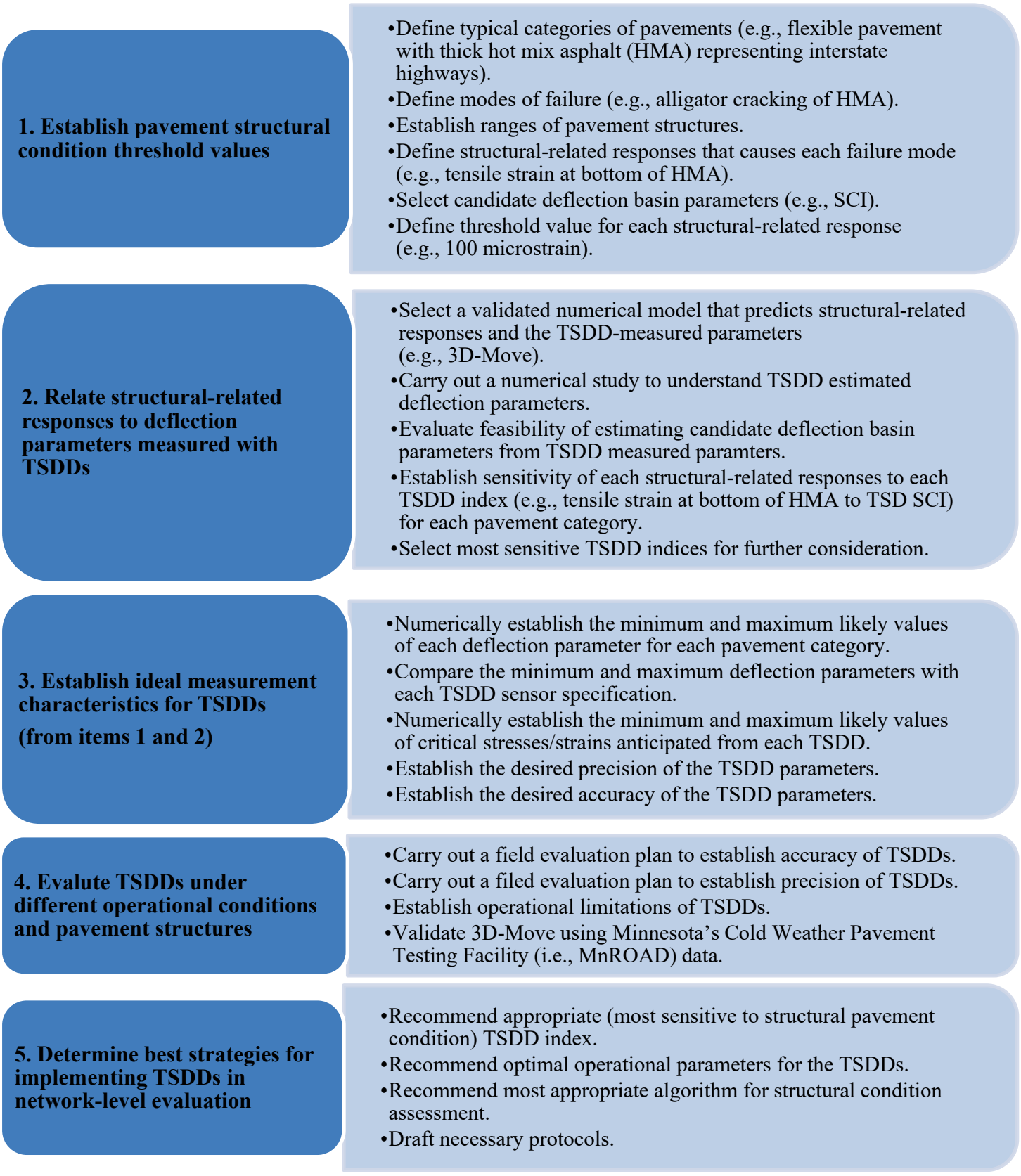

Figure 5. Flowchart. Idealized approach to successful accomplishment of project's objectives.

The five referenced activities also address the remaining project tasks. Activities 1–3 address the validation and evaluation of devices, activity 4 covers the field data collection, and activity 5 addresses the development of analysis methods and processes for incorporation of results into highway agencies' PMS applications. These five activities are detailed next, and changes to the work plan activities are highlighted in future chapters of the report, as applicable.

Activity 1: Establish Pavement Structural Condition Threshold Values

Since current TSDDs are perceived to be less applicable for rigid pavements, the project team decided, in consultation with FHWA, that the focus of the project would be on flexible pavements. As reflected in figure 5, this first activity consisted in addressing the following issues:

- Define typical categories of pavements.
- Define modes of failure.
- Establish ranges of pavement structures.
- Define structural-related responses.
- Select candidate deflection basin parameters.
- Define threshold value for each structural-related response.

Define Typical Categories of Pavements

The magnitude of surface deflection necessary to indicate the potential damage to a pavement structure is controlled by the type of the pavement (rigid versus semi-rigid versus flexible), the characteristics (thickness and stiffness) of the pavement layers above the foundation, the stiffness of the foundation layer, and the traffic volume. Four levels of traffic and representative ranges of pavement structural parameters were proposed (see table 5 and table 6, respectively). Through Monte Carlo simulation, the project team developed an extensive database of pavement sections.[21] Supplementing this database was the pavement responses from *Jacob Uzan Layered Elastic Analysis* (JULEA).[26]

Table 5. Proposed traffic levels for network-level study.

Category	20-Year Traffic (Thousands of Equivalent Single-Axle Loads (ESALs))
Low	< 500
Medium	500–3,000
High	3,000–10,000
Very high	> 10,000

Table 6. Proposed ranges of structural parameters for flexible pavements.

Input	Layer Type	Default	Minimum Value	Maximum Value
Modulus (ksi)	AC	500	300	700
	Base	50	25	250
	Subgrade	10	5	30
Thickness (inches)	AC	5	1	9
	Base	12	6	24

1 ksi = 6.89 MPa
1 inch = 25.4 mm
Note: Subgrades are usually considered as infinite depth. As a result, no data for subgrade thickness are provided.

Define Modes of Failure

Given that the focus of this project was network analysis, the project team proposed to focus on the traditional modes of failure related to fatigue cracking of AC layer and subgrade rutting for flexible pavements.

Establish Ranges of Pavement Structures

The number of 18-kip (1,440-kN) ESALs to failure for each pavement section based on the two failure criteria was established using criteria similar to those recommended by the Asphalt Institute (AI). The AI equation to predict number of repetitions to fatigue cracking is shown in figure 6, while the AI equation for the number of axle loads to cause 0.5 inch (12.7 mm) of rutting is shown in figure 7.[27]

$$N_f = 0.00432 \times 10^{4.84\left(\frac{V_b}{V_b + V_a} - 0.69\right)} \varepsilon_t^{-3.291} E^{-0.854}$$

Figure 6. Equation. AI fatigue prediction.

Where:

N_f = Number of repetitions to fatigue cracking.
V_b = Effective asphalt content in volume (percent).
V_a = Air voids (percent).
ε_t = Tensile strain at the critical location.
E = Stiffness of the material.

$$N_d = 1.365 \times 10^{-9} \varepsilon_c^{-4.47}$$

Figure 7. Equation. AI rutting prediction.

Where:

N_d = Number of axle loads to rut depth failure criteria (0.5 inch (12.7 mm)).
ε_c = Vertical compressive strain on top of the subgrade.

More mechanistic approaches such as those proposed in the American Association of State Highway and Transportation Officials (AASHTO) *Mechanistic-Empirical Pavement Design*

Guide (MEPDG) or CalME, a software program developed by Caltrans/University of California Pavement Research Center using the mechanistic-empirical methodologies for analyzing and designing the performance of flexible pavements were used.[28,29] Pavement structures that preliminarily yielded a design life of 10–40 years for each traffic category were delineated. The distribution of pavement structures along with the mean, median, and standard deviation were used to develop the representative ranges of pavement structures for each traffic category. These results are presented in section 8.4, Relationship Between Indices and Critical Response.

Define Structural-Related Responses

The primary structural responses considered were the tensile strains/stresses at the bottom of the AC and the compressive strains/stresses at the top of subgrade. In addition, the compressive strains/stresses in the middle of the AC and base/subbase were considered as surrogates for the rutting of the AC and base/subbase, respectively, when the rutting failure mode was considered.

Select Candidate Deflection Basin Parameters

Based on the FWD measurements, a number of deflection-basin related parameters that were perceived as strong predictors of the critical structural-related responses and structural conditions of the pavements were proposed. Horak and Emery provided an algorithm for using FWD-derived indices for airfield pavement evaluation, while Thyagarajan et.al. proposed a process for using indices for highway pavements.[30,21] The FWD-measured deflections were simulated for the pavement sections developed under item 1 of this activity (i.e., define typical categories of pavements) and to estimate these and similar deflection basin parameters. Some of these parameters are presented in figure 8 through figure 18.

$$R1 = \frac{r^2}{\left[2D_0\left(1 - {}^{D_r}/_{D_0}\right)\right]}$$

Figure 8. Equation. Definition of radius of curvature *R*1.

Where:

r = Distance from the load.
D_0 = Deflection under the load.
D_r = Deflection at a distance r from load.

$$R2 = \frac{r^2}{\left[2D_0\left({}^{D_0}/_{D_r} - 1\right)\right]}$$

Figure 9. Equation. Definition of radius of curvature *R*2.

$$A = 6\left[1 + 2\left(\frac{D_{12}}{D_0}\right) + 2\left(\frac{D_{24}}{D_0}\right) + \frac{D_{36}}{D_0}\right]$$

Figure 10. Equation. Definition of deflection basin area (*A*).

Where:

D_i = Deflection at i inches away from load.

$$F_1 = \frac{D_0 - D_{24}}{D_{12}}$$

Figure 11. Equation. Definition of shape factor *F*1.

$$F_2 = \frac{D_{12} - D_{36}}{D_{24}}$$

Figure 12. Equation. Definition of shape factor *F*2

$$SCI = D_0 - D_r$$

Figure 13. Equation. Definition of SCI.

$$BCI = D_{24} - D_{36}$$

Figure 14. Equation. Definition of Base Curvature Index (BCI).

$$BDI = D_{12} - D_{24}$$

Figure 15. Equation. Definition of Base Damage Index (BDI).

$$SD = \frac{\tan^{-1}(D_0 - D_r)}{r}$$

Figure 16. Equation. Definition of slope of deflection (SD).

$$AUPP = \frac{5D_0 - 2D_{12} - 2D_{24} - D_{36}}{2}$$

Figure 17. Equation. Definition of area under pavement profile (AUPP).

$$TS = \frac{dD}{dr}$$

Figure 18. Equation. Definition of tangent slope (TS).

Where:

dD = Difference in deflection.
dr = Difference in distance.

Define Threshold Value for Each Structural-Related Response

Ideally, TSDDs are able to provide adequate data accurately and precisely enough so that the performance history of a pavement section can be estimated with reasonable accuracy before any functional or structural distresses are evident. In this ideal process, the critical strains

(e.g., tensile strain at the bottom of the AC) are small enough, and the model for estimating performance of the pavement with time is accurate enough so that highway agencies can conduct what-if analyses (considering life-cycle cost analysis) to make more informed decisions about the best use of their M&R budgets. The project team strived to reach that level of capability. The following items were addressed to evaluate whether the suggested process could be implemented in the near future:

- Do TSDDs provide enough information to reliably estimate critical strains and stresses?
- Do TSDDs provide accurate enough and precise enough information?
- Do highway agencies have enough information about the pavement structure to translate the parameters measured with the TSDDs to critical strains/stresses for network-level studies?
- Are there accurate and calibrated performance models available to predict the performance of pavements?

The subsequent activities, especially activity 4 (field evaluation of devices in figure 5), were designed to answer the first three questions comprehensively. It was thought that the fourth question could be addressed through close collaboration between FHWA and project teams.

An alternative way of establishing the thresholds considered was to conduct simple structural analyses to estimate the remaining life from the time of testing. The relevant structural responses for the representative pavement structures in each traffic category corresponding to 2, 5, and 10 years[1] of remaining life were preliminary considered as the thresholds for deteriorated, marginal, and well-performing pavements, respectively. In other words, if the critical strains/stresses exceeded the 2-year remaining life thresholds, the pavement was considered a candidate for reconstruction, and if the critical strains/stresses were less than the 10-year thresholds, the pavement was considered in good condition. Pavements with remaining lives of 2–5 years were considered candidates for major rehabilitation, and pavements with remaining lives between 5 and 10 years were considered candidates for maintenance or light rehabilitation.

These concepts were revisited after field data with TSDDs became available to develop the best strategies for implementing TSDDs (addressed as part of activity 5).

Activity 2: Relate Structural-Related Responses to Deflection Parameters Measured with TSDDs

The analyses proposed under activity 2 were based on the traditional static layered elastic algorithms. The TSDDs used proprietary hardware and software to estimate dynamic surface deflection parameters imparted by the moving tire loads. Since the trucks carrying the devices often traveled at traffic speeds, the resulting dynamic surface responses were affected by inertia and damping of the layered pavement system. The evaluation of the capabilities of these devices

[1]These values were considered preliminary, for the purposes of the work plan, and are subject to change during the analyses.

was therefore undertaken by a computational model that is capable of modeling moving loads traveling on a layered medium. The five issues addressed under this activity are as follows:

- Using a numerical model to predict structural-related responses and TSDD-measured parameters.
- Understanding TSDD estimated deflection parameters.
- Evaluating feasibility of estimating candidate deflection basin parameters from TSDD-measured parameters.
- Establishing sensitivity of structural-related responses to each TSDD-measured parameter and index.
- Selecting most sensitive TSDD indices for further considerations.

Using a Numerical Model to Predict Structural-Related Responses and TSDD-Measured Parameters

The computer software 3D-Move is ideally suited to evaluate and compare pavement responses measured with TSDDs. 3D-Move estimates the dynamic pavement responses at any point within the pavement structure using a continuum-based finite-layer approach. The 3D-Move model can account for important pavement response factors such as the moving traffic-induced complex three-dimensional contact stress distributions (normal and shear) of any shape, vehicle speed, and viscoelastic material characterization for the pavement layers. (See references 2 and 31–33.) The pavement surface deflection is affected by many factors that include pavement layer characteristics (thickness and stiffness properties), vehicle speed, and damping. Damping in particular plays a major role in the form of time lag between the loaded tire and the deflection response. The 3D-Move model uses viscoelastic formulation and complex frequency domain analyses, such that damping can be specified as either a single value or as a function of frequency. For each of frequency considered in the fast Fourier transform (FFT), the corresponding damping (frequency dependent, if required) was selected and used to obtain the imaginary part of the modulus.

Since rate-dependent (viscoelastic) material properties can be accommodated by 3D-Move, it was considered an ideal tool to study pavement response as a function of vehicle speed through the direct use of the frequency sweep test data (dynamic modulus and damping) of AC mixture.

Several field validations (e.g., Penn State University test track, MnROAD, and University of Nevada-Reno (UNR) Off-Road Vehicle study) that compared a variety of independently measured pavement responses (stresses, strains, and displacements) with those computed by 3D-Move have been reported in the literature. (See references 34, 35, 31, and 33.) Hajj et al. reported that the responses from 3D-Move were within 6 percent of those estimated by ViscoRoute developed by Chabot et al. for thin and thick pavements.[36,37] Those studies demonstrated the applicability and versatility of the 3D-Move approach. Further validation of 3D-Move to strengthen the validity of its application in relating device measurements to structural responses was carried out as part of the field evaluation of the devices as discussed under activity 4.

Understanding TSDD Estimated Deflection Parameters

Each TSDD has its own way of calculating deflection parameters. The TSD measures the surface vertical velocity at as many as nine points[2] (in the front from the mid-point between the dual tires) within the deflection bowl using a Doppler laser technology. The vertical velocity measurements were divided by the vehicle speed to arrive at the slopes of the deflected shape at the measuring locations. These slopes were then fitted to a deflection bowl to estimate the surface deflection at the mid-point between the tires (D_0) and other locations.

The RWD used six spot lasers mounted on a horizontal aluminum beam to measure the deflected pavement surface (longitudinally along the midpoint between the dual tires). Two sensors (sensor D located 7.25 inches (184 mm) behind the axle and sensor F located 7.75 inches (197 mm) in front of the axle in figure 19) were within the deflection bowl, while the other four sensors represent locations within the undeflected pavement surface. The A, B, C, and E sensor readings were used to obtain the load-induced surface deflection at the location of sensors D and F. The following questions were addressed as part of these simulations:

- **Are the algorithms used to estimate surface deflection parameters appropriate?** Routinely used critical surface deflection parameters by the TSD include SCI_{300} ($D_0 - D_{300}$), SCI_{200} ($D_0 - D_{200}$), and D_0. Conversely, the deflection at sensor D (see figure 19) is used by the RWD. A subset of pavement structure database from each traffic category was used as input to 3D-Move to fully explore the strength of the algorithms used to estimate the deflection parameters. The subset was selected based on the results of the linear elastic (LE) analyses performed under activity 1. For example, the appropriateness of the location of sensor D of the RWD needed to be evaluated, as it was not readily apparent whether the maximum deflection occurred 7.25 inches (184.15 mm) behind the axle for all pavement structures and vehicle speed. It was anticipated that the damping characteristics along with stiffness properties (soft versus stiff) governed where the maximum pavement deflection occurred.

- **What are the ideal locations for sensors?** The sensor locations on the TSD are changeable, while they are fixed on the RWD. Accordingly, it was worthwhile to explore whether other sensor locations could better predict pavement layer conditions. An experiment plan as shown in table 7 was adopted to explore the optimal selection of sensor locations. It was also considered possible that the optimal sensor locations may change as the speed of the test vehicle changes and thickness of the AC layer; this matter is addressed next.

- **How does the speed of test vehicle impact the measured deflection parameters?** Field studies revealed that vehicle speed played a significant role in pavement response. Though the devices under consideration were designed to operate at or close to posted traffic speeds, the vehicles may operate at lower speeds for a variety of reasons. The role of vehicle speed on the measured pavement deflection is important, especially if a comparison is to be made between the data from the same TSDD traveling at different speeds. The speed of the vehicle may also impact the optimal location of the sensors.

[2]The TSD that was used in the field trials discussed in chapter 5 only had six points.

- Table 8 provides the experiment plan that was adopted with 3D-Move to investigate the role of vehicle speed. If the speed of the vehicle impacted the optimal location of the sensors, a strategy to recommend the best compromise on the location of the sensors could be developed.

- **How does the seasonal change in material properties of pavement layers (e.g., temperature for AC and moisture for base and subgrade) impact the response?** It was considered important to quantify the variability in the surface deflection (and hence candidate indices or parameters relating to pavement structural condition) caused as a direct consequence of the change in material properties brought on by the seasonal changes. This variation can be used to compare the TSDD measurements taken on a given pavement section at different seasons of the year. Table 9 provides the experiment plan adopted with 3D-Move to investigate the role of seasonal changes. Since the seasonal changes in material properties are not explicitly considered in 3D-Move (i.e., are simulated by increasing or decreasing the properties of different layers), the results from the previous two questions were used to address this question. It was also decided that if a gap in the trends was observed, additional 3D-Move cases would be executed.

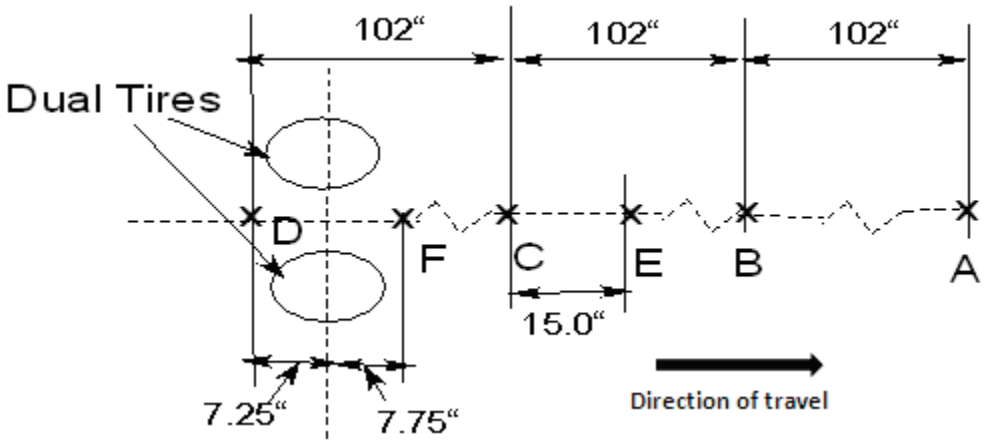

1 inch = 25.4 mm

Figure 19. Illustration. RWD sensor locations.

Table 7. Evaluation of ideal measurement locations.

Activity	Description of Activity
Experiment plan	A subset of as many as 32 cases from database from table 6 based on analyses performed in activity 4.
How	• Select pavement sections and properties as per experiment design. • Execute 3D-Move at traffic speed. • Calculate deflections and velocities at various points on pavement surface (between tires and in front and back of tires) for TSD and RWD. • Use deflection velocities from many combination of points in calculation of surface pavement deflection (TSD). • Compare the deflections under tire center and other surface locations with those calculated from deflection velocities from multiple points (TSD). • Look for the sensitivity of the locations of measurements on TSD measurement locations. • Pay attention to pavement deflections at locations front and back of the axle (5–10-inch (127–254-mm) range) (RWD investigation).
Further action	Synthesize and scrutinize deflections looking for correlation and trend relative to pavement structure and material properties.

1 inch = 25.4 mm

Table 8. Evaluation of test vehicle speed.

Activity	Description of Activity
Experiment plan	Same (up to 32) cases considered in table 7 but with different vehicle velocities.
How	• Select pavement sections and properties as per experiment design. • Execute 3D-Move at three different speeds (slow, intermediate, and fast). • Look for sensitivity of vehicle speed on RWD deflection and deflections at TSD measurement locations.
Further action	Synthesize and scrutinize deflections looking for correlation and trend relative to pavement structure and material properties.

Table 9. Evaluation of seasonal changes.

Activity	Description of Activity
Experiment plan	Use same databases reflected in table 7 and table 8. How does the speed of test vehicle impact the measured deflection parameters? Field studies revealed that vehicle speed played a significant role in pavement response. Though the devices under consideration were designed to operate at or close to posted traffic speeds, the vehicles may operate at lower speeds for a variety of reasons. The role of vehicle speed on the measured pavement deflection is important, especially if a comparison is to be made between the date from the same TSDD traveling at different speeds. The speed of the vehicle may also impact the optimal location of the sensors. Table 8 provides the experiment plan that was adopted with 3D-Move to investigate the role vehicle speed. If the speed of the vehicle impacted the optimal location of the sensors, a strategy to recommend the best compromise on the location of the sensors could be developed (supplement if necessary).
How	• Look for sensitivity of seasonal changes about the control values on RWD deflection and deflections at TSD measurement locations. • Execute 3D-Move with appropriate layer properties that represent the seasonal variations.
Further action	Synthesize and scrutinize deflections looking for correlation and trend relative to pavement structure and material properties

Evaluating Feasibility of Estimating Candidate Deflection-Basin Parameters from TSDD-Measured Parameters:

For practical implementation, it was considered highly desirable to simulate the TSDD-measured parameters and to estimate the candidate deflection-basin parameters established under activity 1 for estimating the pavement structural conditions.

Establishing Sensitivity of Structural-Related Responses to Each TSDD-Measured Parameter and Index

The pavement structure database or its subset was used as input to 3D-Move to estimate the relevant deflection parameters and corresponding indices selected in activity 2 at three vehicle speeds: slow (20 mi/h (32.2 km/h)), intermediate (40 mi/h (64.4 km/h)), and fast (60 mi/h (96.6 km/h)). The two databases were merged for further statistical analyses to address the following:

- How well the surface deflection from static analyses under activity 1 correlated to the surface deflection parameters simulated with 3D-Move for each TSDD.
- How well the critical strains/stresses from static analyses under activity 1 correlated to the maximum critical strains/stresses simulated with 3D-Move.
- How well the critical strains/stresses established earlier under activity 2 correlated to the surface deflection parameters simulated with 3D-Move for each TSDD.

- How well the critical strains/stresses established earlier under item 3 (i.e., evaluating feasibility of estimating candidate deflection basin parameters from TSDD-measured parameters) of activity 2 correlated to candidate indices from activity 2.

- Which candidate indices from item 3 (i.e., evaluating feasibility of estimating candidate deflection basin parameters from TSDD-measured parameters) under activity 2 were more sensitive to the surface deflection parameters simulated with 3D-Move and the critical strains/stresses established for each TSDD.

Selecting Most Sensitive TSDD Indices for Further Considerations

Through correlation and sensitivity analyses explained in the previous item, the most representative indices associated with different modes of failure were identified for further field validation.

Activity 3: Establish Ideal Measurement Characteristics for TSDDs

The outcomes of activities 1 and 2 were used to establish the ideal measurement characteristics. The five issues addressed under this activity were as follows:

1. **Establish the minimum and maximum likely values of deflection parameters anticipated from each TSDD**: The database developed under activity 2 contained the minimum and maximum likely values of deflection parameters for each pavement category selected under activity 1. The distribution of the surface deflection parameter for each TSDD was therefore established. Based on a reasonable confidence level (80–90 percent), the minimum and maximum likely deflection parameters were also established.

2. **Compare the minimum and maximum deflection parameters with each TSDD sensor specifications**: Such statistical comparisons were carried out to establish the likelihood of the success of each device in providing useful data for each pavement category selected in activity 1.

3. **Establish the minimum and maximum likely values of critical strains/stresses anticipated from each TSDD**: The database developed under activity 2 contained the minimum and maximum likely values of critical strains and stresses for each pavement category selected under activity 1. The distributions of the critical strains/stresses for each TSDD were established. Based on a reasonable confidence level (80–90 percent), the minimum and maximum likely critical strains/stresses were also established.

4. **Establish the desired precision of the TSDD raw measurements**: Using the correlation analysis from activity 2 and the distributions from items 1 and 3 under this activity, the sensitivity of the critical strains/stresses to TSDD deflection measurements were established. The sensitivities were then mapped to the desired precision of the measurements for each pavement category.

5. **Establish the desired accuracy of the TSDD parameters**: Using the correlation analysis from activity 2 and the distributions from items 1 and 3 under this activity and the thresholds for weak and strong pavements, the confidence levels for delineating the weak and strong

pavements for each pavement category were established. Based on these confidence intervals, the desired accuracy of the devices was also established. The established preliminary target precisions and accuracies were compared with those obtained from the devices during field study as discussed later under activity 5.

Activity 4: Field Evaluation of Devices

The deflection measurement that defines the minimum requirements for the capable devices include the accuracy of measurements, precision of measurements, and a number of other items that are categorized under operational limitations of devices. To summarize this information, the parameters that support or validate the interpretation of the data collected with a device are not straightforward. This is because the response parameters cannot be measured directly; the raw data collected with a TSDD have to be combined with the pavement structure and pavement conditions through either empirical, analytical, or numerical algorithms to estimate the critical strains/stresses within or at the interfaces of pavement layers. Accordingly, a rigorous field study was required to evaluate, validate, and improve the numerical results and suggested criteria for estimating the structural conditions of the pavements from the parameters measured with the TSDDs. The bulk of the field study activities were carried out at the Minnesota Department of Transportation (MnDOT) MnROAD facility located north of Minneapolis, MN; the basis for selecting this facility for use in the study is provided in section 4.2, Field Trial Locations. The specific issues addressed as part of field study activity include the following:

- Accuracy of deflection measurements.
- Precision of deflection measurements.
- Operational limitations of devices.
- Validation of 3D-Move using MnROAD data.

Accuracy of Deflection Measurements

The accuracy of the measurements was determined by comparing the reported values from each device with the same values from an external sensor. The main focus of the determination of the accuracy was the deflection parameters measured by the devices. The RWD estimated the surface deflection using a spot laser, and the TSD measured the surface velocity using Doppler laser technology. Table 10 summarizes of the objectives and other factors related to this experiment. A comparison of the deflection parameters measured at the densest interval with each device with the deflection parameters measured with embedded sensors at the surface of the pavement was proposed.

Table 10. Evaluation of accuracy of deflection measurements.

Activity	Description of Activity
Hypothesis	TSD/RWD reported deflections or deflection velocities are the same as the deflections or deflection velocities experienced by pavement.
Data requirements	• Deflection parameters measured at densest interval possible with TSD/RWD with time. • Deflection parameters measured with independent surface sensors. • Repeat the first two items three times to ensure that adequate data are available.
Experiment design	• Structure (four levels): Weak, intermediate, and strong flexible pavements and typical rigid pavement • Speed (three levels): Slow, intermediate, and fast (speeds to be determined in consultation with MnROAD and TSD/RWD operators). • Sensors: As many as provided by TSD/RWD.
Pre-testing actions	1. Select test sections for this activity based on FWD data. 2. Decide on test speed based on capabilities of TSD/RWD and instrumentation used. 3. Select a data synchronization technique for the TSDD. 4. Select technique/process to mark/measure wheel location (offset) with respect to instrumentation. 5. Use an FWD and a generic truck to make sure the instrumentation is accurate and operational.
How	• Measure deflection time history as TSD/RWD approaches the embedded sensors. • Obtain synchronized deflection parameters reported by TSD/RWD. • Conduct statistical analysis to test the hypothesis.
Further action	If the hypothesis is rejected: • Consult with manufacturer for possible remedial action. • Request more raw form of data from manufacturer for further analysis.

Based on the status report of the MnROAD sensors that measure displacement parameters (i.e., embedded linear variable differential transformers (LVDTs) and accelerometers), they did not function reliably. As such, the project team decided to retrofit pavement test sections with appropriate surface sensors for this activity. Three alternative sensors (LVDTs, geophones, and accelerometers) were considered as possible candidates for embedded sensors, as outlined in table 11. It was decided to primarily use geophones for accuracy purposes since they are the least expensive, can be easily ruggedized in a steel casing, and have one-to-one correspondence to the deflection parameters measured by the TSD. In addition, one accelerometer was used at each accuracy test section to verify the responses of the retrofitted geophones.

Table 11. Alternative sensors for measuring surface deflection parameters.

Sensor	Advantage	Disadvantage
LVDT	• Measures displacement time history directly. • Works with both static and dynamic loads.	• Requires a reference point deep into pavement foundation. • Installation is difficult and tedious.
Geophone	• Measures velocity time history. • Can be easily ruggedized. • Installation is easy since it does not need a reference point. • Least expensive option.	• Does not respond to static loads. • Should be thoroughly calibrated. • Integration of velocity to calculate displacement should be done carefully.
Accelerometer	• Installation is easy since it does not need a reference point. • Calibration is linear.	• Most models do not respond to static loads. • Double integration of acceleration to calculate displacement should be done carefully. • Most expensive option for sensors appropriate for this study.

A secondary parameter related to the accuracy of the measured deflection parameters is the instantaneous applied load to the pavement. The impact of pavement roughness on the instantaneous load applied to the pavement is documented in the literature.[38,39] The state of the practice in the analyses of the TSDD deflection data is usually based on the assumption that the instantaneous load is equal to the static load, but in this project, the impact of the variation in the instantaneous load on the performance of the devices was studied. The TSD was equipped with instrumentation to measure the instantaneous applied loads concurrent with the deflection measurements. Such measurement is currently lacking from the RWD. Instrumenting the test sections for directly measuring the instantaneous load seemed impractical. However, since the TSD was equipped to estimate the load applied to the pavement, an evaluation of the potential benefits of normalizing measured TSD deflection parameters with loads reported by the device was carried out.

Table 12 summarizes the objectives and other factors related to this experiment.

Table 12. Evaluation of instantaneous applied load.

Activity	Description of Activity
Hypothesis	Instantaneous applied load is equal to static axle load and does not significantly impact results from TSDD analyses.
Data requirements	Dynamic loads measured with TSD concurrent with deflections at the densest interval possible.
Experiment design	Same as table 10 plus all other feasible sections of MnROAD.
Pre-testing actions	1. Measure roughness (e.g., IRI) of test sections shortly before field testing. 2. Measure static axle loads of TSDDs before testing.
How (only on TSD)	• Conduct statistical analysis to obtain average and standard deviation of instantaneous load and deflection parameter for each section. • Conduct correlation analysis to determine whether measured deflections are related to measured instantaneous loads. • Conduct signal analyses on loads and deflections to study the feasibility of delineating spatial variability from variability due to dynamic effects of load.
Further action	Document implication of not measuring instantaneous dynamic loads on evaluating structural condition of pavements.

Precision of Deflection Measurements

The precision of the measurements is estimated by comparing the reported values from replicate measurements in a short period of time. Table 13 summarizes the objectives and other factors related to this experiment.

Table 13. Evaluation of precision of deflection measurements.

Activity	Description of Activity
Hypothesis	TSDD measurements repeated over a short period are adequately precise for network-level analysis of structural condition.
Data requirements	Deflection parameters measured five times with TSDDs at the densest possible intervals.
Experiment design	• All feasible sections at MnROAD and two actual pavement sections near MnROAD. • Speed (three levels): Slow, intermediate (secondary roads), and fast (interstate). • Sensors: As many as provided by the TSDDs. • Ambient conditions: As cool as possible (morning) and as hot as possible (afternoon).
Pre-testing actions	Establish preliminary precision desired for network-level applications.
How	• Conduct statistical analysis to obtain average and standard deviation of measurements for each section. • Conduct student *t*-test and *F*-test to ensure that repeat data belong to same population for each section. • Conduct correlation analysis to relate precision to pavement structure and/or roughness of pavement to address the need for measuring dynamic loads and ranges in deflection parameters.
Further action	Document implication of estimated TSDD precision on delineating structural condition of pavements if hypothesis is rejected.

Operational Limitations of Devices

Although the major technical issues can be conceptually addressed with the established levels of accuracy and precision, many other practical parameters can also impact how well the condition of the pavement can be assessed and were therefore considered in this project. These practical parameters can be optimized to ensure that the maximum information can be robustly extracted from the devices. Marginal additional data collection was needed for this purpose; the data collected under the previous two items of this activity (i.e., accuracy of deflection measurements and precision of deflection measurements) were processed differently to address most of these issues. Those issues were as follows:

- **Desirable reporting interval**: Academically speaking, it would be desirable to collect and store data as densely as possible. In practical terms, however, the data storage requirements for such a dense dataset are prohibitive. Since the goal of this project was network-level analyses, it was suitable to statistically process the data to reasonable reporting intervals. Typically, arithmetic averaging of the data over a certain distance (e.g., 0.1 mi (0.161 km)) is carried out for this purpose. While 0.1 mi (0.161 km) is typical for the network level and is the state of the practice with most other network-level PMS data elements, there are also cases of localized weak sections within the 0.1 mi (0.161 km) that should be identified. This optimum interval is controlled by the size of the network to be tested, the uncertainty of the device measurements (including the

precision and accuracy), and a number of other institutional requirements and practices of local highway agencies.[13] The goals of this effort were to improve the method of statistical processing of the data and to optimize the reporting scheme so that with minimal volume of data the significant areas with structural defect could be identified.

Some of the simple options that were considered include reporting the coefficient of variation (COV) in addition to the average value per 0.1 mi (0.161 km) or the moving average with a base length of 0.1 mi (161 m). Some more advanced improvements considered include supplanting the simple averaging with the more modern geospatial methods or adjusting the reporting interval dynamically based on the COV of a section relative to a threshold COV (set based on the precision of the device). The results of the study were validated on long pavement sections by comparing the lengths of the abnormally high deflection zones from the device and the corresponding lengths of pavements with high FWD deflections or extensive distress. This is addressed in chapter 10.

- **Desirable operating speed**: To expedite the collection of data safely, operating TSDDs at the posted highway speed was preferred. The quality of the data collected at a given speed may also be impacted by the pavement structure, roughness, texture, and geometrical design. It may be possible to relate the optimal operating speed of the devices to these parameters. To that end, statistical analyses were conducted to relate the quality of the deflection parameters collected at the three speeds under items 1 and 2 (i.e., accuracy of deflection measurements and precision of deflection measurements) of this activity to pavement structure. Roughness and geometry of the sections selected were only considered in the context of explaining anomalies. The results of these analyses were used to make some preliminary recommendations on the operating speeds. Where possible and applicable, the data were also correlated to texture to explain the anomalies in the measured data.

- **Temperature adjustment**: The variation in the deflection parameters with temperature, especially for pavement structures with reasonably thick AC layers, is well documented in the literature. Even though several procedures for adjusting the FWD deflections with temperature are proposed (e.g., ASTM D7228, "Standard Test Method for Prediction of Asphalt-Bound Pavement Layer Temperatures"), their applicability to the highway speed devices is not known.[40] Accordingly, a preliminary study was made to see whether the potential differences in deflections measured at the two temperatures for flexible pavements tested under item 1 of this activity could be explained by the changes in temperature and whether the existing FWD-based relationships could be used with the TSDD data. Supplementary data collected at other temperatures during the day were also considered to study the impact of temperature more rigorously. Moreover, the 3D-Move program has been previously used to model temperature variations by treating the AC layer as comprised of many individual sublayers and assigning each sublayer an individual set of frequency-dependent modulus, E^*. E^* can vary as a function of the pavement temperature. Accordingly, a master curve approach was ideally suited to get these temperature-dependent E^* versus frequency curves for the AC sublayers.

- **Compatibility of devices**: Even though the RWD and TSD collect different deflection parameters, ideally they should yield similar structural conditions for the pavement network. To assess whether the devices were interchangeable, the interpreted pavement condition data (not raw measured deflection parameters) was compared. The assessment consisted of relating the TSDDs' structural condition rating from all sections tested to one another to quantify the linearity and bias. Student *t*-tests and *F*-tests were used to determine whether the data from the two devices were from the same population.

Validation of 3D-Move Using MnROAD Data

Existing pavement response measurements on flexible pavements at MnROAD facility include strain responses in longitudinal (vehicle direction) and transverse directions and vertical pressure histories in base and subgrade layers (see table 10). MnROAD contains more than 90 reliably operating longitudinal and transverse dynamic strain gauges in flexible pavement cells and more than 40 dynamic pressure gauges in the foundation layers. These measurements were directly compared with those computed by 3D-Move. Since the project focus was on AC layer condition, attention was given mainly to AC strain measurements. The 3D-Move modeling requires pavement layer configurations and properties and traffic loading. An existing MnROAD database of material properties, which include FWD data and also viscoelastic characterization (dynamic modulus and damping) of AC properties (e.g., master curve of frequency sweep data), were used. The tire load measurements provided the information on the tire-pavement interaction load.

In addition, data collected from the supplementary embedded surface geophones were also used in the validation. The durations of the time histories were variable (based on the vehicle speed) to cover a distance of ±15 ft (4.58 m) from the embedded sensor. Based on preliminary analysis using 3D-Move, the spacing between geophones was determined to ideally be about 5–6 inches (127–152 mm) at a number of locations. The measured velocity time histories from the geophones along with the estimated displacement time histories were relevant since they were the basic measurements that were used by the TSDD under consideration.

Activity 5: Best Strategies for Implementing TSDDs in Network-level Evaluation

The main goal of this activity was to integrate the outcomes from the previous four activities into a coherent set of practical guidelines and protocols for the successful implementation of the TSDDs in network-level structural condition assessments for use in State transportation department PMS applications. Additional data analyses and alternative data interpretation algorithms were considered. Based on the outcomes of the 3D-Move validations, additional simulations were also carried out. The four issues addressed under this activity include the following:

1. **Appropriate TSDD indices**: The main effort associated with this issue was to subject the most promising structural indices selected under activity 2 to the data obtained from relevant MnROAD sections with TSDDs and to evaluate what indices explain the structural conditions of each section as judged by the severity of the distresses, IRI, and FWD deflections. To that end, applicable test sections were subdivided into weak, marginal, and strong (when appropriate) to compare with the predicted structural conditions based on the

TSDD measurements. The outcomes were then applied to the longer pavement test sections as discussed in the next chapter for validation purposes.

2. **Optimal operational parameters for the TSDDs**: The main activity associated with this issue was to evaluate and supplement the numerical results and experimental analyses to recommend the most practical means of utilizing the TSDDs. As part of this item, the following information was provided for each TSDD:

    - Ideal pavement types and those that are not likely to lend themselves to conclusive structural conditions.
    - Speed of operation range for valid measurements as a function of pavement type.
    - Possible limitations due to the road geometry and functional conditions of the pavements.
    - Possible recommendations about the sensor locations.
    - Recommended additional features in the potential TSDDs for better interpretation of structural conditions (like GPR, temperature sensor, etc.).

3. **Most appropriate algorithm for structural condition assessment**: The goal of this effort was to integrate the best means of systematically processing the raw deflection parameters from the TSDDs to obtain the appropriate indices and the preferred statistical or geospatial methods to summarize the processed results into representative structural condition categories for network-level pavement management.

4. **Recommended protocols**: The goal of this effort was to integrate the outcomes from each step into a straightforward generic protocol so that different highway agencies can utilize them for their evaluation and modification based on their specific needs.

4.2 FIELD TRIALS LOCATION

To support the analysis methodologies detailed in the previous section of the report, the field trial location(s) should provide the following pavement factorial parameters:

- Pavement type (flexible, rigid, or composite).
- Pavement surface texture (smooth or rough).
- Pavement thickness (thin to thick).
- Pavement condition (excellent to poor in terms of ride quality and/or distress).
- Horizontal curves.
- Vertical gradients.
- Different unbound layer strength.

Other testing considerations required by the analysis methodologies include varying temperatures and device speeds. These considerations could be taken into account in determining the field location(s) but could also be controlled once the field locations were selected by varying the time of day the testing occurred to control temperature or the speed of the device, provided varying the speed of the device did not pose a safety concern.

Several potential field trial locations were considered to fulfill the requirements mentioned, including the MnROAD facility; instrumented test sections in Kansas, Ohio, and New York; and test sections previously used in the evaluation of the RWD in Louisiana.

4.3 SUMMARY

This chapter presented a detailed work plan developed for the remainder of the project, including analysis methodologies and field trial locations. The details provided in this chapter were developed to accomplish the following two objectives:

- Confirm that the TSDDs met a minimum set of specifications related to the structural evaluation of pavements at the network level.

- Propose processes to incorporate pavement structural information from the successful TSDDs into network-level PMS applications.

The decision was made to hold the field trials at the MnROAD facility because it provides a multitude of test sections in one location and contains readily available information, including environmental and dynamic load response data. In addition to the MnROAD test sections, additional field trial testing was planned on an 18-mi (29-km) loop located in Wright County, MN, near the MnROAD facility.

CHAPTER 5. PROCESS OF EVALUATION AND VALIDATION OF DEVICES

5.1 INTRODUCTION

The main purpose of the field evaluation was to establish the precision and accuracy of the devices considered in this study. A diary of the field activities, including a detailed description of how data were collected, is included in appendix B of this report. Data collected in the field included TSDD data, embedded sensor data, environmental data, and high-speed videos. This chapter describes the process of collecting, reducing, and analyzing the raw data as well as the development of a database. It also covers different methodologies used to evaluate the precision and accuracy of both devices.

5.2 SITE SELECTION

The MnROAD facility was selected as the primary site since it provided a multitude of test sections in one location. The facility consists of a 3.5-mi (5.6-km) mainline roadway (see figure 20) comprising 45 sections with live traffic as part of Interstate 94 near Albertville, MN. In addition, a 2.5-mi (4-km) closed-loop low-volume road (LVR) containing 28 sections was also available (see figure 21). The section lengths were typically about 500 ft (152.5 m) long.

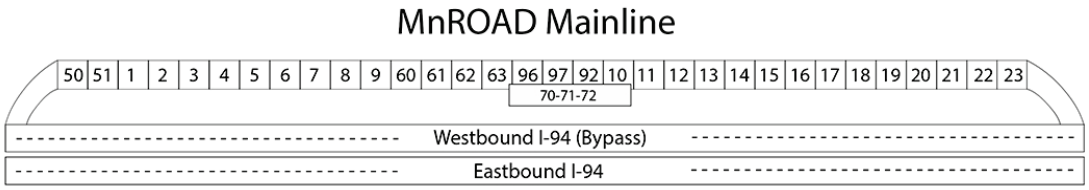

Source: Benjamin Worel

Figure 20. Illustration. MnROAD mainline test cell map.

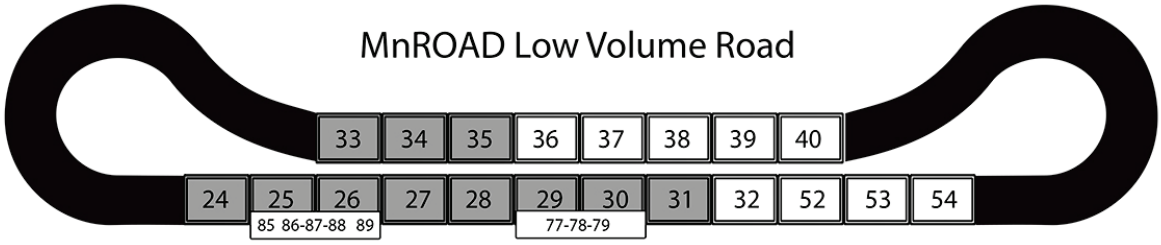

Source: Benjamin Worel

Figure 21. Illustration. MnROAD LVR test cell map.

Table 14 provides a summary of the pavement structure information for the MnROAD test sections. The sections varied in pavement type, with the mainline consisting of 13 AC sections, 15 PCC sections, 14 white-topping sections, and 3 Strategic Highway Research Program composite sections and the LVR consisting of 15 AC sections and 13 PCC sections.

Table 14. Pavement structure of MnROAD test sections.

Section	Pavement Structure	Layer Thickness (inches)			Section Length (ft)		
		Minimum	Maximum	Average	Minimum	Maximum	Average
Mainline	Asphalt	3	6	4.9	462	500	496
	PCC	5	9.5	6.6	210	512	374
	Stabilized full-depth reclamation (FDR)	6	8	6.7	454	500	485
	Unbound concrete overlay	7.5 (PCC)	7.5 (PCC)	7.5 (PCC)	117	153	137
		5 (AC)	5 (AC)	5 (AC)			
	White-topping	4 (PCC)	6 (PCC)	5.6 (PCC)	24	449	137
		5 (AC)	8 (AC)	6.9 (AC)			
LVR	Asphalt	3	5.5	4.1	225	507	389
	PCC	4	12	7	118	508	377

1 inch = 25.4 mm
1 ft = 0.305 m

In addition to the test sections along the mainline and LVR of the MnROAD, an 18-mi (29-km) loop of Minnesota roadway network in Wright County, MN, (see figure 22) was also tested. The loop was located about 20 mi (32 km) from the MnROAD facility and separated into nine sections. MnDOT (through Wright County) provided the pavement structure and IRI data in support of the TSDD study (see table 15). As is the case for many realistic pavement evaluation, a part of section 9 was under construction that might have led to an unanticipated slow down or lane change in a short segment of that section. In addition to providing realistic test sections, the loop also contained tight turns and rolling hills that provided data to evaluate the effects of horizontal and vertical curves.

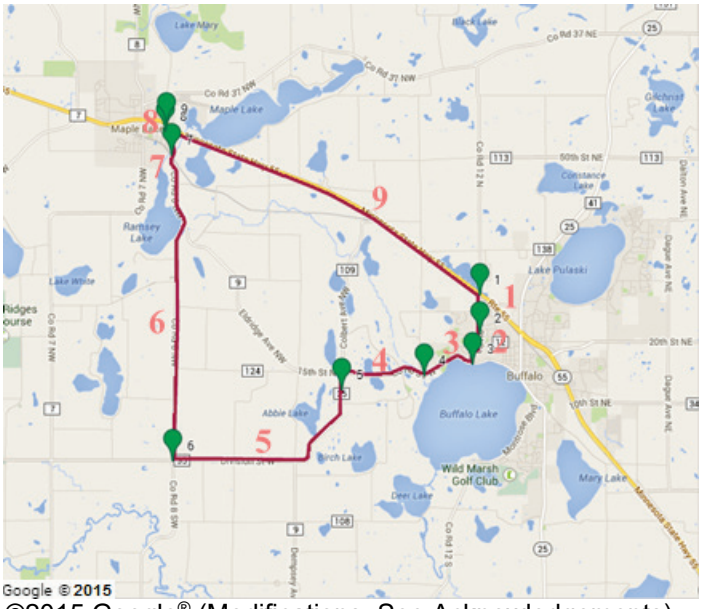

Figure 22. Map. Testing loop in Wright County, MN.[41]

Table 15. Pavement Structures corresponding to nine sections of the 18-mi (29-km) loop shown in figure 22.

Section	Length (mi)	Layer Thickness (inches)			Average IRI (inch/mi)
		AC	Base	Subbase	
1	0.6	3.5	10	—	57
2	0.5	4.0	13	—	70
3	0.9	3.5	10	—	57
4	1.6	3.5	10	—	51
5	3.6	7.0	3	5	146
6	5.0	8.3	12	—	146
7	0.4	5.5	—	—	146
8	0.1	4.5	5	10	310
9	5.8	N/A	N/A	N/A	89

1 mi = 1.61 km
1 inch = 25.4 mm
1 inch/mi = 15.8 mm/km
N/A = Not available.
— Layer was not present.

5.3 SITE INSTRUMENTATION

The MnROAD sections were instrumented with different types of sensors, such as LVDTs, strain gauges, pressure cells, moisture gauges, thermocouples (TCs), and tipping buckets. Distress surveys, rutting measurements, laser profiler measurements, and FWD data were collected regularly on the sections. In addition to existing sensors, four geophones and one accelerometer were installed as embedded sensors to measure deflection velocity and displacement parameters at four MnROAD cells. Based on the criteria discussed in section 4.2 and in consultation with MnROAD staff, three flexible and one rigid pavement sections were selected. The pavement cross sections for the four cells are included in figure 23. The three flexible pavement sections covered three levels of stiffness (cell 34 soft, cell 19 intermediate, and cell 3 stiff as judged by FWD testing and pavement structure). Geophones were primarily used since they are the least expensive and can be easily ruggedized in a steel casing as well as due to their one-to-one correspondence to the deflection parameters measured by the TSD. In addition, one accelerometer was used at each site to verify the responses of the retrofitted geophones. The geophones had nominal resonant frequencies of 4.5 Hz and a measuring range of 160 mil (4 mm). The accelerometers were micro-electro-mechanical system direct current accelerometers with a nominal sensitivity of 28,350 mV/oz (1,000 mV/g). Aluminum holders were machined to provide them the protection needed to withstand the testing process. The geophones were calibrated using a shaker table and a high-precision reference accelerometer to establish their frequency responses after they were placed in the metallic holders.

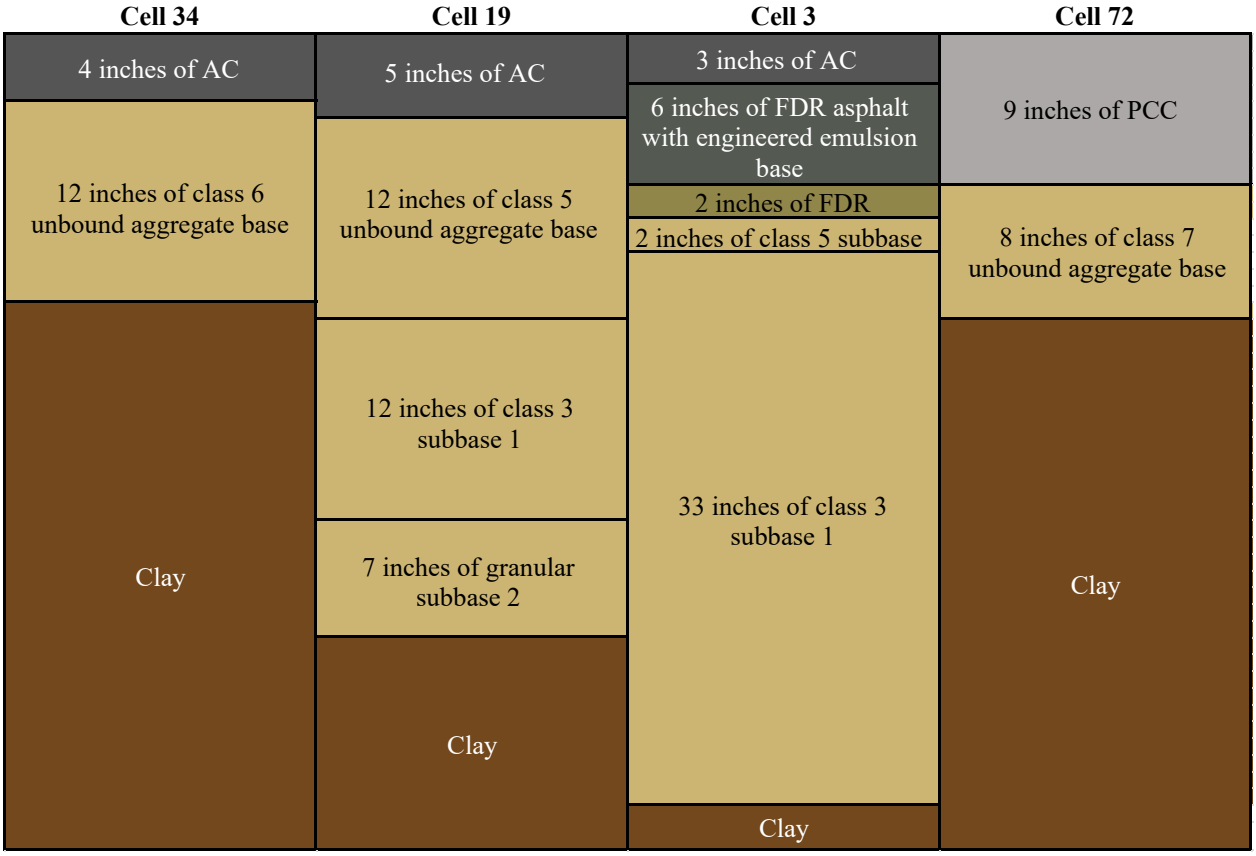

1 inch = 25.4 mm

Figure 23. Illustration. Pavement structure cross section of accuracy cells.

Geophones and accelerometers were embedded in the right wheel path of each selected MnROAD cell, as shown in figure 24. Two of the geophones (marked as 1 and 3) were installed along the center of the wheelpath, while the other two (marked as 2 and 4) had 6 inches (152.4 mm) offset to either side of the wheelpath center. The purpose for this offset was to increase the probability of having the test vehicle sensor pass directly on top of one of the sensors while data from the test vehicle and embedded sensors were being collected. The accelerometer was packaged with geophone 3.

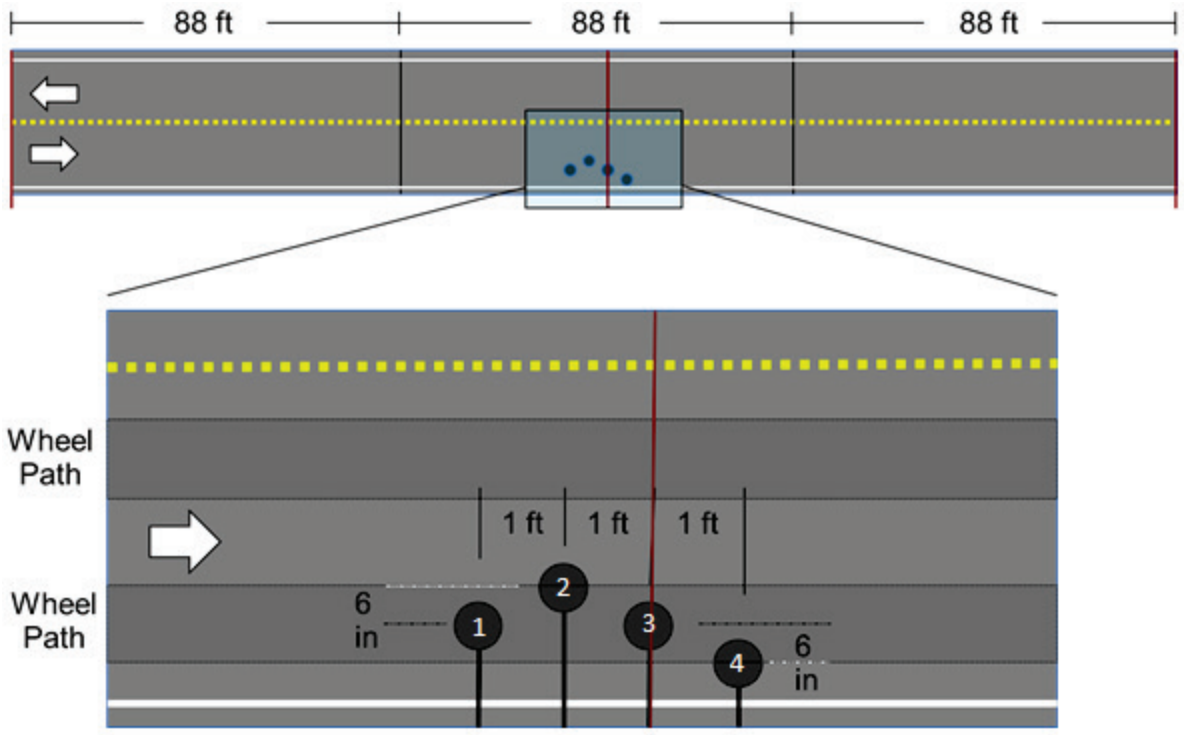

1 ft = 0.305 m
1 inch = 25.4 mm

Figure 24. Illustration. Typical test section of MnROAD cell.

As illustrated in figure 25 through figure 28, 5 sensors were installed at each cell (3, 19, 34, and 72) for a total of 20 sensors. The activities associated with installing the five sensors at each cell included the following:

- Marking the locations of the sensors.
- Coring the pavement down to 2.2 or 2.5 inches (55.88 or 63.5 mm) for sensors containing a geophone and accelerometer.
- Smoothing the bottom of the holes with an air hammer.
- Grooving the pavement to accommodate the sensor wires.
- Partially grouting the sensors in the core holes.

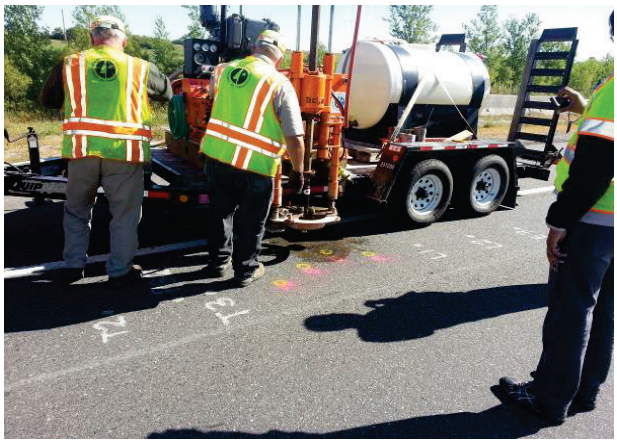

Figure 25. Photo. Pavement coring for sensor installation.

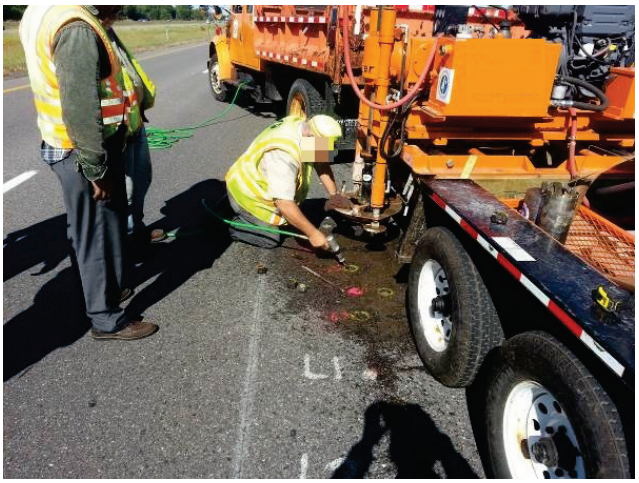

Figure 26. Photo. Smoothing of holes for sensor installation.

Figure 27. Photo. Grooving of pavement for sensor installation.

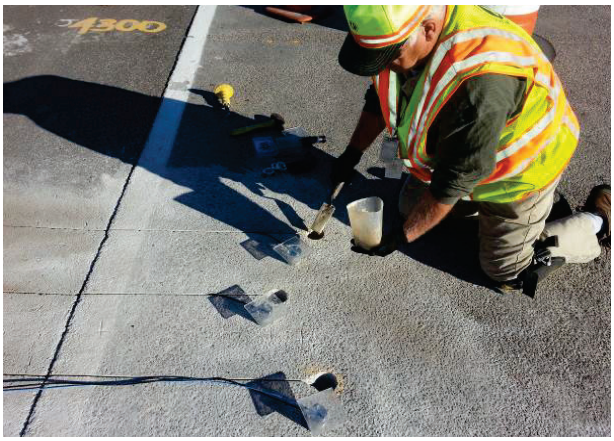

Figure 28. Photo. Partial grouting of the sensors.

As shown in figure 29 and figure 30, the performance of each sensor was then verified using an FWD. For that purpose, one of the FWD sensors was placed directly on top of one of the embedded sensors. The deflections reported by the FWD were then compared with the corresponding deflections reported by the embedded geophones and accelerometers.

Figure 29. Photo. Alignment of project sensor with FWD sensor.

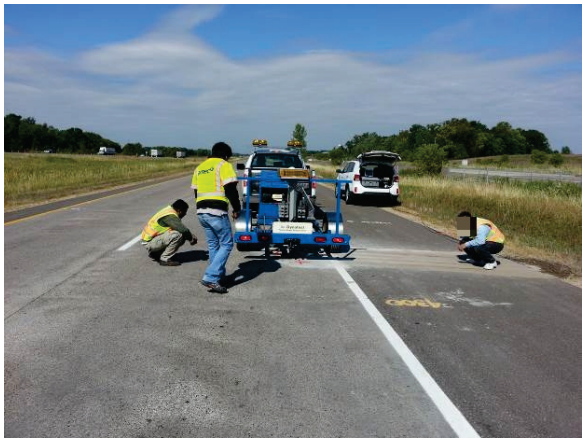

Figure 30. Photo. Sensor verification with FWD.

The results from the sensors installed at the three flexible pavement MnROAD cells are presented in figure 31. The deflections from the FWD sensors and the embedded sensors were quite similar. The typical accuracy of the geophones similar to those used in the FWD and installed at MnROAD was reported by the manufacturer as 2 percent of the measured deflection (no less than ±0.2 mil (0.0051 mm)). Based on the reported statistics in the figure, on average, the deflections of the FWD and installed sensors were within about 0.4 mil (0.010 mm) of one another, which confirms the adequacy of the installed system given the uncertainty associated with measurements with short impulse tests (i.e., FWD).

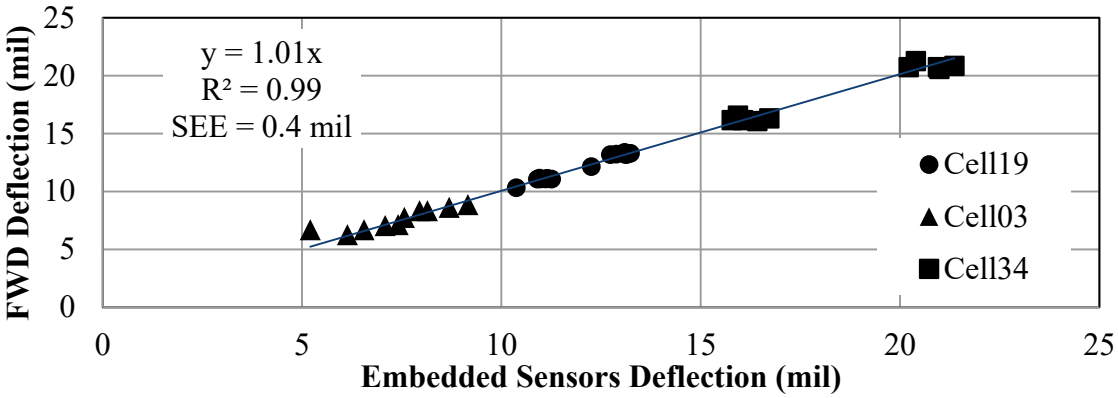

1 mil = 0.0254 mm
SEE = Standard error of estimate.

Figure 31. Graph. Evaluation of performance of embedded sensors with FWD.

Figure 32 shows a comparison of the FWD deflections on top of geophones 1 and 3 from the same exercise. The average difference between the deflections from the two geophones was about 5 percent with an SEE of 0.8 mil (0.02 mm). Figure 33 compares the deflections measured with FWD geophones 3 and 10, located at offsets of 12 and -12 inches, respectively, at the same time and indicates a difference of 1 percent with an SEE of about 0.2 mil (0.005 mm). A review of the data indicated that the reason for the higher uncertainty in the embedded sensors data was related to the inconsistency in the data of one of the embedded sensors at cell 34.

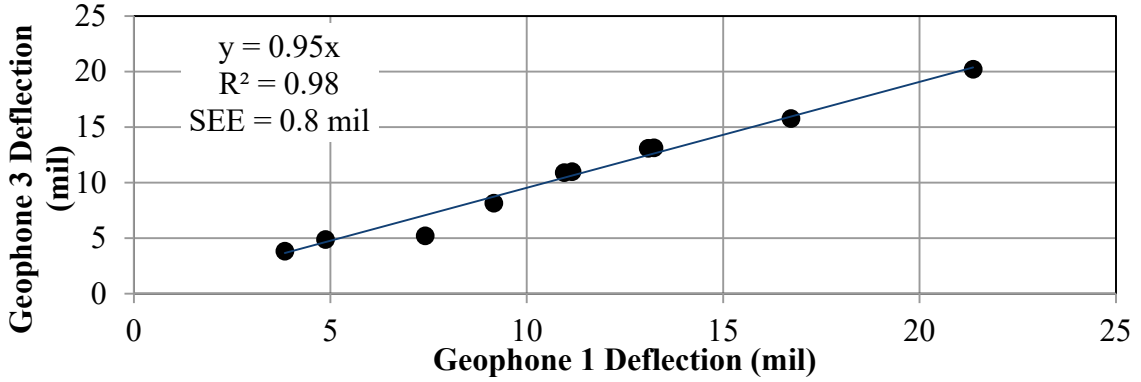

1 mil = 0.0254 mm

Figure 32. Graph. Comparison of deflections for embedded geophones 1 and 3 under FWD loading.

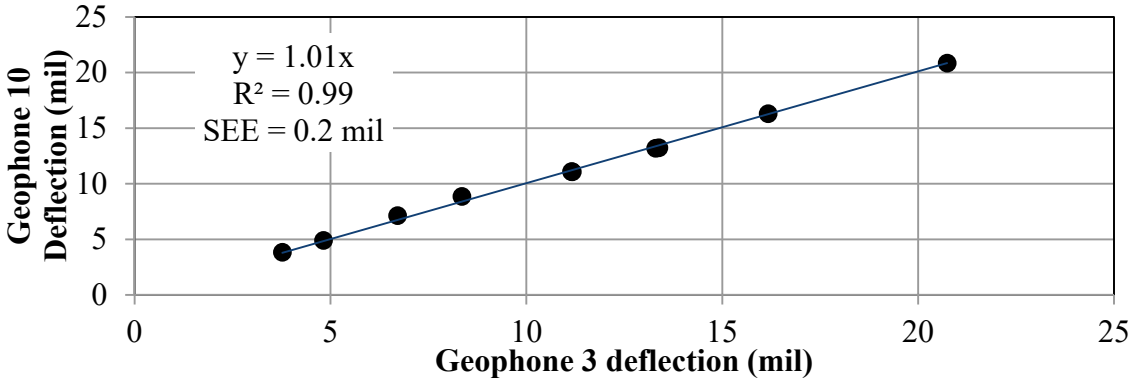

1 mil = 0.0254 mm

Figure 33. Graph. Comparison of deflections for FWD geophones 3 and 10.

After verification of the performance of the embedded sensors, the sensors were then fully grouted (see figure 34). The feasibility of aligning the tires of the moving deflection devices with the sensors was also verified using the MnROAD instrumented truck (see figure 35).

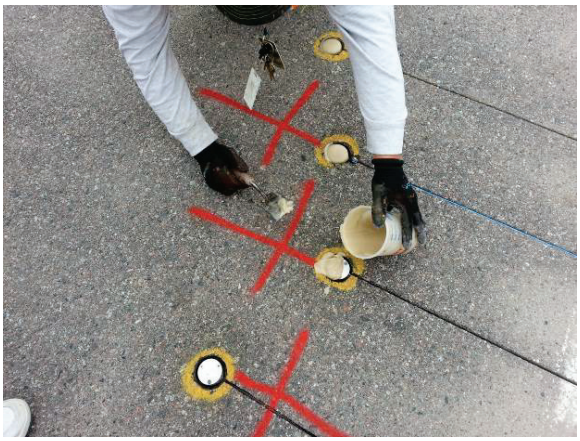

Figure 34. Photo. Final grouting of sensors.

Figure 35. Photo. Verifying the embedded sensor alignment.

To properly trigger the embedded sensors, infrared light-emitting diode (LED) positioning sensors were installed in each of the accuracy testing cells. Figure 36 shows a typical layout of a test section with the positioning sensor arrangement. The positioning sensors consisted of a retro-reflective long-range sensor and a reflector. The sensor was encased in a protective box that was mounted on a metallic base that provided stability and could be maneuvered as needed. The reflector was also mounted on a similar base that offered the same benefits. These sensors had a sensing distance of up to 23 ft (7.02 m) and worked with 12 Vdc with an output pulse of the same amplitude.

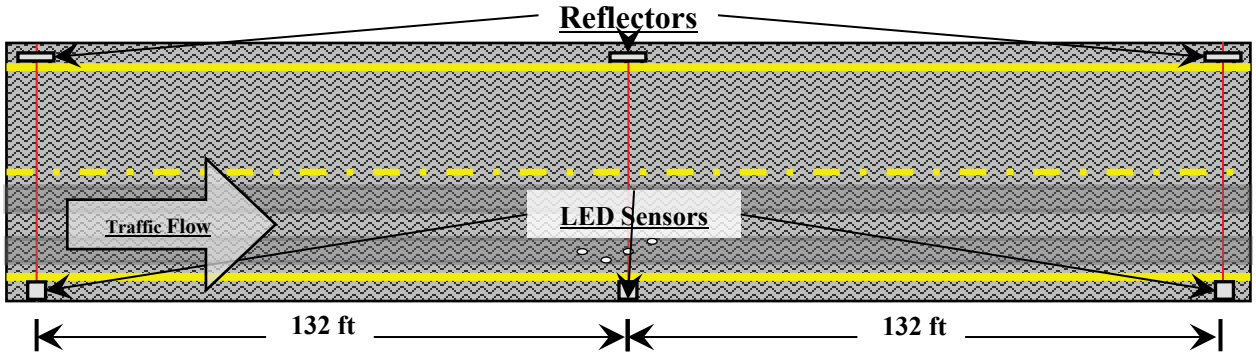

Figure 36. Illustration. Test section layout with positioning sensors placement.

Markings for the trigger sensor positions were placed on the rest of the cells where accuracy testing was to be performed. The data acquisition (DAQ) system program was also modified to capture them in the data files. One positioning sensor was placed directly across from sensor unit 3 (geophone 3), a second positioning sensor was placed 132 ft (40.26 m) before sensor unit 3, and a third positioning sensor was placed 132 ft (40.26 m) after sensor unit 3. The reason behind the trigger spacing was the need to collect at least 3 s of information on each pass. The fastest vehicle speed proposed for testing (i.e., 60 mi/h (96.6 km/h)) resulted in a total length of 264 ft (80.52 m) for the test section. With this arrangement, the trigger sensor was placed 132 ft (40.26 m) before sensor unit 3 and was used to initiate the DAQ. The purpose for the trigger placed across sensor unit 3 was to use it as a reference to compare the shape of the deflection captured with the embedded sensors and the pulse width created by the tire as it crossed the trigger. Two high-speed video cameras were also used to record each pass of the TSDDs to determine the lateral wheel location relative to the installed sensors (see figure 37 and figure 38). The wheel wander for the passes that were used in this study were typically less than 2 inches (50.8 mm).

Figure 37. Photo. Sample video snapshot showing wheel location from TSD pass.

Figure 38. Photo. Sample video snapshot showing wheel location from RWD pass.

5.4 DATA COLLECTION

The DAQ system consisted of a National Instruments™ USB-6211 and a laptop. LabVIEW® software package also provided by National Instruments™ was used to develop the software needed to acquire, save, and analyze the data collected during the testing phase. During data collection, the only setting that needed to be modified was the speed of the vehicle before each test. This variable determined the amount of time needed to collect data with the DAQ system. MnROAD personnel provided the research team with an Arbiter Systems® GPS clock to ensure the collected data were correctly time stamped. While the TSDDs did not have this timing system, their computer clocks were sufficient to ensure their data as well as the data from the MnROAD sensors and installed sensors were correctly matched. To ensure the collected information was correctly assigned, the cell number, TSDD, vehicle speed, surface temperature, and repetition number were all used to name the files when data were saved. The project team encountered a problem while reducing data collected with the accelerometers for 15 out of 64 passes. The problem was tracked down to interference due to the absence of a ground connection, and the associated accelerometer data for the 15 passes in question were dropped from further consideration in the project.

5.5 DATA REDUCTION

Data collected were first subjected to a preliminary quality control. Quality control included classification and discarding of defective or unnecessary data for the purpose of this project.

Since not all existing MnROAD embedded sensors were operational, their data were first visually inspected to identify the sensors that were operational at each cell.

Typical examples of strain gauge and pressure cell data from one location are shown in figure 39 and figure 40. For each TSDD pass, the vehicle speed was calculated using the time between peaks generated by the front and the trailing rear axles and the exact distance between the axles. The vehicle speed obtained in that manner was then compared to the vehicle speed reported by the TSDD. The results were very comparable. Vehicle speed was then used to convert time into distance. Assuming that the peak value from the rear axle was obtained when the axle was directly on top of a sensor, data from -7 to 10 ft (-2.14 to 3.05 m) from the instant they occurred were extracted, as shown in figure 41 and figure 42. These extracted data were further summarized to discrete measurements at 1-ft (0.305-m) intervals to be uploaded into the project database. Given the viscoelastic nature of flexible pavements, a time lag between the time that the tire crosses over the sensor and when the maximum response is measured is anticipated. This time lag was ignored in the presentation of the strains and stresses in figure 39 through figure 42. However, the results were adjusted when the experimental results were compared with the numerical ones in chapter 7 of this report.

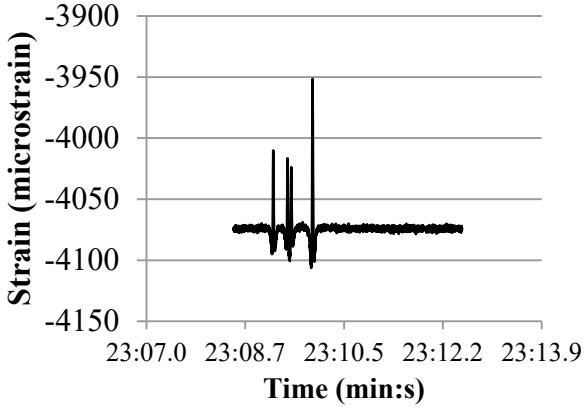

Figure 39. Graph. MnROAD strain gauge data.

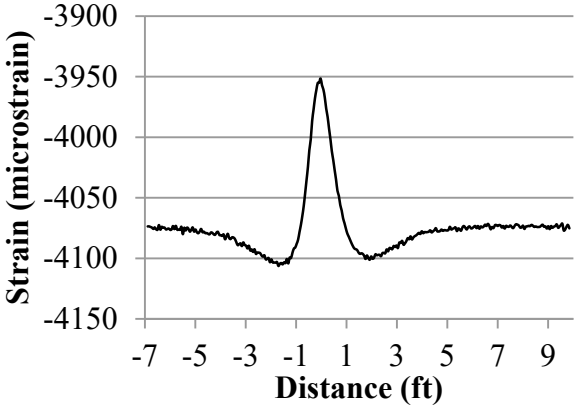

Figure 40. Graph. MnROAD strain gauge reduced data.

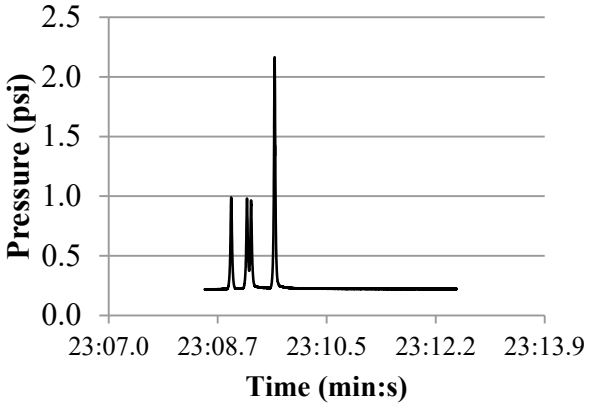

1 psi = 6.89 kPa

Figure 41. Graph. MnROAD soil compression gauge data.

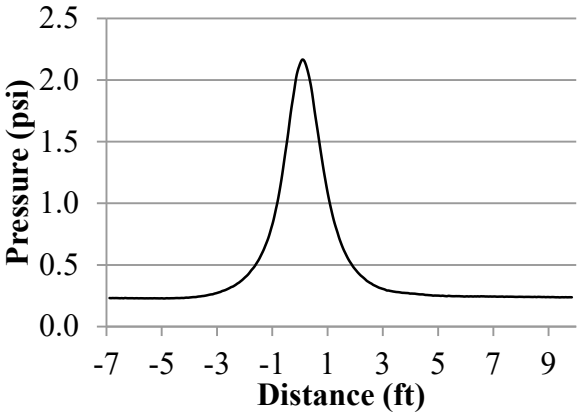

1 psi = 6.89 kPa
1 ft = 0.305 m

Figure 42. Graph. MnROAD soil compression gauge reduced data.

Figure 43 shows a typical voltage time history obtained from an embedded geophone, with the peak voltage outputs created by the front and trailing rear axles marked. As with the other sensors, the time difference between the two peaks was divided by the front-axle-to-rear-axle distance of each TSDD to obtain accurate instantaneous vehicle speed, assuming that the time lags between the maximum displacement parameters and the time the tire passed over a sensor was constant for the front axle and the trailing rear axle.

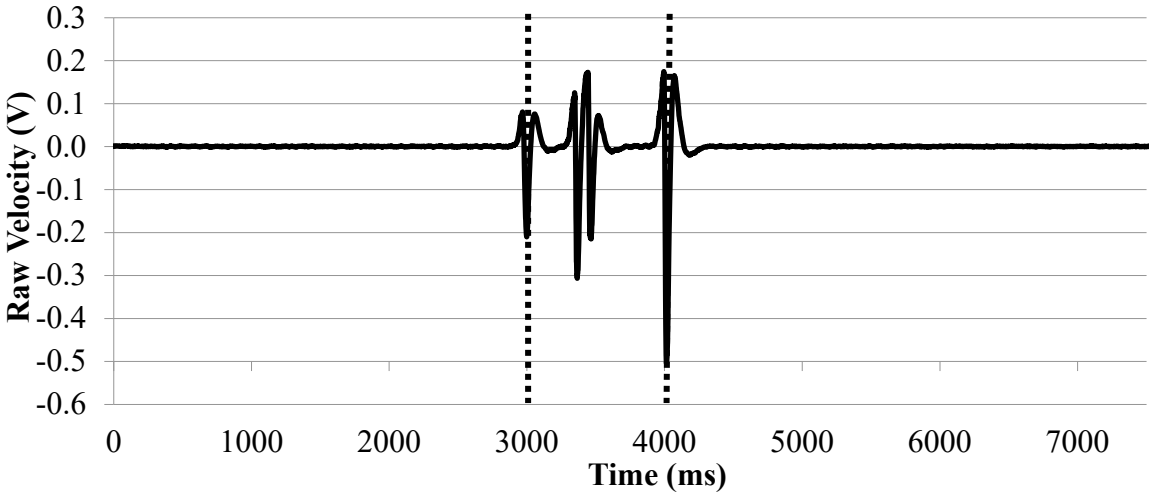

Figure 43. Graph. Embedded sensor full time history with the peaks created by rear and front axles.

The next step of the data analysis was to extract the appropriate range of information from all five newly embedded displacement sensors before, during, and after the rear axle of the TSDD drove over them over an approximate range of -7 to 10 ft (-2.14 to 3.05 m) from sensor unit 3. Figure 44 shows the voltage time histories from the geophone and accelerometer in sensor unit 3 from a typical TSDD pass.

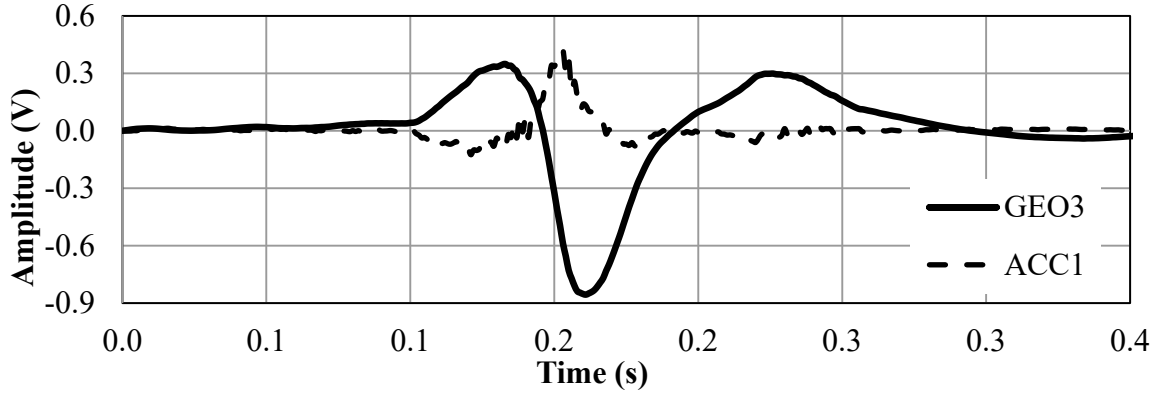

Figure 44. Graph. Geophone and accelerometer time histories.

Since the calibration values of the accelerometers were linear and constant, the accelerometer voltage time history was multiplied by the calibration value to convert it to acceleration. These data were first transformed into the frequency domain using an FFT algorithm integrated once in the frequency-domain to obtain the velocity spectrum and twice to obtain the deflection spectrum. The velocity or deflection spectrum was then subjected to an inverse FFT to obtain velocity or deflection time histories. The velocity results were compared to the TSD measured values, while the deflection results were compared with the RWD measurements.

The process of analyzing the geophone data involved the use of the nonlinear calibration curve in the frequency domain obtained from the geophone calibration. Figure 45 shows a typical

geophone calibration curve. Since the analysis process had to be done in the frequency domain, the first step was to use an FFT algorithm to convert the selected geophone time history from the time domain to the frequency domain. Figure 46 shows the voltage frequency spectrum of the time history of geophone 3 from figure 44, and it also shows the actual velocity spectrum obtained after dividing it by the calibration curve. The shift in the amplitude, especially at low frequencies, demonstrates the importance of implementing a rigorous calibration process to consider the nonlinear behavior of the geophone properly.

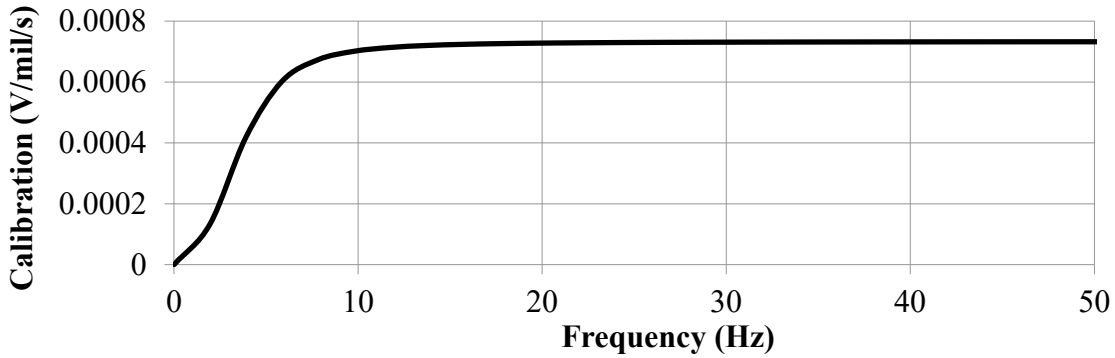

1 V/mil/s = 394 V/mm/s

Figure 45. Graph. Typical geophone calibration curve.

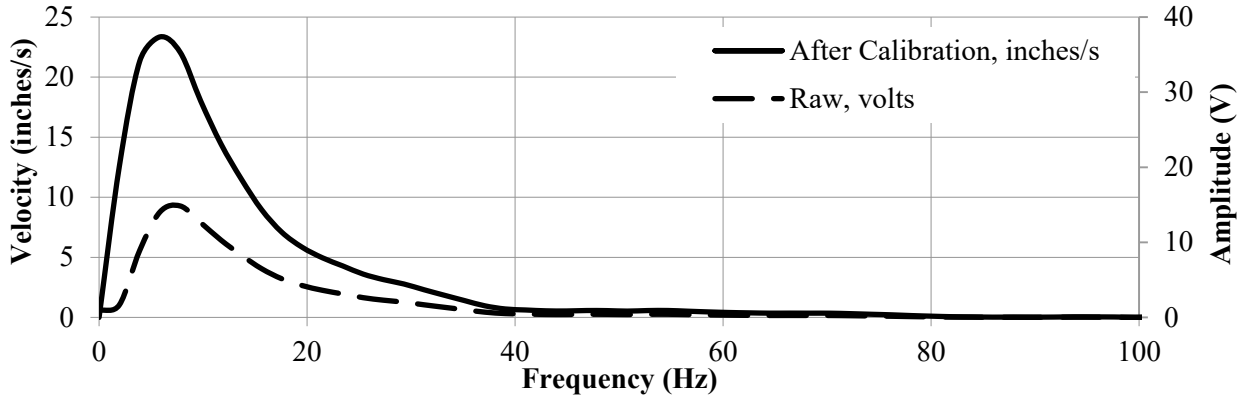

1 inch/s = 25.4 mm/s

Figure 46. Graph. Geophone velocity before and after calibration.

The actual velocity spectrum was then subjected to an inverse FFT algorithm to obtain the actual velocity time history that could be compared with those measured by the TSD. Figure 47 compares the raw geophone voltage time-history with the actual velocity time history, once again to demonstrate the importance of the proper analysis of geophone data. At this time, the time axis was also converted to distance as discussed previously.

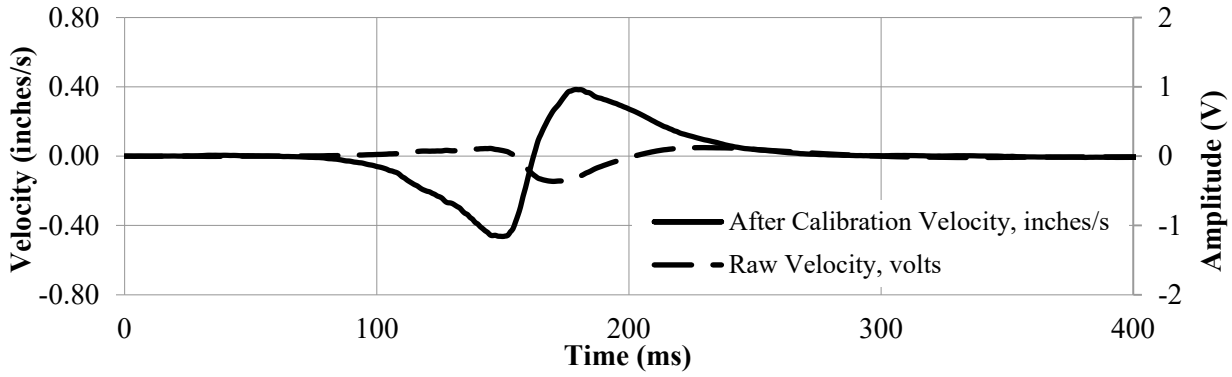

1 inch/s = 25.4 mm/s

Figure 47. Graph. Geophone velocity before and after calibration in the time domain.

To obtain the deflection time history, the actual velocity spectrum illustrated in figure 46 was integrated in the frequency domain and then subjected to an inverse FFT algorithm. Figure 48 shows the analysis results from a typical geophone. Discrete results were extracted from the geophones and accelerometer data at spacings that matched the data reported by the TSDD. For the TSD, these distances included 60, 36, 24, 12, 8, and 4 inches (1,530, 914.4, 609.6, 304.8, 203.2, and 101.6 mm) from the applied load. For the RWD, two data points at -7.25 and 7.75 inches (-184.15 and 196.85 mm) from the applied load were extracted since the device measured vertical displacements with two sensors. The velocity, deflection, strain, and stresses from the MnROAD field sensors were also summarized by extracting the appropriate values at 12-inch (304.8-mm) increments. Based on figure 48 and other similar experiments, the measured deflections with the embedded geophones (and perhaps TSDD sensors) beyond ±2 ft (±0.61 m) were negligible and within the uncertainty band of the measurements.

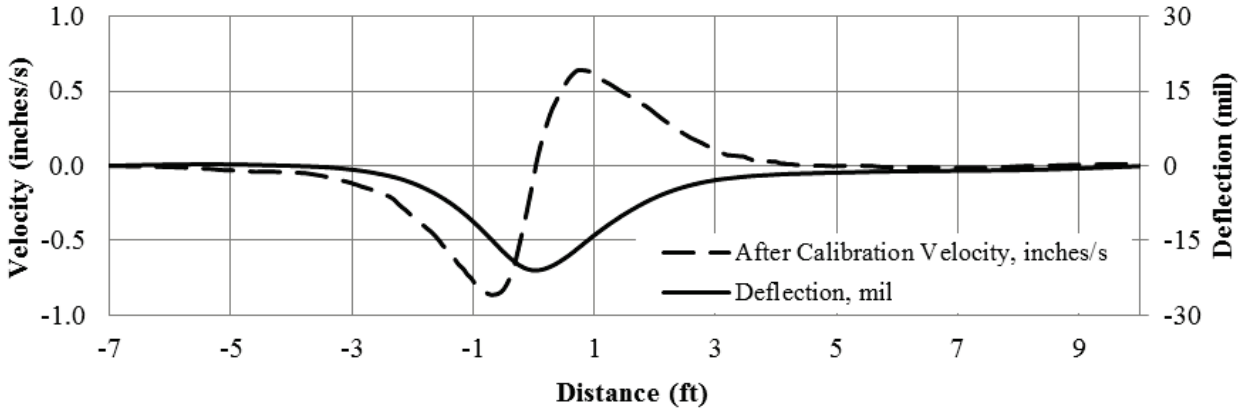

1 inch/s = 25.4 mm/s
1 ft = 0.305 m
1 mil = 0.025 mm

Figure 48. Graph. Deflection velocity in spatial domain.

Figure 48 shows the typical velocities and deflections generated from the installed sensors by the TSDD rear axle after the analysis. The reported results from all sensors were confined to a

distance of -7 to 10 ft (-2.14 to 3.05 m) from the instrumented TSDD rear axle right wheel while passing over the third geophone.

The peak velocities and deflections estimated from the accelerometer and geophone 3 of each cell (excluding the results from the earlier referenced 15 defective accelerometer records) are compared in figure 49 and figure 50, respectively. On average, the velocities from the two sensors differ by 3 percent, and the deflections differ by 7 percent. Even though the accelerometers collected data with less uncertainty than the geophones, the fact that the accelerometer raw data had to be integrated twice introduced more uncertainty in the analyses of deflections. The uncertainties in the reported values as judged by the SEE values are 30 mil/s (0.762 mm/s) and 1.5 mil (0.0381 mm), respectively. In the absence of definite means to attribute these uncertainties to the respective sources, they were fully attributed to the embedded sensors independent of their sources. Given the uncertainty associated with the data collection and analysis, the results were consistent.

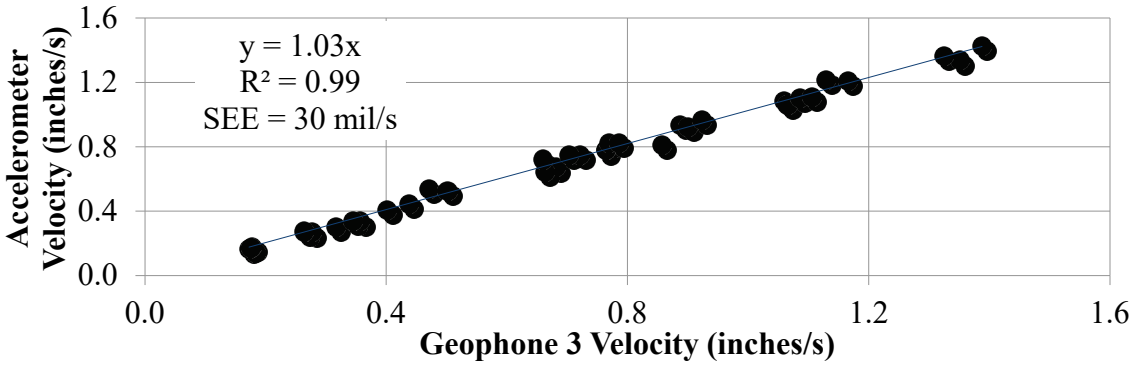

1 inch/s = 25.4 mm/s

Figure 49. Graph. Geophone 3 and accelerometer velocity comparison.

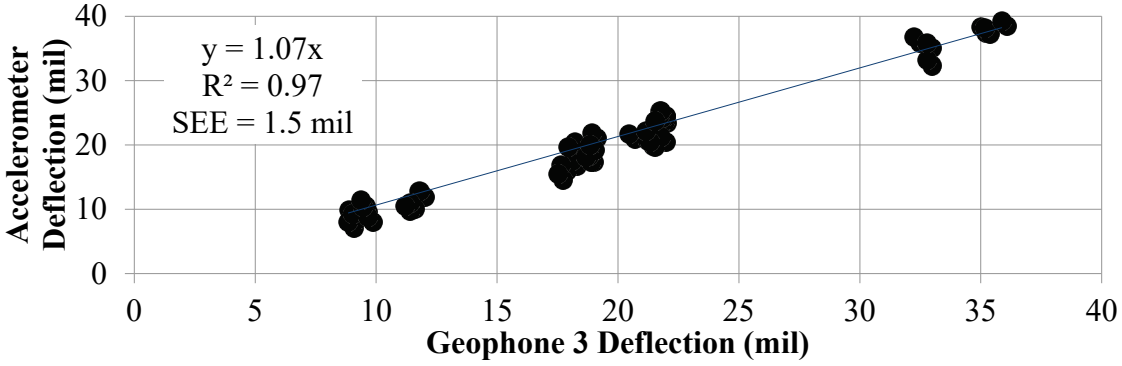

1 mil = 0.025 mm

Figure 50. Graph. Geophone 3 and accelerometer deflection comparison.

Figure 51 and figure 52 compare the peak velocities and deflections from all the accuracy testing results from geophones 1 and 3. A few outliers are evident in the two graphs. The source of these outliers was traced to the inconsistency of the data for geophone 1 at cell 34. Based on these analyses, the TSDD results were compared to the geophone 3 results at each site. Including the outliers in the analysis, the velocities and deflections from the two sensors differed by about 1 percent on average. The uncertainties in the reported values as judged by the SEE values are

137 mil/s (3.5 mm/s) and 1.4 mil (0.036 mm), respectively. Again, these uncertainties were fully attributed to the embedded sensors and not other sources.

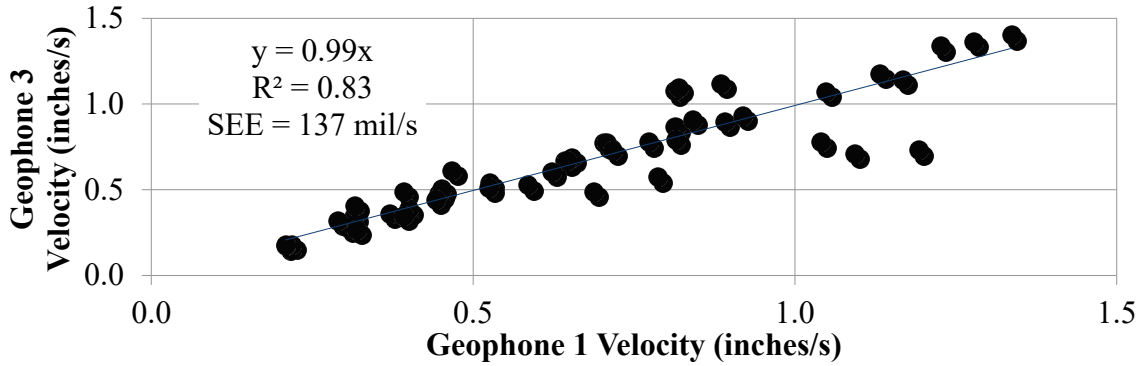

1 inch/s = 25.4 mm/s

Figure 51. Graph. Velocity comparison of geophones 1 and 3.

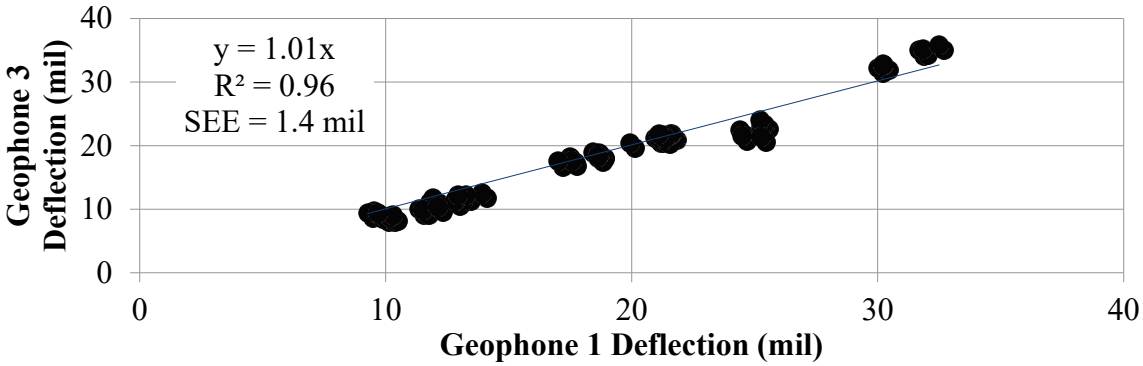

1 mil = 0.025 mm

Figure 52. Graph. Deflection comparison of geophones 1 and 3.

5.6 DATA ANALYSIS

Accuracy

The three AC cells (3, 19, and 34) were used for accuracy analysis. The deflection measurements from PCC cell 72 were not considered because the slab did not show a localized deflection basin, and the magnitudes of the signals reported with the TSDDs and newly installed deflection sensors were too small to be accurate given their stated uncertainties. The accuracy was established by statistically comparing the results measured with the newly embedded sensors with those reported by the TSDDs. Since the TSDDs reported their averaged data at 32 ft (9.76 m) for TSD and 50 ft (15.25 m) for RWD, one-to-one comparisons of the measured and reported data were not possible. As such, the averaged data point closest to the embedded sensors was used for this purpose.

Figure 53 and figure 54 compare the TSD and the RWD discrete measured values with corresponding time histories from the embedded sensors, respectively. Since the TSD sensors measured the pavement surface velocity, the velocities measured with geophone 3 were compared with the TSD velocities in figure 53. On the other hand, the accuracy of the RWD

was evaluated based on the deflections from geophone 3 since the RWD reports the surface displacements (see figure 54).

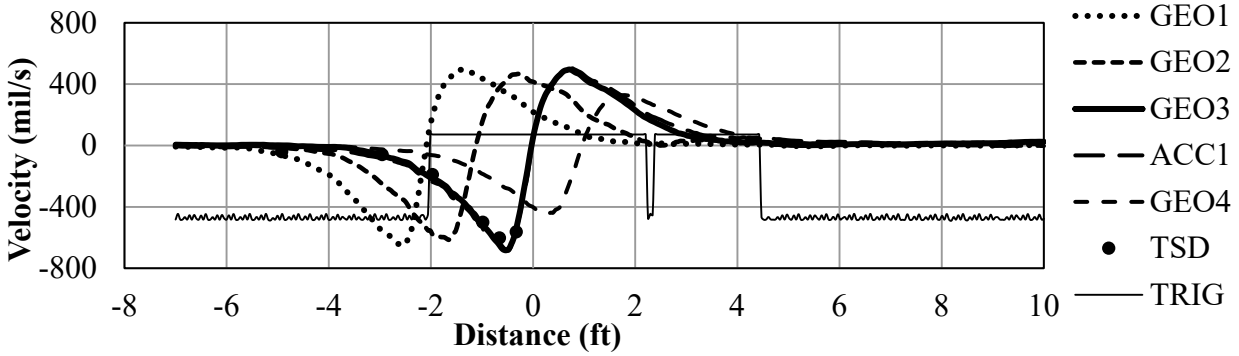

1 mil/s = 0.0254 mm/s
1 ft = 0.305 m

Figure 53. Graph. Comparison between embedded sensor deflection velocity results and TSD measurement.

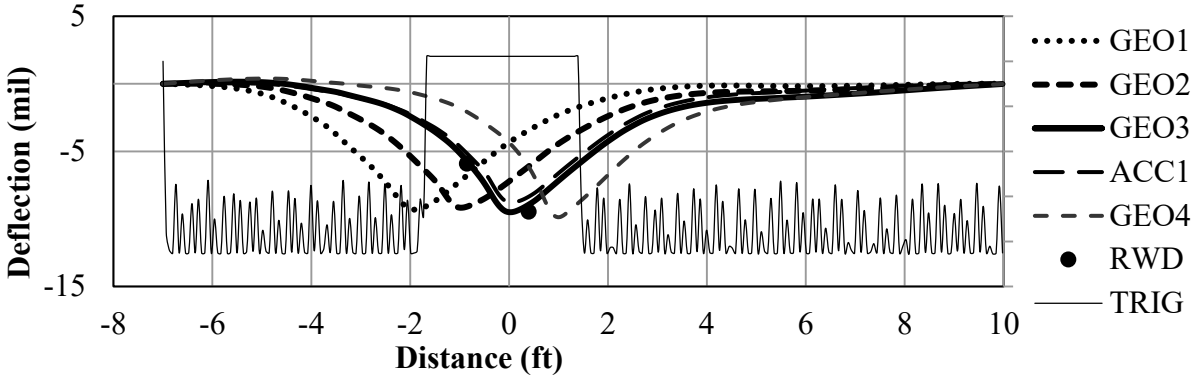

1 mil = 0.0254 mm
1 ft = 0.305 m

Figure 54. Graph. Comparison between embedded sensor deflection results and RWD measurement.

The viscoelastic nature of AC could result in a lag between the time that the tire crosses over the sensor and the time when the maximum response occurs. The deflection parameters shown in figure 53 and figure 54 consider such time lags. Figure 55 presents the process of obtaining this response lag. First, the most probable time that the center of the tire passed over the sensor was determined by estimating the distance where the trigger signal exhibited a high voltage (i.e., the length that the tire interfered with the LED laser reflection in figure 36). The resulting distance was then divided by two to estimate when the tire passed over the sensor (shown with a dotted vertical line in figure 55). The lag was then estimated by subtracting the estimated time when the TSDD sensor passed over the embedded sensor from the time when the maximum deflection measured with the geophone (solid vertical line) occurred. After calculating the lag for each pass, all data points were shifted accordingly. The estimated response lags are reported in table 16. Given the sampling rate of the newly installed geophone data and uncertainty in the process used, the uncertainty associated with the estimation of the phase lags was estimated to be

1–2 inches (25.4–50.8 mm). For the RWD passes, the response lags were estimated based on the measured deflections, while for the TSD, they corresponded to the surface particle velocities. The response lag varied with vehicle speed, temperature, and pavement structure. The time lags for cell 19 had to be determined differently since the body of the TSD interfered with the trigger signal. These time lags were approximated using an average wheel diameter of 3.2 ft (0.98 m) since the trigger signal for this cell covered both of the wheels (rear axle and the distant measuring instrument (DMI) wheel).

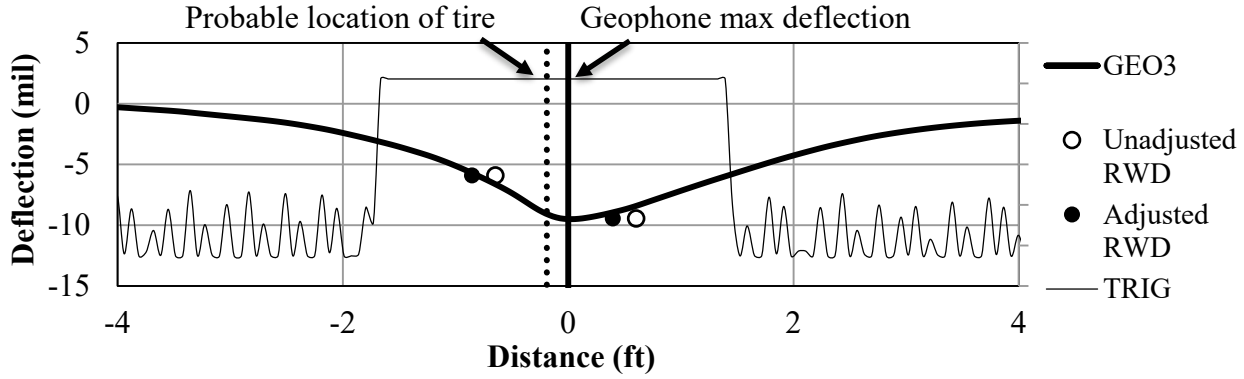

1 mil = 0.0254 mm
1 ft = 0.305 m

Figure 55. Graph. Time lag calculation example.

Table 16. Pavement response lag results.

Cell	Speed (mi/h)	Response Lag (inches)	
		RWD	TSD
34	30	7.3	3.8
	45	6.9	3.4
3	30	4.3	6.6
	45	2.5	5.5
	60	1.6	N/A
19	30	4.5	4.4
	45	3.4	2.8
	60	4.0	2.8

1 mi/h = 1.61 km/h
1 inch = 25.4 mm
N/A = Data were not available.

Figure 56 and figure 57 show typical comparisons between the parameters reported by the TSDDs and those measured by the newly installed embedded sensors. Given the inherent uncertainty in the acquisition and analyses of the embedded sensors' data, tests were repeated three times at every cell for every TSDD. The results from all three replicates were used to maximize the confidence in the data. The constant and the slope of the best fit line through the data were used to assess the closeness of the reported and measured results. The intercept measures the bias in the measurements and should ideally be equal to zero. For a fair comparison, the slope, which is an indication of the proportionality of the measurements, should be equal to unity. Average deviation between the measured and reference of a device under a

given condition was also calculated by determining the absolute difference between the slope of the best fit line directed through the origin and the line of equality. An average deviation close to zero is desirable. The R^2 value was examined as an approximate surrogate indicator of the scatter in the data since, strictly speaking, there are uncertainties in both the reference and measured values. Ideally, that value should be close to unity. In the case of RWD, R^2 was not computed, as it contained only two measurements with repetition. The SEE was judged to be a better indicator of the uncertainty in the results. SEE can be used to estimate how different the deflection parameters from two different pavements should be so that they can be considered different with confidence. The smaller the SEE is, the more subtle changes in pavement structures can be estimated.

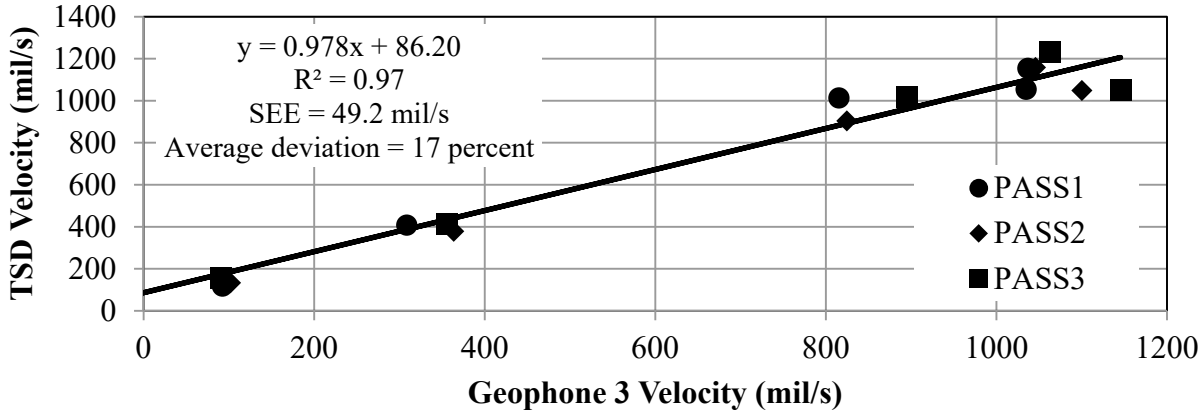

1 mil/s = 0.0254 mm/s

Figure 56. Graph. Comparison of geophone and TSD measurements.

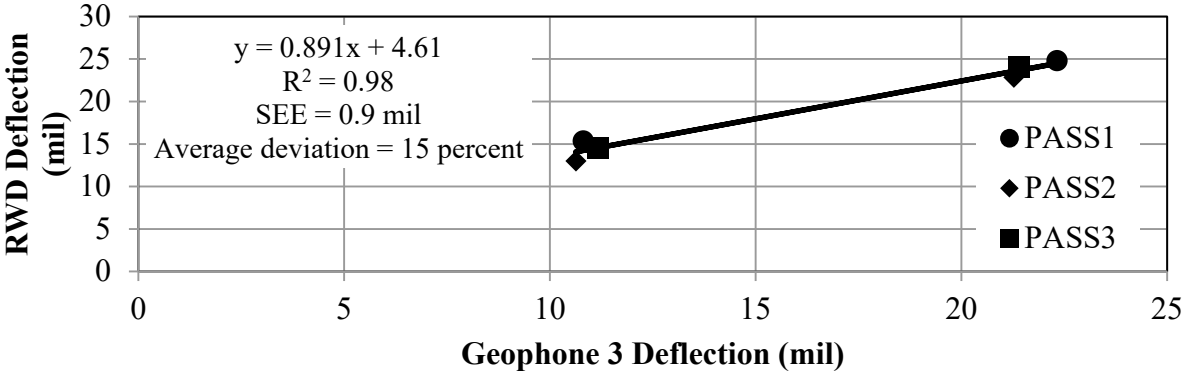

1 mil = 0.0254 mm

Figure 57. Graph. Comparison of geophone and RWD measurements.

The individual difference between the deflection measured by the embedded sensor and the deflection reported by TSDD was estimated from the following:

$$e_{ij} = \text{abs}\left[\frac{\left(d_{ijsensor} - d_{ijTSDD}\right)}{d_{ijsensor}}\right]$$

Figure 58. Equation. Absolute difference between the deflection measured by the embedded sensor and the deflection reported by TSDD.

Where:

e_{ij} = Absolute difference between the deflection measured by the embedded sensor and the deflection reported by TSDD.
i = Sensor.
j = Pass.
$d_{ijsensor}$ = Deflection parameter (either velocity or deflection) measured with the embedded geophone.
d_{ijTSDD} = Deflection parameter reported by the TSDD for its sensor i for pass j.

The average and standard deviation of differences from the three replicates for each sensor were then calculated and reported for each sensor (see table 17). For TSD, values from the sensor spacings of 36 and 60 inches (914.4 and 1,524 mm) were not evaluated since their deflection parameters were considered to be too small to be reliably measured by the embedded geophones.

Table 17. TSDD average difference and standard deviation of difference.

TSD			RWD		
Sensor Distance (inches)	**Average Difference (Percent)**	**Standard Deviation of Difference (Percent)**	**Sensor Distance (inches)**	**Average Difference (Percent)**	**Standard Deviation of Difference (Percent)**
4	12	5	-7.25	11	3
8	4	3	7.75	11	10
12	6	7			
24	11	8			

1 inch = 25.4 mm
Note: Since RWD only had two sensors, the results for the third and fourth sensors were left blank.

Table 18 summarizes the experiments carried out for establishing the accuracy of the TSDDs. The TSD was not able to test cell 3 at 60 mi/h (96.6 km/h) because of safety concerns over the breaking distance. Figures and tables similar to those presented over the remainder of this chapter and in chapter 6 were generated for every combination of device, cell, and nominal speed shown in table 18, but they were not included in the report, as they do not provide further insights. The data used to generate these figures and tables can be obtained directly from FHWA.

Table 18. TSD and RWD accuracy passes.

Device	Cell	Nominal Speed (mi/h)
RWD	3	30
		45
		60
	19	30
		45
		60
	34	30
		45
TSD	3	30
		45
	19	30
		45
		60
	34	30
		45

1 mi/h = 1.61 km/h

The deflection velocities were measured with the TSD. Most algorithms used for estimating the remaining life of pavement structures are based on deflection basins (usually measured with FWDs). To take advantage of the current procedures developed for the structural analysis of pavement structures, the TSD manufacturer suggested two algorithms. The typical outcomes of these two algorithms as well the deflection basins measured with geophone 3 are shown in figure 59. The first algorithm, labeled as "Old Algorithm," is based on utilizing a beam model to estimate the deflection basins at three discrete points, including the deflection between the two wheels.[42,43] The second algorithm, labeled as "New Algorithm," is based on the work by Pedersen et al. and utilizes the measured slope and fits this slope into a sum of two probability density functions to estimate the deflection basin up to 60 inches (1,524 mm) from the load.[44] The same process followed to estimate the accuracy of the TSD deflection velocity was also applied to the deflections estimated by the two algorithms, as discussed in chapter 6.

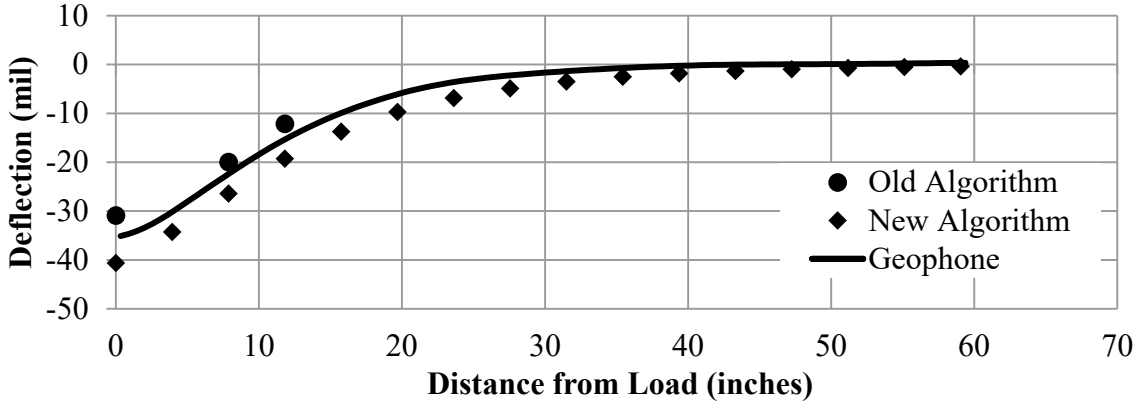

1 mil = 0.0254 mm
1 inch = 25.4 mm

Figure 59. Graph. Typical algorithm deflection comparison.

Precision

Precision analysis included almost all cells of the MnROAD facility and the 18-mi (29-km) Wright County loop to account for different pavement structures. To better evaluate the precision of the two devices, they were tested at different speeds and at different times of the day.

Table 19 describes the number of passes, speeds, and times for each device. Data collection was repeated up to five times at every cell for every TSDD and at two different speeds. Due to safety concerns, the LVR tests were carried out at nominally 30 and 45 mi/h (48 and 72 km/h). These combinations resulted in a total of 78 passes.

Table 19. Precision testing summary.

Test Site	TSDD	Passes Per Speed	Speed (mi/h)	Time of Day
18-mi loop	TSD	3	Traffic speed	Morning
	RWD	3	Traffic speed	Morning
Mainline	TSD	5	45, 60	Morning
		5	45, 60	Afternoon
	RWD	3	45, 60	Morning
		3	45, 60	Afternoon
LVR	TSD	5	30, 45	Morning
		5	30, 45	Afternoon
	RWD	5	30, 45	Morning
		5	30, 45	Afternoon

1 mi = 1.61 km
1 mi/h = 1.61 km/h

Figures and tables similar to those presented over the remainder of this chapter and in chapter 6 were generated for every combination of test site, device, pass, speed, and time shown in table 19, but they are not included in the report, as they do not provide further insights. The data used to generate these figures and tables can be obtained directly from FHWA.

The precision analysis for this project started by developing color-coded Google® maps. An example of one of the maps is shown in figure 60. The average and COV of the deflection parameters for each sensor from replicate passes were calculated for each reported test point. These values were then color-coded using the convention in table 20. This color codification was also applied to the vehicle speed and pavement surface temperature measured by each TSDD since these parameters can influence the precision of the measurements.

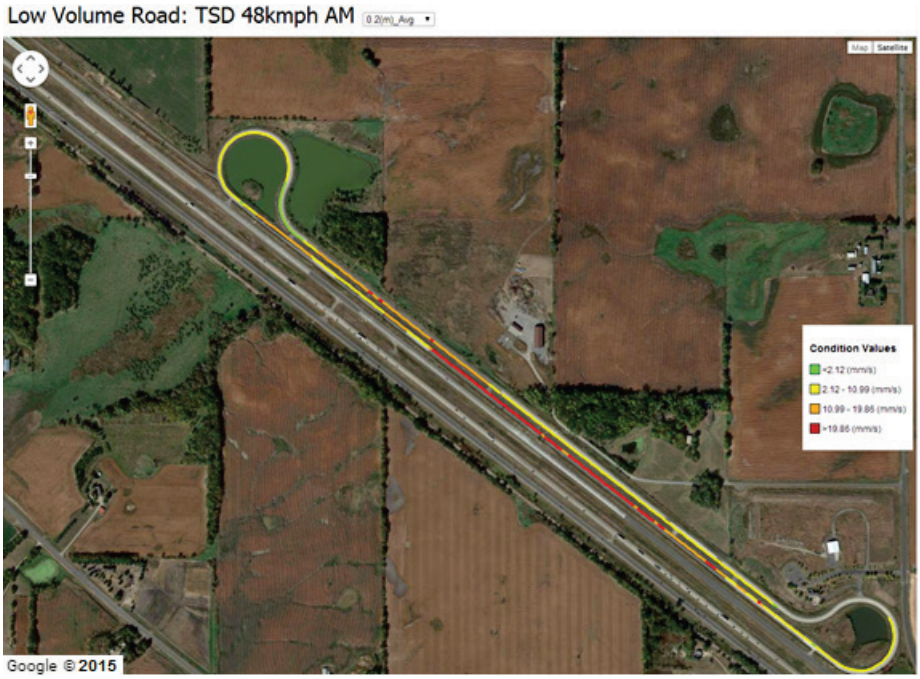

©2015 Google® (Modifications: See Acknowledgements).

1 inch/s = 25.4 mm/s
1 mi/h = 1.61 km/h

Figure 60. Map. Color-coded statistic map.[45]

Table 20. Color-coded legend for statistic map in figure 60.

Parameter	Color			
	Green	**Yellow**	**Orange**	**Red**
Measurement	< Average – Standard Deviation	< Average but > Average – Standard Deviation	<Average + Standard Deviation but > Average	> Average + Standard Deviation
COV	< 5 percent	< 10 percent but > 5 percent	< 20 percent but > 10 percent	> 20 percent

The first step to evaluate the precision was to properly align the starting point of each pass using the GPS coordinates provided by the TSDDs. The second analysis step consisted of comparing the deflection parameters from three or five replicate passes at similar speeds. For the RWD, the reported surface deflections were used for this purpose. The deflection slope, which is the ratio of the deflection velocity and vehicle speed (instead of deflection velocity that was used for the accuracy study), was used for the TSD. The TSD precision evaluation included the sensors from 4–36 inches (101.6–914.4 mm). Unlike the accuracy analysis, where small changes in the deflection parameter may yield high percent differences, the low precision (high variability) of the measurements can impact the analysis of the results negatively. Unlike deflection velocity, deflection slope can potentially reduce the impact of vehicle speed on the results. The appropriate deflection parameters (deflection for RWD and deflection slope for TSD) from different passes were first plotted and visually inspected to confirm the proper alignment of data (see figure 61). In some TSD passes, reported negative numbers were classified as measurement errors and were manually deleted to avoid misleading statistics.

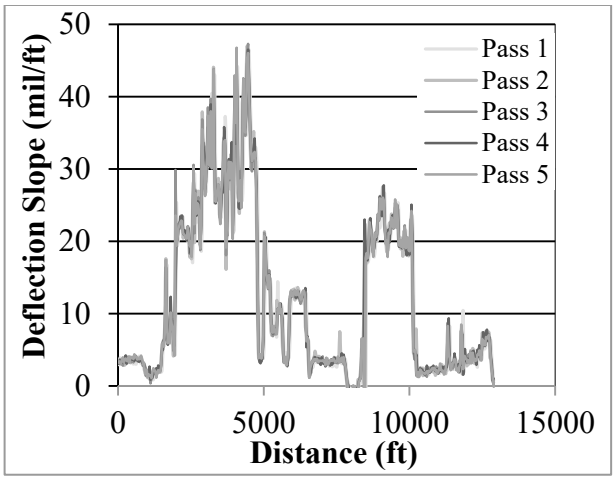

1 mil/ft = 83.3 µm/m
1 ft = 0.305 m

Figure 61. Graph. Precision comparison of passes.

Statistical analyses were then carried out between each two individual pairs of data collected in different passes. As an example, figure 62 demonstrates a comparison of the data from the first and second passes of the TSD. Statistical parameters such as the R^2 value, the slope of the best fit line, and the SEE were estimated for each pair, as shown in table 21. To summarize the extracted data in a manageable form, the minimum, maximum, and median values of each of these statistical parameters were extracted. These results were then presented as box plots. Typical box plots such as the ones presented in figure 63 through figure 66 demonstrate the ranges, 25 and 75 percentiles, and the medians for the slope, R^2, SEE, and the range of measured values.

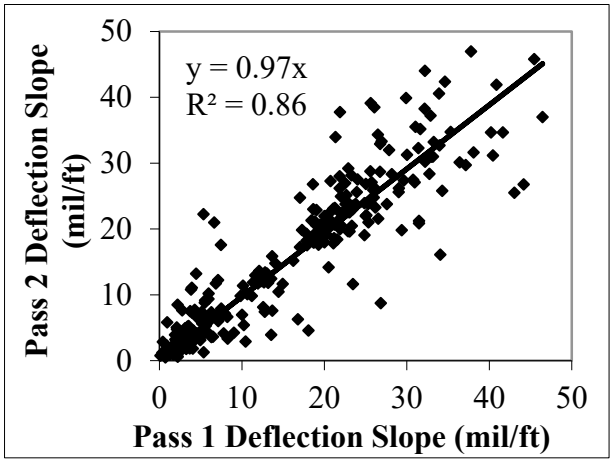

1 mil/ft = 83.3 µm/m

Figure 62. Graph. Precision linear comparison of passes.

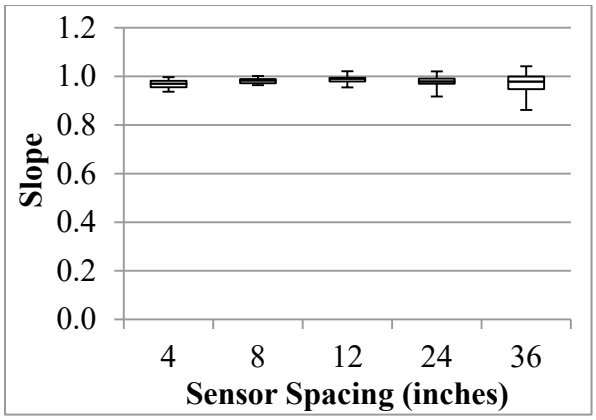

1 inch = 25.4 mm

Figure 63. Graph. Typical slope box plot for precision analysis.

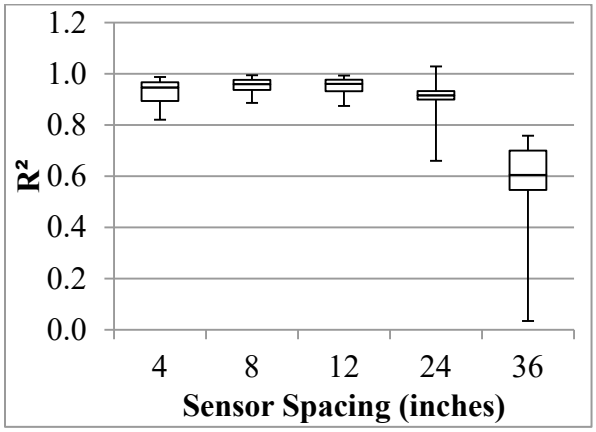

1 inch = 25.4 mm

Figure 64. Graph. Typical R^2 box plot for precision analysis.

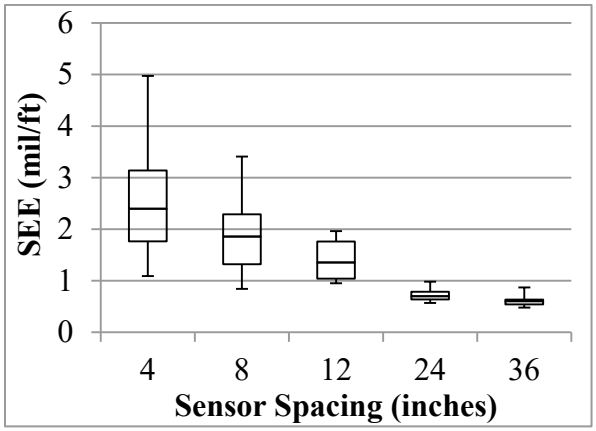

1 mil/ft = 83.3 µm/m
1 inch = 25.4 mm

Figure 65. Graph. Typical SEE box plot for precision analysis.

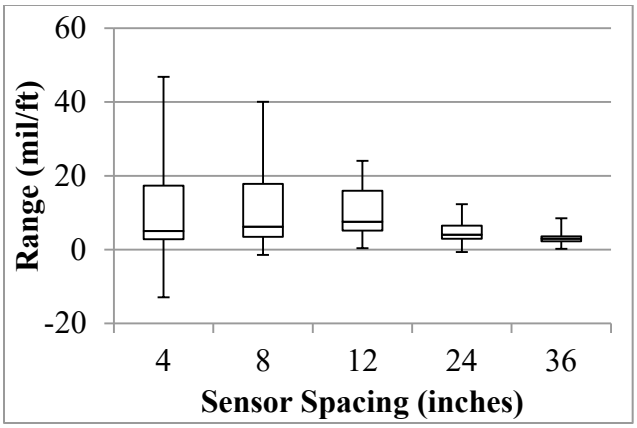

1 mil/ft = 83.3 µm/m
1 inch = 25.4 mm

Figure 66 . Graph. Typical range box plot for precision analysis.

Table 21. Semi-triangular comparison table.

Pass Number	Pass 1	Pass 2	Pass 3	Pass 4	Pass 5
Slope					
Pass 1		0.965	0.962	0.972	0.968
Pass 2			0.983	0.987	0.988
Pass 3				0.992	1.003
Pass 4					0.995
Pass 5					
R^2					
Pass 1		0.864	0.878	0.911	0.887
Pass 2			0.957	0.965	0.959
Pass 3				0.96	0.997
Pass 4					0.967
Pass 5					
SEE					
Pass 1		4.12	3.91	3.34	3.76
Pass 2			2.34	2.08	2.27
Pass 3				2.27	0.65
Pass 4					2.04
Pass 5					

Note: The blank cells correspond to the cells that do not require values as is the standard practice in elementary statistics.

Histograms of the distributions of the reported parameters were also developed to visually evaluate the distributions of the data, as illustrated in figure 67.

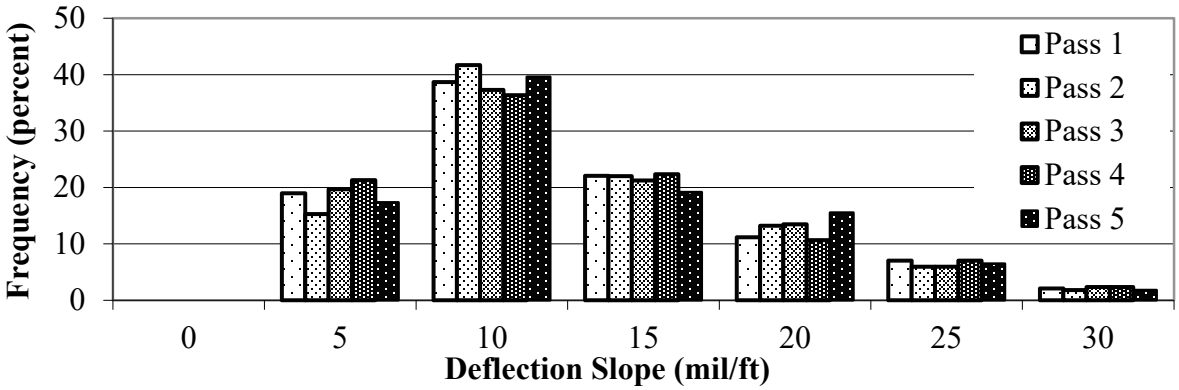

1 mil/ft = 83.3 μm/m

Figure 67. Graph. Typical deflection for a particular sensor.

Such analyses were performed on the first five sensors of the TSD and the two sensors of the RWD. To further evaluate precision, the different passes were grouped together by time of the day (a.m. or p.m.), by speed (30, 45, or 60 mi/h (48.3, 72.45, or 96.6 km/h)), and by pavement structure (AC or PCC). The results from these analyses are presented in chapter 6. The RWD data files included the spatial standard deviations of the reported deflections over 50 ft (15.25 m), corresponding to the average values reported for each data point. The distributions of such spatial COVs for each measurement were also calculated and demonstrated. Such information was not available for the TSD.

5.7 PROJECT DATABASE AND WEB SITE

Given the large quantity of data collected and reduced, a project database was needed to organize data analyses as well as to facilitate communication and accommodate the diverse needs of various team members working on the project. To that end, an online database was developed for ease of update and instant access to various data. The raw, reduced, and analyzed data from the accuracy and precision analyses were placed in the database. This database was also populated with other relevant data such as cell and sensor inventory, ambient conditions, pavement structure, and pavement condition (e.g., IRI measurements).

Figure 68 shows the homepage of the internal Web site containing the database. The structure of the database and the relevant schema and metadata is explained in a write-up within the database. The database is divided into the following sections:

- **Test section inventory**: Includes the GPS location of each individual cell along with sensor location and coding information.
- **Pavement details**: Includes FWD, pavement condition, and pavement structure data. Pavement condition includes texture and IRI data, both from MnROAD and from the TSD at the time of testing.
- **Accuracy/precision data**: Incorporates the TSDD and embedded sensor data, along with the environmental information. This portion of the database includes detailed information

to categorize and describe every test. Climatic measurements were selected from a MnROAD weather station database and matched to the closest time of testing.

- **18-mi (29-km) loop data**: Covers only the TSDD measurements and pavement structure of the loop.

This database was uploaded along with a folder containing all the linked data to a Web site developed for this project. The database and hence information contained therein may be obtained directly from FHWA.

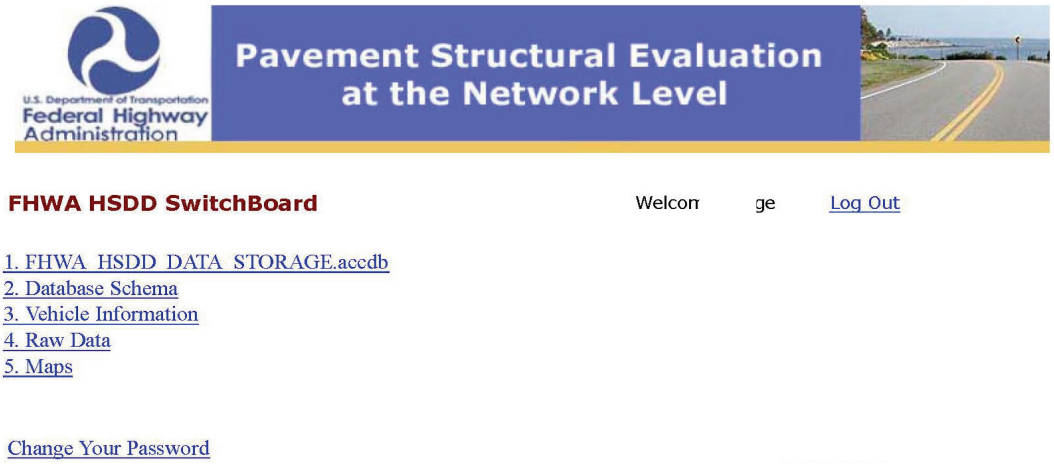

Figure 68. Screenshot. Database Web site homepage.

5.8 SUMMARY

This chapter presents the field trial locations; the instrumentation used and retrofitted to evaluate the TSDDs; the methodologies used to collect, review, reduce, and analyze the data needed for quantifying the accuracy and precision of the TSDDs; and the effort required to store and manage the data so that potential users can take advantage of the wealth of data results generated in this study. These efforts were carried out to accomplish the following two objectives:

- Confirm that the TSDDs meet a minimum set of specifications related to the structural evaluation of pavements at the network level.

- Propose processes to incorporate pavement structural information from the successful TSDDs into network-level PMS applications.

Considering the rationale provided in chapter 4 and the diverse data arranged and generated as discussed in this chapter, subsequent chapters are dedicated to elaborating on these two objectives.

CHAPTER 6. PERFORMANCE EVALUATION OF DEVICES

6.1 INTRODUCTION

The purpose of this chapter is to summarize and evaluate the results obtained from analyzing data collected during the field testing phase of this project based on the work plan in chapter 4. This chapter provides key findings and conclusions relating to the uncertainty (based on the accuracy results) and variability (based on the precision results) of the TSDDs. The conclusions drawn from the study of the two TSDDs were evaluated further to provide optimum operating conditions and device limitations, both of which are addressed in chapter 10 of this report.

6.2 ACCURACY

To evaluate the accuracy of the TSDDs, the variations in the deflections measured by the embedded sensors were compared against the parameters measured by each TSDD. Since the TSDDs generate an average of the measured values over a predetermined distance, the TSDD parameter used to compare to the embedded sensor was obtained using the GPS coordinates of the reference sensor and the GPS coordinates provided by each device. After the TSDD measured parameters closest to the embedded sensor were selected, the data were adjusted according to the response lag and plotted to observe differences and similarities. To quantify these measurements, the discrete values from the embedded sensor and the TSDD were compared against one another to determine the difference in magnitude. Once the data from the TSDDs and the embedded sensors from the cells selected for accuracy testing were analyzed, individual plots for the different TSDDs at different speeds and on different pavement structures were generated. In each of those spreadsheets, a table presenting a quantitative comparison using the TSDDs sensors and showing the average difference and standard deviation of difference was created as well. The data from these spreadsheets were accumulated to observe the overall TSDD behavior through the various speeds and pavement structures. The texture of the pavement surface is known to impact the accuracy of the measurements. This parameter was not studied in this project.

Overall Accuracy of Reported Deflection Parameters

As indicated previously, the uncertainty associated with the measurement with the geophones is specified by the manufacturer as ±2 percent of the measured deflection (no less than ±0.2 mil (0.0051 mm)). Uncertainties associated with the data analysis are on the order of ±7 percent with SEEs of 150 mil/s (3.81 mm/s) for velocity and 1.5 mil (0.0381 mm) for deflection caused by imperfections in installation and alignment of the TSDDs over the sensors. It would have been desirable to carry such comparisons with more refined data from the TSDDs. Neither of the two TSDDs provided raw measurements of their data. The uncertainties associated with the measurements reported by the TSDDs were by far greater than those reported by the embedded sensors given the spatial standard deviations reported by the RWD and the typical raw data reported by Flintsch et al. for TSD.[13] As such, the results provided herein should be considered reasonable.

RWD

The process used to evaluate the RWD from each pass was discussed previously in section 5.6 (Data Analysis). Table 22 contains the overall results obtained at different instrumented cells and at different speeds for the RWD. The column labeled "Constant" can be used to observe whether there was a device-related systematic difference in measurements (e.g., due to sensor calibration). Since the constant values changed with the cell and vehicle speed, the uncertainties in the measurements could not be considered systematic. The slopes of the best fit line varied from 0.84 to 2.41, indicating moderate to significant variability from unity desired from a perfect device. Recall that cell 34 was not tested at 60 mi/h.

Table 22. RWD overall accuracy statistics.

Cell	Speed (mi/h)	Overall Statistics			
		Constant (mil)	Slope	SEE (mil)	Average Deviation (Percent)
3	30	-2.9	1.68	2.0	29
	45	-3.4	1.83	2.2	38
	60	-12.0	2.41	2.3	10
19	30	1.0	0.91	0.9	2
	45	2.7	0.89	1.5	7
	60	-0.1	1.07	1.4	7
34	30	6.2	0.84	0.6	17
	45	4.6	0.89	0.9	15

1 mi/h = 1.61 km/h
1 mil = 0.0254 mm

The SEE was 1.45 mil (0.04 mm) or less for the two less stiff cells (cell 19 and 34) and 2.00 mil (0.05 mm) or greater for the stiffest cell (cell 3). Average deviation for the stiffest cell (cell 3) varied from 10 to 38 percent, while the maximum average deviations for cells 19 and 34 were 7 and 17 percent, respectively. Again, about 7 percent of the average deviation could have been due to the uncertainties in the data collection and analysis of the embedded geophones' records. As is discussed in chapter 8, the SEE in conjunction with the range of deflections is particularly important to assess the minimum level of changes in deflection or damage that the device can delineate.

As discussed in section 5.6 (Data Analysis), another way of evaluating the TSDDs is by calculating the difference associated with each sensor. Table 23 contains that information from all experiments. The average differences from the replicate tests at each cell and speed varied between 7 and 145 percent. The median differences for the sensors at -7.25 and 7.5 inches (-184.15 and 190.5 mm) were 14 and 15 percent, respectively. The median was reported as opposed to the average to ensure that the occasional outlying data did not disproportionately impact the interpreted accuracies.

Table 23. RWD accuracy statistics for individual sensors.

Cell	Speed (mi/h)	Difference of Sensor at -7.25 inches		Difference of Sensor at 7.5 inches	
		Average (Percent)	Standard Deviation (Percent)	Average (Percent)	Standard Deviation (Percent)
3	30	69	23	68	36
	45	83	33	82	20
	60	145	28	137	31
19	30	9	5	10	7
	45	11	5	13	16
	60	9	8	7	9
34	30	16	2	16	6
	45	11	3	11	10
Median		14	—	15	—

1 inch = 25.4 mm
1 mi/h = 1.61 km/h
— Indicates median was not calculated for the standard deviations.

Figure 69 shows the overall plots obtained from the evaluation of the RWD. Overall, the RWD deflections were 11 percent greater than the embedded sensors. The figure also includes 95 percent confidence and prediction intervals. The confidence interval means that there is 95 percent probability that the population will lie within the confidence interval of the regression line calculated from the sample data. However, prediction interval is a range that is likely to contain the response value of a new observation given the linear regression model chosen.

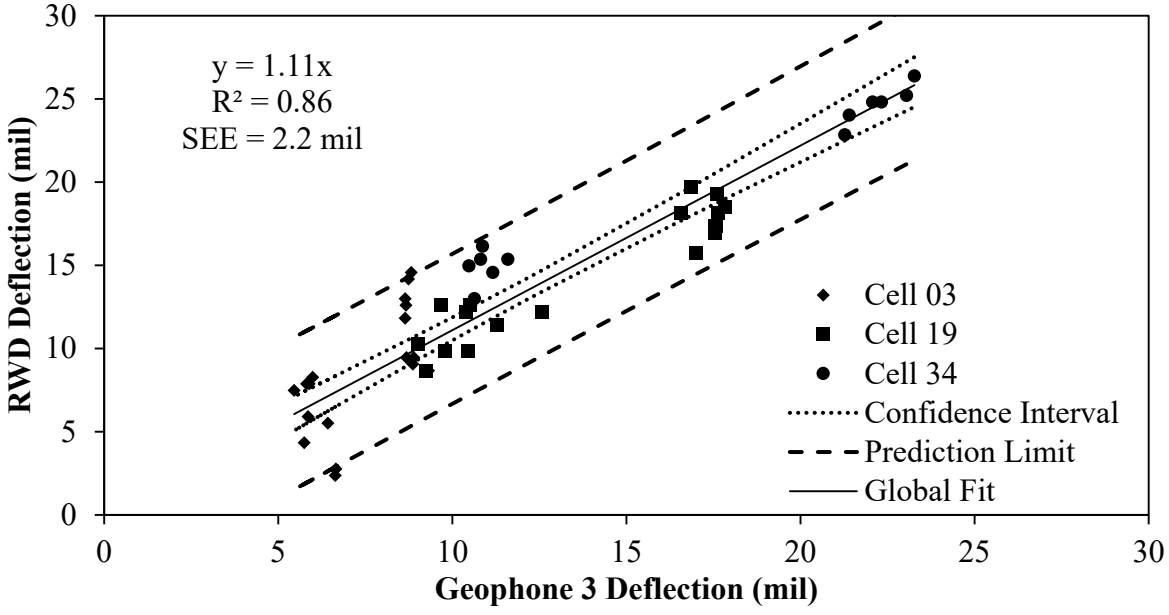

1 mil = 0.0254 mm

Figure 69. Graph. Overall comparison of deflections measured with RWD and embedded sensors.

The impact of the vehicle speed on the performance of the RWD is demonstrated in figure 70. The y-axis corresponds to the median difference measured at all cells at a certain speed. Both sensors' median differences were higher when the RWD was operated at 60 mi/h (96.6 km/h) in comparison to the other two lower speeds.

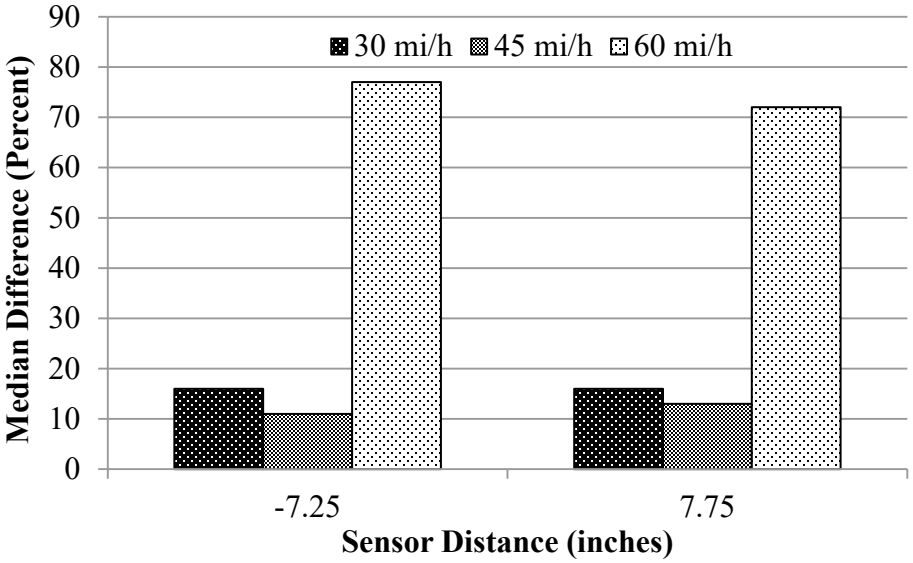

1 mi/h = 1.61 km/h
1 inch = 25.4 mm

Figure 70. Graph. Median sensor difference for RWD with varying speeds.

Cell stiffness seemed to impact the performance of the RWD as presented in figure 71. Sufficient data were not available to determine reason(s) for this impact. The stiffest section (cell 3) demonstrated a median difference ranging from 70 to 140 percent. Cell 19 had the smallest median difference of less than 10 percent for the three speeds. The median values minimized the uncertainties in the reported values related to occasional outliers observed during analysis.

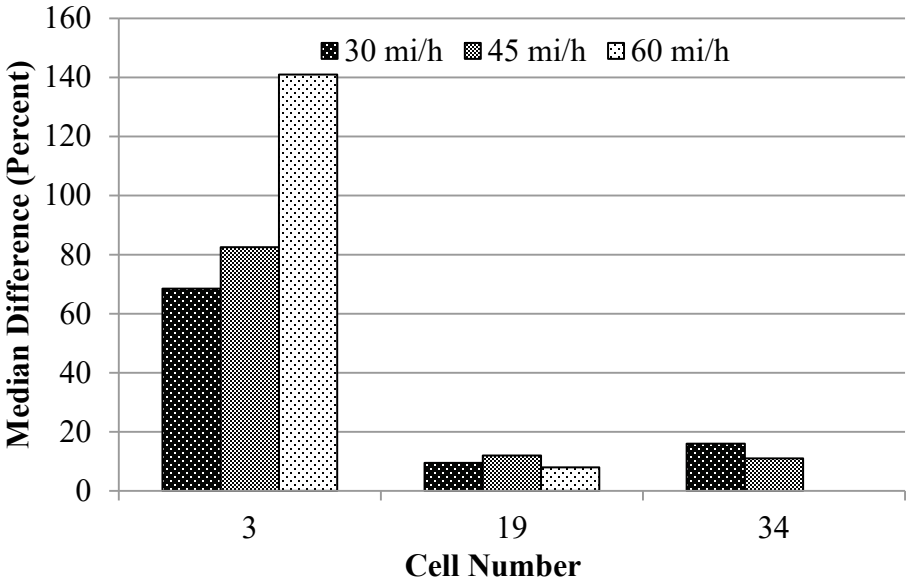

1 mi/h = 1.61 km/h

Figure 71. Graph. Distributions of deflection difference measured with RWD for each cell.

TSD

As indicated, the parameter measured with a TSD is termed "deflection velocity" (i.e., particle velocity of the pavement surface). As such, a similar procedure as discussed for the RWD was followed to evaluate the TSD in terms of the deflection velocity. Table 24 depicts the overall results based on the deflection velocities and the two deflection estimation algorithms explained in section 5.6 (Data Analysis). The evaluation was limited to sensors that were 24 inches (609.6 mm) or less from the load since the deflections measured with the geophones and the TSD farther than that distance are considered to be too small to be sufficiently reliable.

Table 24. TSD overall accuracy statistics.

Parameter	Cell	Speed (mi/h)	Overall Statistics				
			Constant (mil/s or mil)*	Slope	R^2 Value	SEE (mil/s or mil)*	Average Deviation (Percent)
Velocity	3	30	78.80	0.96	0.47	48.66	42
		45	61.37	1.11	0.66	64.29	34
	19	30	163.29	0.86	0.80	83.59	21
		45	109.10	0.94	0.97	44.88	9
		60	97.26	0.97	0.93	89.16	7
	34	30	225.83	0.81	0.92	90.32	6
		45	190.90	1.00	0.99	35.43	17
Deflection method 1	3	30	-1.90	0.97	0.85	0.91	22
		45	-2.52	1.02	0.90	0.73	25
	19	30	-2.71	1.05	0.93	1.39	11
		45	-3.00	1.06	1.00	0.27	12
		60	-4.01	1.14	0.98	0.67	10
	34	30	-3.85	0.99	0.98	1.30	15
		45	-7.81	1.17	0.99	0.70	13
Deflection method 2	3	30	6.21	1.21	0.80	1.74	92
		45	4.41	1.09	0.79	1.62	61
	19	30	8.30	1.02	0.53	6.29	58
		45	9.21	1.04	0.96	1.35	65
		60	3.61	0.87	0.74	3.26	12
	34	30	3.04	0.97	0.98	1.54	9
		45	1.60	1.01	0.99	1.18	7

1 mi/h = 1.61 km/h
1 mil = 0.0254 mm
*Measured in mil/s for velocities and mil for deflections.

The constants from the best fit lines varied between 60 and 225 mil/s (1.5 and 5.7 mm/s). Given the narrow range, the difference may have been partially systematic, and hence it may have been possible to improve them with a more rigorous calibration of the device. For that reason, the constant values were considered systematic in the calculations of the differences. The slopes of the best fit lines varied between 0.81 and 1.11, which was fairly close to the ideal value of unity in most cases. The R^2 values were reasonably close to unity except for the stiffest section (cell 3). The SEE values varied between 35 and 90 mil/s (0.9 and 2.3 mm/s), and they seemed to increase as the pavement became less stiff. Cell 3 also had the highest average deviation (over 34 percent). The average deviation for the less stiff cells (cells 19 and 34) was small, with the highest value being 17 percent. Up to 7 percent of these average deviations could be explained by the uncertainty of the data collection and analysis with the embedded sensors.

A review of the average deviations of the deflections indicates that method 1 was more appropriate for the data collected for this study. Even though method 2 provided more information about the deflection basins, it did not seem to represent the data from the three MnROAD cells as well.

The average and standard deviation of differences of each individual sensor are presented in table 25. In terms of velocities, sensors located 4, 8, and 12 inches (101.6, 203.2, and 304.8 mm) away from the applied load seemed to match the embedded geophones' responses better with median differences of 13, 10, and 9 percent, respectively. Once again, the median values minimized the uncertainties in the reported values related to occasional outliers observed during analysis. The differences for sensors located farther than 24 inches (609.6 mm) from the applied load were in excess of 25 percent. In terms of the two methods proposed for the estimation of deflections, method 1 again seemed to be more representative of the MnROAD data.

Table 25. TSD accuracy statistics for individual sensors.

Parameter	Cell	Speed (mi/h)	Difference of Sensor at (Percent)									
			0 inches		4 inches		8 inches		12 inches		24 inches	
			Mean Value	Standard Deviation	Mean Value	Standard Deviation	Mean Value	Standard Deviation	Mean Value	Standard Deviation	Mean Value	Standard Deviation
Velocity	3	30	NR	NR	18	5	11	4	35	12	51	23
		45	NR	NR	1	1	15	17	49	16	28	7
	19	30	NR	NR	26	11	10	6	9	4	52	26
		45	NR	NR	12	1	2	2	2	1	13	10
		60	NR	NR	13	5	3	3	6	6	11	11
	34	30	NR	NR	25	10	16	10	10	11	45	9
		45	NR	NR	2	2	2	1	3	4	5	7
	Median		**NR**	**NR**	**13**	**—**	**10**	—	**9**	—	**28**	—
Deflection method 1	3	30	9	5	NR	NR	5	3	7	8	NR	NR
		45	5	2	NR	NR	8	9	8	2	NR	NR
	19	30	8	4	NR	NR	10	6	8	2	NR	NR
		45	6	2	NR	NR	7	2	5	2	NR	NR
		60	14	3	NR	NR	18	4	11	5	NR	NR
	34	30	1	1	NR	NR	7	1	8	2	NR	NR
		45	17	1	NR	NR	17	4	17	5	NR	NR
	Median		**8**	—	**NR**	**NR**	**8**	—	**8**	—	**NR**	**NR**
Deflection method 2	3	30	19	16	20	15	20	20	26	15	41	19
		45	19	17	14	13	17	14	17	16	32	20
	19	30	31	7	34	11	42	14	52	22	148	71
		45	15	7	6	6	7	6	9	9	37	13
		60	14	7	13	14	17	20	22	18	79	72
	34	30	10	2	4	4	7	3	7	6	23	17
		45	17	4	7	4	4	4	5	4	41	18
	Median		**19**	—	**14**	—	**18**	—	**21**	—	**34**	—

1 mi/h = 1 km/h
1 inch = 25.4 mm
NR = Not reported.
— Indicates that the median was not calculated for the standard deviations.

The TSD deflection velocities and estimated deflections from the two algorithms were compared with the corresponding deflection parameters from the embedded geophones in figure 72 through figure 74. The slope of the global fit depicted a difference of about 12 percent. The slope and an R^2 value of 0.94 demonstrate the overall level of performance of the TSD. Most of the data points fall close to the global fit, generating a tight confidence interval and prediction limit with an SEE of about 80 mil/s (2.0 mm/s).

Sensors were also evaluated with varying vehicle speeds, and results are shown in figure 75. The median difference was the greatest for vehicle speeds of 30 mi/h (48.3 km/h) and usually the smallest at 45 mi/h (72.45 km/h).

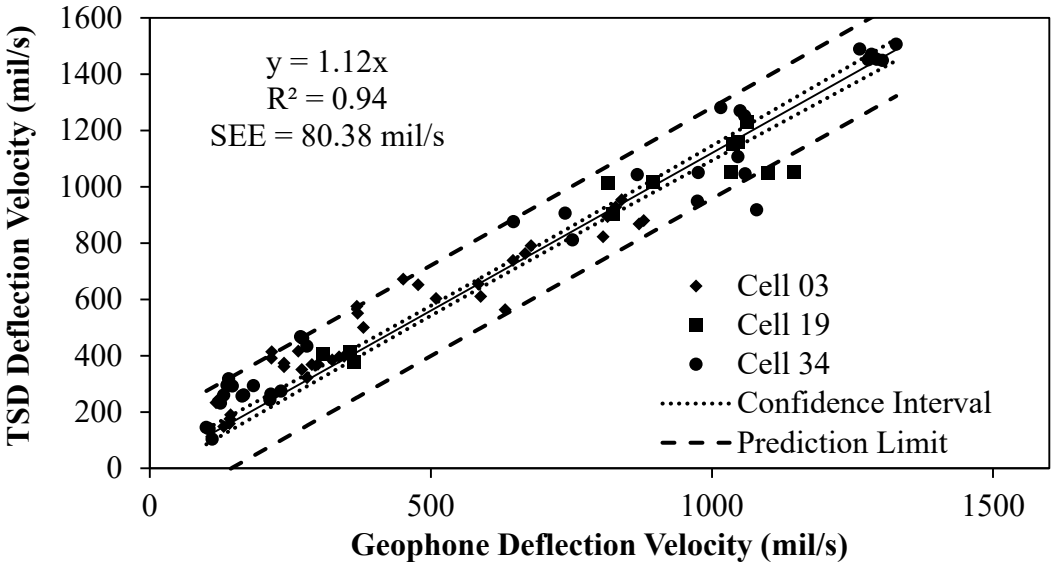

1 mil/s = 0.0254 mm/s

Figure 72. Graph. Overall comparison of deflection velocities measured with TSD and embedded sensors.

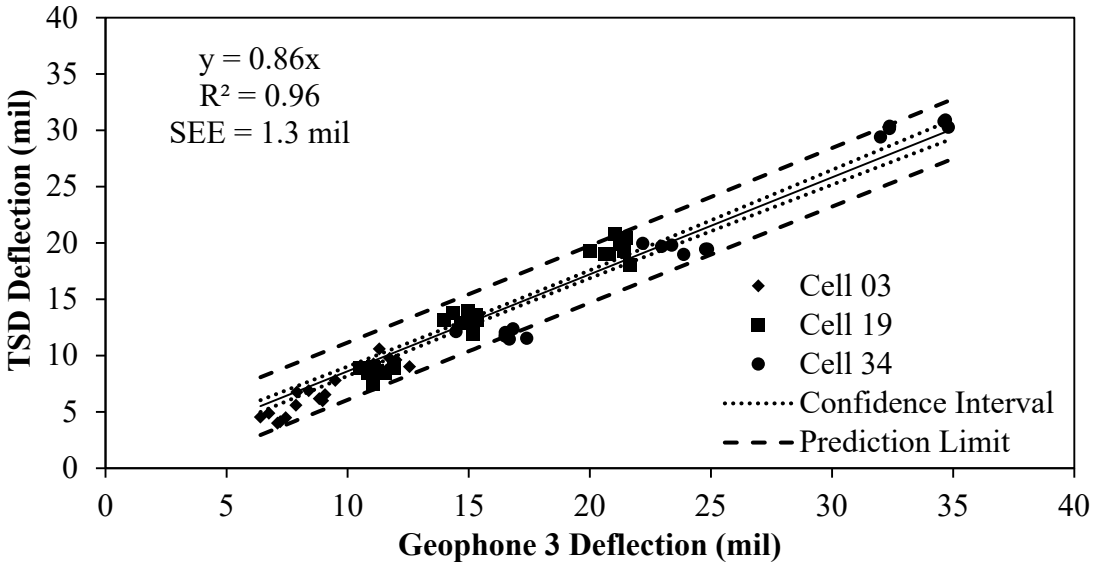

1 mil = 0.0254 mm

Figure 73. Graph. Overall comparison of TSD deflection method 1 and embedded sensors.

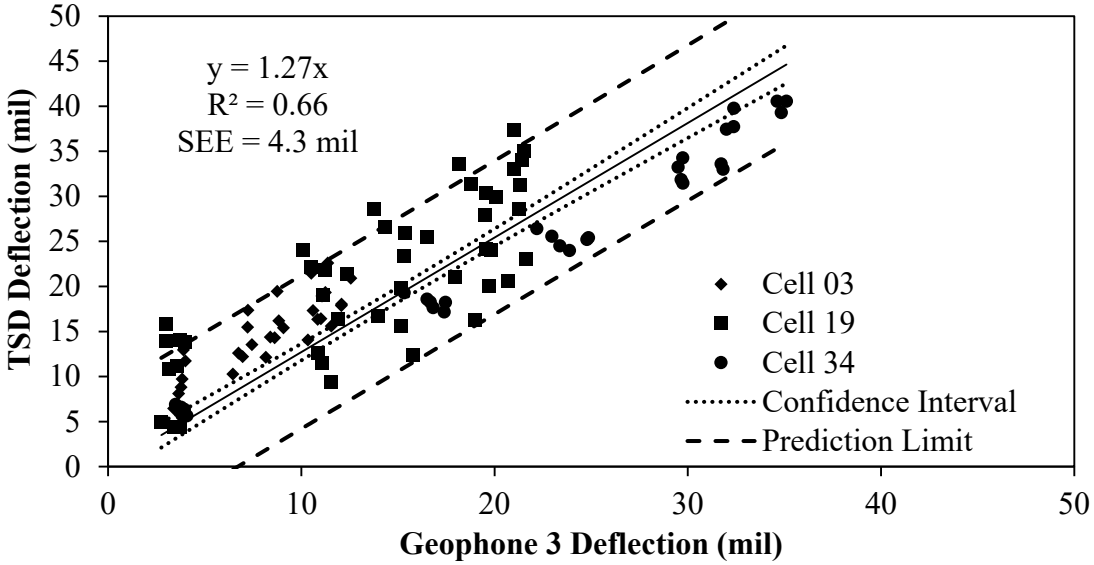

1 mil = 0.0254 mm

Figure 74. Graph. Overall comparison of TSD deflection method 2 and embedded sensors.

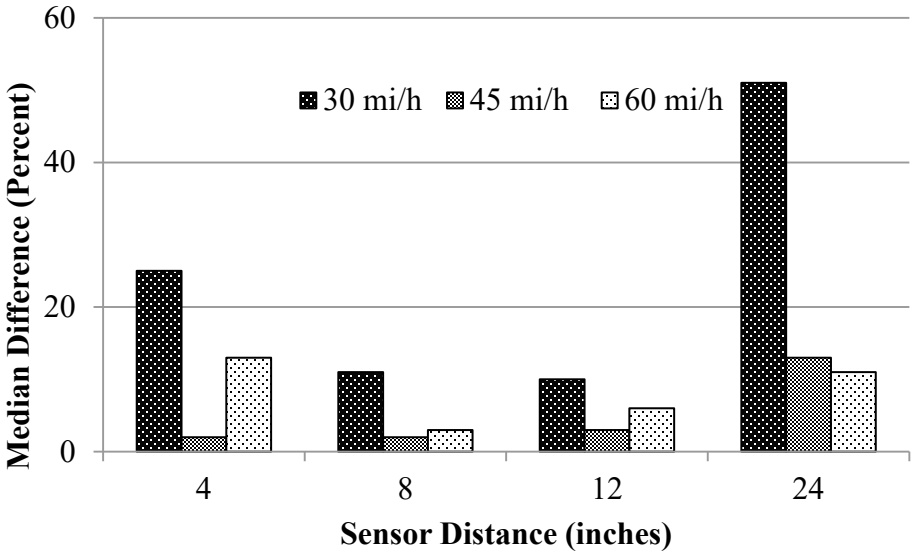

1 mi/h = 1.61 km/h
1 inch = 25.4 mm

Figure 75. Graph. Median sensor difference for TSD sensors with varying speeds.

The variations in differences with pavement structure are summarized in figure 76. Median differences were obtained from all of the sensors' differences except for the one at 36 and 60 inches (914.4 and 1,524 mm). The stiffest cell (cell 3) had a median difference ranging from 22 to 27 percent at 30 and 45 mi/h (48.3 and 72.45 km/h). Cells 34 exhibited the lowest median difference (around 3 percent) at 45 mi/h (72.45 km/h).

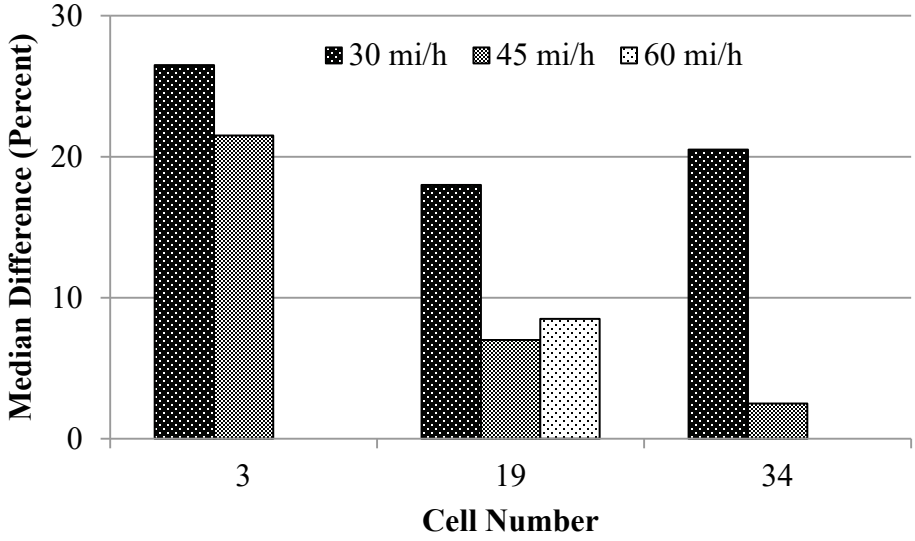

1 mi/h = 1.61 km/h

Figure 76. Graph. Distribution of differences measured with TSD for each cell.

6.3 PRECISION

The evaluation of precision was carried out by analyzing the results obtained as discussed in section 5.6 (Data Analysis) for almost all MnROAD cells and the 18-mi (29-km) loop. To evaluate the influence of speed, temperature, and pavement structure and roughness in precision, each individual cell was also analyzed so that the variation in precision could be directly related to each of those factors. Several other factors such as the road geometry (slope and curves) were also studied less quantitatively using the 18-mi (29-km) loop data. Some other parameters such as the surface texture that are known to impact the precision could not be studied due to a lack of texture data. The results are discussed in the following subsection.

Overall Results

The RWD deflections were directly used for the precision analysis. However, the deflection slopes (i.e., deflection velocity divided by the vehicle speed) were used instead of the deflection velocity for the evaluation of TSD to reduce the speed-related variability in the results. The data from the TSD sensor placed 60 inches (1,524 mm) from the load were not considered in the precision analysis due to their high variability and small reported values.

Typical box plots, such as those shown in figure 63 through figure 66, were developed to delineate the median, upper, and lower quartiles and minimum and maximum values. The y-axis consisted of the slope, R^2 value, SEE (as discussed in section 5.6, Data Analysis) and the range of measured values for all sections at all three speeds and during morning and afternoon. The precision of each sensor was evaluated individually.

RWD

Overall results from the RWD along the MnROAD LVR and the mainline are presented in figure 77 through figure 84. The reported RWD data related to the PCC sections were limited to seven sections. As such, the results reported here are more relevant to the flexible and composite sections.

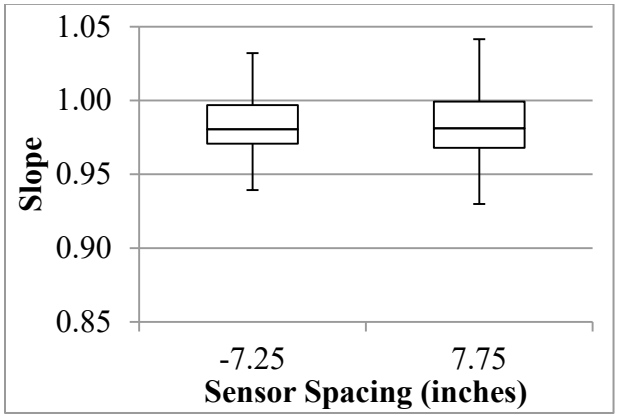

1 inch = 25.4 mm

Figure 77. Graph. RWD overall precision slope in the LVR.

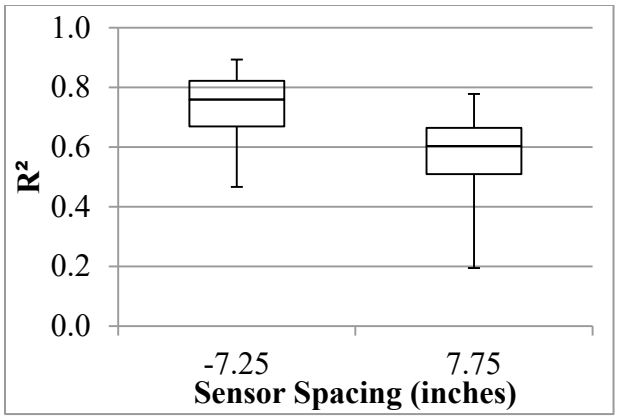

1 inch = 25.4 mm

Figure 78. Graph. RWD overall precision R^2 in the LVR.

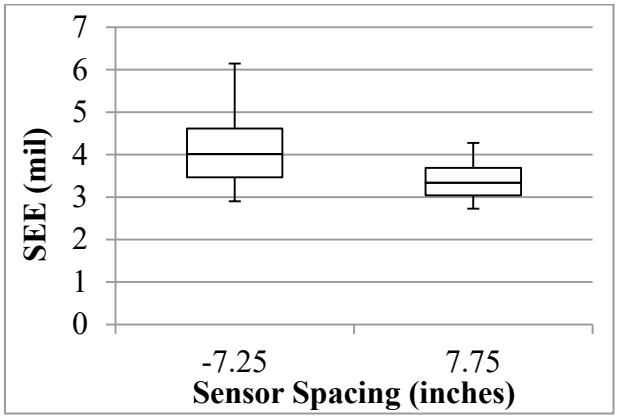

1 mil = 0.0254 mm
1 inch = 25.4 mm

Figure 79. Graph. RWD overall precision SEE in the LVR.

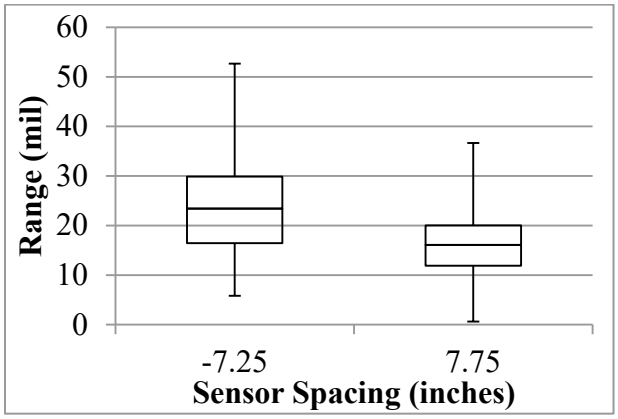

1 mil = 0.0254 mm
1 inch = 25.4 mm

Figure 80. Graph. RWD overall precision range in the LVR.

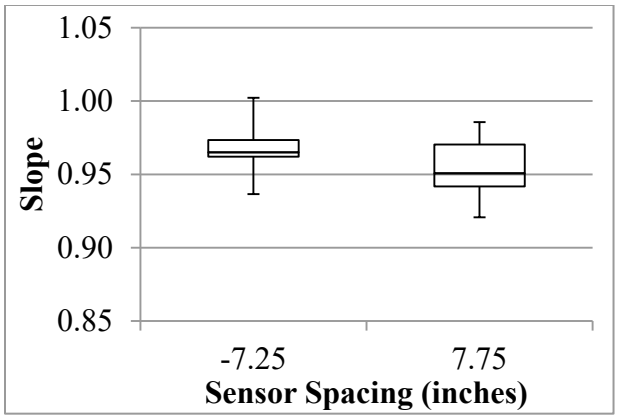

1 inch = 25.4 mm

Figure 81. Graph. RWD overall precision slope in the mainline.

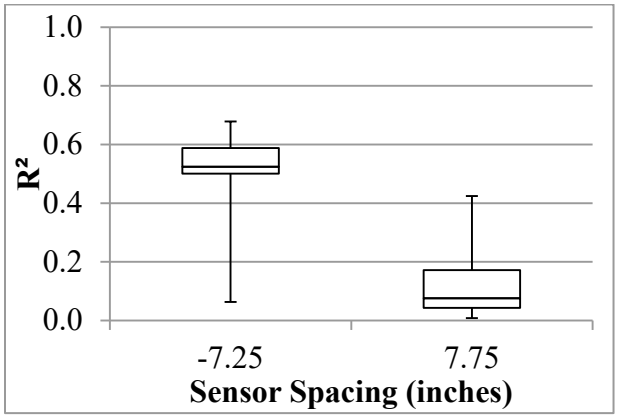

1 inch = 25.4 mm

Figure 82. Graph. RWD overall precision R^2 in the mainline.

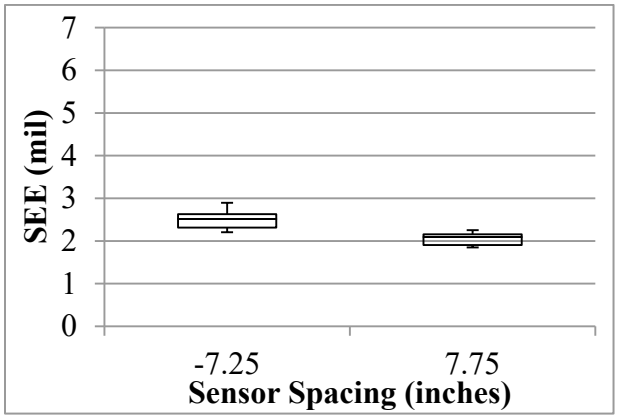

1 mil = 0.0254 mm
1 inch = 25.4 mm

Figure 83. Graph. RWD overall precision SEE in the mainline.

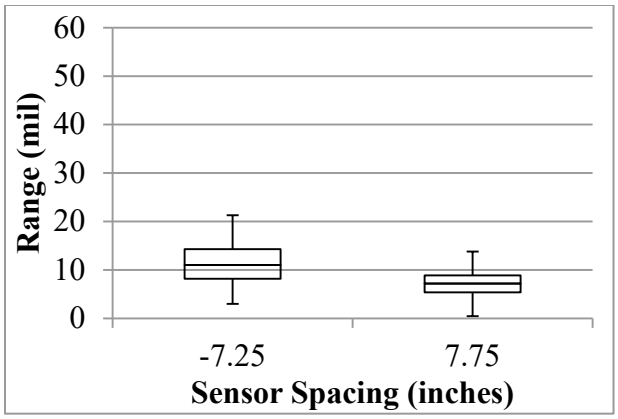

1 mil = 0.0254 mm
1 inch = 25.4 mm

Figure 84. Graph. RWD overall precision range in the mainline.

With slopes between the deflections from different passes averaging above 95 percent, both sensors exhibited satisfactory overall reproducibility. However, the median R^2 values of 0.8 and lower indicate high scatter among deflections collected at each test point among different runs. The sensor located 7.25 inches (184.15 mm) behind the axle exhibited greater R^2 values, especially along the LVR.

The median SEE from relating the deflections from different passes and sensors were 4 mil (0.1 mm) or less. The uncertainty of the measurements could be evaluated by comparing SEE with the range of deflections measured along the test sections. The median deflections were 24 mil (0.6 mm) or less for the sensor behind the axle and 16 mil (0.4 mm) or less for the sensor located 7.75 inches (196.85 mm) in front of the axle. As such, the median SEE was about 15 to 25 percent less than the median deflections measured by sensors.

Figure 85 through figure 88 depict the Wright County 18-mi (29-km) loop overall results, including the minimum, median, and maximum deflection parameters. The upper and lower quartiles are not shown because the experiments consisted of only three passes. Overall, the RWD exhibited a reasonable performance when tested under realistic environment. The slopes of the relationships among different passes typically yielded values equal or greater than 0.95 (i.e., close to the ideal value of unity). The R^2 values were also above 0.86 for both sensors. The median SEE values were about 10 percent less than the median deflections for the sensor 7.25 inches (184.15 mm) behind and about 15 percent less than the sensor located 7.75 inches (196.85 mm) in front of the load. It should be mentioned that the data provided for the 18-mi (29-km) loop were averaged over 0.1 mi (0.161 km), whereas the data used in the precision and accuracy along the MnROAD were provided at 50-ft (15.25-m) intervals. This may explain the apparent higher precision of the RWD along the 18-mi (29-km) loop as compared to the MnROAD sections.

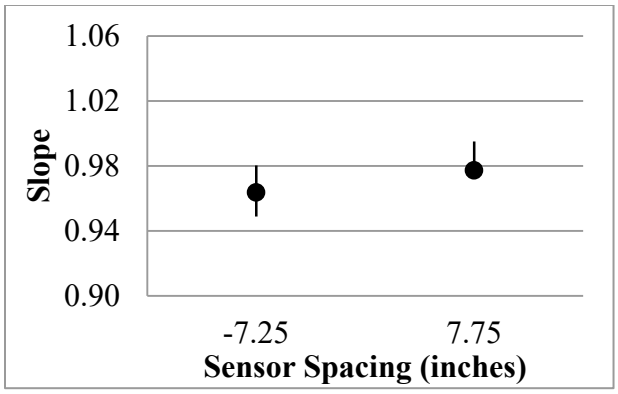

1 inch = 25.4 mm

Figure 85. Graph. RWD overall precision slope in the 18-mi (29-km) loop.

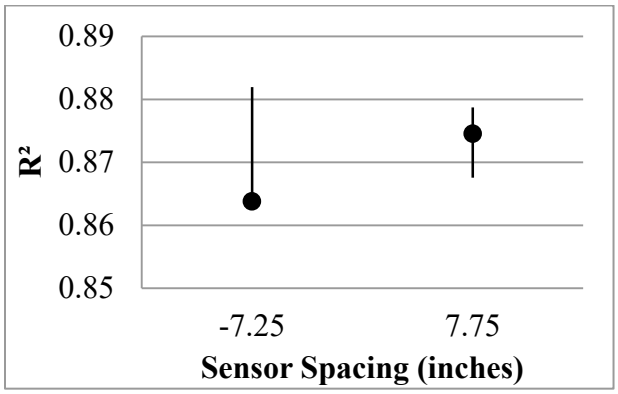

1 inch = 25.4 mm

Figure 86. Graph. RWD overall precision R^2 in the 18-mi (29-km) loop.

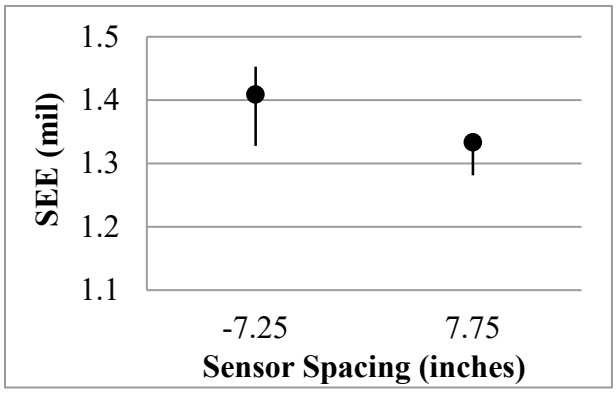

1 mil = 0.0254 mm
1 inch = 25.4 mm

Figure 87. Graph. RWD overall precision SEE in the 18-mi (29-km) loop.

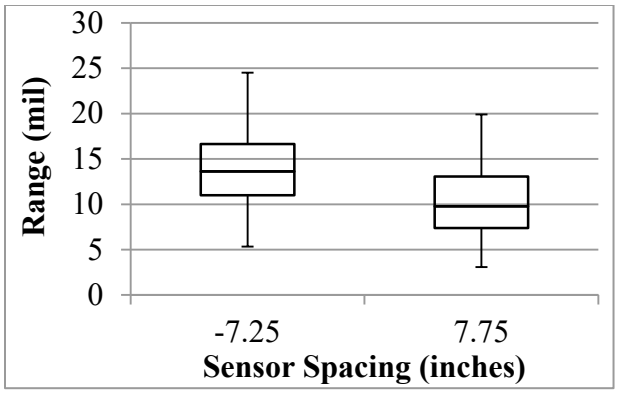

1 mil = 0.0254 mm
1 inch = 25.4 mm

Figure 88. Graph. RWD overall precision range in the 18-mi (29-km) loop.

TSD

The TSD precision analyses were carried out based on deflection slopes and deflections estimated with the two methods discussed in section 5.6. Precision of the deflection slope varied with sensor spacing, as presented in figure 89 through figure 96. The median of the best fit slopes for all sensors was greater than 95 percent, indicating that the replicate data were in general agreement. The R^2 values of the relationships between different passes were in excess of 0.9 for the first three sensors, indicating high certainty in the repeatability of the results from different passes. The farthest three sensors (including the sensor spaced 60 inches (1,524 mm) that is not shown here) yielded median R^2 values that were less than desirable. A study by the manufacturer to assess the sources of the uncertainties of the last three sensors is warranted. The median SEE values were less than 1 mil/ft (0.08 mm/m) for the mainline sections and less than 2.5 mil/ft (0.20 mm/m) for the LVR sections. The repeatability of the sensor located at 36 inches (914.4 mm) might be of concern given that most of the measured deflection slopes were less than 3 mil/ft (0.08 mm/m).

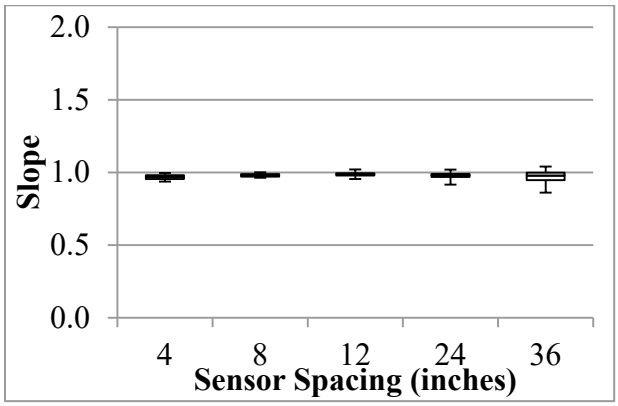

1 inch = 25.4 mm

Figure 89. Graph. TSD overall precision slope in the LVR.

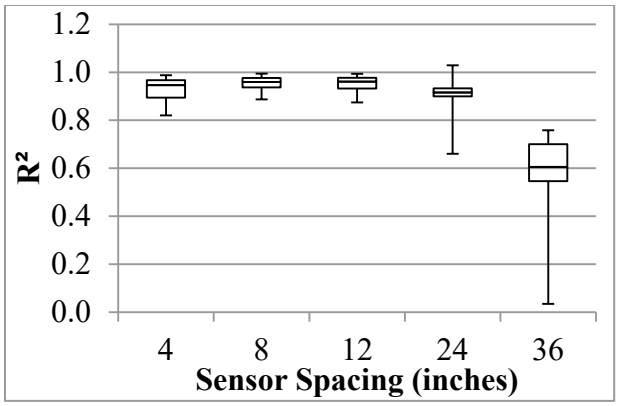

1 inch = 25.4 mm

Figure 90. Graph. TSD overall precision R^2 in the LVR.

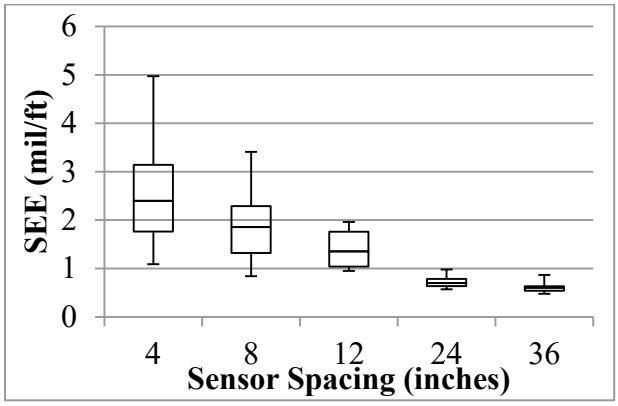

1 mil/ft = 83.3 µm/m
1 inch = 25.4 mm

Figure 91. Graph. TSD overall precision SEE in the LVR.

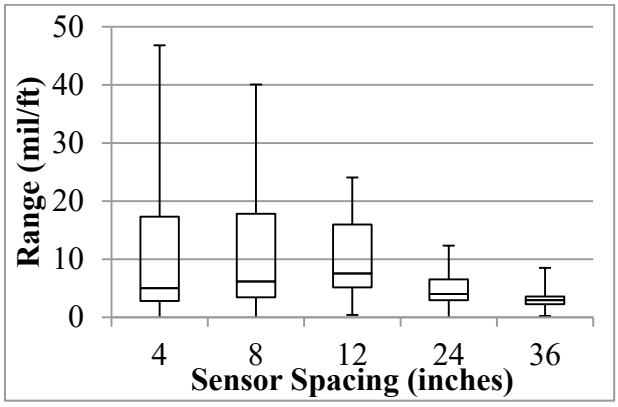

1 mil/ft = 83.3 µm/m
1 inch = 25.4 mm

Figure 92. Graph. TSD overall precision range in the LVR.

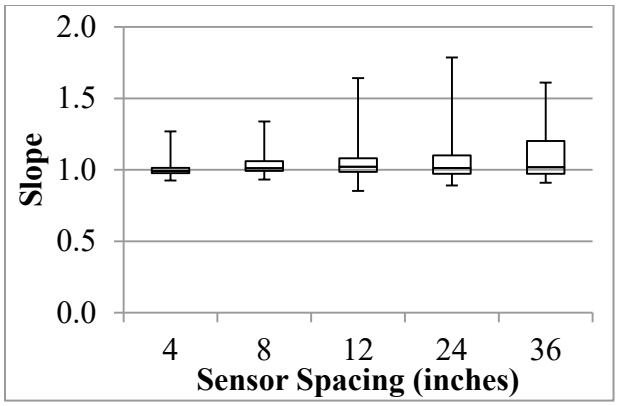

1 inch = 25.4 mm

Figure 93. Graph. TSD overall precision slope in the mainline.

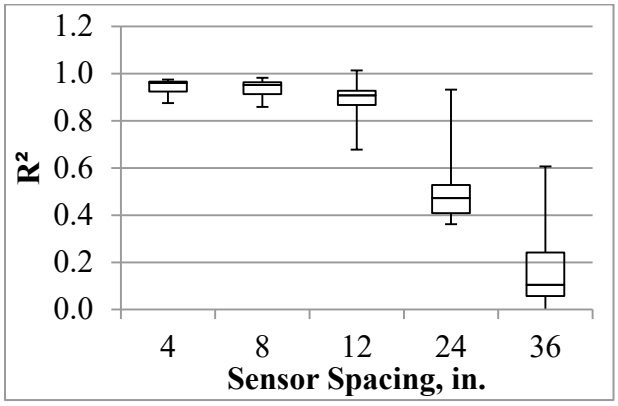

1 inch = 25.4 mm

Figure 94. Graph. TSD overall precision R^2 in the mainline.

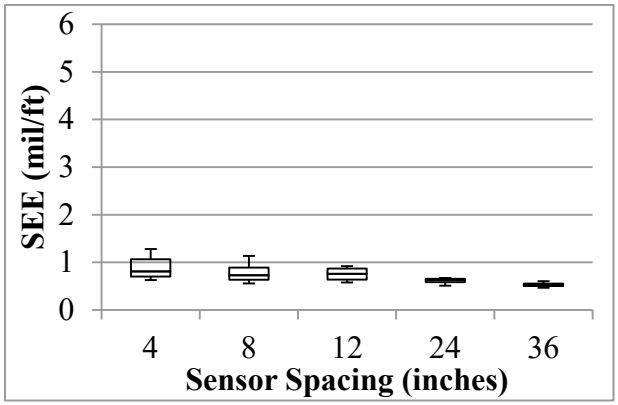

1 mil/ft = 83.3 µm/m
1 inch = 25.4 mm

Figure 95. Graph. TSD overall precision SEE in the mainline.

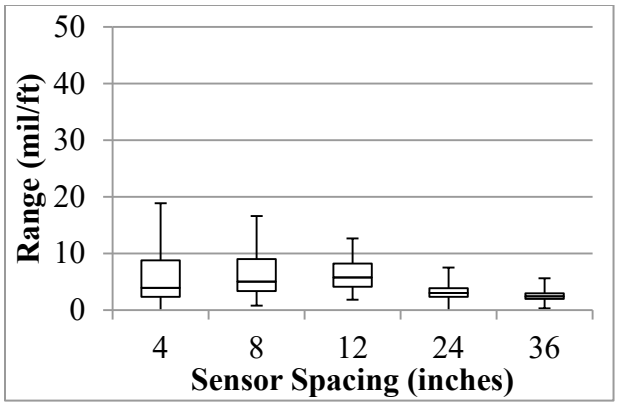

1 mil/ft = 83.3 µm/m
1 inch = 25.4 mm

Figure 96. Graph. TSD overall precision range in the mainline.

Table 26 and table 27 contain the medians of the slope, R^2, and SEE at different distances from the wheel's centerline. Both deflection algorithms estimated the deflection 0 inches (0 mm) from the centerline. For the available distances, both deflection methods resulted in an acceptable best fit slope. The median R^2 and SEE values from deflection method 1 indicate a more precise method relative to method 2.

Table 26. Overall precision results for the close sensors.

Parameter	Test Section	Median Statistical Parameters								
		0 inches			4 inches			8 inches		
		Slope	R^2	SEE	Slope	R^2	SEE	Slope	R^2	SEE
Deflection slope	LVR	NR	NR	NR	0.97	0.95	2.40	0.98	0.96	1.86
	Mainline	NR	NR	NR	0.99	0.96	0.81	1.01	0.95	0.73
	18-mi loop	NR	NR	NR	0.93	0.71	1.31	0.96	0.78	1.11
Deflection method 1	LVR	0.99	0.95	2.23	NR	NR	NR	0.99	0.91	1.63
	Mainline	1.02	0.82	1.35	NR	NR	NR	1.02	0.66	1.12
	18-mi loop	0.98	0.81	1.87	NR	NR	NR	0.98	0.82	1.46
Deflection method 2	LVR	0.97	0.71	5.66	0.97	0.63	4.92	0.97	0.40	4.54
	Mainline	1.03	0.16	4.68	1.03	0.30	4.42	1.03	0.46	4.13
	18-mi loop	0.99	0.48	5.22	0.99	0.45	5.05	0.99	0.41	4.84

1 inch = 25.4 mm
1 mi = 1.61 km
NR = Not reported.

Table 27. Overall precision results for far sensors.

Parameter	Test Section	Median Statistic Parameters								
		12 inches			24 inches			36 inches		
		Slope	R^2	SEE	Slope	R^2	SEE	Slope	R^2	SEE
Velocity	LVR	0.99	0.96	1.35	0.98	0.92	0.70	0.98	0.61	0.60
	Mainline	1.02	0.91	0.76	1.01	0.47	0.63	1.02	0.10	0.52
	18-mi loop	0.95	0.79	1.00	0.99	0.80	0.65	1.01	0.72	0.59
Deflection method 1	LVR	0.99	0.79	1.32	—	—	—	—	—	—
	Mainline	1.02	0.47	0.95	—	—	—	—	—	—
	18-mi loop	0.98	0.81	2.00	—	—	—	—	—	—
Deflection method 2	LVR	0.96	0.19	4.15	0.93	0.24	3.87	0.89	0.29	3.66
	Mainline	1.02	0.49	3.97	1.00	0.48	3.84	0.97	0.49	3.57
	18-mi loop	0.99	0.35	4.65	0.97	0.09	4.30	0.94	0.15	3.90

1 inch = 25.4 mm
1 mi = 1.61 km
— Indicates that method 1 did not report these values.

Figure 97 through figure 100 present the overall TSD results from the Wright County 18-mi (29-km) loop data averaged at a 33-ft (10 m) spacing. The precision of the TSD along the 18-mi (29-km) loop was similar or slightly worse in comparison to the MnROAD sections. The slopes of the best fit lines between repeat passes were greater than 0.92, but the R^2 values were less than 0.8. The SEE gradually decreased from 1.3 to 0.6 mil/ft (0.11 to 0.05 mm/m), while the median range decreased from about 8 to 4 mil/ft (0.67 to 0.33 mm/m). Once again, the precision of the farther sensors was considered low.

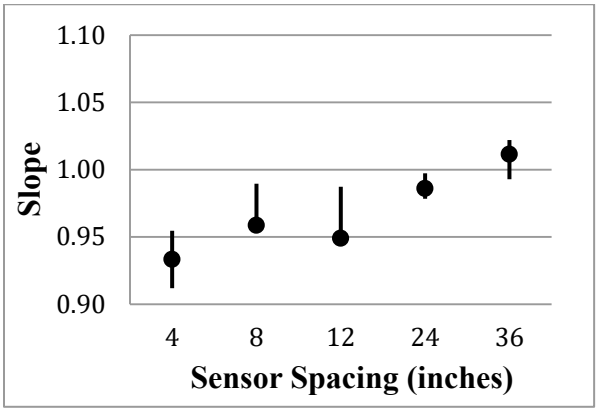

1 inch = 25.4 mm

Figure 97. Graph. TSD overall precision slope in the 18-mi (29-km) loop.

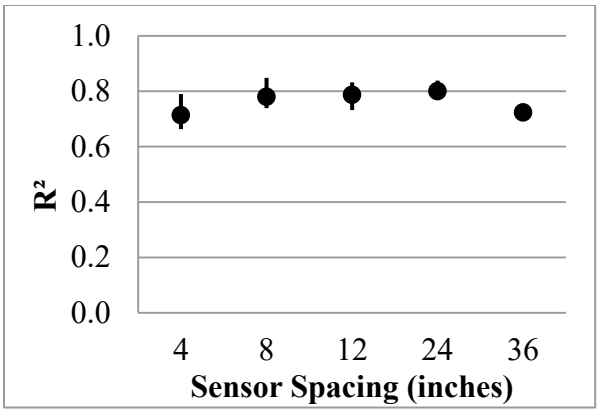

1 inch = 25.4 mm

Figure 98. Graph. TSD overall precision R^2 in the 18-mi (29-km) loop.

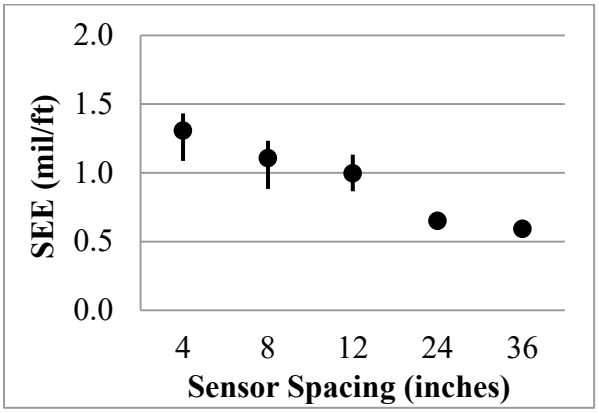

1 mil/ft = 83.3 µm/m
1 inch = 25.4 mm

Figure 99. Graph. TSD overall precision SEE in the 18-mi (29-km) loop.

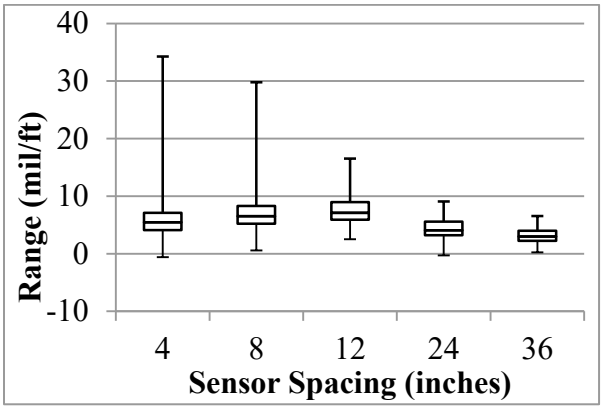

1 mil/ft = 83.3 µm/m
1 inch = 25.4 mm

Figure 100. Graph. TSD overall precision range in the 18-mi (29-km) loop.

Correlation to Pavement Structure

The stiffness of the pavement structure was defined using the average FWD deflection of the sensor directly under the load (center deflection) normalized to 11 kip (50 kN). MnROAD performs periodic FWD measurements. For this project, the FWD measurements at dates closest to the day of precision/accuracy testing were used. The precision of the device in each cell was also correlated to pavement roughness. The average IRI for each cell reported by the TSD during precision testing was used for this purpose. While the plots generated for this section were divided into flexible and rigid pavement, the trend lines corresponded to all sections.

TSDD precision for this and the following sections was evaluated using the median COVs of deflection parameters from each sensor within each cell. The COV of the deflection parameter from the three or five test repetitions at each individual data point within each cell was calculated. The median of these COV values was then extracted and used to avoid a statistical error from single marginal data point. For this section the median COVs from different times of day and different speeds were then averaged since this section only focuses on the correlation to pavement structure.

RWD

Figure 101 and figure 102 present the trends between the median coefficients of variation of deflection for each cell with the average FWD central deflection (as an indication of the structural stiffness of each cell). As the FWD deflection increased (i.e., the cell became structurally weaker), the COV of the RWD measurements decreased (i.e., the precision of the RWD increased). Based on limited accuracy data (see figure 71), the accuracy of the RWD measurements also decreased with an increase in stiffness.

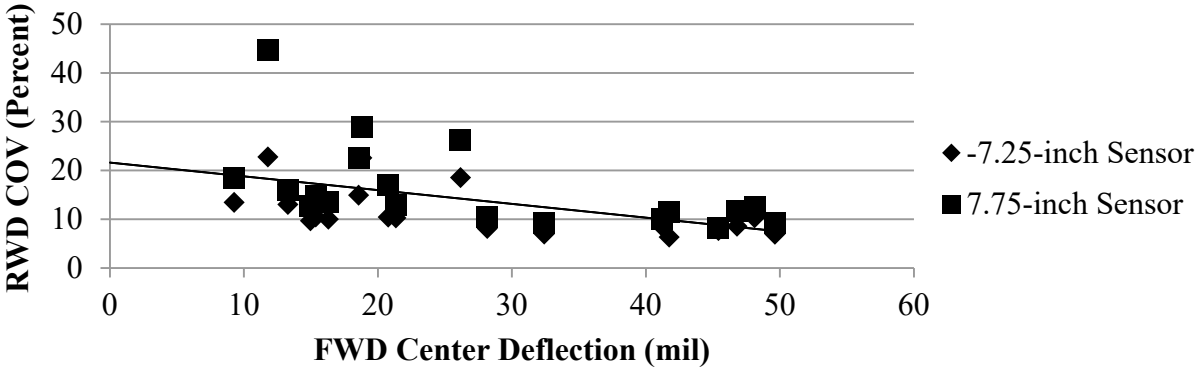

1 mil = 0.0254 mm
1 inch = 25.4 mm

Figure 101. Graph. Comparison of RWD COV with pavement stiffness over flexible pavement.

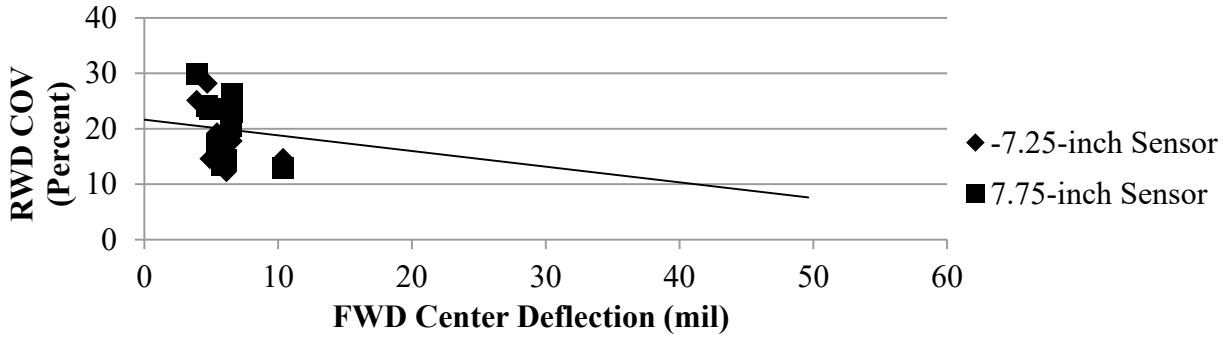

1 mil = 0.0254 mm
1 inch = 25.4 mm

Figure 102. Graph. Comparison of RWD COV with pavement stiffness over rigid pavement.

Figure 103 and figure 104 depict the comparison between the RWD median COV of deflection and IRI. It is difficult to draw a conclusion on the influence of the IRI on the precision of the RWD given the scatter in the results.

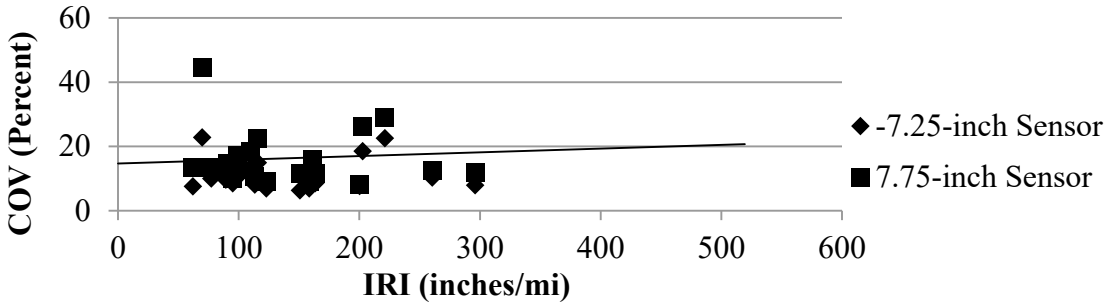

1 inch/mi = 0.0158 m/km
1 inch = 25.4 mm

Figure 103. Graph. Comparison of RWD COV with IRI over flexible pavement.

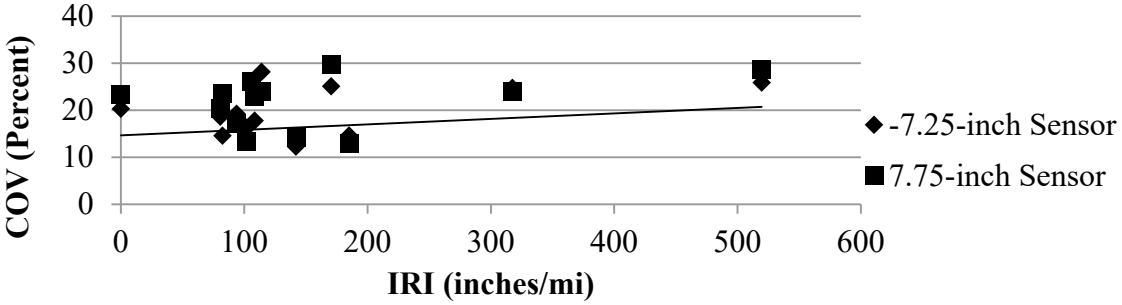

1 inch/mi = 0.0158 m/km
1 inch = 25.4 mm

Figure 104. Graph. Comparison of RWD COV with IRI over rigid pavement.

TSD

Figure 105 and figure 106 depict the relationship between the median COV of the deflection slope for each cell and the average FWD deflection as a surrogate for the overall stiffness of the pavement structures. The spatial COVs associated with the first four sensors decreased as the FWD central deflection increased for the flexible pavements. The closest sensor exhibited higher COVs than the other sensors for the rigid pavements. From figure 76, the accuracy of the TSD for the flexible pavements was also impacted by the pavement stiffness. The median COVs of the deflection slopes are also correlated to the IRI measurements in figure 107 and figure 108. Once again, these two parameters are not strongly correlated.

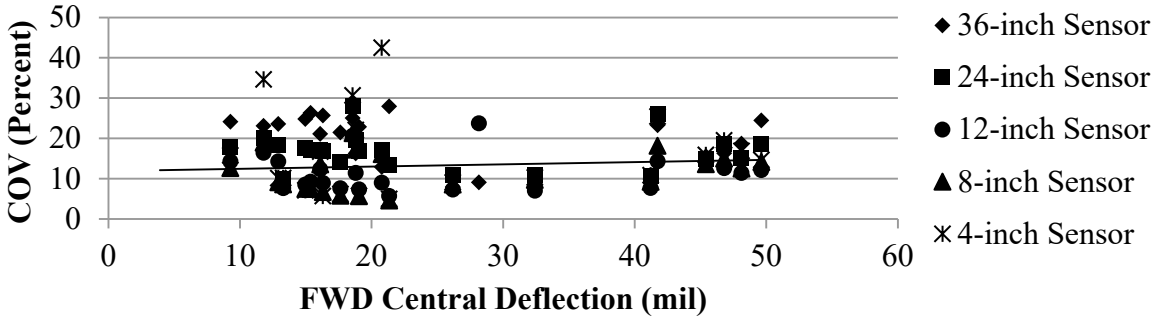

1 mil = 0.0254 mm
1 inch = 25.4 mm

Figure 105. Graph. Precision TSD COV with pavement stiffness over flexible pavement.

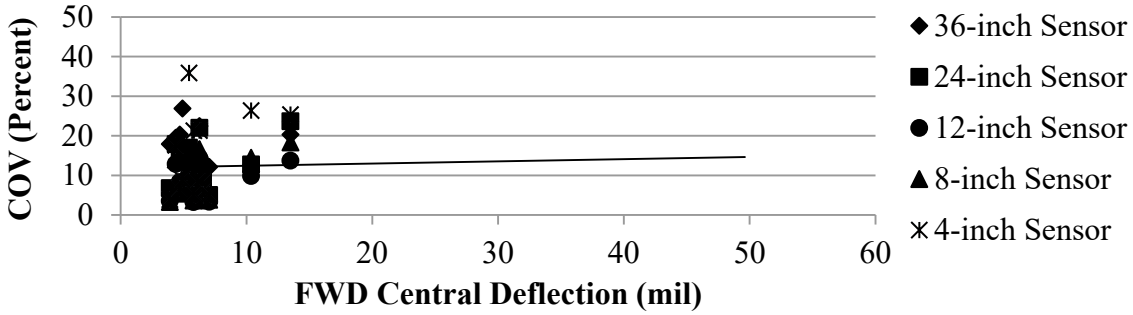

1 mil = 0.0254 mm
1 inch = 25.4 mm

Figure 106. Graph. Precision TSD COV with pavement stiffness over rigid pavement.

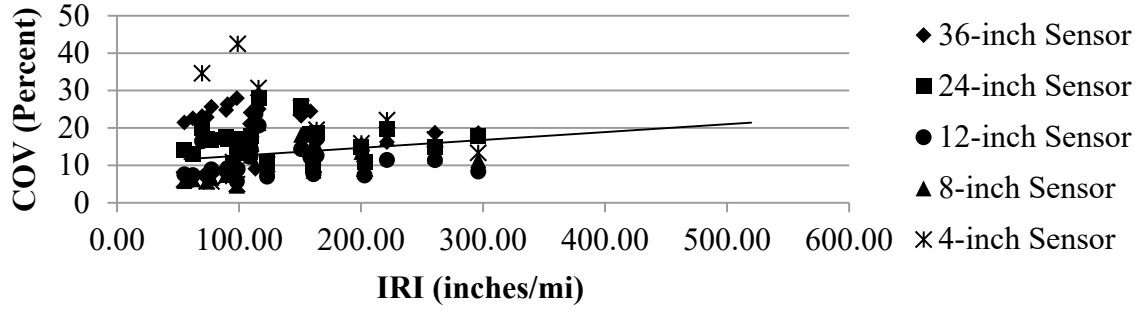

1 inch/mi = 0.0158 m/km
1 inch = 25.4 mm

Figure 107. Graph. Precision TSD COV with IRI over flexible pavement.

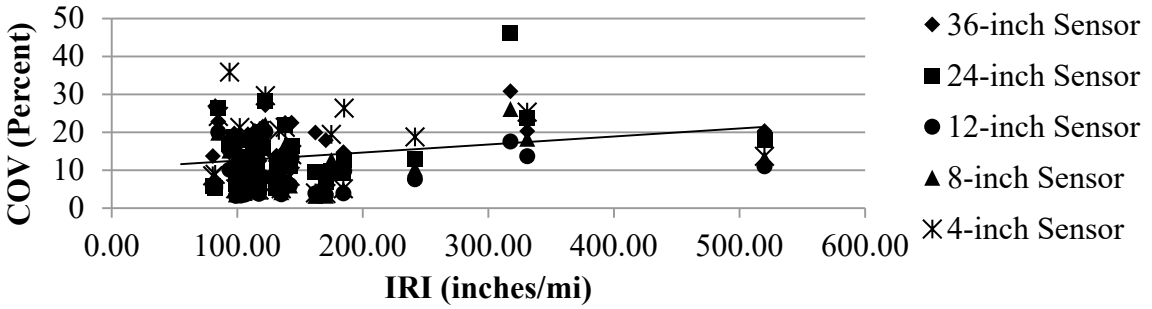

1 inch/mi = 0.0158 m/km
1 inch = 25.4 mm

Figure 108. Graph. Precision TSD COV with IRI over rigid pavement.

Operating Speed

To demonstrate the variation of the precision of the TSDDs with the vehicle speed, the median COVs of the deflection parameter from different passes within a cell of each sensor were calculated at different vehicle speeds as explained in the subsection, Correlation to Pavement Structure. The plots had to be separated between the MnROAD LVR and the mainline since the precision tests were carried out at different speeds along these two facilities. The LVR cells were tested at 30 and 45 mi/h (48.3 and 72.45 km/h), while the mainline tests were carried out at 45 and 60 mi/h (72.45 and 96.6 km/h). The common vehicle speed of 45 mi/h (72.45 km/h) was used as the common abscissa for reference.

RWD

Based on the slopes of the best fit lines shown in figure 109 and figure 110, the RWD became mildly (5 to 10 percent) less precise as the operational speed increased. The relationship shown in figure 109 for the LVR cells was stronger (i.e., exhibited higher R^2 value) than the relationship from the mainline cells, as shown in figure 110. This trend could be attributed to the fact that the mainline cells were generally stiffer than the LVR cells. The RWD seemed to exhibit more precise measurements at lower speeds. Although measurements were not greatly affected by vehicle speed, the optimum operational speed should be the slowest one that is a compromise between operational costs and safety. Similar results were observed in figure 70 where the performance of the RWD was also negatively affected at a vehicle speed of 60 mi/h (96.6 km/h).

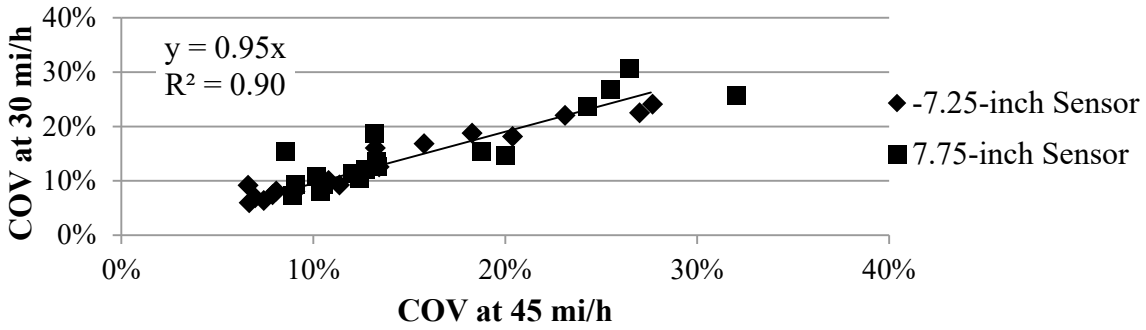

1 mi/h = 1.61 km/h
1 inch = 25.4 mm

Figure 109. Graph. Comparison of RWD COV at different speeds in the LVR.

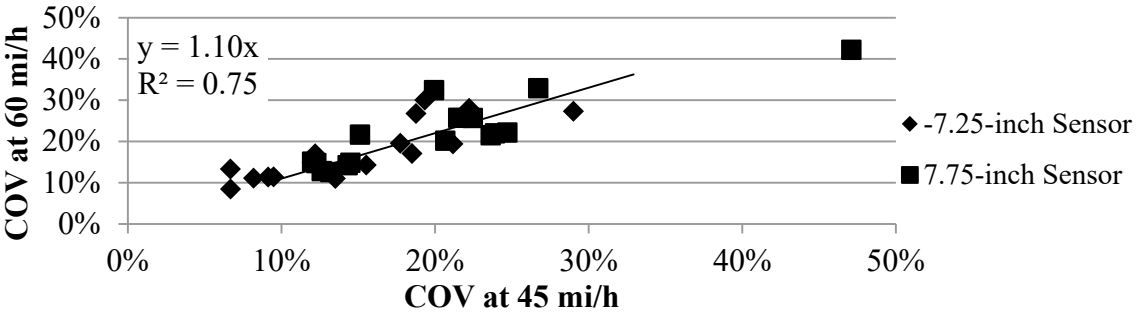

1 mi/h = 1.61 km/h
1 inch = 25.4 mm

Figure 110. Graph. Comparison of RWD COV at different speeds in the mainline.

TSD

The relationships between the median COVs of the deflection slope at different vehicle speeds for the TSD are shown in figure 111 and figure 112. Although deflection slope was the parameter used for the TSD precision evaluation, the results appear to be affected by the vehicle speed. The COVs from tests at 30 mi/h (48.3 km/h) along the LVR were around 24 percent less than those measured at 45mi/h (72.45 km/h). The COVs from tests at 60 mi/h (96.6 km/h) were about 38 percent greater than the COVs measured at 45 mi/h (72.45 km/h) along the mainline.

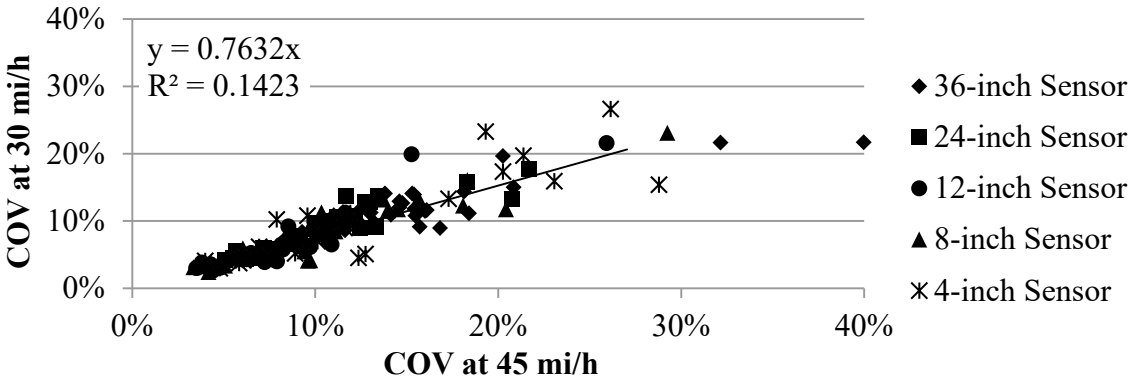

1 mi/h = 1.61 km/h
1 inch = 25.4 mm

Figure 111. Graph. Comparison of TSD COV at different speeds in the LVR.

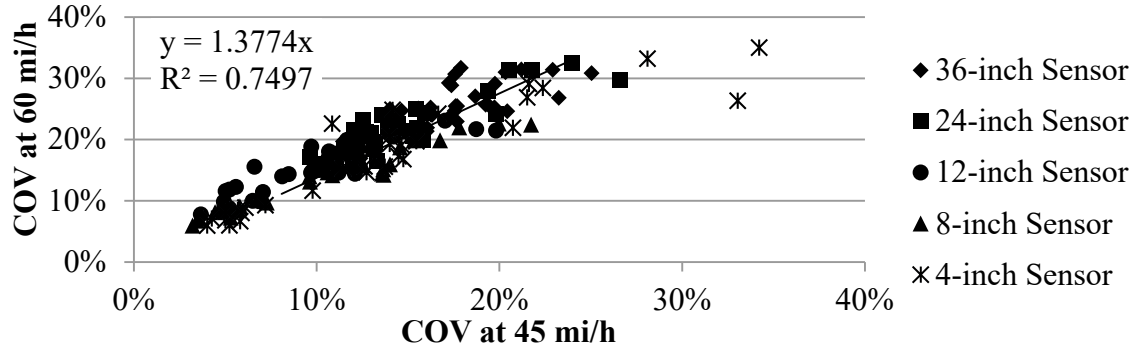

1 mi/h = 1.61 km/h
1 inch = 25.4 mm

Figure 112. Graph. Comparison of TSD COV at different speeds in the mainline.

Temperature Variation

The same procedure followed for vehicle speed was used to estimate the impact of temperature variation on the precision of the TSDDs. Similar plots were developed to compare the median COVs of deflection slopes from morning runs with those from afternoon runs. Table 28 includes the average and COVs of the pavement temperature during precision testing as measured by both TSDDs.

Table 28. Average pavement temperature during precision testing.

Test Section	Morning Temperature		Afternoon Temperature	
	Average (°F)	COV (Percent)	Average (°F)	COV (Percent)
LVR	68	6.4	92	5.2
Mainline	80	9.1	92	5.4

1 °F = 1.8 °C + 32

RWD

RWD results are presented in figure 113. A weak correlation between the afternoon and morning COVs of the deflections could be observed considering that the R^2 value was 0.61. Afternoon runs were around 7 percent more precise than morning runs. One reason for this pattern could be that high temperatures create a softer surface layer that increases the measured deflections. For the same sensors, higher precision is expected as the measured parameter increases. RWD consistently showed lower precision when the measured deflections were small for stiffer pavement or when the device was operated at higher vehicle speed.

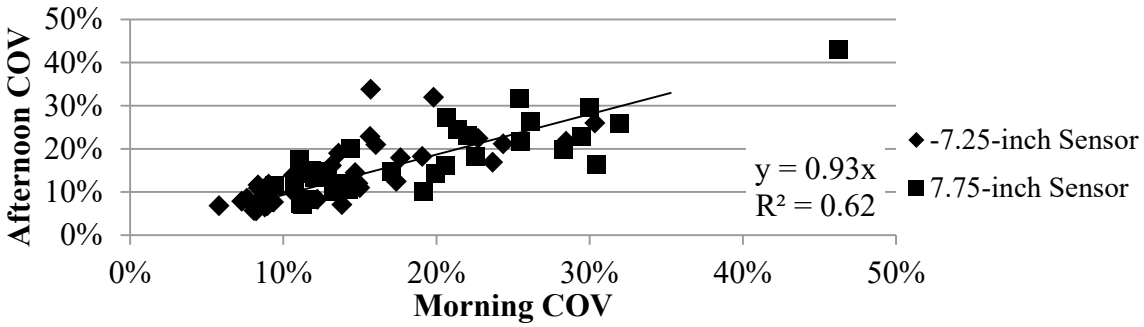

1 inch = 25.4 mm

Figure 113. Graph. Comparison of RWD COV at different afternoon temperatures.

TSD

Change in pavement temperature affected the TSD differently. The precision of the TSD, presented in figure 114, seemed to decrease with higher temperatures. Afternoon runs yielded COVs that were 32 percent greater than the measurements in the morning. With an R^2 value of 0.87, the precisions from the morning and afternoon tests were more correlated than from the RWD.

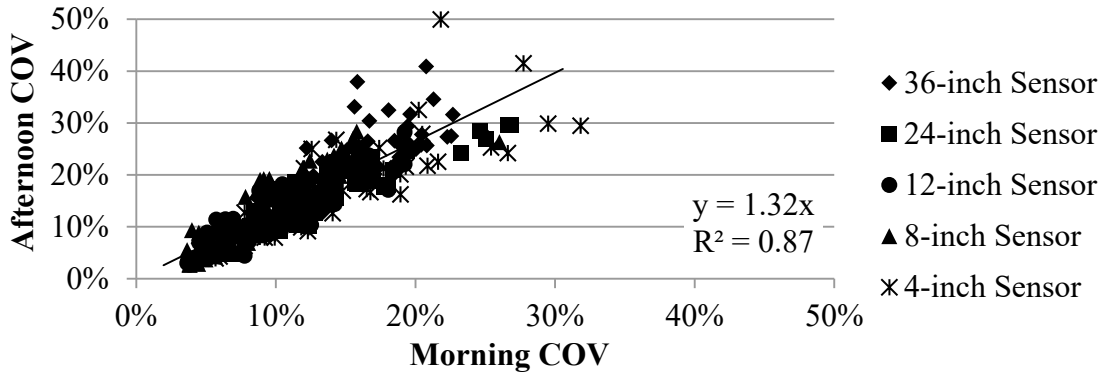

1 inch = 25.4 mm

Figure 114. Graph. Comparison of TSD COV at different afternoon temperatures.

Vertical and Horizontal Curves

The impact of the vertical gradient and horizontal curves on the precision of the TSD was studied only for the 18-mi (29-km) loop using the data reported at 33-ft (10-m) intervals. Such analysis

was not feasible for the RWD because the data were reported every 0.1 mi (0.161 km). Enough data were not available to carry out a conclusive study with the RWD.

Correlation to Vertical Gradient

The 18-mi (29-km) loop was first divided into 0.2-mi (0.322-km) increments. The vertical gradient of the road was estimated for each subsection by dividing the change in elevation as measured by the TSD by the horizontal distance (0.2 mi (0.322 km)). The median COV within each increment was determined and plotted against the vertical gradient. Figure 115 and figure 116 detail the results from the five closest sensors for the TSD. A zero elevation change was denoted with a dashed line, delineating the downhill sections from uphill sections. No clear correlation related to a vertical gradient was found.

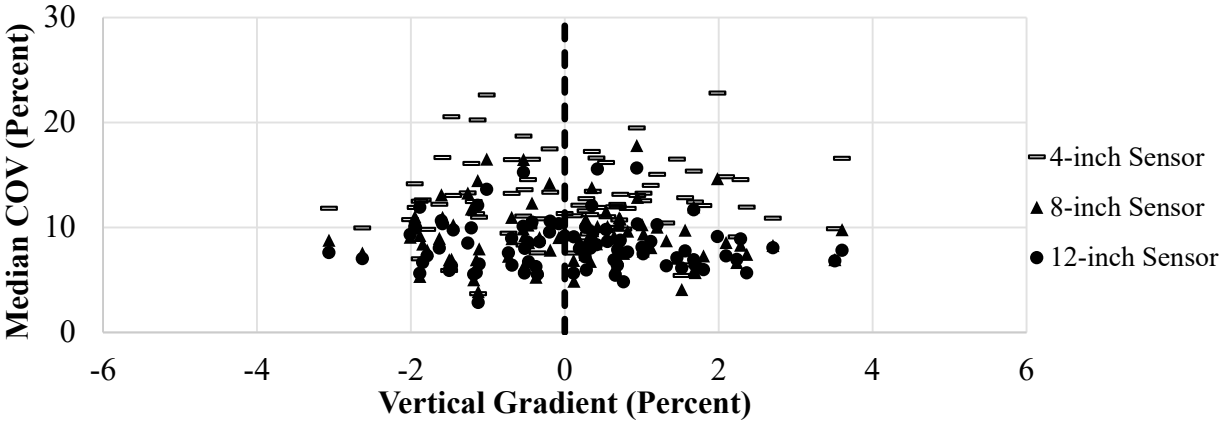

1 inch = 25.4 mm

Figure 115. Graph. Precision TSD COV with vertical gradients for the closer sensors.

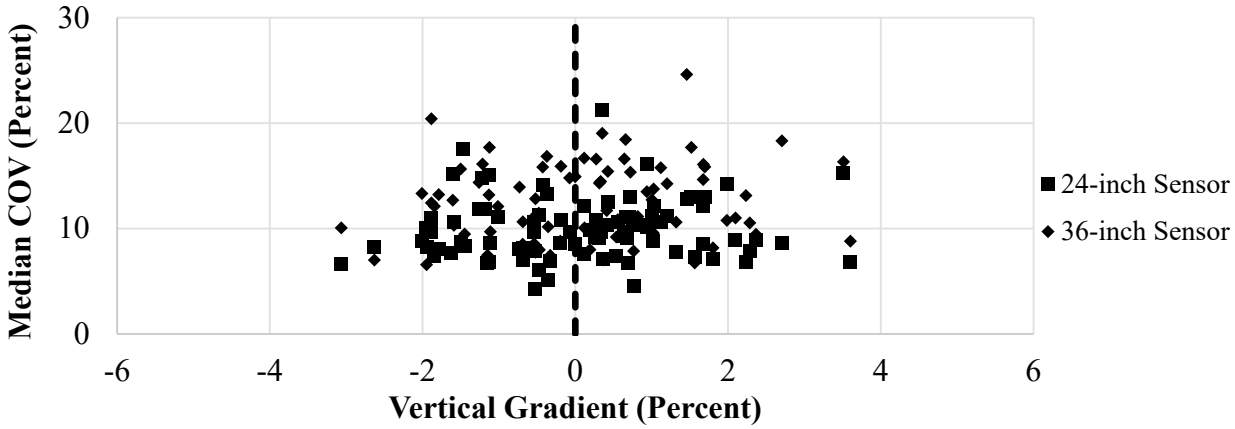

1 inch = 25.4 mm

Figure 116. Graph. Precision TSD COV with vertical gradients for the further sensors.

Correlation to Horizontal Curves

Google© maps of the COVs of the deflection slopes from repeated runs for the first five sensors are shown in figure 117 through figure 121. Qualitatively, most of the relatively high COVs (i.e., red and orange sections) correspond to sharp turns and/or locations of the stop signs.

In order to quantify the horizontal curvature of the road, the horizontal curvature index was obtained for each 0.2-mi (0.322-km) subsection. This index was approximated using the GPS coordinates. The horizontal curvature index was estimated by dividing the straight distance between the beginning and ending of each subsection by the total traveled distance between those two points. A straight section of the road would result in a horizontal curvature index of unity since the direct distance and the traveled distance are the same. The smaller the curvature index, the curvier the 0.2-mi (0.322-km) subsection will be. Figure 122 and figure 123 depict the correlation between the median COV of the TSD measurements and the horizontal curvature index of the subsections. Most subsections in the 18-mi (29-km) loop constituted straight roads denoted by value of 1. A clear correlation was not present in the plot. All subsections including those with sharp horizontal curvatures resulted in a COV ranging between 5 and 25 percent.

Figure 117. Map. Wright County 18-mi (29-km) loop TSD 36-inch (914.4-mm) sensor COV.[46]

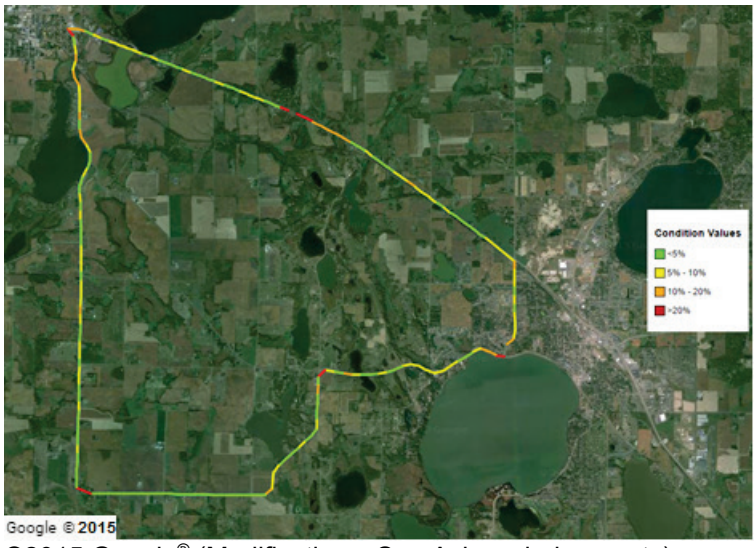

©2015 Google® (Modifications: See Acknowledgements).

Figure 118. Map. Wright County 18-mi (29-km) loop TSD 24-inch (609.6-mm) sensor COV.[47]

©2015 Google® (Modifications: See Acknowledgements).

Figure 119. Map. Wright County 18-mi (29-km) loop TSD 12-inch (304.8-mm) sensor COV.[48]

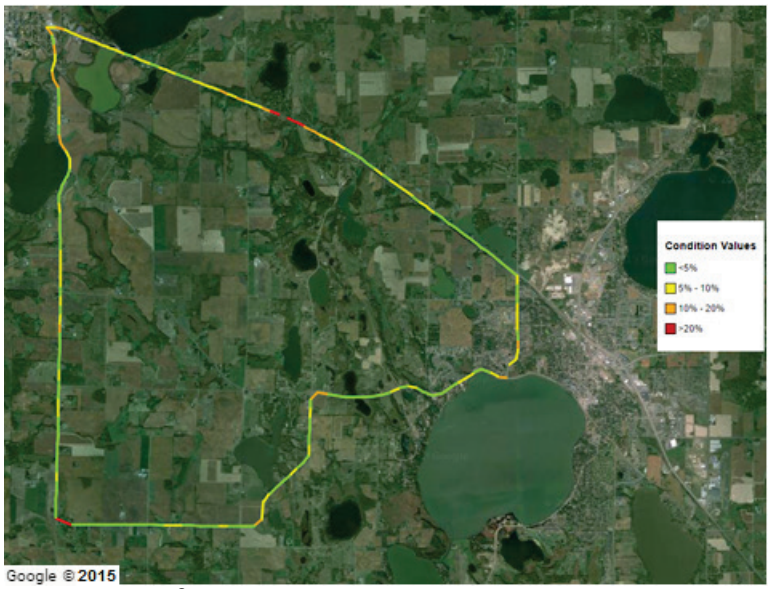

©2015 Google® (Modifications: See Acknowledgements).

Figure 120. Map. Wright County 18-mi (29-km) loop TSD 8-inch (203.2-mm) sensor COV.[49]

©2015 Google® (Modifications: See Acknowledgements).

Figure 121. Map. Wright County 18-mi (29-km) loop TSD 4-inch (101.6-mm) sensor COV.[50]

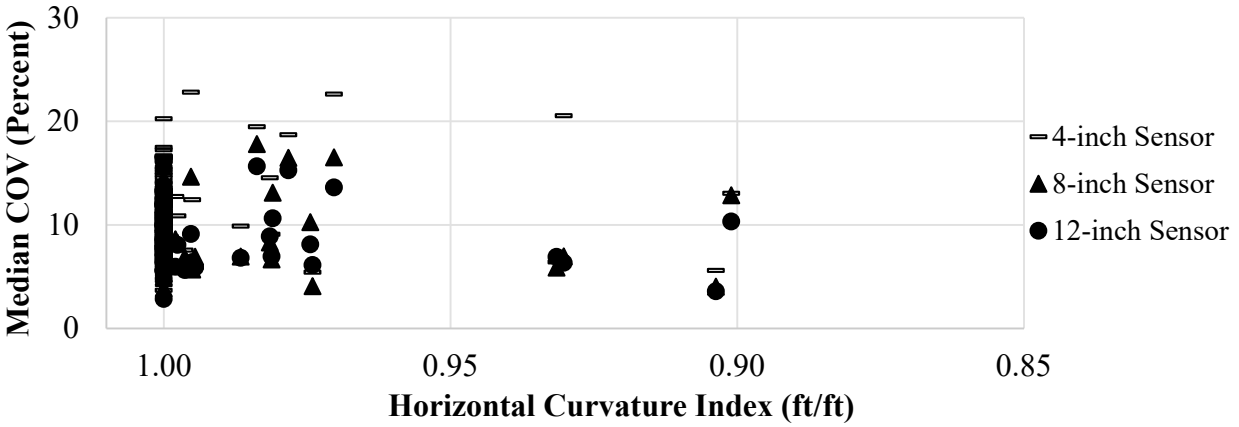

1 ft/ft = 1 m/m
1 inch = 25.4 mm

Figure 122. Graph. Precision TSD COV with horizontal curves for the closer sensors.

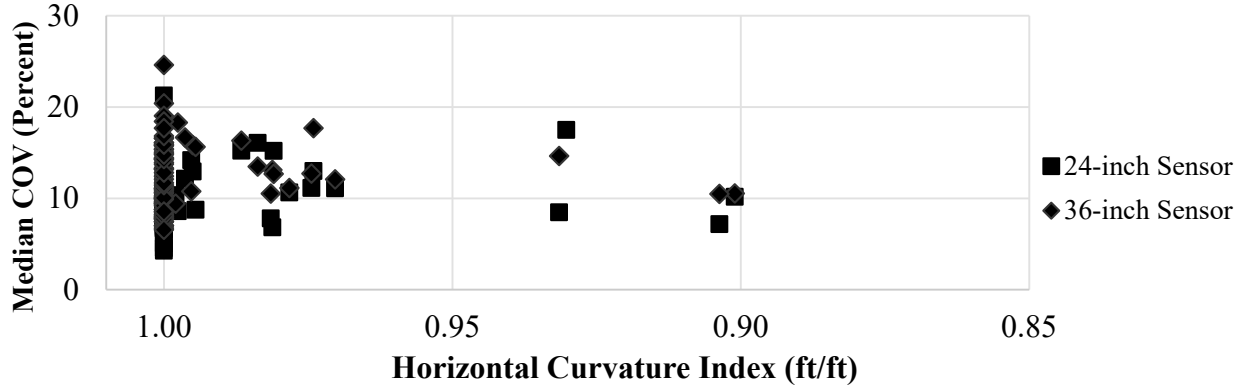

1 ft/ft = 1 m/m
1 inch = 25.4 mm

Figure 123. Graph. Precision TSD COV with horizontal curves for the further sensors.

6.4 SUMMARY

This chapter includes the overall evaluation of the RWD and TSD. The performance of both TSDDs varied under different conditions. Based on the results of the analyses presented in this chapter, it was found that both devices were capable of providing reasonably accurate and precise pavement response measurements. The information presented in this chapter can also be used to recommend the optimum operational conditions and to identify device limitations, both of which are addressed in chapter 10 of this report. Conclusions and recommendations within this chapter were limited by the amount of data available for this project.

CHAPTER 7. 3D-MOVE CALIBRATION

7.1 INTRODUCTION

This chapter presents the results of the 3D-Move software calibration using data collected from installed sensors at the MnROAD facility during the September 2013 TSDD field trials. The objective of this calibration was to enable the use of the 3D-Move software in the development of methodologies and/or procedures for incorporating TSDD measurements into network-level PMS applications. This software was chosen because it is ideally suited to evaluate and compare pavement responses measured with TSDDs. It estimates the dynamic pavement responses at any given point within the pavement structure using a continuum-based finite layer approach.

The dynamic pavement surface deflections measured by TSDDs are affected by many factors, which include pavement layer characteristics (e.g., thickness, stiffness, and damping properties), vehicle loading (e.g., tire configuration and contact stress distribution), and vehicle speed. Since rate-dependent (viscoelastic) material properties can be accommodated by 3D-Move, it is an ideal tool to study pavement response as a function of vehicle speed through the direct use of the frequency sweep test data (dynamic modulus and damping) of AC mixture.

The applicability and versatility of the 3D-Move approach has been reported in literature.[35,31] Measured pavement responses with the existing and newly installed geophones and accelerometers during MnROAD trials provided a great opportunity to validate the applicability of 3D-Move due to loading from TSDDs. This chapter focuses on details relating to the 3D-Move calibration effort.

Purpose and Overview of Calibration Effort

One of the major tasks of this project was to simulate pavement surface deflections using numerical models with a focus on understanding the parameters that affect the TSDD measurements. Those parameters include changes in TSDD vehicle speed, pavement layer properties (e.g., age and moisture), and vehicle loading (e.g., tire configuration, load, and inflation pressure). To accomplish this, calibration of the analytical tool that simulates TSDDs was required (i.e., it is critical to verify that the analytical tool and the corresponding software are used correctly to assess pavement responses and that they provide reliable results). Toward this end, calibration of 3D-Move relative to TSDDs was undertaken first, and the calibrated software was subsequently used in the simulations of pavement responses.

As noted earlier in this report, during the September 2013 TSDD field trials, data were collected from the embedded geophones and accelerometers (which were installed as a part of this project) as well as also by the two TSDDs. The measured velocity time histories from the geophones along with the computed displacement time histories (referred to as “project measurements”) are important since they are the basic measurements made by the TSDDs and subsequently used for pavement condition evaluations. In addition, the MnROAD facility had existing sensors (subsequently referred as MnROAD sensors) capable of measuring earth pressures and pavement strain responses under vehicle loading (i.e., dynamic). Those MnROAD sensor data were included in the project database (see section 5.7). The resulting data were used to create a comprehensive database of

independently measured pavement responses (i.e., stresses, strains, and displacements) from different sources, including MnROAD sensors, project sensors, and TSDDs.

The material properties that are appropriate for the conditions (e.g., temperature and moisture) that existed at the time of TSDD trials are critical inputs to 3D-Move. Some pavement layer properties are sensitive to temperature changes, while others are affected by moisture changes. Consequently, some of the TSDD trials were conducted at different times of the day (e.g., early morning and late afternoon). A study of the effects of moisture changes was not possible within the project schedule. Data from FWD testing that was conducted prior to the TSDD field trials were available. An iterative procedure that involved selecting numerous case scenarios where 3D-Move computed responses for a wide range of inputs were compared with those actually measured at the MnROAD facility. The main variables relative to the 3D-Move inputs were the pavement layer configuration and material properties. These material properties must be reasonable and consistent with available data (e.g., FWD measurements). It is important that the appropriate case scenarios should bracket the measured responses in a consistent manner covering all independent measurements (i.e., stresses, strains and displacements).

7.2 3D-MOVE PROGRAM OVERVIEW AND CALIBRATION

The 3D-Move program was developed at UNR to evaluate pavement response. The program can account for important pavement response factors such as the moving traffic-induced complex 3D contact stress distributions (normal and shear) of any shape, vehicle speed, and viscoelastic material characterization for the pavement layers. The finite-layer approach used in the formulation of the program treats each pavement layer as a continuum and uses the Fourier transform technique; therefore, it can handle complex surface loadings such as multiple loads and non-uniform tire pavement contact stress distribution. This approach is suitable to analyze tire imprints of any shape, including those generated by wide-base tires.[32,33,2] The finite-layer method is much more computationally efficient than the moving load models based on the finite element method.[51,52] This is because often times, the pavements are horizontally layered, and pavement responses are required only at a few selected locations. For such problems, the finite layer approach of 3D-Move is ideally suited. The frequency domain solutions along with complex modulus formulation adopted in 3D-Move enables a direct use of the frequency sweep test data of AC mixture in the analysis.

A number of field calibrations (e.g., Penn State University test track, MnROAD, and UNR Off-Road Vehicle study) that compared a variety of independently-measured pavement responses (i.e., stresses, strains, and displacements) with those computed by 3D-Move have been reported in the literature.[35,31] ViscoRoute, which is a semi-analytical dynamic multi-layer model, is currently the only other available software capable of handling loaded areas with uniform contact vertical pressure.[10] It is an ideal program that can be compared with 3D-Move in terms of incorporating viscoelastic properties in its formulation. Hajj et al. compared computed maximum transverse strains by 3D-Move and ViscoRoute at the bottom of thin and thick AC layers.[36] The computed responses were found to be within 6 percent in the 60 cases considered. These verification studies demonstrate the validity, applicability, and versatility of the 3D-Move approach. Since details of 3D-Move are available in the literature, they are not addressed in this report. (See references 35, 31–33, and 2.) However, details concerning the application of 3D-Move to this project (e.g., inputs and response outputs) are presented next.

7.3 MATERIALS CHARACTERIZATION OF MnROAD ACCURACY CELLS

MnROAD Accuracy Cells

Cells 3 and 19 in the MnROAD mainline and cell 34 in the MnROAD LVR were selected to evaluate the accuracy of the TSDDs and hence are referred to as the "accuracy cells." All three cells consisted of AC pavements. As described in chapter 5, each cell was instrumented with four geophones and one accelerometer during the project. These cells were also previously instrumented during construction by MnROAD with sensors such as strain gauges, pressure cells, LVDTs, moisture gauges, TCs, and tipping buckets. In the calibration process, only load-induced measured response values of strains, stresses, and displacements from the referenced sensors at the three accuracy cells were compared with those computed with 3D-Move.

Material Characterization

The characterization of the material properties for the three accuracy cells is an important step in the calibration process.

The required 3D-Move inputs for the surface layer (AC considered viscoelastic) were as follows:

1. Thickness.
2. Unit weight.
3. Dynamic modulus and damping as a function of temperature and frequency.
4. Poisson's ratio.

The required 3D-Move inputs for unbound layers (base and subgrade, which were considered LE) were as follows:

1. Thickness.
2. Unit weight.
3. Resilient modulus.
4. Poisson's ratio.

MnROAD maintains a database containing laboratory and field-testing results on soils, aggregates, asphalt mixtures, asphalt binders, concrete mixtures, and other materials. The database also contains cell-specific information, including layer thickness, type of layers, and cross sections of cells at time of construction and subsequent treatments. Figure 124 shows the pavement structure for the three MnROAD accuracy cells. As shown in table 29, FWD testing was done a few days prior to the TSDD field trials, which facilitated the characterization of existing material properties for the pavement layers in the accuracy cells.

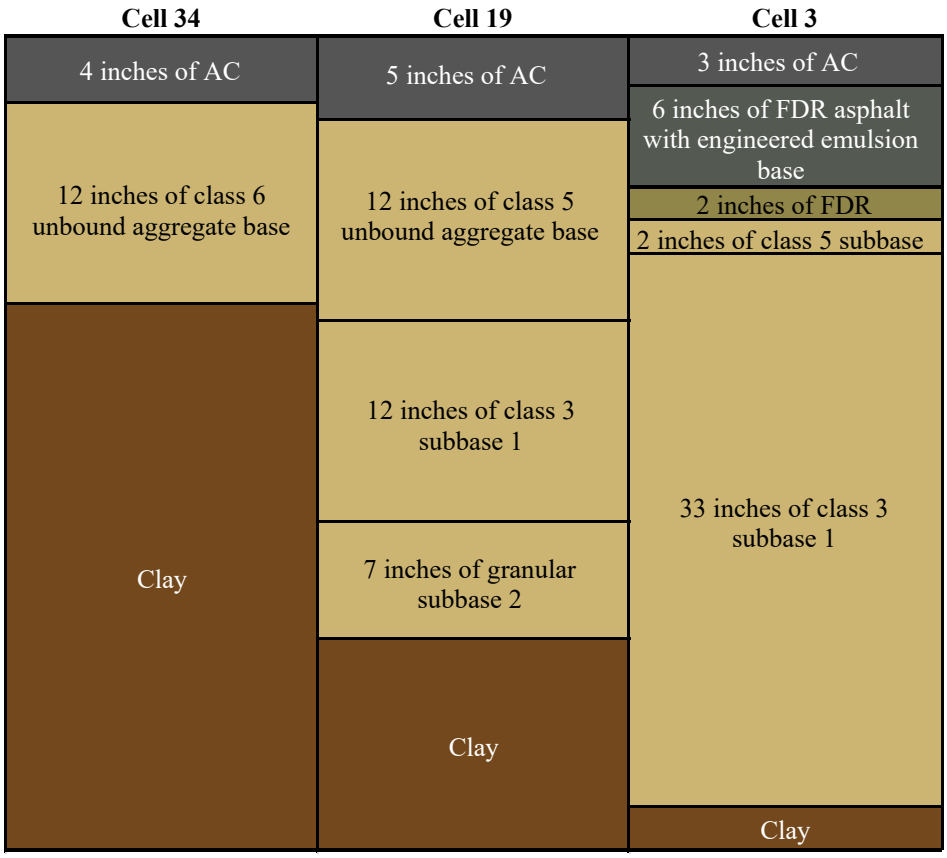

1 inch = 25.4 mm

Figure 124. Illustration. Pavement structure of MnROAD accuracy cells.

Table 29. Date and time of FWD and TSDD testing.

Device	Accuracy Cell Date and Time		
	Cell 3	Cell 19	Cell 34
FWD	9/16/2013 at 2 p.m.	9/20/2013 at 2 p.m.	9/5/2013 at 3 p.m.
TSD	9/26/2013 at 12:30 p.m.	9/26/2013 at 10 a.m.	9/24/2013 at 3 p.m.
RWD	9/23/2013 at 2:30 p.m.	9/23/2013 at 9 a.m.	9/23/2013 at 5 p.m.

Table 30 shows the backcalculated layer moduli for the accuracy cells, which were estimated using the widely used program MODULUS.[53] Other outputs of the program include standard deviation of the backcalculated moduli computed from multiple FWD drop data. These backcalculated moduli may be considered appropriate for the site at the time of FWD testing. The AC layer moduli shown in table 30 had to be adjusted to actual temperature at the time of the TSDD testing for the purposes of the 3D-Move simulations. The procedure used for temperature adjustment is detailed in the subsection, Pavement Material Properties at the Time of TSDD Trials, later in this chapter.

Table 30. Backcalculated moduli of pavement layers for accuracy cells.

Cell	Material	Thickness (inches)	Average Modulus (ksi)	Standard Deviation (ksi)	COV (Percent)
3	AC	3	554	34	14.0
	Base	43	68.8	13.6	19.8
	Subgrade	122.4	17.7	2.2	12.3
19	AC	5	301	65	22.0
	Base	31	32	5.8	18.0
	Subgrade	18.1	6.1	0.6	10.2
34	AC	4	299	67	22.0
	Base	12	15.7	3.1	19.9
	Subgrade	46.3	8.5	0.9	10.2

1 inch = 25.4 mm
1 ksi = 6.89 MPa

The properties of the unbound layers (base and subgrade) were generally unaffected by temperature (as long as there was no freezing), but moisture could play a significant role. However, the FWD and TSDD testing were performed within a short period of each other, and a careful review of climate at the site revealed that no significant changes in moisture (i.e., no rain or snow) occurred. Therefore, the FWD backcalculated moduli for the unbound layers at the three MnROAD accuracy cells were used without adjustments in the 3D-Move runs.

Evaluation of AC Pavement Temperature During FWD Testing

Accurate estimates of the AC layer temperatures at the time of FWD testing were necessary since AC stiffness is significantly affected by temperature. Accordingly, adjustments to the AC stiffness to reflect actual temperatures at the time of TSDD testing were needed. A TC tree device was used for the MnROAD accuracy cells to measure temperature within the pavement layers. A typical MnROAD TC tree is 6 ft (1.83 m) long. Sensor depths were selected during construction to provide a temperature profile within the AC, base, and subbase layers. Table 31 shows the TC sensor depths from the surface at the MnROAD accuracy cells, while table 32 shows the AC layer temperatures recorded by the TC device at the three cells.

Table 31. Depths of TC sensors in accuracy cells.

Cell 3		Cell 19		Cell 34	
Sensor	**Depth (inches)**	**Sensor**	**Depth (inches)**	**Sensor**	**Depth (inches)**
101	**0.5**	**101**	**0.5**	**201**	**0.5**
102	**1.5**	**102**	**1.5**	**202**	**1.6**
103	**2.5**	**103**	**2.5**	**203**	**2.5**
104	3.5	**104**	**3.5**	204	3.5
105	5	**105**	**4.5**	205	7
106	7	106	6	206	9
107	9	107	9	207	11
108	11	108	12	208	13
109	13	109	15	209	15
110	15	110	18	210	20
111	24	111	24	211	24
112	28	112	30	212	30
113	36	113	36	213	36
114	48	114	48	214	48
115	60	115	60	215	60
116	72	116	72	216	72

1 inch = 25.4 mm

Note: Bolded cells indicate the sensors were located within the AC layer.

Table 32. Measured temperature within AC at the time of FWD test.

			Temperature at Location from Surface (ºF)								
Cell	**Day**	**Hour**	**Sensor 101**	**Sensor 102**	**Sensor 103**	**Sensor 104**	**Sensor 105**	**Sensor 201**	**Sensor 202**	**Sensor 203**	**Sensor 204**
3	9/16/13	14	126	93	90	84	N/A	N/A	N/A	N/A	N/A
19	9/20/13	14	84	**	135*	73	72	N/A	N/A	N/A	N/A
34	9/5/13	15	N/A	N/A	N/A	N/A	N/A	**	108	**	**

1 °F = 1.8° C + 32

*Possible incorrect data.

**Missing data.

N/A = Not applicable.

As shown in table 32, there are missing and possibly incorrect data from the MnROAD TC devices. Although AC temperature depth coverage seemed adequate for cell 3, which had the lowest thickness of 3 inches (76.2 mm), coverage in the other cells were not. For example, in cell 19, there are four data points, but one of them (sensor 103) was unreliable. For cell 34, only one data point is available. Accordingly, an alternate robust and defensible approach was adapted to estimate temperatures within the AC layers during FWD testing and also during the TSDD field trials. Towards this end, the BELLS equation was selected for a number of reasons, including its extensive calibration using data from the Long-Term Pavement Performance (LTPP) Program.[40,54]

The BELLS equation was used to predict temperatures within the AC layer for cells 19 and 34 at locations other than those for which field measurements were available. The BELLS equation is given by the following:

$$T_d = 0.95 + 0.892 \times IR + \{\log(d) - 1.25\}\{-0.448 \times IR + 0.621 \times (1\text{-day}) + 1.83 \times \sin(hr_{18} - 15.5)\} + 0.042 \times \text{IR} \times \sin(hr_{18} - 13.5)$$

Figure 125. Equation. BELLS equation.

Where:

T_d = Pavement temperature at depth d.
IR = Pavement surface temperature.
d = Depth at which pavement temperature is to be predicted.
1-day = Average air temperature the day before testing.
hr_{18} = Time of day, in a 24-h clock system, calculated using an 18-h AC and temperature rise-and-fall time cycle**.**

Figure 126 shows the variation of air temperature in Monticello, MN, which is close to the MnROAD facility, during September 2013, which is when the FWD testing and TSDD field trials under consideration took place.

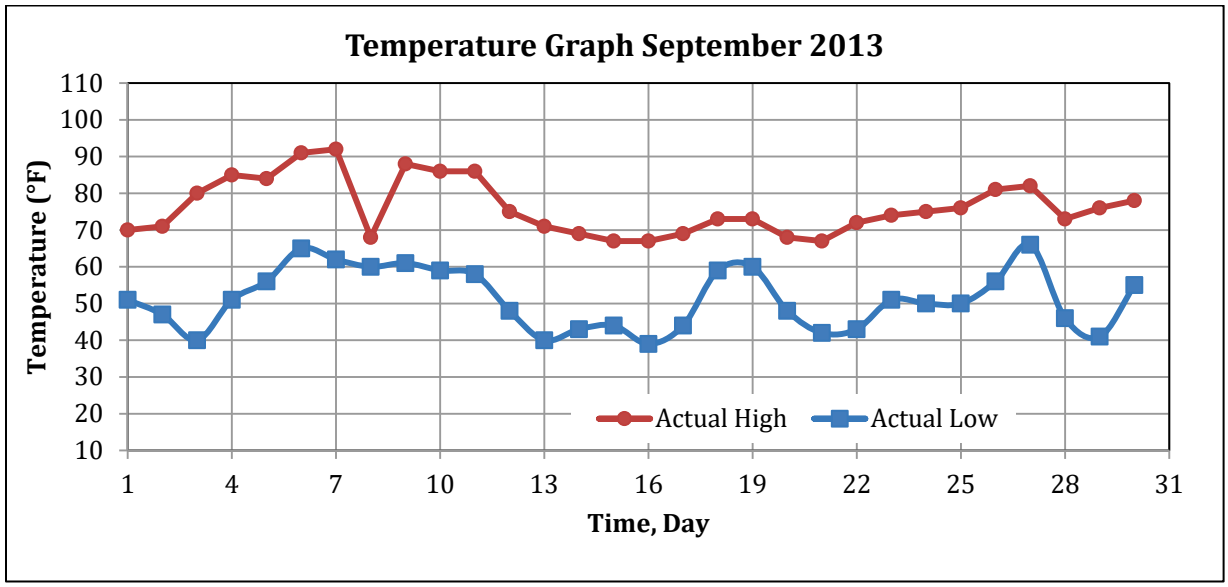

1 °F = 1.8 °C + 32

Figure 126. Graph. September 2013 temperature variations in Monticello, MN.

Figure 126 was used to find the average air temperature of the day before FWD testing, which was 66 °F (18.9 °C) on September 19, 2013, and 69 °F (20.6 °C) on September 4, 2013, for cells 19 and 34, respectively. Appropriate surface temperatures were determined based on the data available from the top-most sensor (sensor 101 in cell 19 and sensor 202 in cell 34) of the TC device and matching the prediction by the BELLS equation. Having estimated the required surface temperatures, the BELLS equation was used to predict the variation of temperature with

depth within the AC layer at both cells in question. Table 33 and table 34 show the estimated temperatures within AC layer for cells 19 and 34 at the time of FWD testing.

Table 33. Temperature within AC from BELLS equation in cell 19 during FWD test.

Matched Surface Temperature (°F)	Time	Depth (inches)	1-Day Temperature (°F)	Temperature from BELLS Equation (°F)
87.3	2 p.m.	0.5	65.5	84.2
	2 p.m.	1.5	65.5	82.4
	2 p.m.	2.5	65.5	80.6
	2 p.m.	3.5	65.5	78.8
	2 p.m.	4.5	65.5	78.8

1 °F = 1.8 °C + 32
1 inch = 25.4 mm

Table 34. Temperature within AC from BELLS equation in cell 34 during FWD test.

Matched Surface Temperature (°F)	Time	Depth (inches)	1-Day Temperature (°F)	Temperature from BELLS Equation (°F)
119.3 (48.5)	3 p.m.	0.5	68.9	116.6
	3 p.m.	1.6	68.9	107.6
	3 p.m.	2.5	68.9	104
	3 p.m.	3.5	68.9	102.2

1 °F = 1.8 °C + 32
1 inch = 25.4 mm

The data presented in table 32 to table 34 were then used to estimate representative average AC layer temperatures at the time of FWD testing for cells 3, 19, and 34, which resulted in temperatures of 99, 81, and 108 °F (37.2, 27.2, and 42.2 °C), respectively.

Pavement Material Properties at the Time of TSDD Trials

The 3D-Move program requires viscoelastic characterization (frequency dependent) of the AC layers to evaluate pavement responses as a function of vehicle speed. Since the TSDD field trials were conducted under different temperature conditions, a master curve approach was adopted so that the AC layer modulus versus frequency relationship could be determined at any given temperature.

The FWD backcalculated AC layer modulus was appropriate for the temperature at the time of testing and a loading frequency of about 30 Hz.[55] Using this AC layer modulus and frequency as an anchoring point, the AC master curve (i.e., modulus versus frequency) could be established.

The first step in the development of the AC master curves was determining the representative AC layer temperatures during TSDD testing. The same procedure used to determine the AC layer temperatures during FWD testing was used to estimate the average AC layer temperatures during TSDD testing. Table 35 summarizes the average AC layer temperatures at the time of FWD and TSDD testing.

Table 35. Average temperatures within AC layer.

Cell	Temperature at Time of FWD Testing (°F)	Temperature at Time of TSD Testing (°F)	Temperature at Time of RWD Testing (°F)
3	99	91	99
19	81	68	63
34	108	91	90

1 °F = 1.8 °C + 32

Using the average AC layer temperature, damping was estimated using dynamic modulus test data available in the MnROAD database. In those tests, the phase angels of the AC layer at several temperatures and frequencies were measured. In its complex form, the dynamic modulus is given by the following:

$$E^* = E'(1+2i \times \zeta_{AC})$$

Figure 127. Equation. Complex dynamic modulus.

Where:

E^* = Complex dynamic modulus.
E' = Elastic (or storage) modulus.
i = Unit imaginary number.
ζ_{AC} = Measure of internal damping of AC.

For viscoelastic layers, E^* can be presented as the sum of the real and imaginary components, which is given by the following:

$$E^* = E' + iE''$$

Figure 128. Equation. Modified modulus equation.

Where:

E'' = Damping (or loss) modulus.

The equations may be re-written as follows:

$$\zeta_{AC} = E''/(2E') = 0.5 \tan(\varphi)$$

Figure 129. Equation. Rewritten modulus equation.

Where:

φ = Phase angle.

Table 36 and table 37 show the values of damping associated with the TSDD field trials. The procedure used to obtain these values consisted of fitting a best curve through the available AC dynamic modulus test (phase angle measured at given frequencies) results and then interpolating the phase angles for the temperature corresponding with the TSDD field trials.

Table 36. Phase angle and damping for accuracy cells for TSD field trials.

Cell 3 (91 °F)			Cell 19 (68 °F)			Cell 34 (91 °F)		
Frequency (Hz)	Phase Angle (Degree)	Damping (Percent)	Frequency (Hz)	Phase Angle (Degree)	Damping (Percent)	Frequency (Hz)	Phase Angle (Degree)	Damping (Percent)
0.1	36.3	36.8	0.1	34.2	33.9	0.01	29.0	27.8
0.5	36.7	37.3	0.5	26.4	24.8	0.1	32.0	31.2
1	36.2	36.6	1	23.7	21.9	1	31.6	30.7
5	33.2	32.7	5	19.1	17.3	25	27.6	26.1
10	34.4	34.2	10	16.9	15.1	N/A	N/A	N/A
25	31.6	30.7	25	13.5	11.9	N/A	N/A	N/A

1 °F = 1.8 °C + 32
N/A = Not available.

Table 37. Phase angle and damping for accuracy cells for RWD field trials.

Cell 3 (99 °F)			Cell 19 (63 °F)			Cell 34 (90 °F)		
Frequency (Hz)	Phase Angle (Degree)	Damping (Percent)	Frequency (Hz)	Phase Angle (Degree)	Damping (Percent)	Frequency (Hz)	Phase Angle (Degree)	Damping (Percent)
0.1	36.8	37.4	0.1	32.7	32.1	0.01	29.7	28.5
0.5	36.6	37.2	0.5	22.6	20.8	0.1	33.0	32.4
1	36.4	36.9	1	19.4	17.6	1	32.5	31.9
5	34.7	34.6	5	15.4	13.7	25	28.0	26.5
10	36.7	37.2	10	12.4	10.9	N/A	N/A	N/A
25	34.6	34.5	25	9.4	8.3	N/A	N/A	N/A

1 °F = 1.8 °C + 32
N/A = Not available.

Undamaged Modulus of AC Layer:

The procedure used to develop the appropriate AC master curves took into account the following considerations:

- Undamaged AC modulus as determined from Witczak's equation.(56)
- FWD backcalculated modulus (in situ or existing modulus).
- Existing modulus correction approach (fatigue damage factor) used in the MEPDG overlay design.(57)

One of the most comprehensive AC mixture stiffness models is Witczak's dynamic modulus predictive equation. This model predicts modulus as a function of temperature and frequency based on volumetric AC mix design information. The Witczak-Andrei AC dynamic modulus equation is given by the following:(56)

$$\log E^* = -1.25 + 0.029\rho_{200} - 0.0018(\rho_{200})^2 - 0.0028\rho_4 - 0.058V_a - 0.822\frac{V_{beff}}{V_{beff} + V_a} + \frac{3.872 - 0.0021\rho_4 + 0.003958(\rho_{38}) - 0.000017(\rho_{38})^2 + 0.0055\rho_{34}}{1 + e^{(-0.603313 - 0.313351\log(f) - 0.393532\log(\eta))}}$$

Figure 130. Equation. Witczak equation.

Where:

ρ_{200} = Percent passing #200 (0.075 mm) sieve.
ρ_4 = Cumulative percent retained on #4 (4.76 mm) sieve.
ρ_{38} = Cumulative percent retained on 0.375-inch (9.5 mm) sieve.
ρ_{34} = Cumulative percent retained on 0.75-inch (19 mm) sieve.
V_a = Air void, percent by volume.
V_{beff} = Effective binder content, percent by volume.
e = Euler's number.
f = Loading frequency, Hz.
η = Viscosity (cP).

The Witczak equation requires input such as gradation and viscosity. The gradation data for the three MnROAD accuracy cells were available from the MnROAD database, while viscosity values were estimated as a function of temperature based on the regression intercept, *A*, and the regression slope of viscosity temperature susceptibility (VTS) as shown in figure 131.[58]

$$\log\log\eta = A + VTS \times \log T_R$$

Figure 131. Equation. Temperature-viscosity relationship.

Where:

A = Regression intercept.
T_R = Temperature at which the viscosity is estimated (Rankine).

AASHTO T315-10 gives guidelines for calculating *A* and *VTS*.[59] The dynamic shear rheometer test results are available in the MnROAD databases for the three cells under consideration. The performance grade (PG) for these cells, which were estimated from available data, are PG 70-16, PG 64-22, and PG 58-34 for cells 3, 19, and 34, respectively. Accordingly, the calculated *A* and *VTS* values were 10.641 and -3.548 for cell 3, 10.98 and -3.68 for cell 19, and 10.149 and -3.359 for cell 34.

Having determined the *A* and *VTS* values, the equation given in figure 130 was used to estimate the undamaged AC modulus as a function of temperature and frequency. The next step entailed the derivation of the existing AC modulus at various frequencies and at the AC layer temperature corresponding to the time of the TSDD testing based on the FWD backcalculated layer moduli. This step is explained next.

Obtaining Existing AC Modulus for Use with 3D-Move:

The existing AC moduli as a function of frequency was estimated by using the backcalculated AC layer moduli as anchor points and shifting the Witczak-derived AC modulus relationships as shown in figure 132. In this figure, E_{NDT} and t_r are the AC modulus and reduced time from the non-destructive testing (NDT), respectively. E_{PRED} is the AC modulus from the prediction equation and δ is the minimum AC modulus.

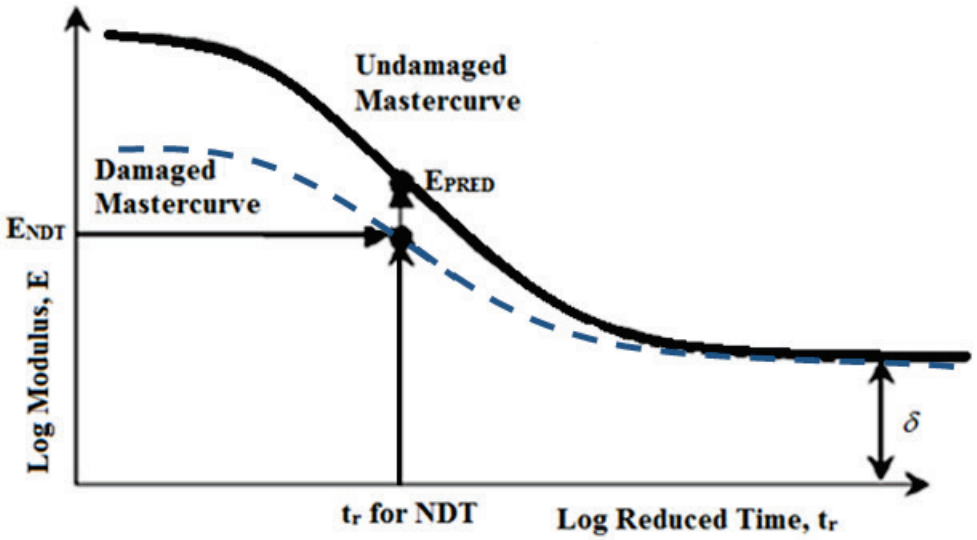

Figure 132. Graph. Development of existing AC modulus master curves from undamaged AC moduli.

The AC existing modulus master curve was obtained by applying the following equation to E^* computed from the original master curve:

$$E^*_{dam} = 10^{\delta} + \frac{E^* - 10^{\delta}}{1 + e^{-0.3+5\times\log(d_{AC})}}$$

Figure 133. Equation. Existing modulus equation.

Where:

E^*_{dam} = Existing modulus.
δ = Regression parameter (from master curve), it is also the minimum AC modulus.
d_{AC} = Fatigue damage in AC layer.

As stated earlier, the AC moduli obtained from the backcalculation of FWD deflection data reflect the temperatures at the time of FWD testing as well as for a frequency of about 30 Hz. Figure 132 illustrates the procedure used to derive the AC existing modulus master curves from the undamaged AC moduli.

Accordingly, using Witczak's equation and taking into consideration the fatigue damage factor, a reasonable AC modulus master curve can be generated. Moreover, this approach is similar to that proposed by Seo et al.[60]

AC Master Curves During TSDD Field Trials:

AC modulus master curves for the three MnROAD accuracy cells were developed using the procedure described in the previous subsection. Figure 134 through figure 136 show the resulting master curves for the temperatures associated with the TSDDs field tests. These curves appear realistic, with smooth variation in both the low and high frequencies. Hence, they were used as input to 3D-Move.

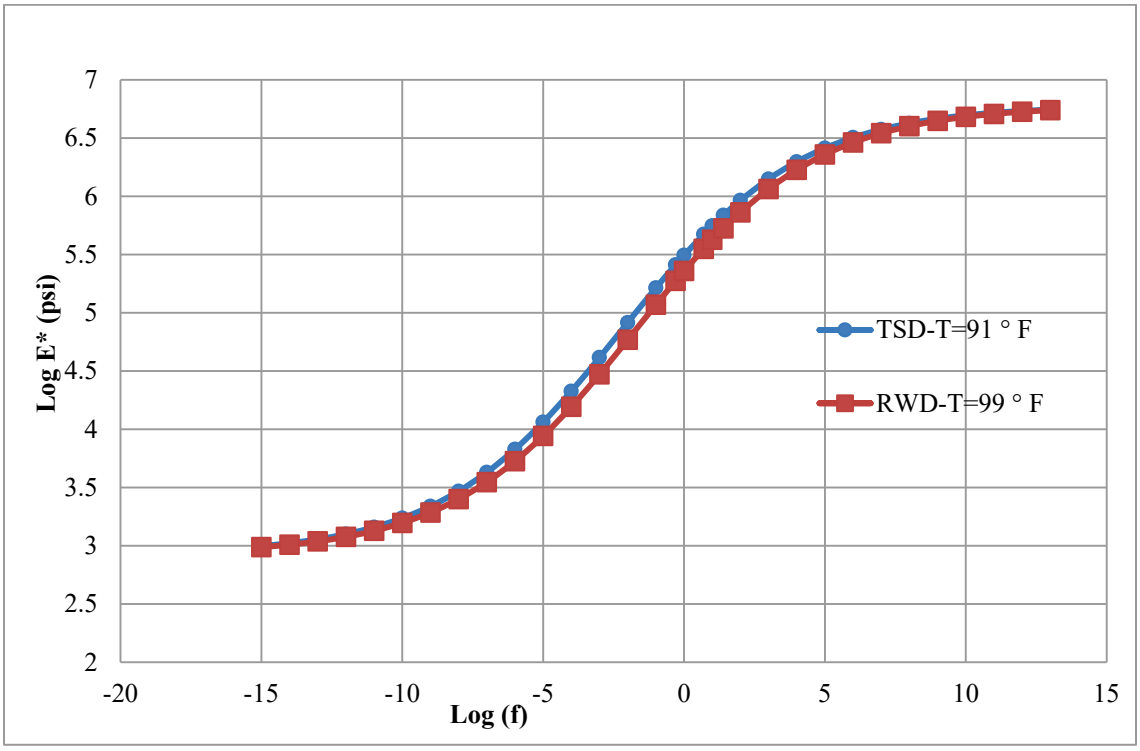

1 psi = 6.89 kPa
1 °F = 1.8 °C + 32

Figure 134. Graph. Master curves for cell 3 in TSDD field trials.

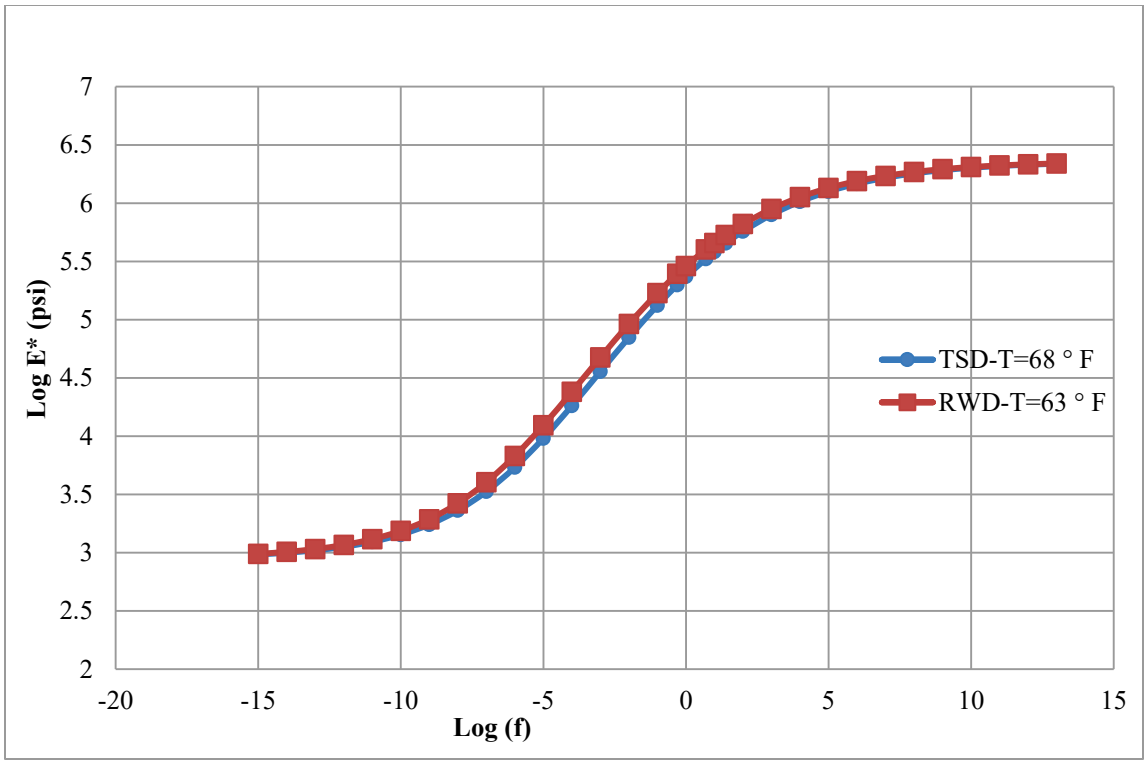

1 psi = 6.89 kPa
1 °F = 1.8 °C + 32

Figure 135. Graph. Master curves for cell 19 in TSDD field trials.

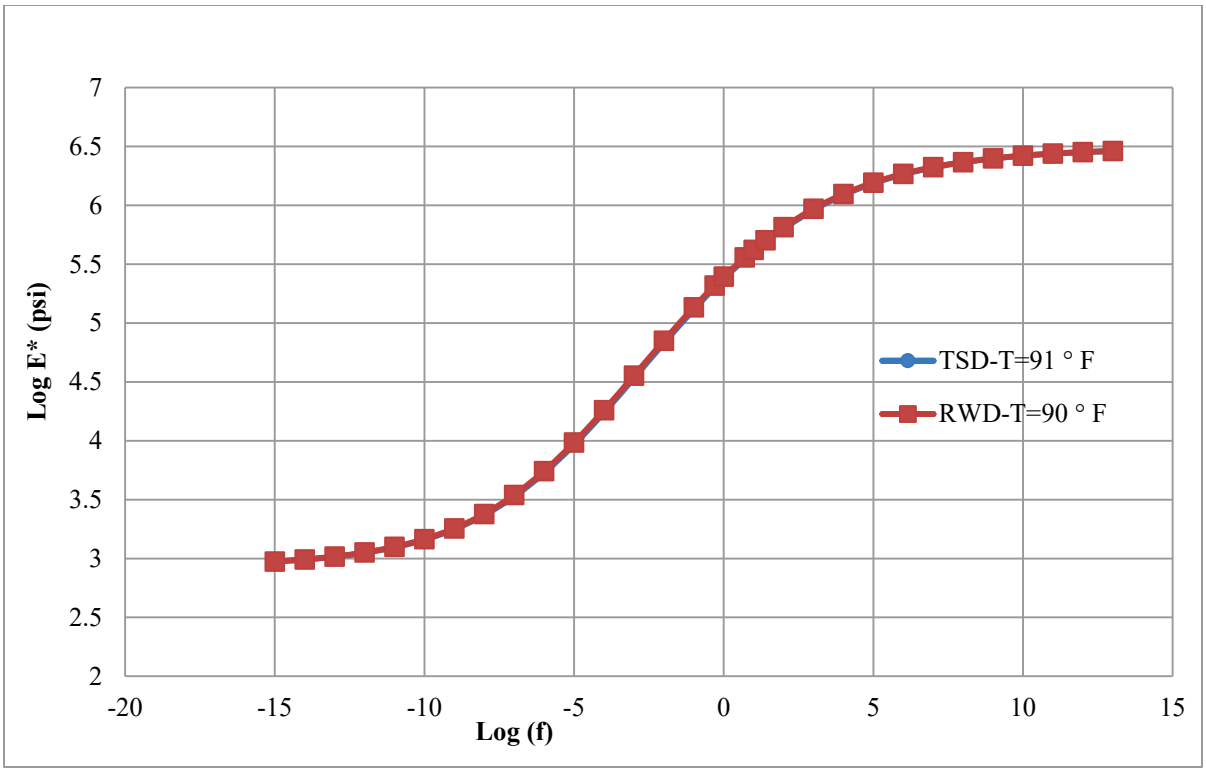

1 psi = 6.89 kPa
1 °F = 1.8 °C + 32

Figure 136. Graph. Master curves for cell 34 in TSDD field trials.

Summary

This section detailed the procedure that was used to obtain the pavement layer material properties, including viscoelastic characterization of the AC layers. The procedure relied on three data sources for estimating material properties: (1) laboratory testing, which included inspection, sampling, and testing data for various pavement materials used at MnROAD; (2) MnROAD cell specifications, which included layer thickness and type of layers; and (3) FWD deflection test results, which were done a few days before the TSDD field trials. Accordingly, it was possible to estimate the existing material layer properties for the three MnROAD accuracy cells. For unbound materials, layer moduli backcalculated from the FWD deflection measurements (see table 30) were used without modification. Table 38 presents the values used in 3D-Move for the unbound layers properties.

Table 38. Unbound layer properties used in 3D-Move.

Cell	Layer	Modulus (ksi)	Thickness (inches)	Poisson's Ratio	Unit Weight (pcf)	Damping Ratio (Percent)
3	Base	68.8	43	0.35	105	5
	Subgrade	17.7	122.4	0.4	105	5
19	Base	32	31	0.35	105	5
	Subgrade	6.1	18.1	0.4	105	5
34	Base	15.7	12	0.35	110	5
	Subgrade	8.5	46.3	0.4	110	5

1 ksi = 6.89 MPa
1 inch = 25.4 mm
1 pcf = 16 Kg/m^3

Table 39 provides the AC layer moduli corresponding to the temperature at the time of the TSDD field trials at frequency of 30 Hz, where standard deviation was obtained from MODULUS backcalculation shown in table 30.

Table 39. AC modulus at the time of TSDD trials for frequency of 30 Hz.

Parameter	Device	Cell 3	Cell 19	Cell 34
Average AC temperatures, °F	RWD	99	63	90
	TSD	91	68	91
Existing modulus at *f* = 30 Hz (mean), ksi	RWD	554	550.1	522
	TSD	716.8	468.5	506.5
Existing modulus at *f* = 30 Hz (mean minus standard deviation), ksi	RWD	520	431.2	404.9
	TSD	672.8	367.2	392.9

1 °F = 1.8° C + 32
1 ksi = 6.89 MPa

7.4 LOADING CHARACTERISTICS OF TSDDs

Characterization of the applied load is an important input for analyzing pavement structures. During the TSDD field trials, the loads carried by the axles were determined using a static scale owned and operated by MnROAD. Details concerning the axle configuration and contact pressure distribution of the TSD and RWD are presented next.

Because the weights of the devices were measured using a static scale, the 3-D Move results should be used with caution when simulating moving vehicles. Figure 137 illustrates the variation in the rear trailing axle load for a five-axle truck semitrailer traveling 25–30 mi/h (4.25–48.3 km/h). The dynamic load could vary by as much as 33 percent of the static load. This suggests that the variation of axle load, which has a direct influence on the computed deflection response, should be addressed.

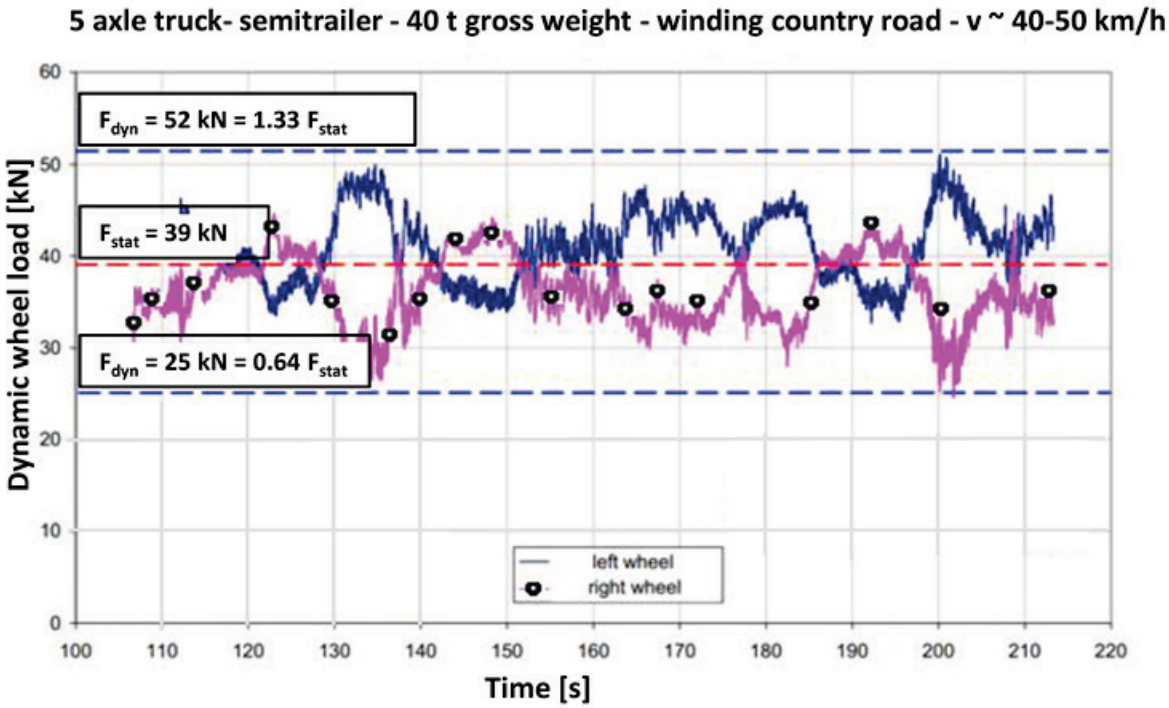

1 mi/h = 1.61 km/h
1 lbf = 0.0044 kN

Figure 137. Graph. Variation of five-axle truck semitrailer.[61]

Axle Configurations and Contact Pressure Distribution

Figure 138 shows TSD axle configuration and axle loads, while figure 139 shows RWD axle configuration and axle loads. Since the deflection measuring sensors for the two TSDDs were mounted close to the dual tire of the rear trailing axles (shown in red box in the figures), the 3D-Move comparisons in this calibration effort focused on the responses generated by those axles. Because data on the pavement-tire contact pressure distribution were not available, the rear axles were modeled as dual circular loads with uniform contact pressure in the 3-D Move analyses. Based on the information presented in figure 137, the static loads measured with the two TSDDs were increased by 25 percent in two 3D-Move scenarios to explore the impact of axle load variations caused by the dynamic interaction with pavements.

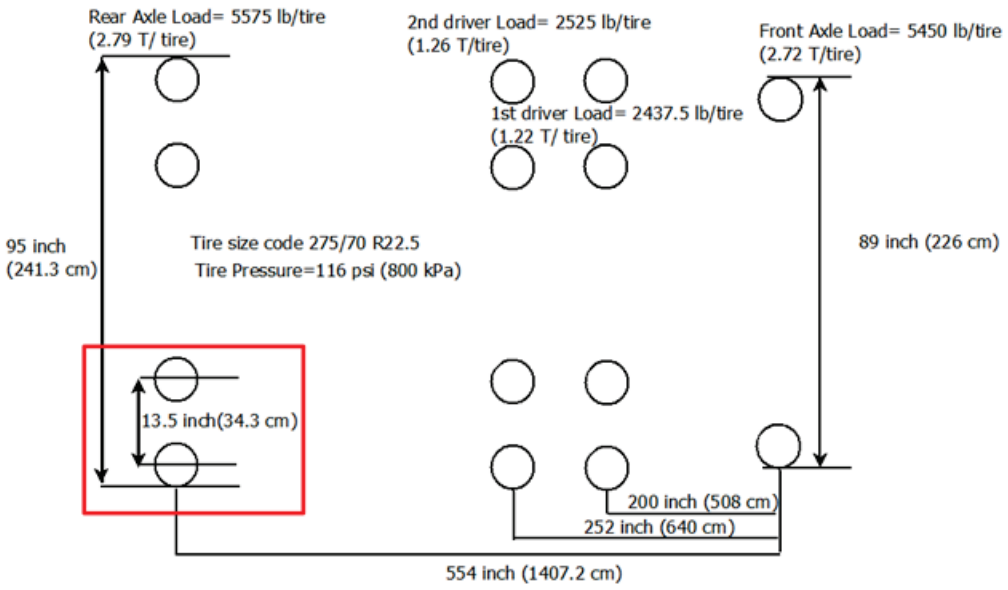

1 inch = 25.4 mm
1 T = 0.907 Mg
1 lb = 0.454 kg
1 psi = 6.89 kPa

Figure 138. Illustration. TSD axle configuration and loads.

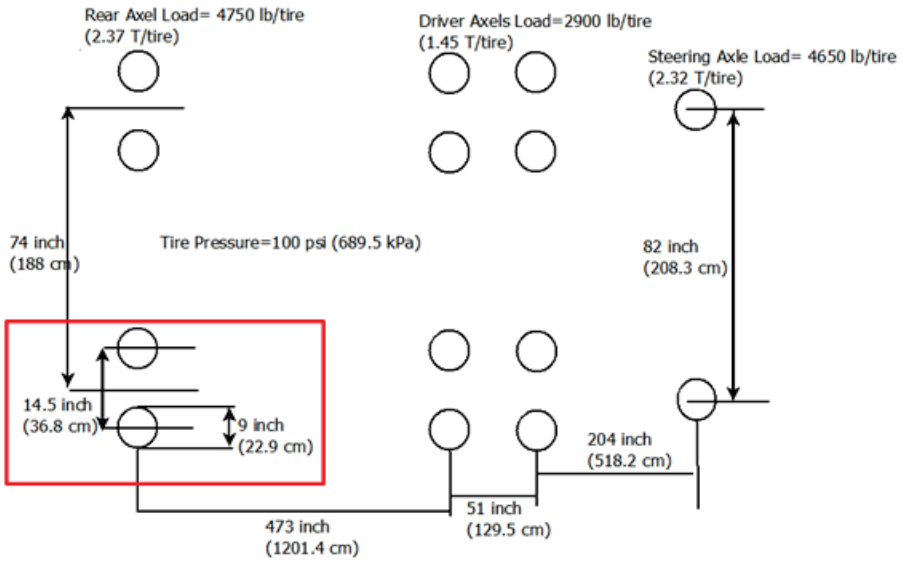

1 inch = 25.4 mm
1 T = 0.907 Mg
1 lb = 0.454 kg
1 psi = 6.89 kPa

Figure 139. Illustration. RWD axle configuration and loads.

7.5 3D-MOVE CALIBRATION USING PROJECT SENSOR DATA

Project Sensors

As discussed in chapter 5, four geophones and one accelerometer were installed near the pavement surface at each of the MnROAD accuracy cells. Since the measurement sensors for both TSDDs were located along the midline of the rear axle tires, two geophones (GEO 1 and GEO 3) were located along this midline plane, as shown in figure 140. To estimate the lateral wheel location relative to installed sensors, two video cameras were also used to record each pass of the TSDDs. A laser trigger device was also installed across the travel lane (transverse plane) for timing purposes. The location of the rear wheels relative to the location of the maximum displacement (i.e., lag distance) could be determined by superimposing the data from the laser device and measured displacement bowls. As noted in chapter 5, the geophone data were filtered and analyzed to arrive at the final surface deflection data. The TSDD field trials were conducted at various vehicle speeds, as summarized in table 40**.** Figure 141 provides a sketch of the pavement sections and average FWD backcalculated layer moduli and the standard deviation of cells 3, 19, and 34. These pavement structures represent pavements with AC thickness varying from 3–5 inches (76.2–127 mm) and a base thickness varying from 12–43 inches (304.8–1,092.2 mm).

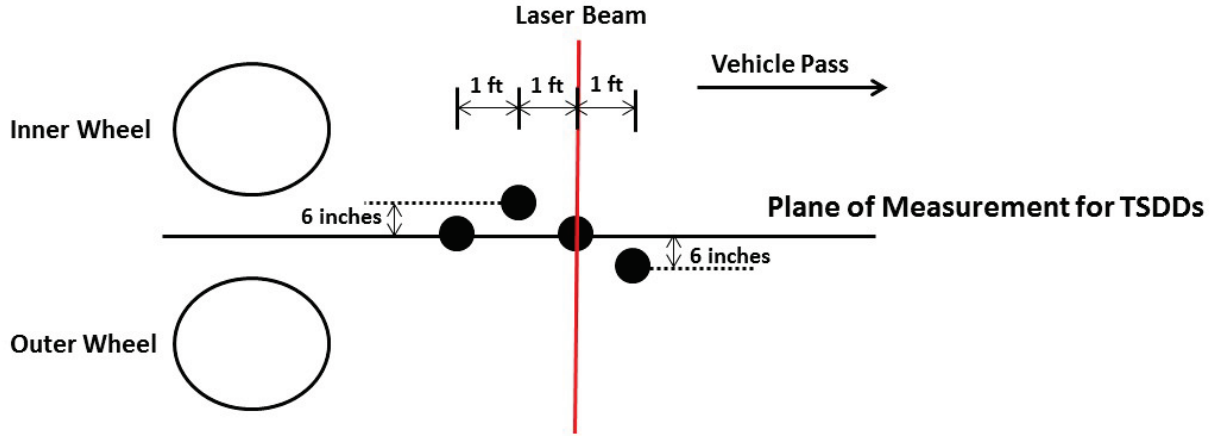

1 inch = 25.4 mm
1 ft = 0.305m

Figure 140. Illustration. Configuration and spacing of embedded project sensors.

Table 40. TSDD accuracy runs at MnROAD.

Cell	TSDD	Velocity (mi/h)
3	TSD	30 and 45
	RWD	30, 45, and 60
19	TSD	30, 45, and 60
	RWD	30, 45, and 60
34	TSD	30 and 45
	RWD	30 and 45

1 mi/h = 1.61 km/h

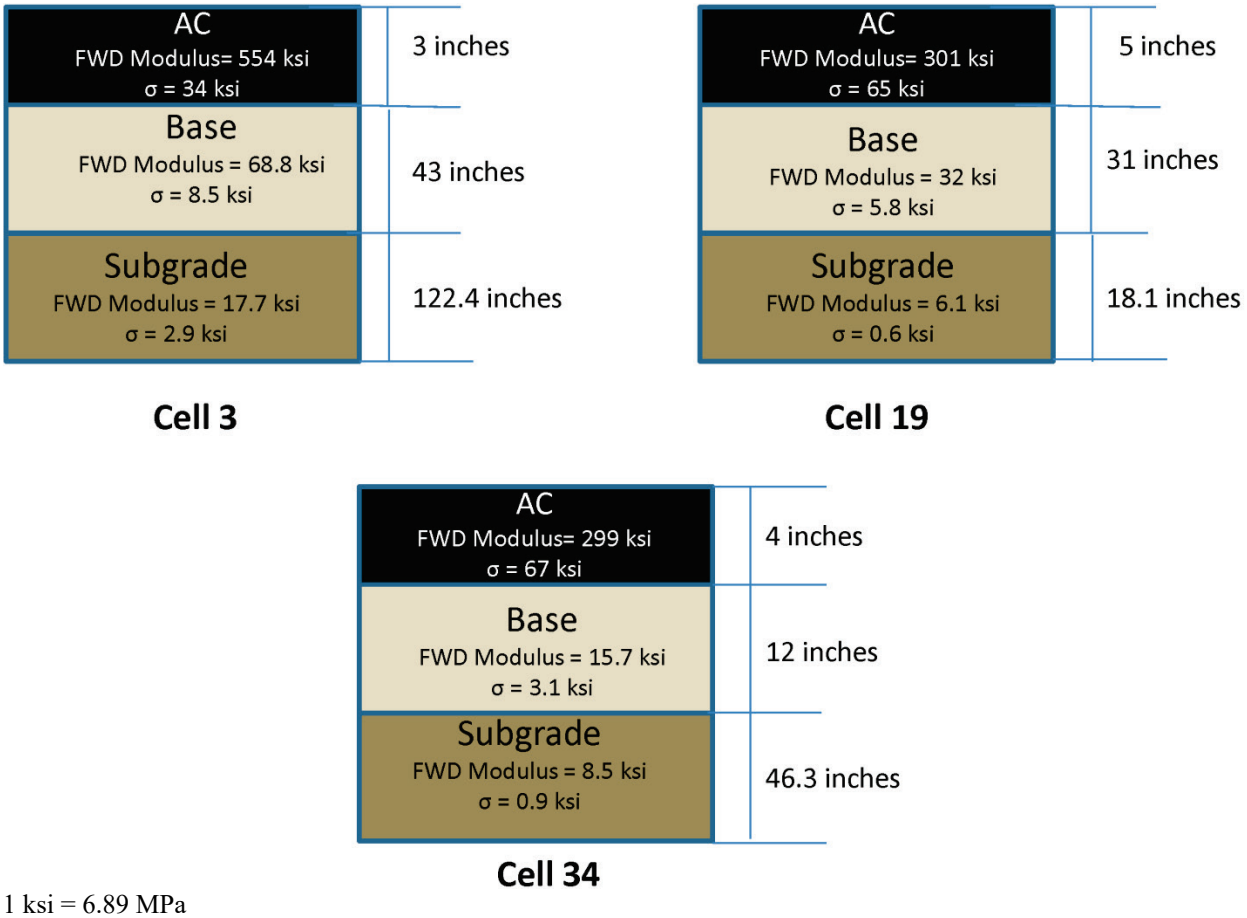

1 ksi = 6.89 MPa
1 inch = 25.4 mm
σ = Standard deviation.

Figure 141. Illustration. Sketch of pavement structures used for cells 3, 19, and 34.

Case Scenarios for 3D-Move to Bracket the Project Sensor Results

Initial attempts revealed that surface displacements computed from the 3D-Move analyses with mean tire loads and material properties did not match well with those given by the project sensors. The 3D-Move displacement basins were wider and of a smaller magnitude for all three accuracy cells and passes. Many possible factors might have contributed to this. They include the following:

- **Transverse wheel wander**: While it was hoped that the TSDDs would operate such that the midline of the rear axle tires coincided with the plane of the project sensor measurements (i.e., plane of GEO 1 and GEO 3 in figure 140), this might not have happened. The interaction between the rear axle tires plays a role, such that wheel wander could result in either higher or lower measured deflection data depending on the extent of the wheel wander. The 3D-Move program is capable of providing the dispalcement basin as a fuction of wheel wander (i.e., at various wheel locations). Since precise location of the midline relative to the plane of measurement was not available, it was decided to use only the maximum possible displacement given by 3D-Move. Therefore, it was expected that the deflection bowls given by 3D-Move would be wider.

- **Material properties**: As noted earlier, the pavement layer moduli and subgrade thickness used as input into 3D-Move were based on FWD backcalculated values. The backcalculation process assumes static loading conditions, and the results of the backcalculation are sensitive to small variations in input (e.g., thickness of AC and base layers). Geology in the area suggests that the subgrade thickness at the accuracy cell locations were substatially greater than those that were predicted from the backcalculation effort. In addition, the viscoelastic characterization used for the AC layers was based on undamaged moduli determined using Witczak's equation as well as by shifting the master curve to get the AC modulus versus frequency relationship for the existing pavements. The damping characteristics of the AC material were determined based on laboratory tests done on fresh AC samples. These steps have limitations, especially their applicability to aged AC layers (more than 5 years old) present at the sites is questionable. A possible solution to address this issue is that 3D-Move analyses should consider changes to material properties and layer thicknesses when comparisons are made.

- **Variation in axle load**: As noted earlier, the axle loads were measured under static conditions, but these loads were expected to vary during operation at high speeds. It was shown in figure 137 that the five-axle truck semitrailer wheel load variations could be as high as 33 percent when moving across a pavement. To account for these variations in tire load under moving conditions, adjustments to the tire loads used in the 3D-Move runs were considered.

Accordingly, after an extensive trial and error process, acceptable bracketing of the measured deflection responses was obtained with the following three 3D-Move case scenarios:

- **Case 1**: Three-layer pavement structure with same thicknesses as used in the FWD backcalculation and corresponding mean layer moduli derived from the FWD backcalculation results.

- **Case X**: Three-layer pavement with: (1) thicknesses used in the FWD backcalculation except decreasing the AC layer thickness by 1 inch (25.4 mm); (2) (mean – standard deviation) of FWD backcalculated layer moduli for AC and base layers; (3) (mean + standard deviation) of FWD backcalculated layer moduli for subgrade; and (4) +25 percent of nominal tire load.

- **Case X1**: Same as case X, but with no reduction in AC layer thickness. This case was used for cells 3 and 34, which had the thinner AC thickness.

Case X was only used for cell 19 to bracket the measured values. As is shown later in this chapter, the 3D-Move predictions based on the above three scenarios bracketed well the measured responses (stresses, strains, and displacements) collected by the project and MnROAD sensors as well as with those measured by TSDDs.

3D-Move Results for Accuracy Runs

The results from the analyses with 3D-Move using the case scenarios described in the previous section were initially compared with the measured values from the project sensors. TSDD measurements were also included in the comparisons. It should also be noted that TSD provided surface velocities at six points ahead of the wheels, while RWD measured displacement at two points.

Figure 142 illustrates the comparison of 3D-Move results and measured deflections for cell 34 based on testing done by the TSD at a vehicle velocity of 30 mi/h (48.3 km/h). Since the main focus is the comparison of the deflection bowls (shape and maximum value), the plots were shifted to align so that the maximum displacement locations coincided. Since GEO 1 and GEO 3 are located along a plane parallel to the vehicle direction, they were expected to have similar deflection bowls. Therefore, the responses from these two sensors are shown in the figure. The variation between the deflection bowls given by these two sensors may be viewed as a measure of the overall variability in the measurements made by the project sensors and possibly any spatial variability between 2 ft (0.61 m) of distance between geophones (figure 140). The lower and upper bound of the project sensor data were determined by treating GEO 1 and GEO 3 data as independent datasets in figure 142 and figure 143. In all cases, 3D-Move adequately captured the maximum and shape of measured displacements. Case X1 provided the closest deflection basin to that measured. Figure 143 compares predicted and measured TSD surface velocities (maximum from field trials). While all 3D-Move case results had similar shapes as the measured ones, the case X1 predictions were closer to both project sensors and TSD measurements.

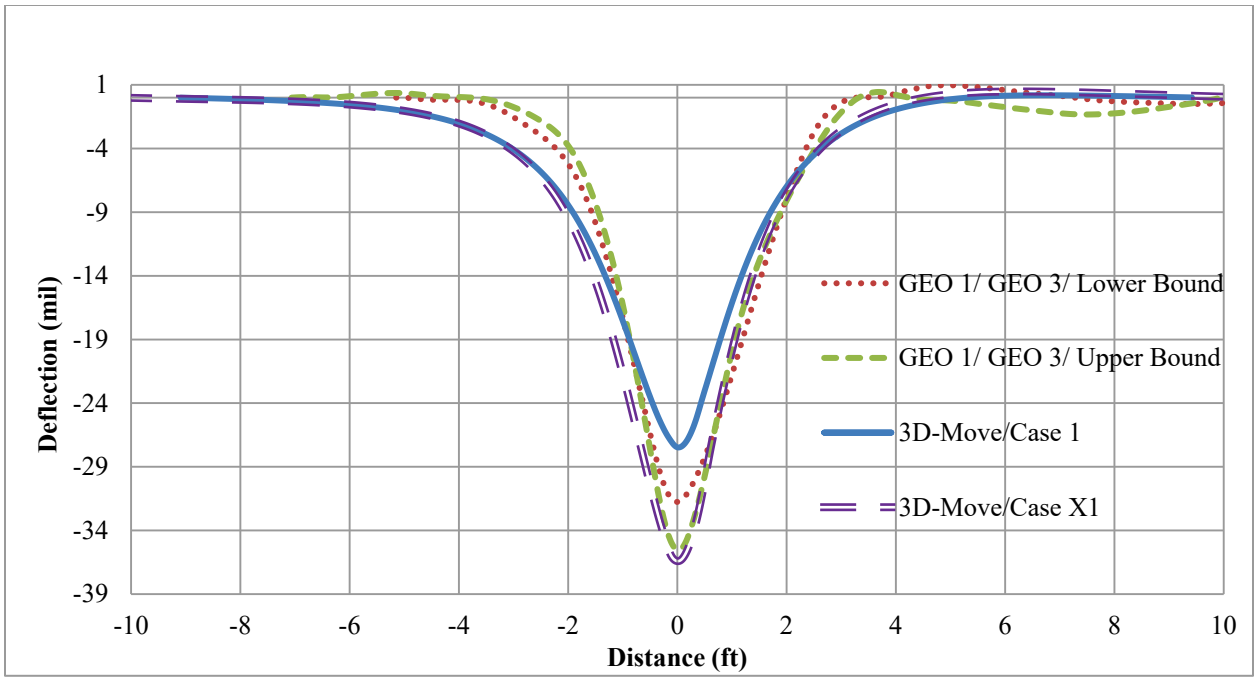

1 mil = 0.025 mm
1 ft = 0.305 m

Figure 142. Graph. 3D-Move predictions and measured deflections for cell 34 in TSD trials (device velocity = 30 mi/h (48.3 km/h)).

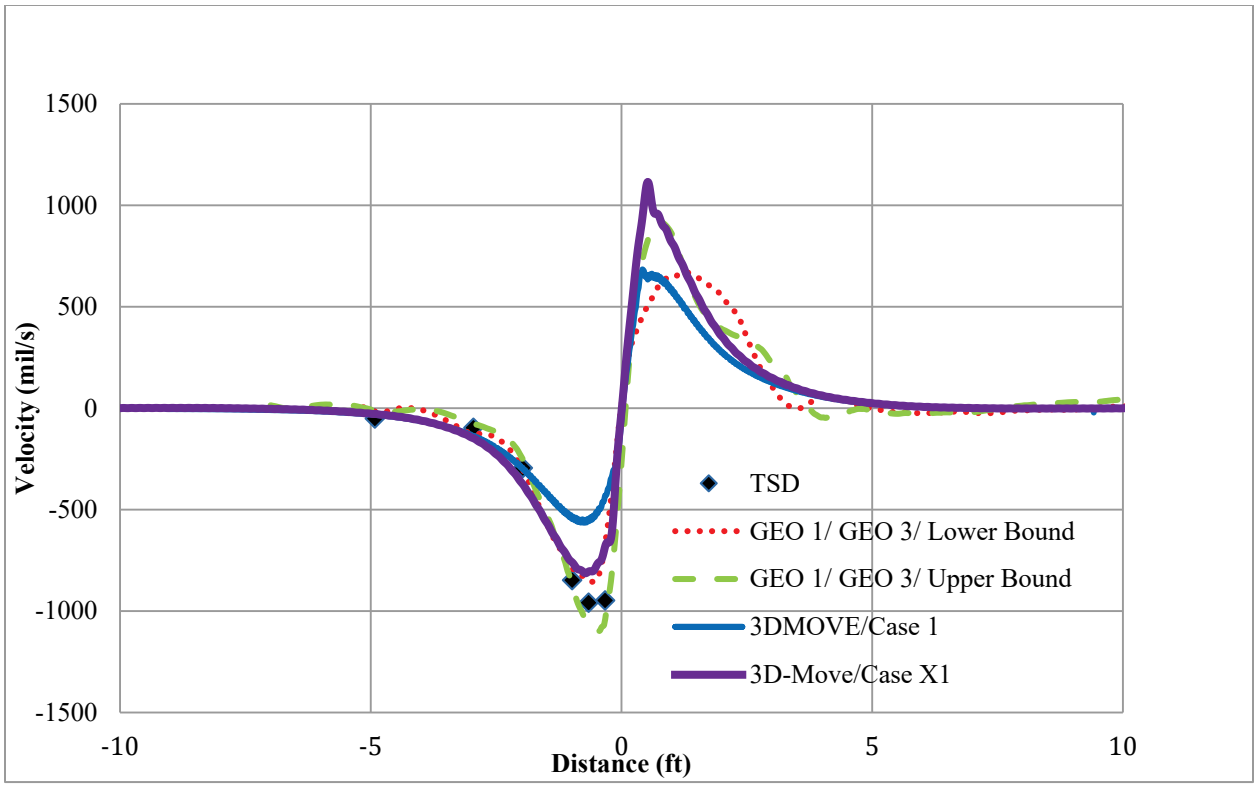

1 mil/s = 0.0254 mm/s
1 ft = 0.305 m

Figure 143. Graph. 3D-Move predictions and measured velocities for cell 34 in TSD trials (device velocity = 30 mi/h (48.3 km/h)).

To compare the shapes of the computed and measured basins, normalized deflection basins were used. This was done by dividing each deflection basin by its maximum value. Figure 144, which shows normalized basins, reveals that the differences in shape among the computed and measured deflection basins were small. A comparison between the normalized basins can be achieved by using the widths of the deflection basins at three levels as shown in figure 145. Figure 146 shows the comparison of the pulse widths at various levels of normalized deflection. This figure shows that 3D-Move produced comparable normalized deflection basins. Similar plots were developed for all possible combinations of TSDD speeds and accuracy cells, and they showed the same trends as shown in the example figures (i.e., figure 144 and figure 146 through figure 150) included within this chapter. The data used to generate all of these figures may be obtained directly from FHWA.

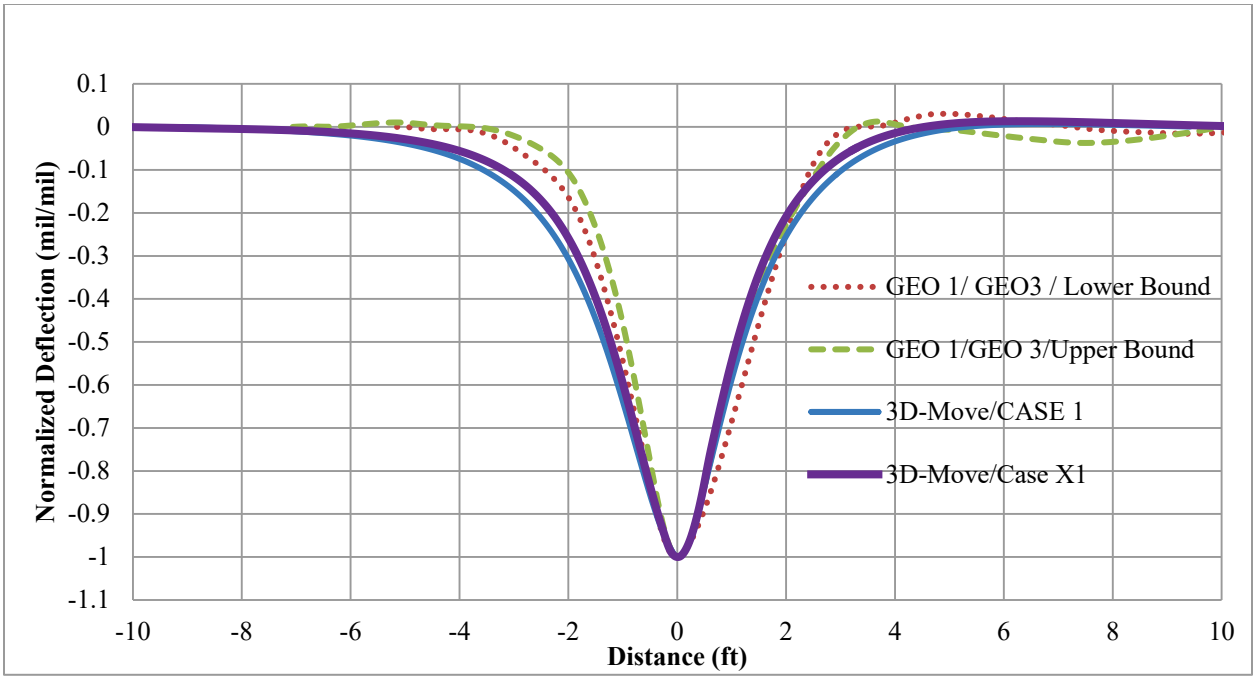

1 mil/mil = 1 mm/mm
1 ft = 0.305 m

Figure 144. Graph. Normalized basins of 3D-Move predictions and measured deflections for cell 34 in TSD trials (device velocity = 30 mi/h (48.3 km/h)).

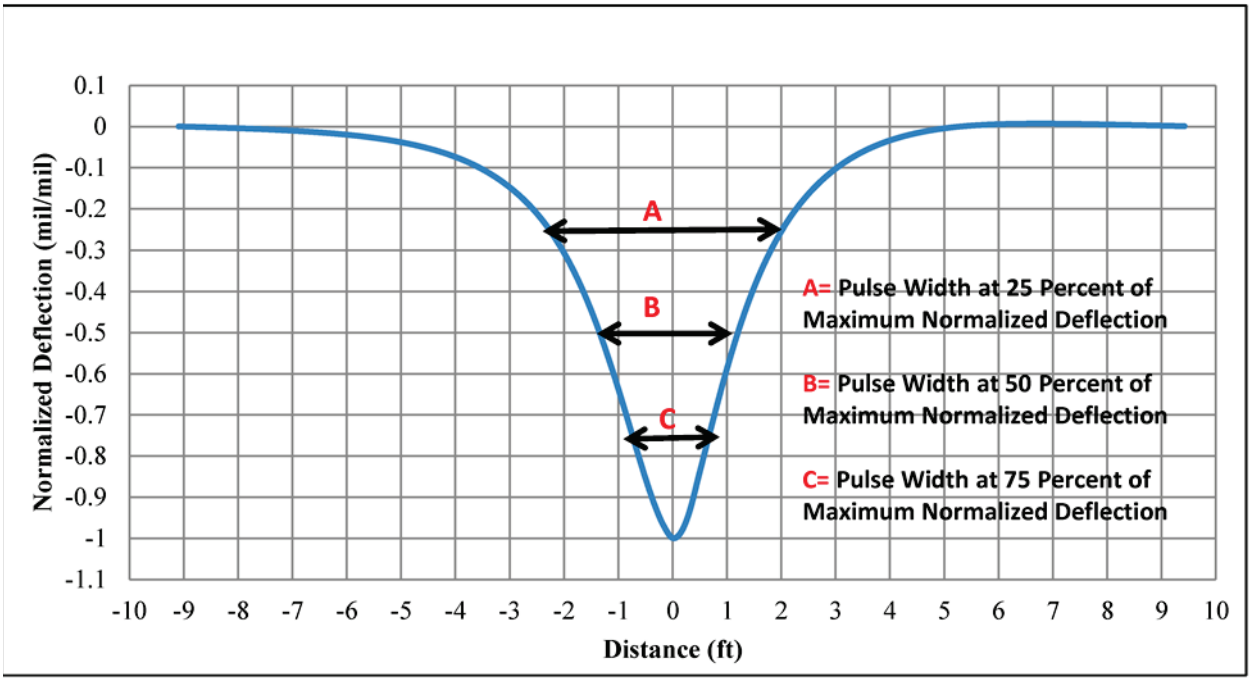

1 mil/mil = 1 mm/mm
1 ft = 0.305 m

Figure 145. Graph. Definition of percentage of maximum displacement.

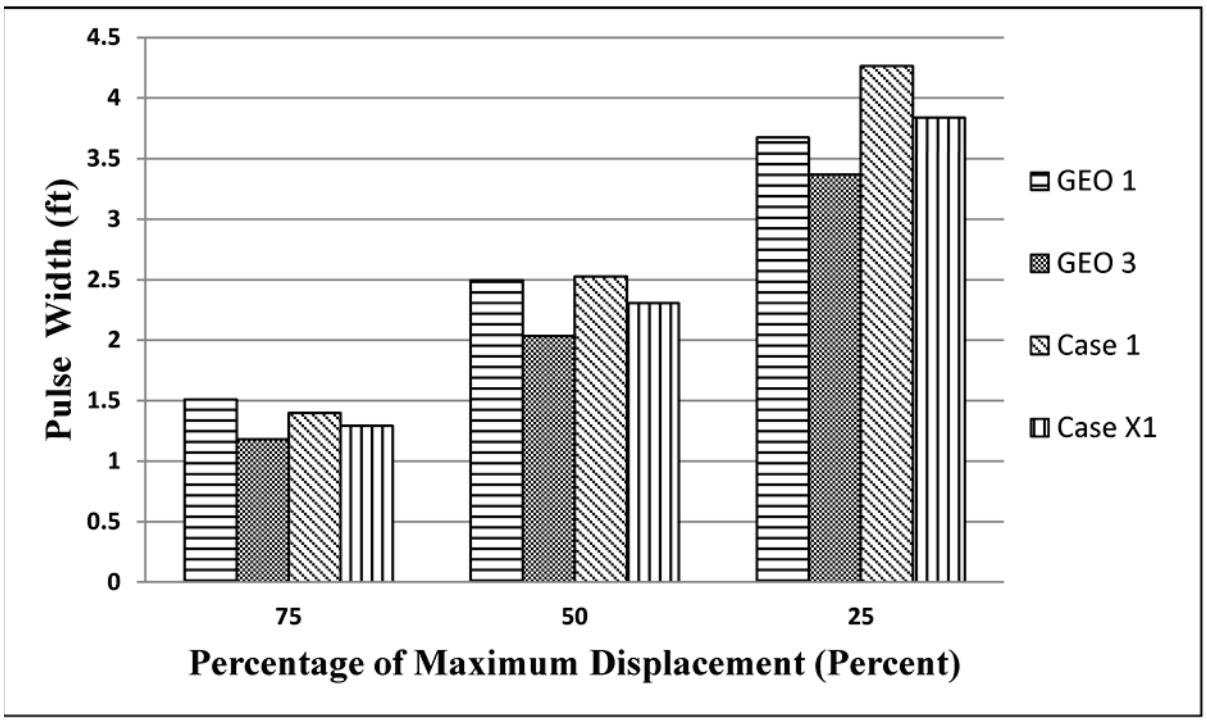

1 ft = 0.305 m

Figure 146. Graph. Comparison of normalized deflection basins at various levels for cell 34 in TSD trials (device velocity = 30 mi/h (48.3 km/h)).

Figure 147 shows the comparison of 3D-Move and measured deflection basins for cell 19 during TSD testing at 30 mi/h (48.3 km/h). Unlike cell 34, case X yielded closer results to those measured. Figure 148 compares the prediction and measured surface velocities. Figure 149 and figure 150 present the comparison of the normalized deflection basins. Again, a close match can be observed between the 3D-Move predictions and those measured.

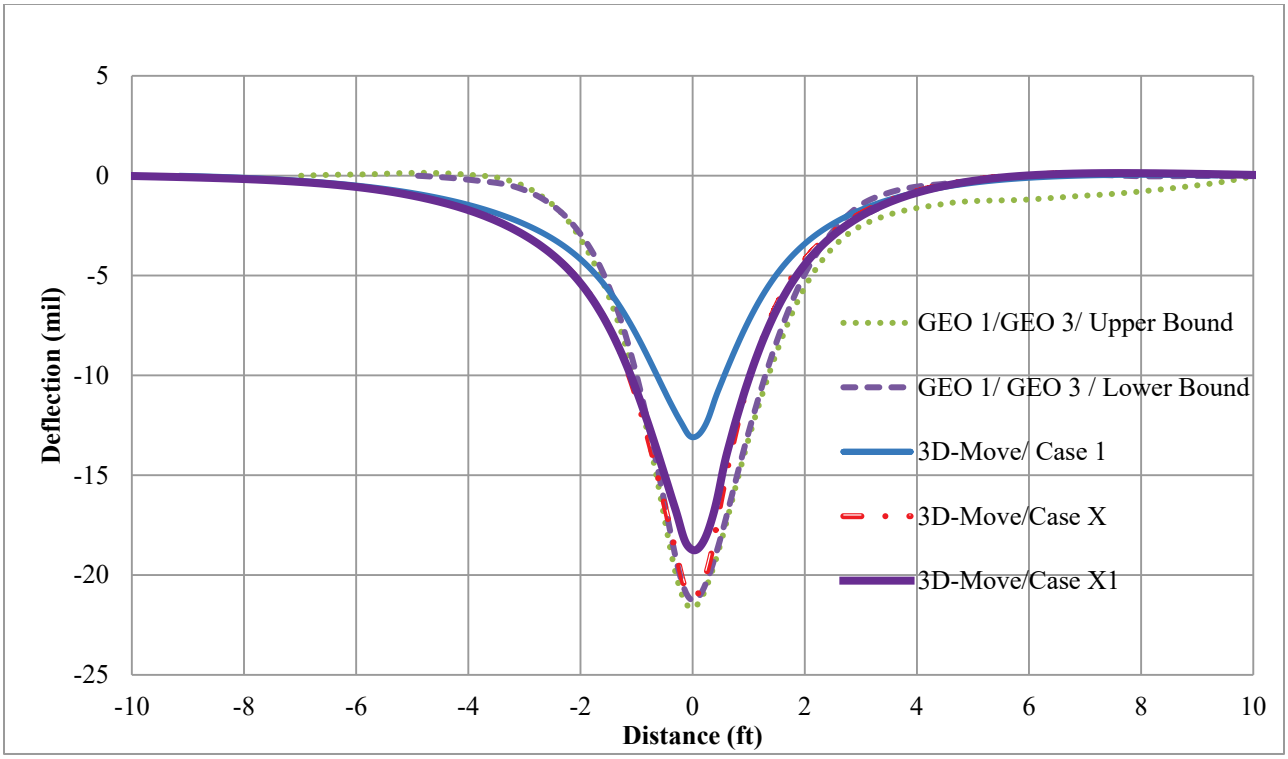

1 mil = 0.0254 mm
1 ft = 0.305 m

Figure 147. Graph. 3D-Move predictions and measured deflections for cell 19 in TSD trials (device velocity = 30 mi/h (48.3 km/h)).

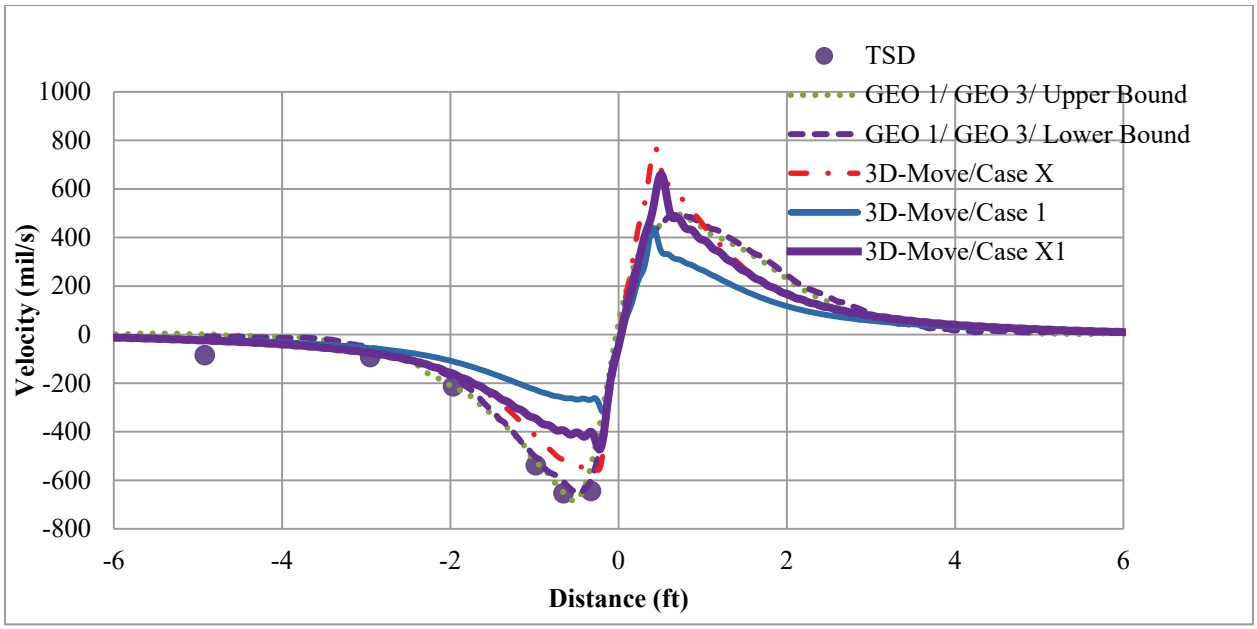

1 mil/s = 0.0254 mm/s
1 ft = 0.305 m

Figure 148. Graph. 3D-Move predictions and measured velocities for cell 19 in TSD trials (device velocity = 30 mi/h (48.3 km/h)).

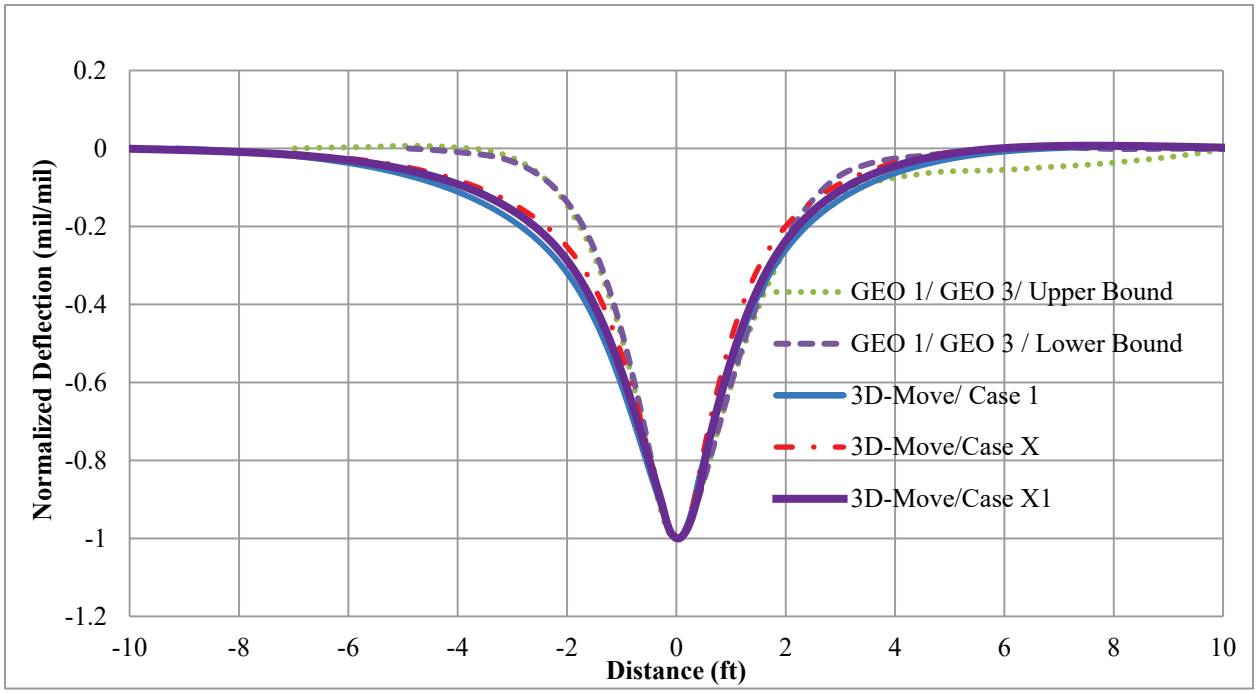

1 mil /mil = 1 mm/mm
1 ft = 0.305 m

Figure 149. Graph. Normalized basins of 3D-Move predictions and measured deflections for cell 19 in TSD trials (device velocity = 30 mi/h (48.3 km/h)).

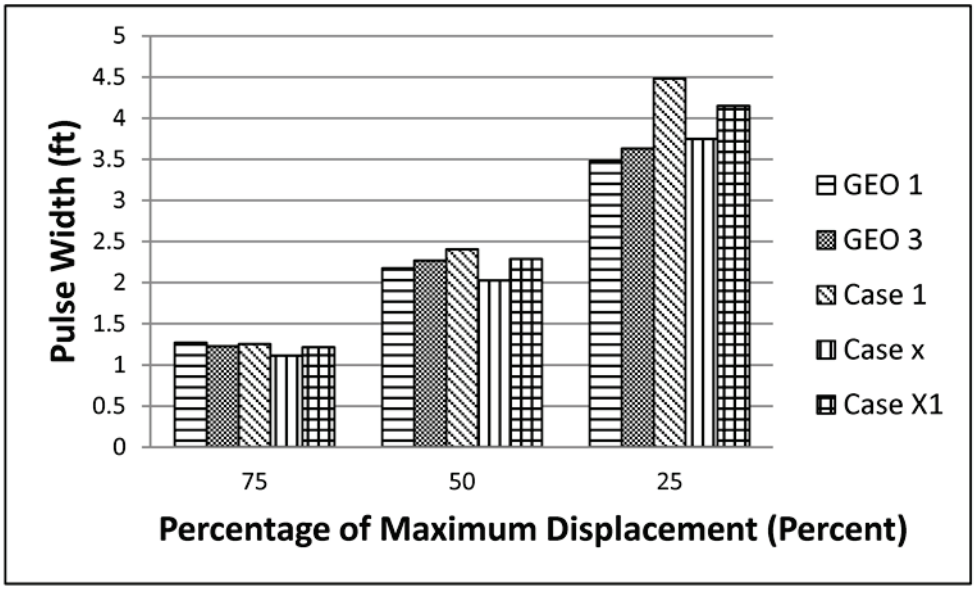

1 ft = 0.305 m

Figure 150. Graph. Comparison of normalized deflection basins at various levels for cell 19 in TSD trials (device velocity = 30 mi/h (48.3 km/h)).

The 3D-Move results were also compared with those from the RWD device. Again as a representative plot, figure 151 shows 3D-Move and measured deflection bowls as well as the two measured deflection values from RWD. 3D-Move results fall within the geophone measured responses, and the RWD measurements were close to the predicted results. The pulse widths of the normalized deflection basins shown in figure 152 and figure 153 were also similar.

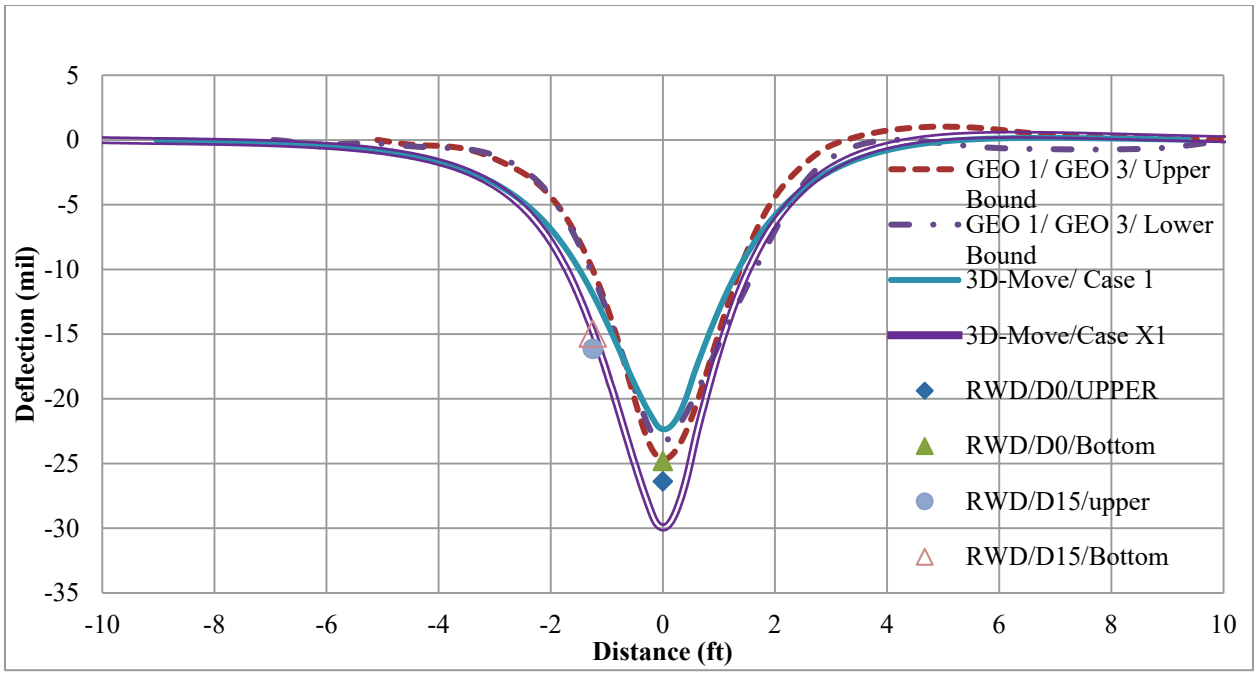

1 mil = 0.0254 mm
1 ft = 0.305 m

Figure 151. Graph. 3D-Move predictions and measured deflections for cell 34 for RWD trials (device velocity = 30 mi/h (48.3 km/h)).

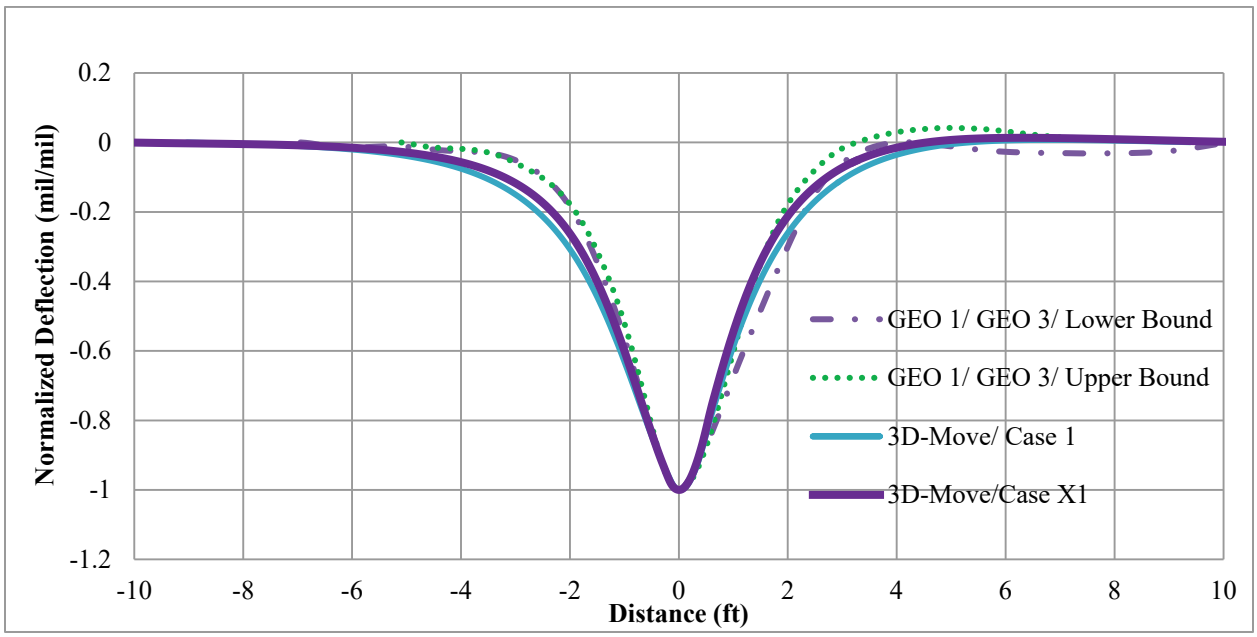

1 mil/mil = 1 mm/mm
1 ft = 0.305 m

Figure 152. Graph. Normalized basins of 3D-Move predictions and measured deflections for cell 34 in RWD trials (device velocity = 30 mi/h (48.3 km/h)).

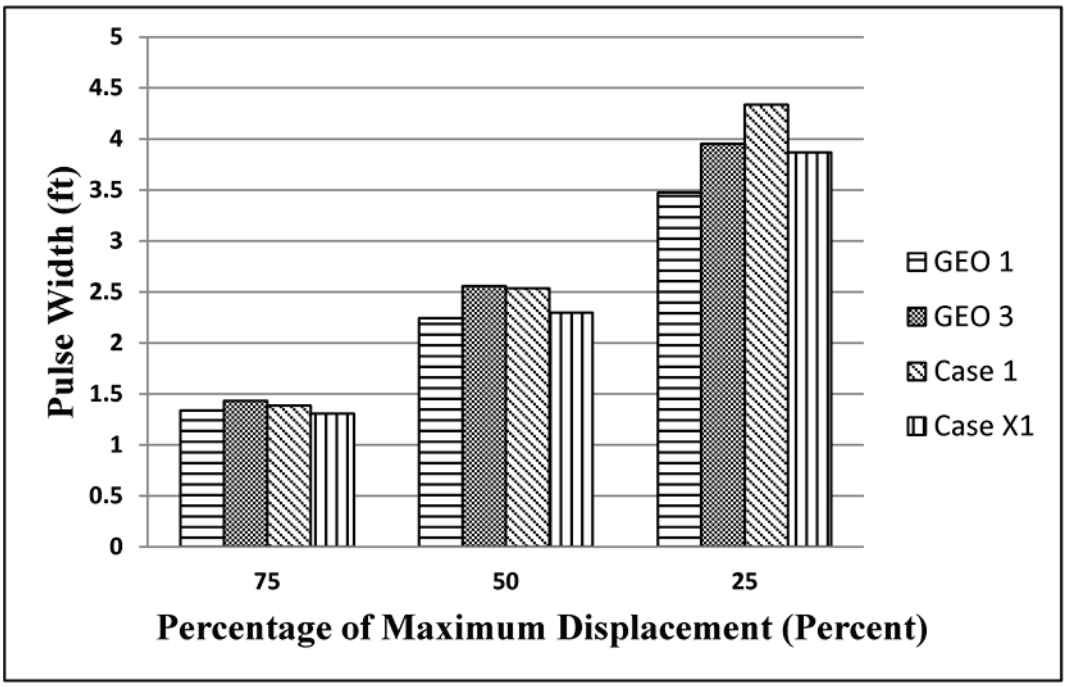

1 ft = 0.305 m

Figure 153. Graph. Comparison of normalized deflection basins at various levels for cell 34 in RWD trials (device velocity = 30 mi/h (48.3 km/h)).

Summary

The 3D-Move analyses were conducted using inputs derived based on the following considerations:

- Existing MnROAD database of pavement layer properties (thicknesses and physical properties) and recent FWD deflection data.
- Representative layer material properties based on backcalculation of FWD deflection data and subsequently, viscoelastic AC properties as a function of frequency extrapolated for the TSDD field trial temperatures using Witczak's model. In some cases because of lack of data, there was a need to extrapolate the AC layer temperatures at interior points using the BELLS equation.
- Static tire loads that were measured at the MnROAD facility weighing station.
- Role of wheel wander was addressed by selecting the transverse location that gave the highest 3D-Move deflection predictions.

Several 3D-Move analyses were undertaken in an attempt to bracket the measured surface deflection data (peak and basin shape). In the process, due consideration was given to the selection of 3D-Move inputs (material properties and loading) so that they were rationally determined and the adjustments were defensible.

It was shown that 3D-Move results fell within the measured time histories from project geophones. Figure 154 shows the comparison of maximum displacements computed by 3D-Move and those measured by the project sensors for all accuracy runs made with the TSD and RWD. In this comparison, case X1 was used for cells 3 and 34, and case X was used for cell 19. When project sensor measurements were plotted, the largest displacement given by either GEO 1 or GEO 3 (from all field trials) was selected. The figure shows a good match between computed and measured maximum displacements.

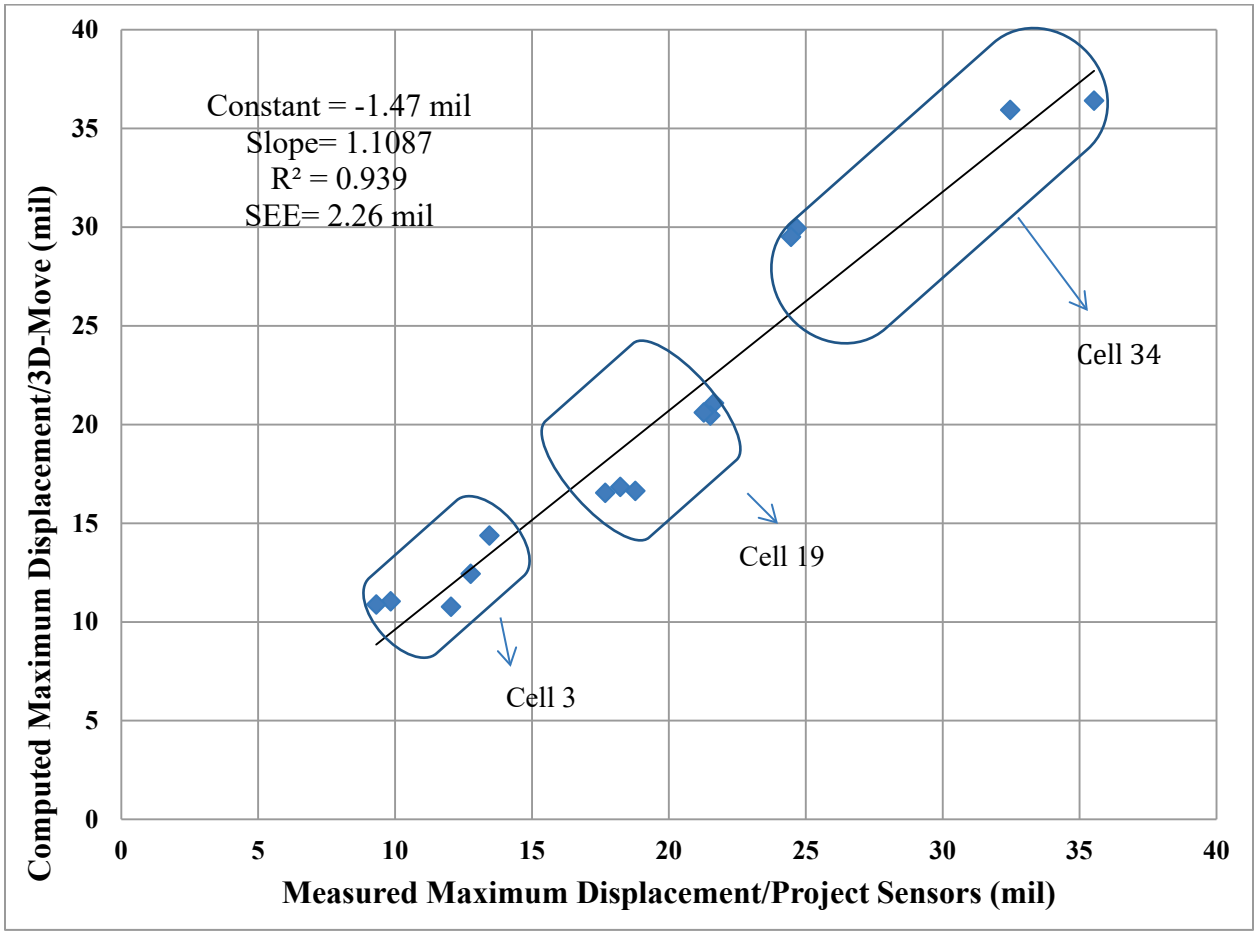

1 mil = 0.0254 mm

Figure 154. Graph. 3D-Move computed maximum displacement versus measured displacement for all cells and vehicle velocities during RWD and TSD trials.

In addition to maximum displacement, it was also important to have a good representation of the deflection bowls since TSDDs use deflections at various points of a bowl to predict pavement layer condition. Figure 155 shows the comparison of the shapes of normalized deflection bowls that gave the maximum deflection with 3D-Move analyses and sensor measurements (GEO 1 and GEO 3). Three levels of the normalized deflection bowls (75, 50, and 25 percent of maximum displacement) are reported. In this figure, w_{max} is the normalized maximum deflection. Based on this information, it was concluded that 3D-Move can predict the displacement bowl similar to those measured by geophones.

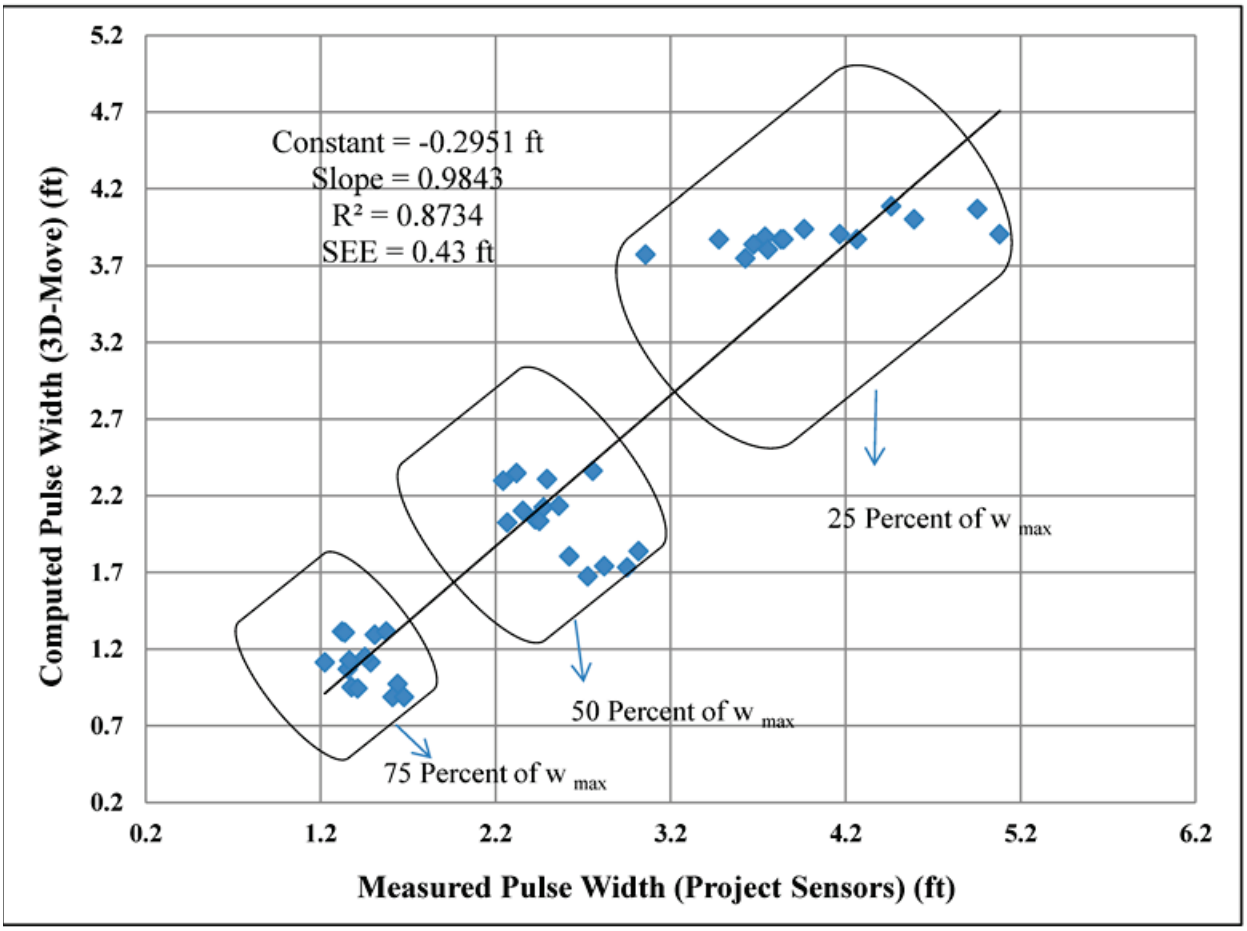

1 ft = 0.305 m

Figure 155. Graph. 3D-Move computed pulse width versus measured pulse for all cells and velocities in RWD and TSD trials.

7.6 3D-MOVE CALIBRATION USING MNROAD SENSOR DATA

MnROAD Sensors

This subsection provides a comparison between the 3D-Move results and the measured MnROAD sensor data. Unlike the earlier sensor comparisons, which focused on surface deflections, the comparisons presented in this subsection consider stresses and strains at various interior pavement locations. Since the load-induced stresses and strains are critical inputs to pavement performance predictions, this effort is important in the validation of the applicability of the 3D-Move for pavement response predictions to be used in identifying the most promising indices from TSDD measurements that best relate to pavement structure.

The existing instrumentations at the MnROAD facility include normal strain responses in the longitudinal direction and in some cases in the transverse direction as well as vertical pressure histories in unbound base and subgrade layers. The measurements from these sensors can be directly compared with those computed by 3D-Move. However, it is important to recognize that measurements made by these sensors reflect an average value over the entire dimensions of the

sensors (e.g., pressure cell measurements reflect an average Earth pressure over a diameter of 9 inches (228.6 mm)). Table 41 presents the sensors that were monitored during the accuracy runs.

Table 41. Available sensor data in cells 3, 19, and 34 (used in 3D-Move calibration).

Sensor ID	Cell Number	Facility	Sensor Type	Latitude (Degree)	Longitude (Degree)	Depth (inches)
03LE101	3	ML	Longitudinal SG	45.27331792	-93.73110608	9.3
03LE102	3	ML	Longitudinal SG	45.27332065	-93.73111185	9.4
03LE103	3	ML	Longitudinal SG	45.27332372	-93.73111822	9
03PG103	3	ML	Pressure cell	45.27329061	-93.73105228	14
19LE101	19	ML	Longitudinal SG	45.25624056	-93.69966629	4.9
19LE104	19	ML	Longitudinal SG	45.2562641	-93.69970936	4.7
19PG101	19	ML	Pressure cell	45.25621817	-93.69962245	18
19PG103	19	ML	Pressure cell	45.25625157	-93.69968785	18.2
34LE202	34	LVR	Longitudinal SG	N/A	N/A	3.5
34LE203	34	LVR	Longitudinal SG	N/A	N/A	3.5
34PG201	34	LVR	Pressure cell	N/A	N/A	15.9
34PG202	34	LVR	Pressure cell	N/A	N/A	15.9
34PG203	34	LVR	Pressure cell	N/A	N/A	15.9

1 inch = 25.4 mm
ML = Main line.
SG = Strain gauge.
N/A = Not available.

3D-Move Results for Accuracy Runs

The MnROAD pressure cells measured the average dynamic pressure applied to the entire plate, while the 3D-Move responses were computed point by point (i.e., at any given single location). Therefore, an average estimate of the computed pressure over the entire plate diameter was used for comparison purposes. Since the location of the wheel during the field trials were not known precisely, it was decided to compute 3D-Move responses at many transverse locations as an attempt to bracket the possible variation in the responses as a result of wheel wander. Figure 156 shows the response points considered along the transverse direction in 3D-Move runs. These points are located at 2-inch (50.8-mm) intervals with enough coverage so that the role of the wheel wander can be investigated. The difference between the average pressure on the plate and pressure at the center of the plate was less than 5 percent.

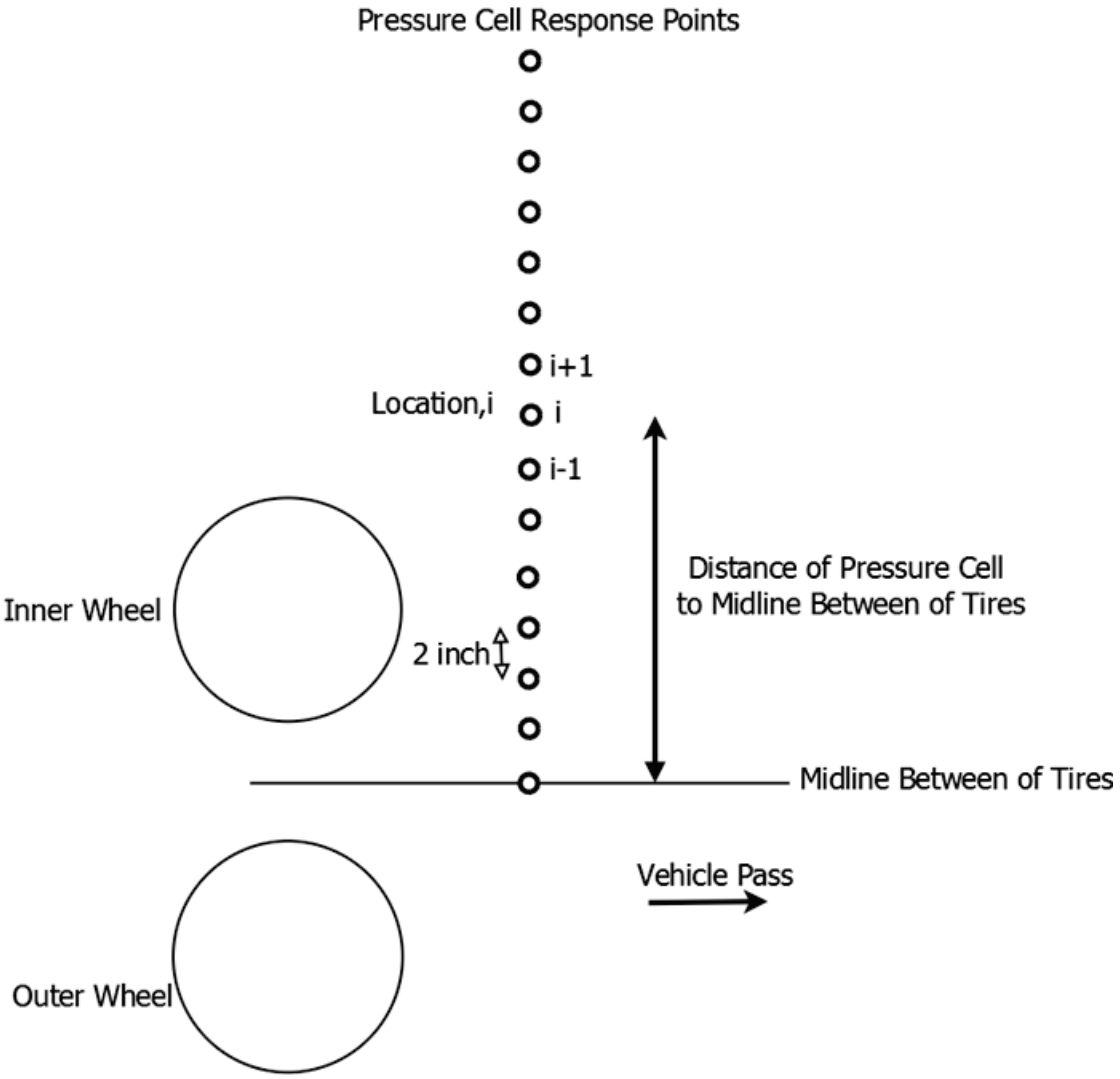

1 inch = 25.4 mm

Figure 156. Illustration. Response points for normal pressure in 3D-Move.

The average MnROAD strain responses were computed over the length of the strain gauges, which were 6 inches (152.4 mm) long. Figure 157 shows the locations used in 3D-Move to determine the role of wheel wander in the comparison of strain responses.

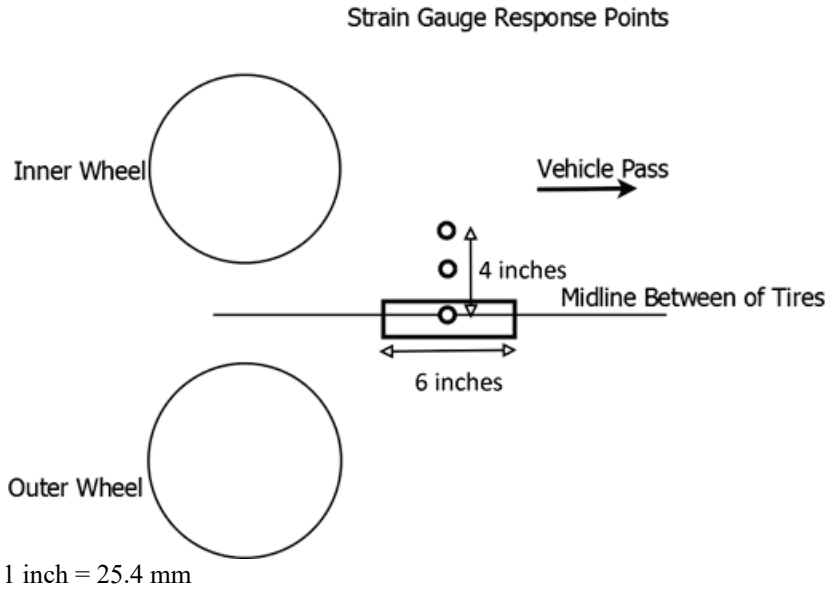

Figure 157. Illustration. Response points for strain gauges in 3D-Move.

In the 3D-Move versus project sensor comparison, the following same three scenarios for analyses were found to be appropriate:

- **Case 1**: Three layer pavement structure with same thicknesses as used in the FWD backcalculation and corresponding mean layer moduli derived from the FWD backcalculation results.

- **Case X**: Three layer pavement with: (1) thicknesses used in the FWD backcalculation except decreasing the AC layer thickness by 1 inch (25.4 mm); (2) (mean – standard deviation) of FWD backcalculated layer moduli for AC and base layers; (3) (mean + standard deviation) of FWD backcalculated layer moduli for subgrade; and (4) +25 percent of nominal tire load.

- **Case X1**: Same as case X, but with no reduction in AC layer thickness. This case was used for cells 3 and 34 which had thinner AC thicknesses.

These cases were used to compare the MnROAD sensor measurements with the 3D-Move responses.

It became apparent from the start that the earth pressures predicted by 3D-Move were substantially greater than those measured by the MnROAD sensors. The differences were larger than what could be realistically attributed to the wheel wander. To reconcile this difference, other sources where earth pressures had been predicted and measured were reviewed. As a first step, the static LE software WESLEA results were evaluated for the TSDDs loading. Unlike 3D-Move, WESLEA cannot provide the response time history nor can it provide the results as a function of vehicle speed. The results of WESLEA were compared only with the responses from the slowest TSDD speed, which was 30 mi/h (48.3 km/h) for both the RWD and TSD. The 3D-Move and WESLEA pressures were compared mainly to determine whether the measured earth pressures were reasonable.

Table 39, which was presented earlier, contains the AC moduli used in the WESLEA analyses. The existing AC moduli at a frequency of 30 Hz were adjusted to the temperature at the time of the TSDDs trials. The FWD backcalculated values were directly used for unbound layers.

Table 42 and figure 158 show the 3D-Move and WESLEA computed vertical normal pressures along various transverse offsets for the TSD pass along cell 34. The values for each case are close to one another. Minor differences could be attributed to issues related to the viscoelastic characterization of the AC layer and to vehicle speed in 3D-Move. As seen in figure 158, the values measured by the MnROAD sensors were significantly lower (a factor of about 4 to 6). Conversely, the normalized predicted and measured earth pressures shown in figure 159 agree closely, leading to questioning of the correctness of the measurements. These sensors were installed during construction about 5 years before the TSDDs trials, and hence it is possible that the calibration was off or they are damaged. It should also be noted that the earth pressures measured in cell 19 in both TSDDs had substantial negative values, which were unrealistic. This information, coupled with the close match with 3D-Move comparisons with WESLEA, led to the conclusion that the MnROAD earth pressure sensor data were suspect.

Table 42. 3D-Move versus WESLEA predictions at various offsets for cell 34 during TSD trials (device velocity = 30 mi/h (48.3 km/h)).

Offset Distance (inches)	Pressure From 3D-Move Case 1 (psi)	Pressure From WESLEA Analyses Case 1 (psi)	Pressure From 3D-Move Case X1 (psi)	Pressure from WESLEA Analyses Case X1 (psi)
0	7.7	7.2	10.6	10.2
2	7.5	7.2	10.4	10.1
4	7.2	7	10	9.9
6	6.8	6.8	9.4	9.5
8	6.3	6.4	8.6	8.9
10	5.7	5.9	7.8	8.2
12	5	5.4	6.8	7.4
14	4.4	4.8	5.9	6.6
16	3.7	4.2	5	5.7
18	3.2	3.6	4.2	4.9
20	2.7	3.1	3.5	4.1
22	2.2	2.6	2.8	3.5
24	1.9	2.2	2.3	2.9

1 inch = 25.4 mm
1 psi = 6.89 kPa

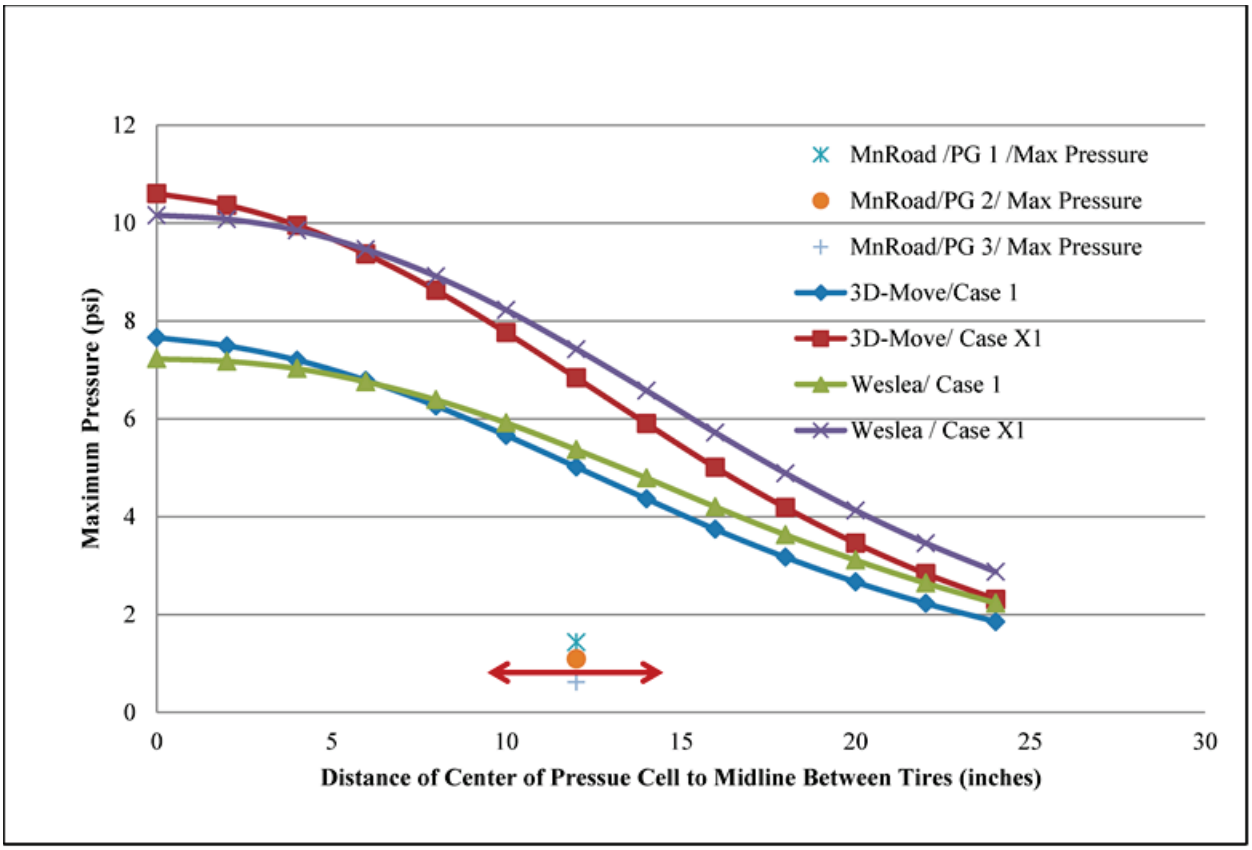

1 psi = 6.89 kPa
1 inch = 25.4 mm

Figure 158. Graph. 3D-Move versus WESLEA predictions and MnROAD pressure cell for cell 34 in TSD trials (device velocity = 30 mi/h (48.3 km/h)).

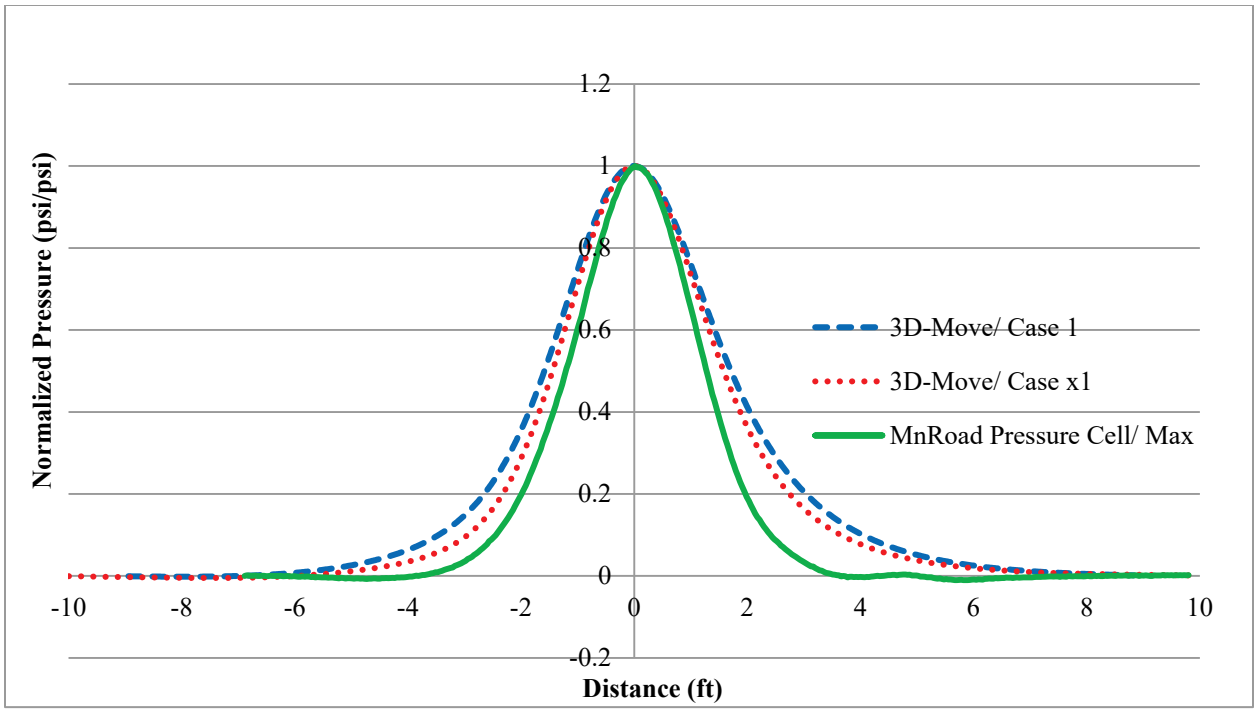

1 psi/psi = 1 kPa/kPa
1 ft = 0.305 m

Figure 159. Graph. Normalized basins of 3D-Move predictions and MnROAD pressure cell measurement for cell 34 in TSD trials (device velocity = 30 mi/h (48.3 km/h)).

Figure 160 compares the measured and predicted longitudinal strains in cell 34 for the TSD runs. Unlike the case of the earth pressures, the calculated longitudinal strains from 3D-Move matched well with the measured data from the MnROAD strain gauges. Table 43 and figure 161 through figure 163 show the comparison of the measured and calculated vertical pressure, normalized vertical pressure, and longitudinal strains for the RWD runs for cell 3. Similar to the TSD findings, the values for longitudinal strain were predicted closely by 3D-Move.

Similar plots were developed for all possible combinations of TSDD speeds and accuracy cells, and they showed the same trends as shown in the example figures included with in this chapter. The data used to generate all of these figures/tables may be obtained directly from FHWA.

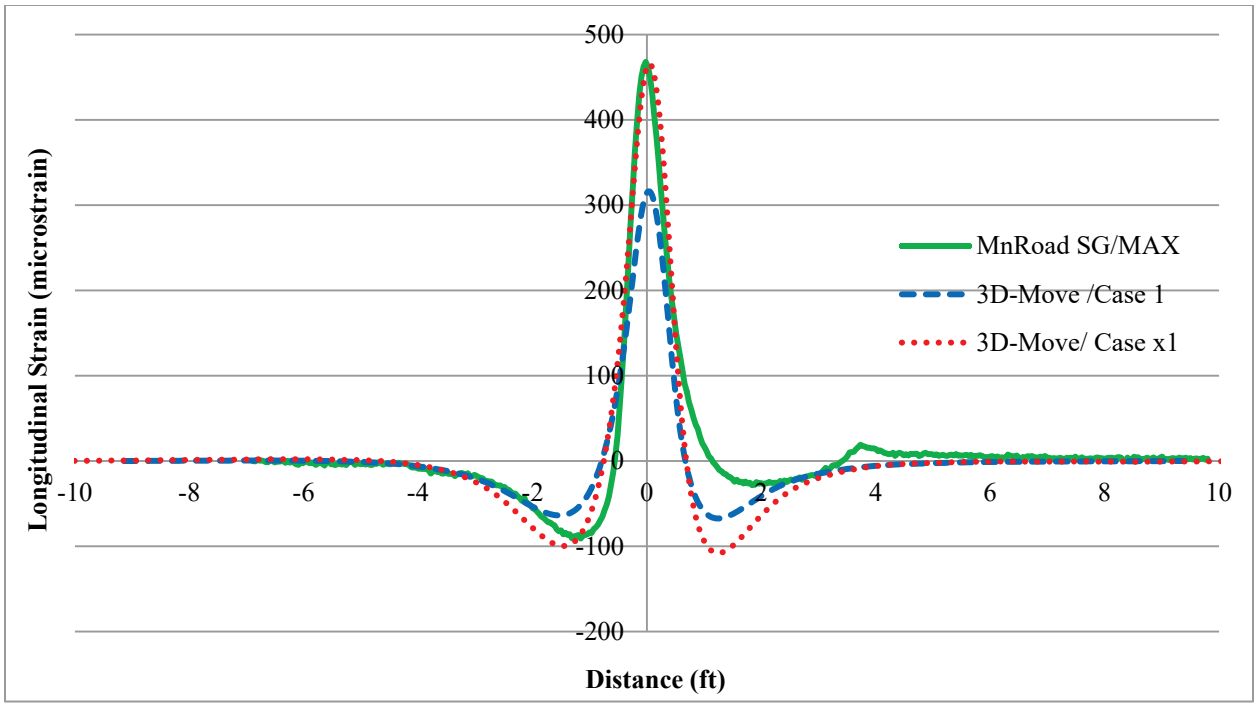

1 ft = 0.305 m

Figure 160. Graph. 3D-Move versus MnROAD strain gauge measurement for cell 34 in TSD trials (device velocity = 30 mi/h (48.3 km/h)).

Table 43. 3D-Move versus WESLEA predictions in various offsets for cell 3 RWD trials (device velocity = 30 mi/h (48.3 km/h)).

Offset Distance (inches)	Pressure From 3D-Move Case 1 (psi)	Pressure From WESLEA Analyses Case 1 (psi)	Pressure From 3D-Move Case X1 (psi)	Pressure From WESLEA Analyses Case X1 (psi)
0	10.5	10.7	12.9	13.2
2	10.4	10.7	12.8	13.2
4	10.2	10.7	12.5	13.1
6	9.7	10.4	11.8	12.7
8	8.8	9.8	10.7	12
10	7.7	8.9	9.2	10.8
12	6.3	7.6	7.6	9.4
14	5	6.2	6.1	7.7
16	3.8	4.9	4.6	6.1
18	2.8	3.7	3.4	4.7
20	2	2.7	2.5	3.5
22	1.4	2	1.8	2.6
24	1	1.4	1.3	1.8

1 inch = 25.4 mm
1 psi = 6.89 kPa

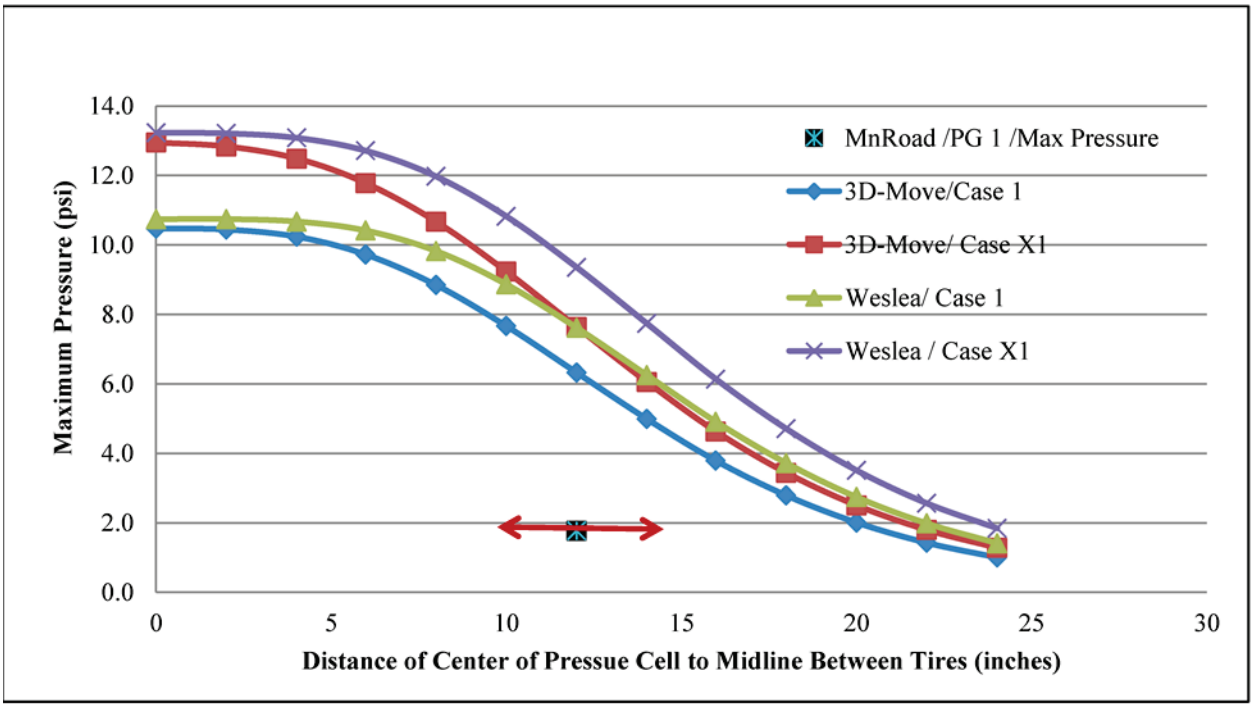

1 psi = 6.89 kPa
1 inch = 25.4 mm

Figure 161. Graph. 3D-Move versus WESLEA predictions and MnROAD pressure cell for cell 3 in RWD trials (device velocity = 30 mi/h (48.3 km/h)).

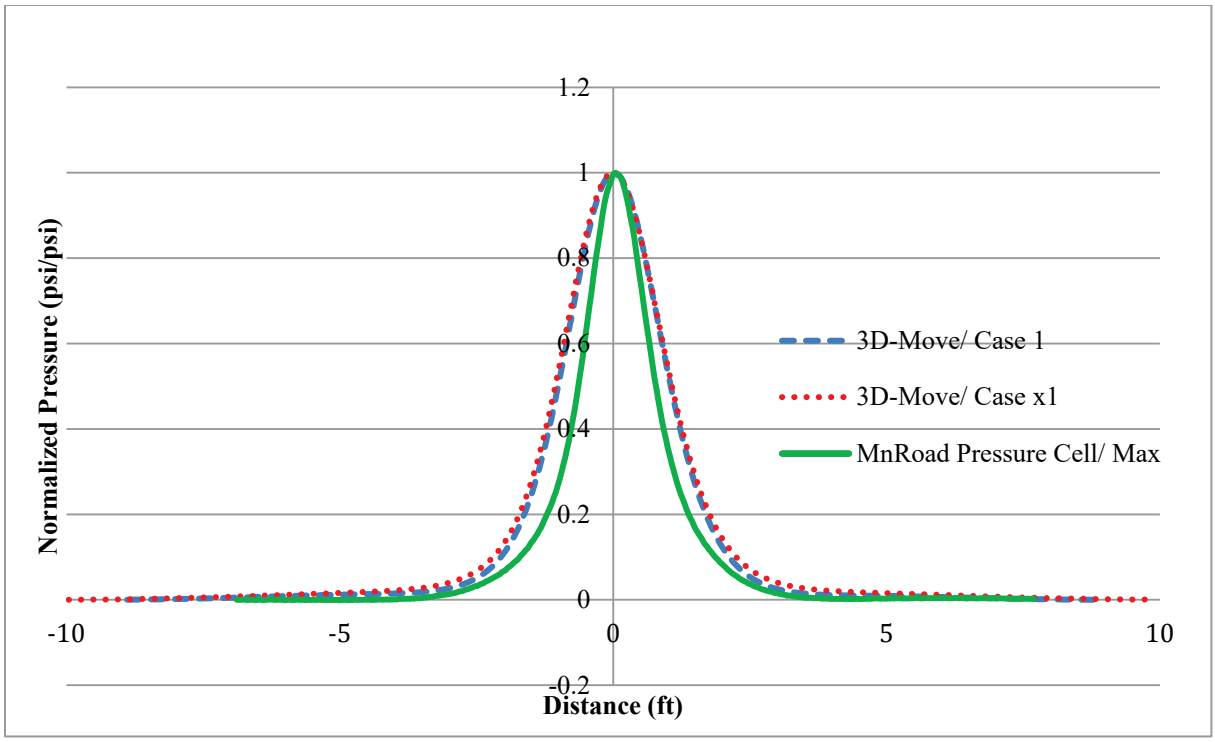

1 psi/psi = 1 kPa/kPa
1 ft = 0.305 m

Figure 162. Graph. Normalized basins of 3D-Move predictions and MnROAD pressure cell measurement for cell 3 in RWD trials (device velocity = 30 mi/h (48.3 km/h)).

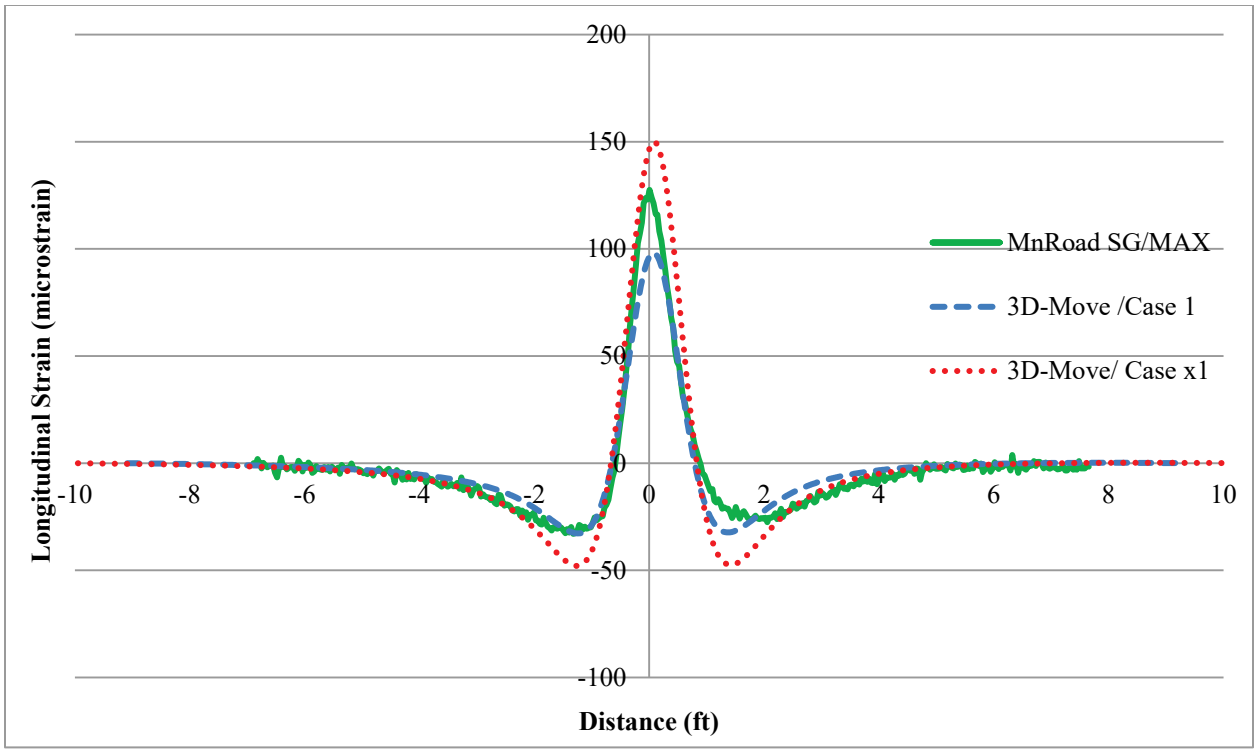

1 ft = 0.305 m

Figure 163. Graph. 3D-Move versus MnROAD strain gauge measurement from cell 3 in RWD trials (device velocity = 30 mi/h (48.3 km/h)).

Summary

The vertical pressures measured by MnROAD sensors were significantly less by a factor of 4 to 6 than those computed by 3D-Move. The possible transverse wheel wander could not explain the differences. However, the shapes of the pressure histories, when normalized, closely matched with those given by 3D-Move. Figure 164 shows the comparison of 3D-Move prediction of normal pressures and those computed from WESLEA for all accuracy passes and cells. In this graph, only the 3D-Move results computed with the lowest vehicle speed are shown. The 3D-Move normal pressure values were consistent and reasonable with WESLEA predictions, unlike those measured with MnROAD sensors.

The maximum longitudinal strains from the MnROAD measurements and 3D-Move predictions were similar (see figure 165). Accordingly, it can be concluded that 3D-Move is capable of predicting field measured surface displacement histories and interior pavement responses (stresses and strains) and could be used to evaluate pavement responses under TSDD loadings.

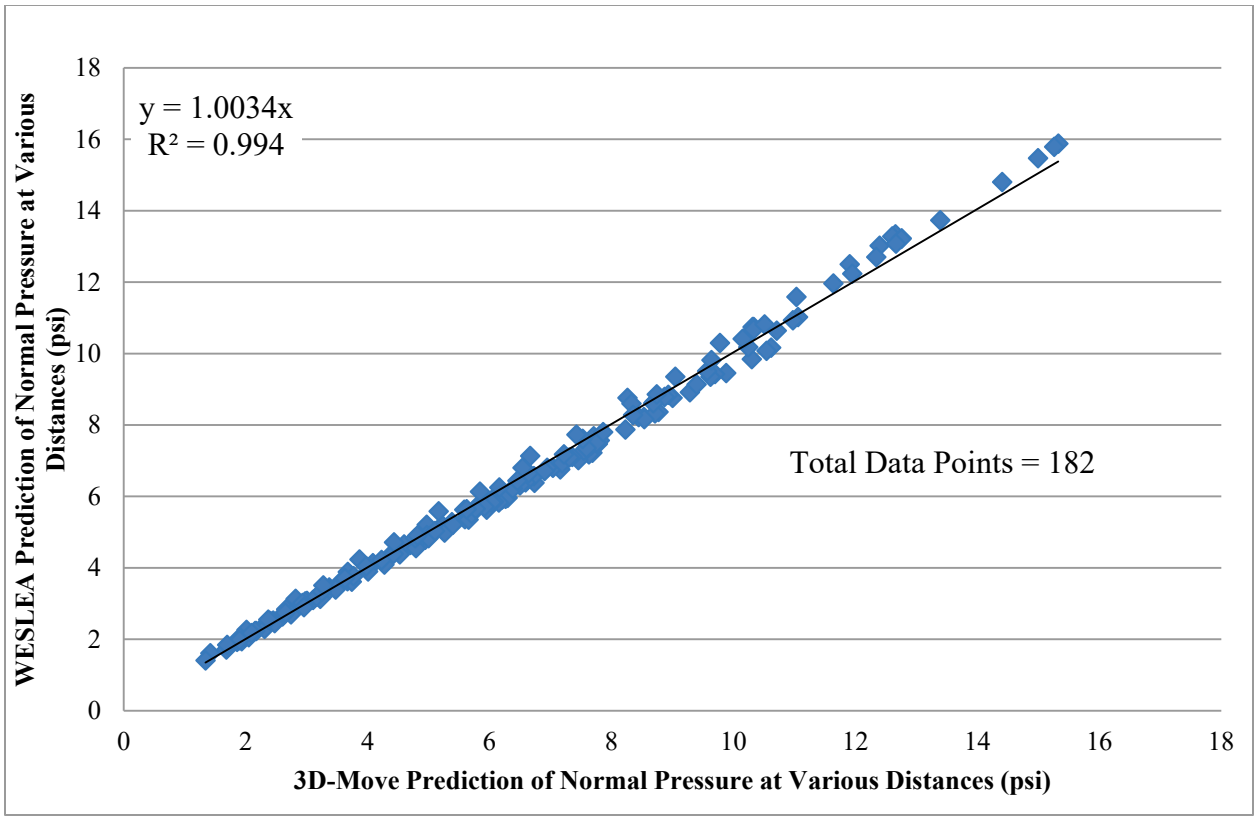

1 psi = 6.89 kPa

Figure 164. Graph. Computed normal pressure for 3D-Move versus WESLEA.

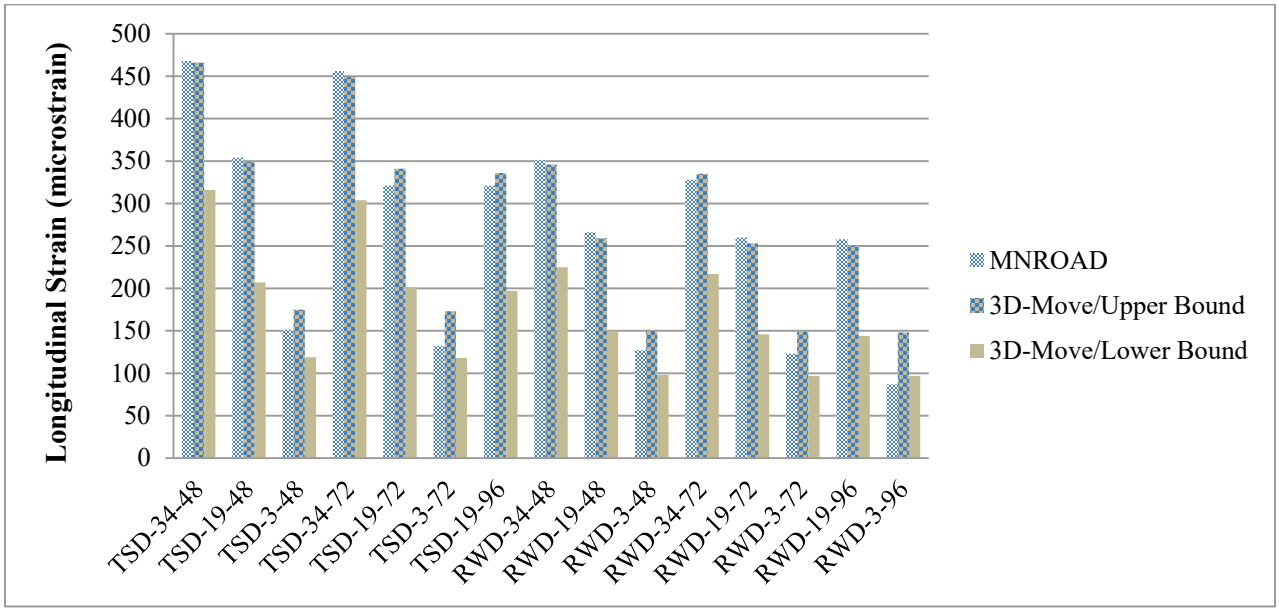

Figure 165. Graph. Maximum longitudinal strains from MnROAD sensors and 3D-Move computations.

CHAPTER 8. DEFLECTION BASIN INDICES

8.1. INTRODUCTION

This chapter presents details concerning the analytical investigation undertaken to explore relationships between load-induced structural-related responses of a pavement system and the corresponding surface deflection basin-related indices. This investigation and associated results were considered an important effort toward the development of methodologies for incorporating TSDD measurements into network-level PMS applications.

Pavement failure (or structural capacity), in terms of fatigue or rutting can be estimated from performance prediction equations.[27,57] These equations relate load-induced pavement responses to the following two important pavement distresses: (1) certain level of AC fatigue cracking and (2) rutting failure in the subgrade. The critical load-induced pavement responses that relate to the two referenced distresses are the maximum tensile horizontal strain (also known as fatigue strain) at the bottom of the AC layer and the vertical compressive strain on top of the subgrade, respectively. In addition, there are studies that postulate the existence of reliable correlations between deflection basin- related indices and load-induced pavement structural responses, which suggest it is possible to correlate deflection basin indices to structural capacity (or distress).[62,63,21]

Specific TSDD deflection basin measurements depend on the device under consideration. For example, the TSD device measures surface vertical velocity at as many as nine locations within the deflection bowl, and subsequently, the surface vertical deflection basin is determined based on a certain assumption for the shape of the defection basin. Conversely, only two surface measurements within the deflection bowl are taken by the RWD. In turn, this means that the selection of deflection basin indices for correlation to structural capacity (or distress) must take into consideration the capabilities of the specific TSDD.

Chapter 7 of this report detailed the validation of the 3D-Move program, for the purposes of the project in question, using a variety of independent pavement responses that included surface deflection bowls (measured using project sensors) as well as horizontal strains at the bottom of the AC layers and vertical stresses at the top of the subgrade (measured using MnROAD sensors). Accordingly, the program was ready for the evaluation of the critical pavement responses and corresponding deflection-based indices, thus enabling the investigation of correlations between the two. Because 3D-Move uses a dynamic moving load model, important factors such as viscoelastic properties and vehicle speed can be accounted for in the evaluation of pavement response time histories.

A number of previous studies have proposed many surface vertical deflection-based indices, and they have also postulated that these indices relate to the structural capacity of pavements.[62,63,21] However, for the purposes of this project, it was important to identify those indices that best relate to the two critical pavement responses. The identification of the appropriate indices was undertaken using the following three-step procedure:

1. **Step 1**: Identified the surface deflection indices that correlated well with the critical pavement responses using the 3D-Move simulation results presented in chapter 7, which were based on the TSDD field trials carried out at the MnROAD facility.

2. **Step 2**: Used a set of 36 pavement structures (different combinations of layer thicknesses and moduli) and vehicle speed combinations (hereafter referred to as combinations) as input to 3D-Move to perform a sensitivity analysis of the correlations associated with various deflection indices (not limited to those indices identified in step 1).

3. **Step 3**: Used the JULEA layered elastic program to further explore the robustness of the correlations identified in the first two steps by considering a much larger database (approximately 15,000 different pavement combinations) of pavements.[26] There were limitations (e.g., stationary, static, and elastic) associated with JULEA relative to realistic modeling of pavement response. However, if narrowly constrained correlations irrespective of pavement material properties were found through the use of the large JULEA database, then the impact of these limitations may not have been significant.

These three steps used to identify the most appropriate indices are described in greater detail in the following subsections.

8.2 STEP 1: USING EXISTING 3D-MOVE SIMULATION RESULTS

As a part of the calibration process described in chapter 7, pavement responses using 3D-Move were computed for three MnROAD accuracy cells with the TSDDs travelling at various vehicle speeds. By trial and error, three pavement case scenarios were identified for each of the accuracy cells, which bracketed the vertical surface deflection bowls computed by 3D-Move with those measured by the project sensors. In all, 42 datasets of pavement responses and corresponding vertical surface deflections datasets were generated using 3D-Move.

Defining Response Points in 3D-Move Runs

The 3D-Move program can output many response time histories (e.g., stresses, strains, displacements, and velocities) as a vehicle travels on at any specified location of the pavement surface. The TSDDs measured (or estimated) vertical surface deflections at many predetermined locations in the longitudinal direction along the midline between the rear tires (see figure 166). From the vertical displacement time history computed by 3D-Move at a point (observation point) on the midline between the tires, it was possible to determine the displacements at various individual locations along the midline using time space superposition. The 3D-Move output includes the time of the maximum displacement (t_{max}) and also the time (t_o) at which the instantaneous deflection at the midpoint between tires (D_0) reached the point of observation (see figure 167). Since 3D-Move modeled the damping characteristics of the pavement layers, there was an offset between t_{max} and t_o. The location D_r refers to a point at a distance r in inches in front of D_0. The maximum displacement that occurred at the location D_{max} and other displacements at many locations shown along the midline between the tires in figure 166 could be readily determined using time-space superposition.

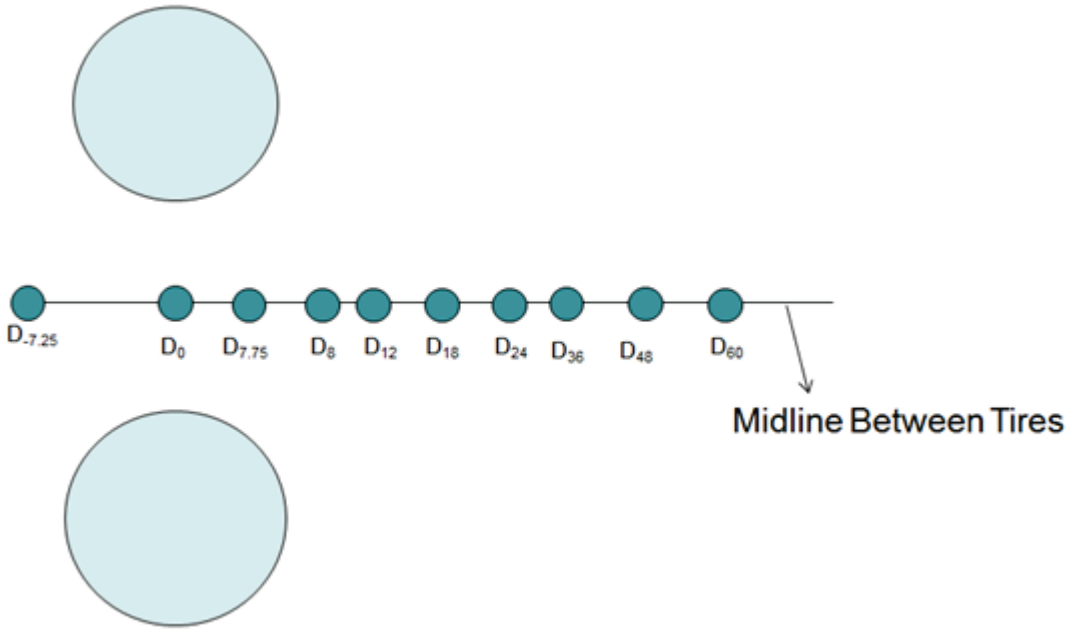

Figure 166. Illustration. Predetermined locations for estimation of vertical surface deflections in TSDDs.

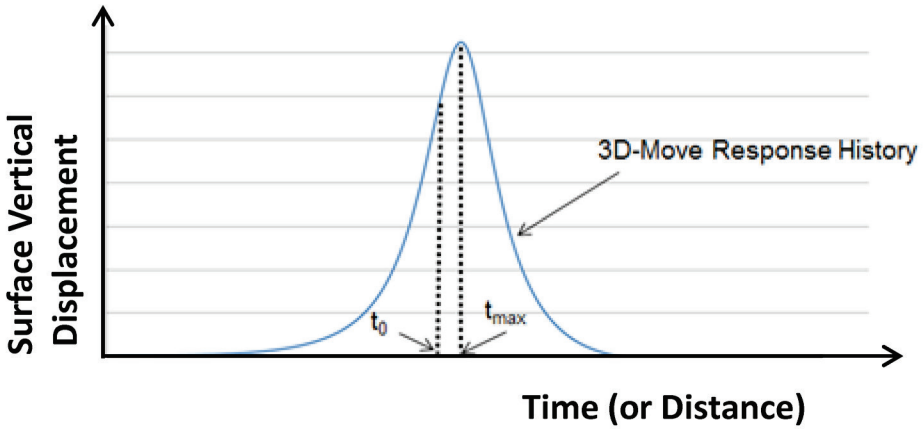

Figure 167. Illustration. Surface displacement from 3D-Move displacement time history.

Conversely, when other 3D-Move pavement responses (e.g., maximum AC tensile strain) were considered, it was necessary to select multiple transverse locations (the depth was fixed) in the computations. This is because the location of the maximum value of the response was not known a priori. After computing responses at many multiple transverse locations, the maximum response value could be determined.

Though the focus of this project was on the horizontal (or fatigue) strains at the bottom the AC and to a lesser extent on the vertical strains at the top of subgrade, a larger database of pavement responses was assembled from the 3D-Move runs. The list of the locations and corresponding responses and the distress mode includes the following (see figure 168):

- Bottom of AC tensile strains in x and y direction for bottom-up fatigue cracking.

- Tensile strains at surface and 0.5 inch (12.7 mm) from surface of AC for top-down cracking.
- Vertical strain/stress 2 inches (50.8 mm) from AC surface for rutting estimate of AC.
- Vertical stress/strain at mid-point of base for base rutting.
- Vertical strains on top of the subgrade for subgrade rutting.

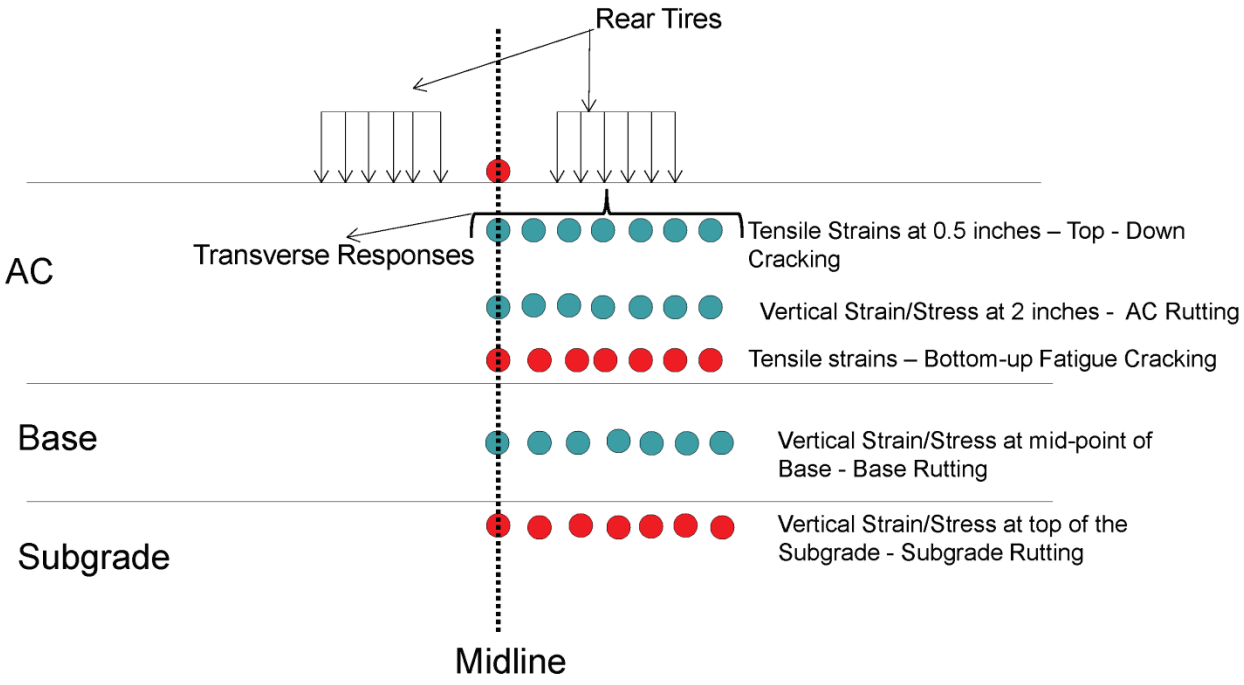

1 inch = 25.4 mm

Figure 168. Illustration. Selection of response points when using 3D-Move.

Pavement Properties and Loading in 3D-Move Runs

The initial focus of the simulations was on the three MnROAD cells (cells 3, 19, and 34), where project sensor measurements were taken during the TSDD field trials. A sketch of the pavement structures at these three cells was presented earlier in figure 141 (see chapter 7). Since the AC thickness varied from 3 to 5 inches (76.2 to 127 mm) along these cells, the sections could be categorized as pavements with relatively thin AC. Other pavement layer thicknesses and moduli are also shown in this figure. To compare the 3D-Move results to measured data from the MnROAD and project sensors, the AC moduli corresponding to the temperatures at the time of the TSDD field trials were required. The procedure to get the AC layer modulus versus frequency relation at any given temperature based on FWD backcalculated layer moduli was described in chapter 7. Figure 138 and figure 139 in chapter 7 showed the axle configuration and loads for the TSD and RWD. These two cases of loading (tire loads, pressure, and spacing) could be used to determine the role of loading conditions on the correlations between surface deflection indices and pavement responses as described later in this chapter.

Selection of Deflection Basin Indices

A number of deflection basin-related indices have been proposed by researchers and are perceived as strong predictors of the critical structural-related responses and structural conditions (or capacity) of the pavements. Experimental and analytical studies have reported strong correlations between some deflection basin indices and pavement responses.[62,63,21] Horak proposed two different equations for *R* referred as R1 and R2 as in Figure 8 and Figure 9.[63,64]

As noted previously, the 3D-Move deflection basin parameters were computed based on surface vertical displacement along the midline between the two rear tires, while the maximum pavement responses were determined by considering many transverse response locations. The 3D-Move runs initially used both the TSD and RWD loadings individually, and then the combined dataset were used when exploring the correlations. A power curve generally described the data better than a linear fit, as judged by improved correlation coefficients (R^2).

SCI is typically defined as the difference in displacements between D_0 and D_r. D_0 is the reference displacement; however, the locations D_0 and D_{max} were not the same due to viscous lag of the response due to the moving load. Accordingly, it was important to determine whether a better correlation existed if D_{max} was used as the reference displacement. Parameter *SCIm* is defined by using D_{max} instead of D_0 as the reference displacement in the calculations of the indices. Since both TSD and RWD did not directly measure deflection at D_0, another observation made during the investigation was the need to also consider D_4, $D_{-7.25}$, and D_8 (i.e., displacements at 4, -7.25, and 8 inches (101.6, -184.15, and 203.2 mm), respectively) as reference displacement locations. In the case of the TSD, because of its capacity to measure multiple deflection points, a theoretical algorithm was used to compute D_0. However, to minimize additional computations and associated errors, the possibility of utilizing direct TSD measurements at D_4 and D_8 were proposed. More specifically, a new index called Deflection Slope Index (DSI) was proposed based on reference at D_4, D_8, D_{12}, D_{18}, and D_{24}. DSI is the difference between the deflection at reference location and D_r. In addition, indices representing deflection slope at a given location defined as Tangent Slope (TS) was also considered.

Table 44 shows these indices. A total of 75 individual indices are listed in this table. The deflection basin indices included in table 44 correlated with the two pavement structural-related responses presented earlier in this chapter. The deflection basin parameters that did not yield strong correlations to the structural-related responses were not considered further under the third step.

Table 44. Deflection basin indices used in the evaluation.

Parameter and Number of Indices	Indices for Evaluation
*R*1 (7)	$R1_8$
	$R1_{12}$
	$R1_{18}$
	$R1_{24}$
	$R1_{36}$
	$R1_{48}$
	$R1_{60}$
*R*2 (7)	$R2_8$
	$R2_{12}$
	$R2_{18}$
	$R2_{24}$
	$R2_{36}$
	$R2_{48}$
	$R2_{60}$
Surface displacement (2)	D_0
	D_{60}
Area (1)	A
Shape factors (2)	F_1
	F_2
SCI (7)	SCI_8
	SCI_{12}
	SCI_{18}
	SCI_{24}
	SCI_{36}
	SCI_{48}
	SCI_{60}
	$D_{-7.25} - D_{7.75}$ (for RWD)
BCI (1)	BCI
BDI (1)	BDI
AUPP (1)	AUPP
SD (7)	SD_8
	SD_{12}
	SD_{18}
	SD_{24}
	SD_{36}
	SD_{48}
	SD_{60}
TS (8)	TS_4*
	TS_8*
	TS_{12}*
	TS_{18}
	TS_{24}*
	TS_{36}*

	TS_{48}
	TS_{60}*
SCIm (7)	$SCIm_{8}$
	$SCIm_{12}$
	$SCIm_{18}$
	$SCIm_{24}$
	$SCIm_{36}$
	$SCIm_{48}$
	$SCIm_{60}$
$DSI_{4\text{-}r}$ (7)	DSI_{4-8}
	DSI_{4-12}
	DSI_{4-18}
	DSI_{4-24}
	DSI_{4-36}
	DSI_{4-48}
	DSI_{4-60}
DSI_{8-r} (6)	DSI_{8-12}
	DSI_{8-18}
	DSI_{8-24}
	DSI_{8-36}
	DSI_{8-48}
	DSI_{8-60}
DSI_{12-r} (4)	DSI_{12-18}
	DSI_{12-24} (same as BDI)
	DSI_{12-36}
	DSI_{12-48}
	DSI_{12-60}
DSI_{18-r} (4)	DSI_{18-24}
	DSI_{18-36}
	DSI_{18-48}
	DSI_{18-60}
DSI_{24-r} (2)	DSI_{24-36} (same as BCI)
	DSI_{24-48}
	DSI_{24-60}

*TSD sensor location.
Note: Numbers within parentheses in left column indicate the number of indices for each deflection basin parameter.

The goodness of the correlations between the indices and pavement responses were categorized into three classes. Class 1 indices had an R^2 greater than 0.9 and were considered the most appropriate indices. Class 2 indices were those with an R^2 between 0.7 and 0.9, and class 3 indices were those with an R^2 less than 0.7.

Two options were used when horizontal strains at the bottom AC were considered:
(1) maximum tensile strains in transverse and longitudinal direction of vehicle travel and

(2) maximum tensile strains at a location directly below the midpoint between the rear tires. For the purpose of brevity, only the following tables and figures that showed the highest (and therefore the most appropriate) correlations are included in this chapter:

- Table 45, table 46, figure 169, and figure 170 show the relationships with *R*1 shown in table 44.
- Table 47, table 48, figure 171, and figure 172 show the relationships with SCI, where D_0 was used as the reference displacement.
- Table 49, table 50, figure 173, and figure 174 show the relationships with *SCIm*, where D_{max} was used as the reference displacement.
- Table 51, table 52, figure 175, and figure 176 show the relationships with DSI, where D_4 was used as the reference displacement.

The equations with R^2 values more than 0.90 are presented bold. The example tables and figures provide results for TSD loadings only and also for the combined TSD and RWD loadings. There are 17 data points available for the TSD loadings and 43 for the combined dataset. Similar tables and figures looking at the fatigue strain relationship were developed for every index in table 44, but they are not included in the report, as they do not provide further insights. The data used to generate these tables and figures can be obtained directly from FHWA.

Based on the information presented in table 45 through table 52 and the review of the correlations for other indices, it was concluded that indices based on maximum horizontal strains were better than horizontal strains at the location directly below the midpoint between the tires. It was also concluded that the role of the difference in load characteristics (TSD versus RWD) on the relationships were minimal. However, *SCIm*, which used D_{max} as the reference displacement, had a slightly better correlation. It also appears that using D_4 instead of D_0 to calculate SCI yielded better correlations.

Table 45. Relationships between *R*1 and horizontal strains at bottom of AC with TSD loading data.

Index	Relation with Midline Horizontal Strain*		Relation with Maximum Horizontal Strain*	
	Equation	R^2	Equation	R^2
$R1_8$	$y = 3.3238x^{-1.02}$	0.75	$y = 1.2327x^{-0.896}$	0.88
$R1_{12}$	$y = 1.3707x^{-0.912}$	0.85	**$y = 0.4438x^{-0.775}$**	**0.94**
$R1_{18}$	$y = 0.5819x^{-0.791}$	0.88	**$y = 0.1802x^{-0.655}$**	**0.92**
$R1_{24}$	$y = 0.4157x^{-0.73}$	0.88	$y = 0.1241x^{-0.595}$	0.89
$R1_{36}$	$y = 0.397x^{-0.684}$	0.87	$y = 0.1115x^{-0.551}$	0.86
$R1_{48}$	$y = 0.5396x^{-0.682}$	0.87	$y = 0.1395x^{-0.547}$	0.85
$R1_{60}$	$y = 0.7837x^{-0.69}$	0.87	$y = 0.1866x^{-0.553}$	0.85

*At the bottom of AC layer.
y = Horizontal strain.
x = Index.
Note: There were 17 TSD loading data points. Bold cells indicate indices in class 1.

Table 46. Relationship between *R*1 and horizontal strains at bottom of AC with all loading data.

Index	Relation with Midline Horizontal Strain*		Relation with Maximum Horizontal Strain*	
	Equation	R^2	Equation	R^2
$R1_8$	$y = 6.2386x^{-1.091}$	0.74	$y = 1.2078x^{-0.895}$	0.88
$R1_{12}$	$y = 2.2986x^{-0.968}$	0.87	**$y = 0.3945x^{-0.763}$**	**0.95**
$R1_{18}$	**$y = 0.9436x^{-0.843}$**	**0.91**	**$y = 0.1584x^{-0.643}$**	**0.93**
$R1_{24}$	**$y = 0.6542x^{-0.778}$**	**0.91**	**$y = 0.1079x^{-0.583}$**	**0.90**
$R1_{36}$	**$y = 0.6504x^{-0.733}$**	**0.90**	$y = 0.0994x^{-0.542}$	0.87
$R1_{48}$	$y = 0.9188x^{-0.732}$	0.89	$y = 0.125x^{-0.539}$	0.85
$R1_{60}$	$y = 1.3733x^{-0.742}$	0.89	$y = 0.1666x^{-0.545}$	0.85

*At the bottom of AC layer.
y = Horizontal strain.
x = Index.
Note: There were 43 data points from both TSD and RWD loading. Bold cells indicate indices in class 1.

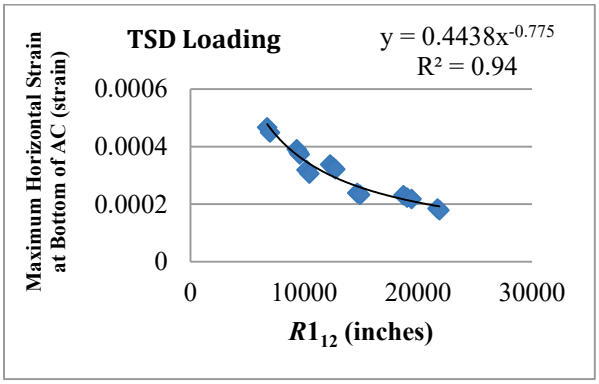

1 inch = 25.4 mm

Figure 169. Graph. Relationship between $R1_{12}$ and horizontal strains at bottom of AC with TSD loading data.

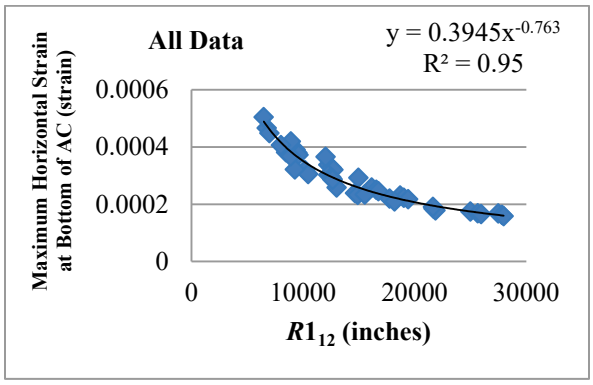

1 inch = 25.4 mm

Figure 170. Graph. Relationship between $R1_{12}$ and horizontal strains at bottom of AC with all loading data.

Table 47. Relationship between SCI and horizontal strains at bottom of AC with TSD loading data.

Index	Relation with Midline Horizontal Strain*		Relation with Maximum Horizontal Strain*	
	Equation	R^2	Equation	R^2
SCI_8	$y = 0.0969x^{1.0201}$	0.75	$y = 0.0553x^{0.8958}$	0.88
SCI_{12}	$y = 0.0277x^{0.9119}$	0.85	**$y = 0.0161x^{0.775}$**	**0.94**
SCI_{18}	$y = 0.0104x^{0.7911}$	0.88	**$y = 0.0064x^{0.6547}$**	**0.92**
SCI_{24}	$y = 0.0067x^{0.73}$	0.88	$y = 0.0043x^{0.5948}$	0.89
SCI_{36}	$y = 0.0047x^{0.6841}$	0.87	$y = 0.0031x^{0.551}$	0.86
SCI_{48}	$y = 0.0044x^{0.6817}$	0.87	$y = 0.003x^{0.547}$	0.85

*At the bottom of AC layer.
y = Horizontal strain.
x = Index.
Note: There were 17 TSD loading data points. Bold cells indicate indices in class 1.

Table 48. Relationship between SCI and horizontal strains at bottom of AC with all loading data.

Index	Relation with Midline Horizontal Strain*		Relation with Maximum Horizontal Strain*	
	Equation	R^2	Equation	R^2
SCI_8	$y = 0.142x^{1.0914}$	0.74	$y = 0.0543x^{0.8949}$	0.88
SCI_{12}	$y = 0.0365x^{0.9684}$	0.87	**$y = 0.0151x^{0.7626}$**	**0.95**
SCI_{18}	**$y = 0.0129x^{0.8432}$**	**0.91**	**$y = 0.006x^{0.6427}$**	**0.93**
SCI_{24}	**$y = 0.008x^{0.778}$**	**0.91**	**$y = 0.004x^{0.5827}$**	**0.90**
SCI_{36}	**$y = 0.0056x^{0.7335}$**	**0.90**	$y = 0.003x^{0.5422}$	0.86
SCI_{48}	$y = 0.0053x^{0.7324}$	0.89	$y = 0.0028x^{0.5392}$	0.85

*At the bottom of AC layer.
y = Horizontal strain.
x = Index.
Note: There were 43 data points from both TSD and RWD loading. Bold cells indicate indices in class 1.

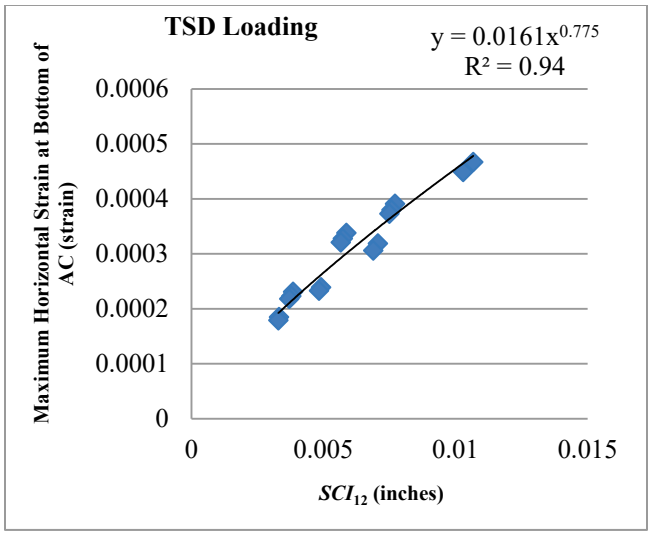

1 inch = 25.4 mm

Figure 171. Graph. Relationship between SCI_{12} and horizontal strains at bottom of AC with TSD loading data.

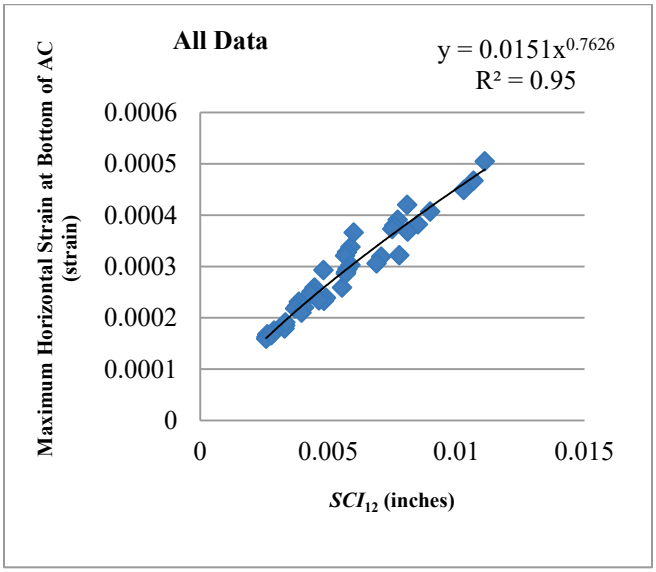

1 inch = 25.4 mm

Figure 172. Graph. Relationship between SCI_{12} and horizontal strains at bottom of AC with all loading data.

Table 49. Relationship between *SCIm* and horizontal strains at bottom of AC with TSD loading data.

Index	Relation with Midline Horizontal Strain*		Relation with Maximum Horizontal Strain*	
	Equation	R^2	Equation	R^2
$SCIm_8$	$y = 0.0713x^{0.9751}$	0.76	$y = 0.0417x^{0.854}$	0.89
$SCIm_{12}$	$y = 0.0234x^{0.883}$	0.84	**$y = 0.014x^{0.7505}$**	**0.92**
$SCIm_{18}$	$y = 0.0096x^{0.7774}$	0.88	**$y = 0.0061x^{0.6437}$**	**0.92**
$SCIm_{24}$	$y = 0.0063x^{0.7211}$	0.87	$y = 0.0041x^{0.5879}$	0.89
$SCIm_{36}$	$y = 0.0046x^{0.6782}$	0.87	$y = 0.0031x^{0.5465}$	0.86
$SCIm_{48}$	$y = 0.0043x^{0.6763}$	0.86	$y = 0.0029x^{0.5429}$	0.85

*At the bottom of AC layer.
y = Horizontal strain.
x = Index.
Note: There were 17 TSD loading data points. Bold cells indicate indices in class 1.

Table 50. Relationship between *SCIm* and horizontal strains at bottom of AC with all loading data.

Index	Relation with Midline Horizontal Strain*		Relation with Maximum Horizontal Strain*	
	Equation	R^2	Equation	R^2
$SCIm_8$	$y = 0.1022x^{1.0439}$	0.77	**$y = 0.0407x^{0.8526}$**	**0.91**
$SCIm_{12}$	$y = 0.0306x^{0.9386}$	0.87	**$y = 0.0131x^{0.739}$**	**0.95**
$SCIm_{18}$	$y = 0.012x^{0.8292}$	0.91	**$y = 0.0057x^{0.6323}$**	**0.93**
$SCIm_{24}$	**$y = 0.0076x^{0.7689}$**	**0.91**	$y = 0.0038x^{0.5763}$	0.89
$SCIm_{36}$	**$y = 0.0055x^{0.7274}$**	**0.90**	$y = 0.0029x^{0.538}$	0.86
$SCIm_{48}$	$y = 0.0051x^{0.7268}$	0.89	$y = 0.0027x^{0.5354}$	0.85

*At the bottom of AC layer.
y = Horizontal strain.
x = Index.
Note: There were 43 data points from both TSD and RWD loading. Bold cells indicate indices in class 1.

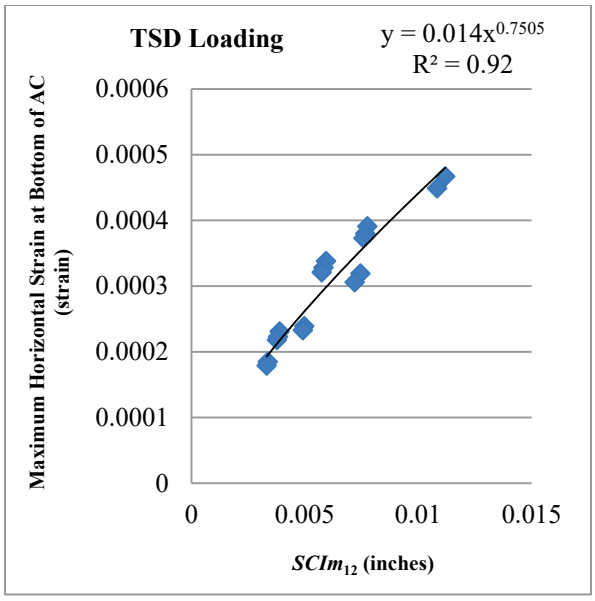

1 inch = 25.4 mm

Figure 173. Graph. Relationship between *SCIm*$_{12}$ and horizontal strains at bottom of AC with TSD loading data.

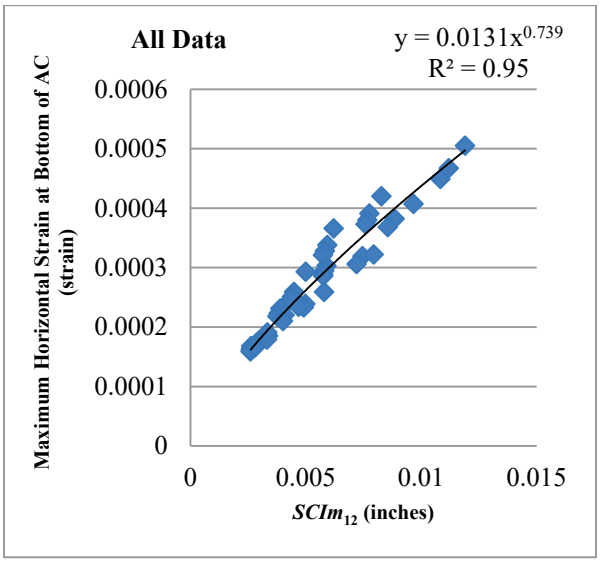

1 inch = 25.4 mm

Figure 174. Graph. Relationship between *SCIm*$_{12}$ and horizontal strains at bottom of AC with all loading data.

Table 51. Relationship between DSI_{4-r} and horizontal strains at bottom of AC with TSD loading data.

Index	Relation with Midline Horizontal Strain*		Relation with Maximum Horizontal Strain*	
	Equation	R^2	Equation	R^2
DSI_{4-8}	$y = 0.0641x^{0.9153}$	0.79	**$y = 0.0357x^{0.7917}$**	**0.90**
DSI_{4-12}	$y = 0.0201x^{0.8324}$	0.84	**$y = 0.0119x^{0.7019}$**	**0.91**
DSI_{4-18}	$y = 0.0086x^{0.7386}$	0.87	**$y = 0.0054x^{0.6079}$**	**0.90**
DSI_{4-24}	$y = 0.0057x^{0.6872}$	0.87	$y = 0.0037x^{0.5573}$	0.87

*At the bottom of AC layer.
y = Horizontal strain.
x = Index.
Note: There were 17 TSD loading data points. Bold cells indicate indices in class 1.

Table 52. Relationship between DSI_{4-r} and horizontal strains at bottom of AC with all loading data.

Index	Relation with Midline Horizontal Strain*		Relation with Maximum Horizontal Strain*	
	Equation	R^2	Equation	R^2
DSI_{4-8}	$y = 0.0891x^{0.9776}$	0.82	**$y = 0.0337x^{0.7862}$**	**0.93**
DSI_{4-12}	$y = 0.0257x^{0.8833}$	0.88	**$y = 0.0111x^{0.6886}$**	**0.94**
DSI_{4-18}	**$y = 0.0104x^{0.7857}$**	**0.91**	**$y = 0.005x^{0.5947}$**	**0.91**
DSI_{4-24}	**$y = 0.0067x^{0.7313}$**	**0.90**	$y = 0.0035x^{0.5445}$	0.88

*At the bottom of AC layer.
y = Horizontal strain.
x = Index.
Note: There were 43 data points from both TSD and RWD loading. Bold cells indicate indices in class 1.

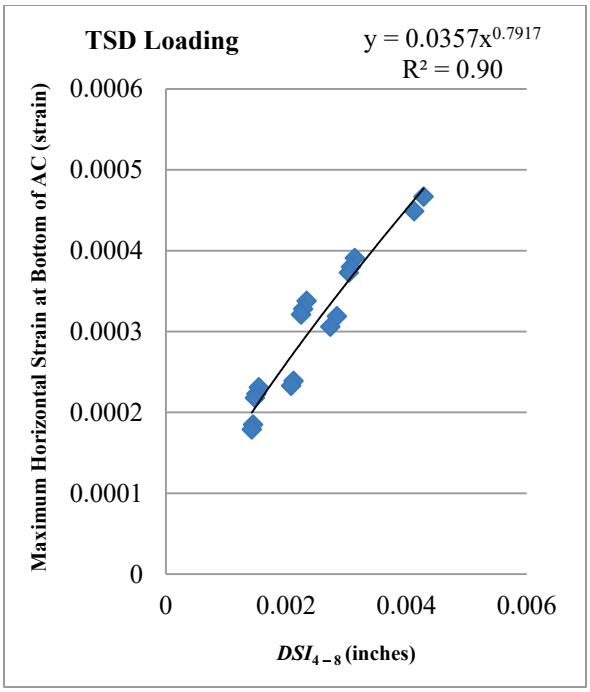

1 inch = 25.4 mm

Figure 175. Graph. Relationship between DSI_{4-8} and horizontal strains at bottom of AC with TSD loading data.

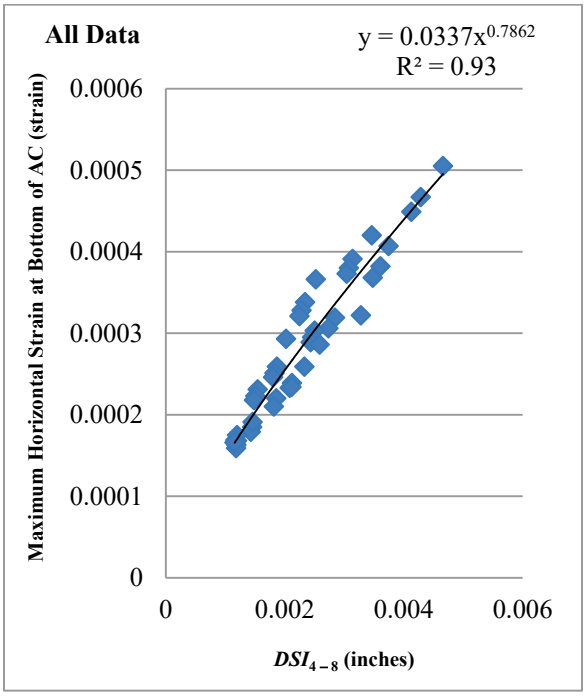

1 inch = 25.4 mm

Figure 176. Graph. Relationship between DSI_{4-8} and horizontal strains at bottom of AC with all loading data.

Because vertical strain at the top of the subgrade is an important response that relates to subgrade rutting, the deflection basin indices considered were also correlated with those strains.

Table 53, table 54, figure 177, and figure 178 show the relationships between SCI and vertical strain at the top of the subgrade. While SCI (e.g., SCI_{12}) was one of the most appropriate indices related to maximum horizontal strain at the bottom of AC, it cannot be used to relate to subgrade strain because of poor correlation.

Table 53. Relationship between SCI and maximum vertical strains on top of the subgrade with TSD loading data.

Index	Relation with Maximum Vertical Strain*	
	Equation	**R^2**
SCI_8	$y = 1E+07x^{1.7785}$	0.38
SCI_{12}	$y = 6E+06x^{1.904}$	0.62
SCI_{18}	$y = 2E+06x^{1.7981}$	0.76
SCI_{24}	$y = 815968x^{1.7374}$	0.84
SCI_{36}	$y = 447767x^{1.6776}$	0.88
SCI_{48}	$y = 402727x^{1.6869}$	0.89
SCI_{60}	$y = 414955x^{1.7136}$	0.89

*On top of subgrade.
y = Vertical strain.
x = Index.
Note: There were 17 TSD loading data points.

Table 54. Relationship between SCI and maximum vertical strains on top of the subgrade with all loading data.

Index	Relation with Maximum Vertical Strain*	
	Equation	**R^2**
SCI_8	$y = 9E+06x^{1.752}$	0.39
SCI_{12}	$y = 4E+06x^{1.8178}$	0.62
SCI_{18}	$y = 1E+06x^{1.7333}$	0.78
SCI_{24}	$y = 621344x^{1.6678}$	0.84
SCI_{36}	$y = 360860x^{1.6188}$	0.88
SCI_{48}	$y = 328608x^{1.63}$	0.89
SCI_{60}	**$y = 335884x^{1.654}$**	**0.90**

*On top of subgrade.
y = Vertical strain.
x = Index.
Note: There were 43 data points from both TSD and RWD loading. Bold cells indicate indices in class 1.

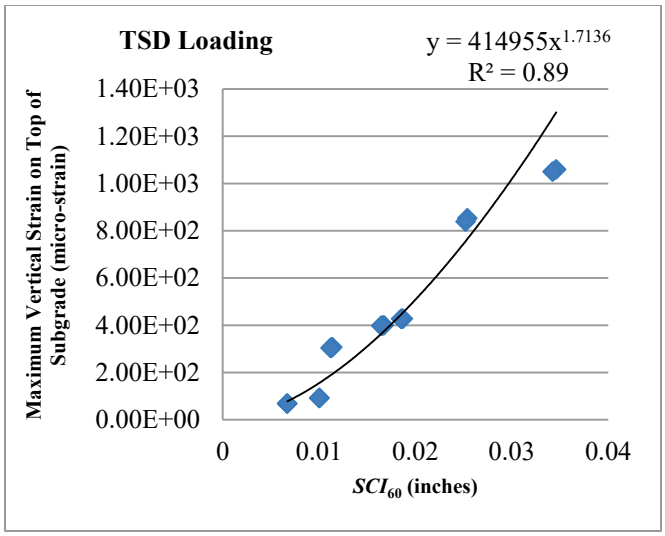

1 inch = 25.4 mm

Figure 177. Graph. Relationship between *SCI*$_{60}$ and maximum vertical strain on top of the subgrade with TSD loading data.

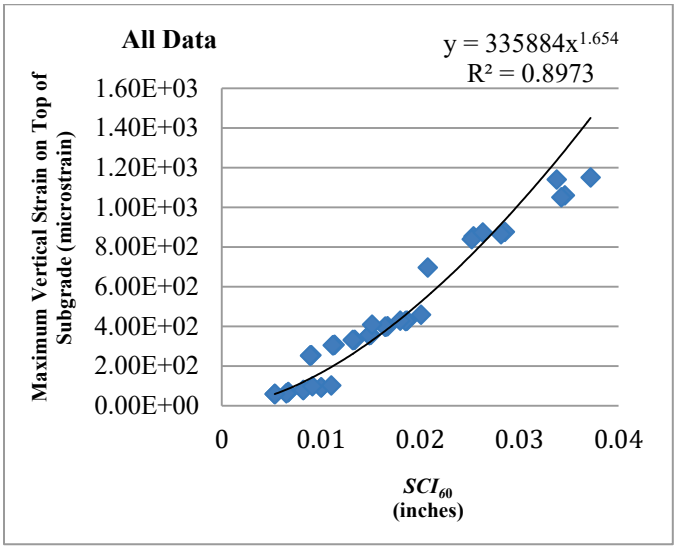

1 inch = 25.4 mm

Figure 178. Graph. Relationship between *SCI*$_{60}$ and maximum vertical strain on top of the subgrade with all loading data.

Table 55, table 56, figure 179, and figure 180 show the relationships between DSI_{24-r} and vertical strain at the top of the subgrade. DSI_{24-36}, which is also known as BCI, had a good correlation, indicated by class 1 classification. Moreover, it was observed that those indices based on displacements at far away locations from the loaded area were better related to vertical strain at the top of the subgrade. This is because these indices reflect the influence of the lower portion of the pavement system.[62,63] Similar tables and figures looking at the rutting strain relationship were developed for every index in table 44, but they are not included in this report as they do not provide further insights. The data used to generate these tables and figures can be obtained directly from FHWA.

Table 55. Relationship between DSI_{24-r} and maximum vertical strain on top of the subgrade with TSD loading data.

Index	Relation with Maximum Vertical Strain*	
	Equation	R^2
DSI_{24-36}	**$y = 937463x^{1.3155}$**	**0.97**
DSI_{24-48}	**$y = 994720x^{1.4238}$**	**0.97**
DSI_{24-60}	**$y = 1E+06x^{1.5332}$**	**0.97**

*On top of subgrade.
y = Vertical strain.
x = Index.
Note: There were 17 TSD loading data points. Bold cells indicate indices in class 1.

Table 56. Relationship between DSI_{24-r} and maximum vertical strain on top of the subgrade with all loading data.

Index	Relation with Maximum Vertical Strain*	
	Equation	R^2
DSI_{24-36}	**$y = 880697x^{1.3031}$**	**0.98**
DSI_{24-48}	**$y = 936915x^{1.4106}$**	**0.97**
DSI_{24-60}	**$y = 1E+06x^{1.5125}$**	**0.97**

*On top of subgrade.
y = Vertical strain.
x = Index.
Note: There were 43 data points from both TSD and RWD loading. Bold cells indicate indices in class 1.

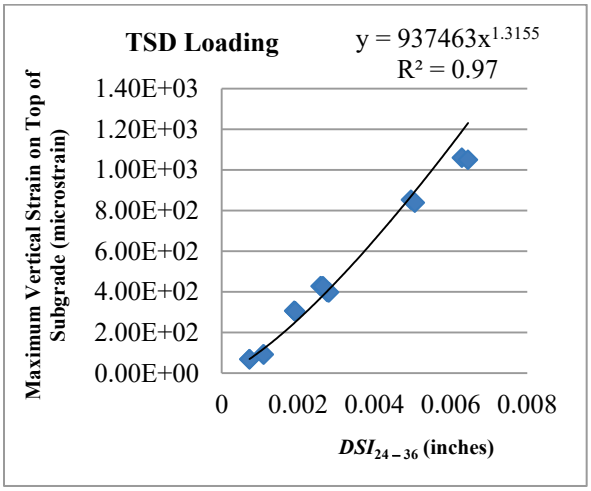

1 inch = 25.4 mm

Figure 179. Graph. Relationship between DSI_{24-36} and maximum vertical strain on top of the subgrade with TSD loading data.

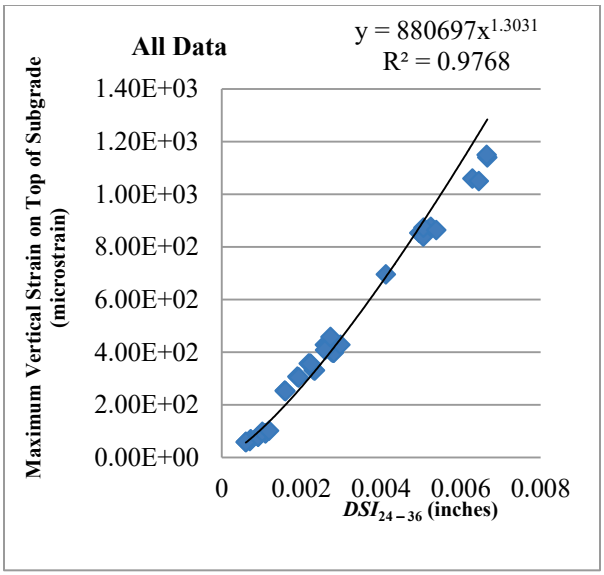

1 inch = 25.4 mm

Figure 180. Graph. Relationship between DSI_{24-36} and maximum vertical strain on top of the subgrade with all loading data.

Summary of Evaluation of Indices

Table 57 through table 60 summarize the most appropriate indices for TSD and for the combined data (TSD and RWD) against maximum horizontal strain at the bottom of the AC and maximum vertical strain on the top of subgrade, respectively. Some of the most significant observations from these tables are as follows (see table 44 for definitions of indices):

- Load characteristics (TSD versus RWD) did not appear to have much influence on the respective indices used to develop the correlations with important critical pavement responses needed for pavement performance evaluations.
- The best indices that related to the maximum horizontal strain at the bottom of the AC layer were $R1_{12}$, and $R2_{18}$, SCI_{12}, or SD_{12}. All these indices related deflections that occurred close to the center of the load.
- Using D_{max} instead of D_0 to calculate SCI did not noticeably improve the correlation; however, slightly better correlations, indicated by a higher R^2 value, existed when using *SCIm*.
- Using D_4 instead of D_0 to calculate SCI seemed reasonable. In turn, if D_4 from the TSD is more reliable than D_0, it should be used as the reference displacement in SCI calculations.
- Indices based on far away deflections (i.e., beyond 12 inches (304.8 mm)) seemed to relate well with maximum subgrade vertical strain. For example, BCI reflected the role of the lower portion of the pavement system, and it had a good correlation, as indicated by class 1 classification with vertical strain on top subgrade.

- The appropriate indices for maximum subgrade vertical strain ($R^2 > 0.95$) were $DSI_{12-r} = D_{12} - D_r$, $DSI_{18-r} = D_{18} - D_r$, and $DSI_{24-r} = D_{24} - D_r$.

While SCI_{12} was found to be one of the most appropriate indices for maximum horizontal strain at the bottom of the AC ($R^2 = 0.95$), it was not a good index for subgrade vertical strain ($R^2 = 0.62$).

Table 57. Most appropriate indices using TSD data related to maximum horizontal strain at bottom of AC layer.

Best Indices with TSD Loading (Relationship with Maximum Horizontal Strain)	Index	R^2
$R1$	$R1_{12}$	0.94
	$R1_{18}$	0.92
$R2$	$R2_{18}$	0.92
	$R2_{24}$	0.94
	$R2_{36}$	0.90
SCI	SCI_{12}	0.94
	SCI_{18}	0.92
	$SCIm_{12}$	0.92
	$SCIm_{18}$	0.91
DSI	DSI_{4-8}	0.90
	DSI_{4-12}	0.91
	DSI_{4-18}	0.90
SD	SD_{12}	0.93
	SD_{18}	0.92
TS	TS_8	0.93
	TS_{24}	0.91
AUPP	A_m	0.90

Table 58. Most appropriate indices using all data related to maximum horizontal strain at bottom of AC layer.

Best Indices with All Data (Relationship with Maximum Horizontal Strain)	Index	R^2
*R*1	$R1_{12}$	0.95
	$R1_{18}$	0.93
*R*2	$R2_{18}$	0.95
	$R2_{24}$	0.94
SCI	SCI_{12}	0.95
	SCI_{18}	0.93
	$SCIm_{8}$	0.91
	$SCIm_{12}$	0.95
	$SCIm_{18}$	0.93
DSI	DSI_{4-8}	0.93
	DSI_{4-12}	0.94
	DSI_{4-18}	0.91
	DSI_{8-12}	0.92
SD	SD_{12}	0.95
	SD_{18}	0.93
TS	TS_{8}	0.94
AUPP	A_m	0.91

Table 59. Most appropriate indices using TSD data related to maximum vertical strain at top of subgrade.

Best Indices with TSD Loading (Relationship with Maximum Vertical Strain at Top of Subgrade)	Index	R^2
*R*2	$R2_{60}$	0.92
DSI	DSI_{4-48}	0.90
	DSI_{4-60}	0.90
	DSI_{8-36}	0.92
	DSI_{8-48}	0.93
	DSI_{8-60}	0.93
	DSI_{12-18}	0.90
	DSI_{12-24}*	0.94
	DSI_{12-36}	0.95
	DSI_{12-48}	0.95
	DSI_{12-60}	0.95
	DSI_{18-24}	0.97
	DSI_{18-36}	0.97
	DSI_{18-48}	0.97
	DSI_{18-60}	0.97
	DSI_{24-36}**	0.97
	DSI_{24-48}	0.97
	DSI_{24-60}	0.97
TS	TS_{12}	0.90
	TS_{18}	0.92
	TS_{36}	0.95
Shape factor	F_2	0.91

*Indicates BDI.
**Indicates BCI.

Table 60. Most appropriate indices using all data related to maximum vertical strain at top of subgrade.

Best Indices with All Data (Relationship with Maximum Vertical Strain at Top of Subgrade)	Index	R^2
*R*2	$R2_{48}$	0.90
	$R2_{60}$	0.93
DSI	DSI_{4-48}	0.91
	DSI_{4-60}	0.91
	DSI_{8-24}	0.91
	DSI_{8-36}	0.93
	DSI_{8-48}	0.94
	DSI_{8-60}	0.94
	DSI_{12-18}	0.92
	DSI_{12-24}*	0.95
	DSI_{12-36}	0.96
	DSI_{12-48}	0.96
	DSI_{12-60}	0.96
	DSI_{18-24}	0.97
	DSI_{18-36}	0.98
	DSI_{18-48}	0.97
	DSI_{18-60}	0.97
	DSI_{24-36}**	0.98
	DSI_{24-48}	0.97
	DSI_{24-60}	0.97
TS	TS_{18}	0.91
	TS_{24}	0.91
	TS_{36}	0.94

*Indicates BDI.
**Indicates BCI.

Evaluating Indices Using MnROAD Measured Data

During the September 2013 TSDD field trials, pavement response data were collected using both project and MnROAD sensors. The project sensors collected surface displacements, while pavement responses (longitudinal AC strain and vertical stresses at the top of the subgrade) were collected by the MnROAD sensors.

The correlations between deflection indices and pavement responses can also be explored based solely on the measured data. From project sensors embedded at the pavement surface, the surface displacements along the midline of the tires in the longitudinal direction can be estimated. However, adjustments should be made to account for the time lag that exists between D_{max}

and D_0. In addition, as pointed out in chapter 7, the lateral wheel wander can also affect the estimation of the midline deflections.

MnROAD sensors collected responses at interior pavement locations (see table 41), and they were also affected by the lateral wheel wander. In other words, the maximum responses given by the MnROAD sensors may not have been the actual maxima for the responses in question. Also, because MnROAD sensors that measured vertical stresses were considered unreliable (section 7.6), only the measured data from the longitudinal AC strain gauges were correlated.

Table 61 shows the best correlated indices from 3D-Move computed displacement bowls with respect to 3D-Move computed maximum AC strains and the measured maximum horizontal AC strains. R^2 values of the correlations with computed displacements and maximum strains (i.e., both 3D-Move derived) are higher. It should be noted R^2 values that are shown in the table correspond to the respective best curve-fit equations obtained for the relationship.

Table 61. Comparison of most appropriate indices with respect to maximum horizontal strain: 3D-Move results and MnROAD measured data.

Best Indices with All Data (Relationship with Maximum Horizontal Strain for 3D-Move and Measured Strain)	Index	R^2 from 3D-Move Relationships	R^2 from Measured Relationships
*R*1	$R1_{12}$	0.95	0.86
	$R1_{18}$	0.93	0.87
*R*2	$R2_{18}$	0.95	0.88
	$R2_{24}$	0.94	0.89
SCI	SCI_{12}	0.95	0.86
	SCI_{18}	0.93	0.87
	$SCIm_{8}$	0.91	0.83
	$SCIm_{12}$	0.95	0.88
	$SCIm_{18}$	0.93	0.90
DSI	DSI_{4-8}	0.93	0.83
	DSI_{4-12}	0.94	0.85
	DSI_{4-18}	0.91	0.86
	DSI_{8-12}	0.92	0.85
SD	SD_{12}	0.95	0.86
	SD_{18}	0.93	0.87
TS	TS_8	0.94	0.91
AUPP	A_m	0.91	0.87

Evaluation of RWD Sensor Location from Project Sensor Measurements

As noted previously, the RWD used two sensors within the deflection bowl to characterize the deflected pavement surface. The sensors were located 7.25 inches (184.15 mm) behind the rear wheels and 7.75 inches (196.85 mm) in front of the rear wheels, as shown in figure 19 in chapter 4. In addition to the accuracy evaluation of RWD laser sensor presented in chapter 6, a deflection basin measured from the project sensor was used to evaluate the effectiveness of positioning the sensor 7.25 inches (184.15 mm) behind the wheels in capturing the maximum deflection. The response lag between the time that the rear tire crosses over the sensor and the time when the maximum response occurred in the project sensor signal is reproduced in table 62 for RWD testing. Table 62 also shows the percent difference between the deflections measured 7.25 inches (184.15 mm) behind the rear axle ($D_{-7.25}$) and D_{max}. Response lag is a function of pavement stiffness and vehicle speed. Cell 3, which was the stiffest of the three cells tested, had the least response lag and percent difference. Also, as expected, response lag decreased as vehicle speed increased. In summary, for stiffer pavements, the maximum deflection occurred closer to the center of the tire when tested at 60 mi/h (96.9 km/h). The hypothesis that maximum deflection occurs 7.25 inches (184.15 mm) behind the tire is valid only for less stiff pavements tested at relatively lower traffic speeds and may not be valid for stiff pavements tested at 60mi/h (96.9 km/h).

As noted, a number of previous studies have concluded that curvature indices, which are evaluated based on the difference in surface deflection at two points, reflect the characteristics of the AC layer.[62,63,21] The only possible curvature index from RWD, $D_{-7.25} - D_{7.75}$ was evaluated further in this study. Table 62 also summarizes the percent difference between the computed index ($D_{-7.25} - D_{7.75}$) and SCI_{15} as computed from the deflection basin measured in project sensor. SCI_{15} is the difference between maximum deflection and the deflection 15 inches (381 mm) in front of maximum deflection. When the response lag was less than 7.25 inches (184.15 mm) as in stiff pavements, the two deflection measurements $D_{-7.25}$ and $D_{7.75}$ were made on either side of the deflection basin, thus increasing the difference between the actual and computed index. The accuracy of the index computed from RWD deflection was hampered by the measurement location, especially in stiff pavements. In order to improve the compatibility of the RWD device to wider pavement sections, it is suggested that the location of the sensor be positioned in front of the rear axle.

Table 62. Effect of RWD laser position on deflection and computed index.

Cell	Speed (mi/h)	RWD Response Lag (inches)	Percent Difference Between Deflection at $D_{-7.25}$ and D_{max}		Percent Difference Between Index ($D_{-7.25} - D_{7.75}$) and SCI_{15}	
34	30	7.3	0.04	0.15	-0.49	-0.11
	45	6.9	0.25		0.27	
19	30	4.5	3.42	4.04	22.11	28.75
	45	3.4	5.33		32.98	
	60	4	3.38		31.17	
3	30	4.3	3.47	6.84	28.95	41.91
	45	2.5	5.80		42.30	
	60	1.6	11.26		54.49	

1 mi/h = 1.6 km/h
1 inch = 25.4 mm

8.3 STEP 2: CORRELATING DEFLECTION BASIN INDICES USING 3D-MOVE ANALYSIS OF SIMULATED PAVEMENT SECTIONS

In the previous section, 3D-Move runs for the MnROAD accuracy cells were used to find the surface deflection indices that correlated best with pavement responses. However, the pavements for the MnROAD accuracy cells were relatively thin, with AC layer thicknesses varying between 3 and 5 inches (76.2 and 127 mm). Factors such as AC layer thickness, modulus and vehicle speed can and do influence the deflection correlations. Accordingly, in this section, the details of the 3D-Move-based correlation investigation that used a variety of pavement structures with differing properties (thickness and modulus) and vehicle speeds are presented.

Simulated Pavements for 3D-Move Based Correlations

Figure 181 shows a generic pavement structure used in the analyses. For the AC layer, three thickness (3, 6, and 12 inches (76.2, 152.4, 304.8 mm)) and three moduli (200, 500, and 800 ksi (1.37, 3.44, and 5.51 GPa)) were considered. The base layer thickness and modulus were fixed at 12 inches (304.8 mm) and 60 ksi (0.41 GPa), respectively. Moduli of 10 and 20 ksi (0.07 and 0.14 GPa) were used for the subgrade layer. In addition, vehicle speeds of 30 and 60 mi/h (48.3 and 96.6 km/h) were used in the 3D-Move runs. This resulted in 36 combinations of pavement structures and vehicle speeds, as shown in table 63.

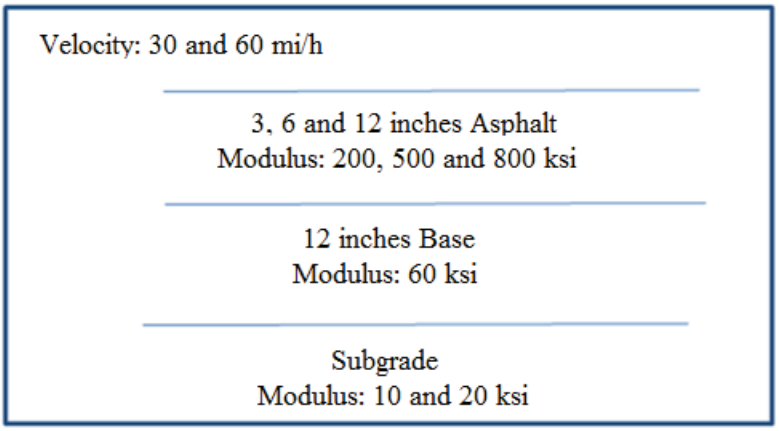

1 mi/h = 1.61 km/h
1 inch = 25.4 mm
1 ksi = 6.89 MPa

Figure 181**. Illustration. Pavement structures used with 3D-Move analyses.**

Table 63. Pavement considered in 3D-Move analyses and corresponding identification key.

Identification Key	AC Modulus at 30 Hz (ksi)	AC Thickness (inches)	Subgrade Modulus (ksi)	Vehicle Speed (mi/h)
B200-3-10-30	200	3	10	30
B200-3-10-60	200	3	10	60
B200-3-20-30	200	3	20	30
B200-3-20-60	200	3	20	60
B200-6-10-30	200	6	10	30
B200-6-10-60	200	6	10	60
B200-6-20-30	200	6	20	30
B200-6-20-60	200	6	20	60
B200-12-10-30	200	12	10	30
B200-12-10-60	200	12	10	60
B200-12-20-30	200	12	20	30
B200-12-20-60	200	12	20	60
B500-3-10-30	500	3	10	30
B500-3-10-60	500	3	10	60
B500-3-20-30	500	3	20	30
B500-3-20-60	500	3	20	60
B500-6-10-30	500	6	10	30
B500-6-10-60	500	6	10	60
B500-6-20-30	500	6	20	30
B500-6-20-60	500	6	20	60
B500-12-10-30	500	12	10	30
B500-12-10-60	500	12	10	60
B500-12-20-30	500	12	20	30
B500-12-20-60	500	12	20	60
B800-3-10-30	800	3	10	30
B800-3-10-60	800	3	10	60
B800-3-20-30	800	3	20	30
B800-3-20-60	800	3	20	60
B800-6-10-30	800	6	10	30
B800-6-10-60	800	6	10	60
B800-6-20-30	800	6	20	30
B800-6-20-60	800	6	20	60
B800-12-10-30	800	12	10	30
B800-12-10-60	800	12	10	60
B800-12-20-30	800	12	20	30
B800-12-20-60	800	12	20	60

1 ksi = 6.89 MPa
1 inch = 25.4 mm
1 mi/h = 1.61 km/h

The impact of pavement temperature was reflected in the AC modulus; therefore, it was not considered an independent parameter. The AC modulus as a function of frequency (a master curve) needs to be specified as input when the viscoelastic material characteristics are considered

in 3D-Move. The procedure to build a master curve from AC mix properties is explained in chapter 7. The AC modulus given in table 63 was considered appropriate for a frequency of 30 Hz when estimating the AC moduli as a function of frequency. Table 64 shows the AC mix properties used to develop the master curve for the effort in question.

Table 64. AC mix properties used with 3D-Move analysis.

Variable	Value
Air Voids (percent)	7
Effective binder content (percent)	11
Void filled with asphalt (percent)	61
Percent retained for 0.75 inch	11.62
Percent retained for 0.375 inch	35.3
Percent retained #4 sieve	52.64
Percent passing #200 sieve	7.28
PG grade	58-28
Binder—regression intercept	11.01
Binder—VTS	-3.701

1 inch = 25.4 mm

3D-Move Results and Sensitivity Analysis

The 75 indices listed in table 44 were reevaluated using the 3D-Move results from the 36 pavement structure and vehicle speed combinations detailed in the previous section. The sensitivity of those indices was investigated with respect to the following parameters: AC thickness and modulus, subgrade modulus, and vehicle speed. A major objective of this analysis was to isolate the parameters that most affect the indices. Once identified, those parameters could be used as a starting point in categorizing the pavements in the next step using JULEA.[26]

For the purpose of brevity, only selected figures showing notable conclusions are presented in this chapter. Similar figures to those presented in this chapter were developed for other deflection indices, but they are not included in this report, as they do not provide further insights. The data used to generate these figures can be obtained directly from FHWA.

Figure 182 shows the variation of SCI_{12} for the pavement combinations considered. The x-axis shows the key that can be used to identify easily a specific pavement combination (see table 63). In this graph, nine categories are shown with different fill patterns. For each category, the AC surface layer properties (AC thickness and AC modulus) remained constant. As shown, SCI_{12}, which has been often viewed as an indicator of the influence of the AC layer, is strongly influenced by the AC thickness and modulus.

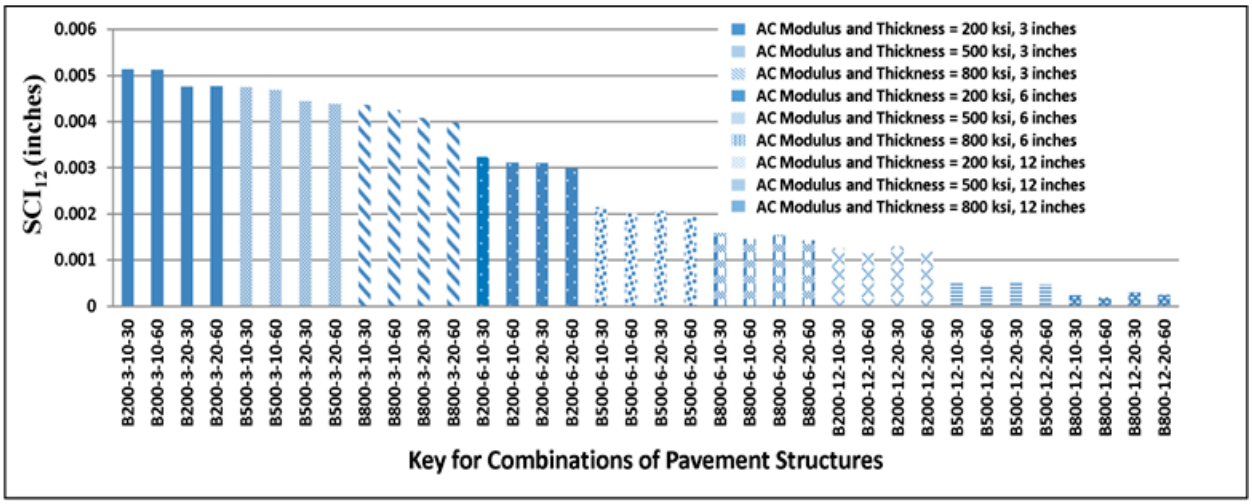

1 inch = 25.4 mm

Figure 182. Graph. Variation of SCI_{12} calculated with 3D-Move in simulated pavement combinations.

TS is potentially considered an important index because it is measured directly by the TSD, and thus uncertainties associated with algorithms needed to convert the measured deflection velocities to surface deflections are avoided. In general, TS showed high sensitivity to changes in the pavement layer properties (stiffness and thickness). In particular, TS_{48} and TS_{60} seemed to be mostly affected by subgrade modulus. For example, TS_{60} is clearly influenced by subgrade modulus (see figure 183). As is shown later in this chapter, TS_4 and TS_8 are better correlated with the maximum horizontal strain at the bottom of thin and thick AC layers, respectively.

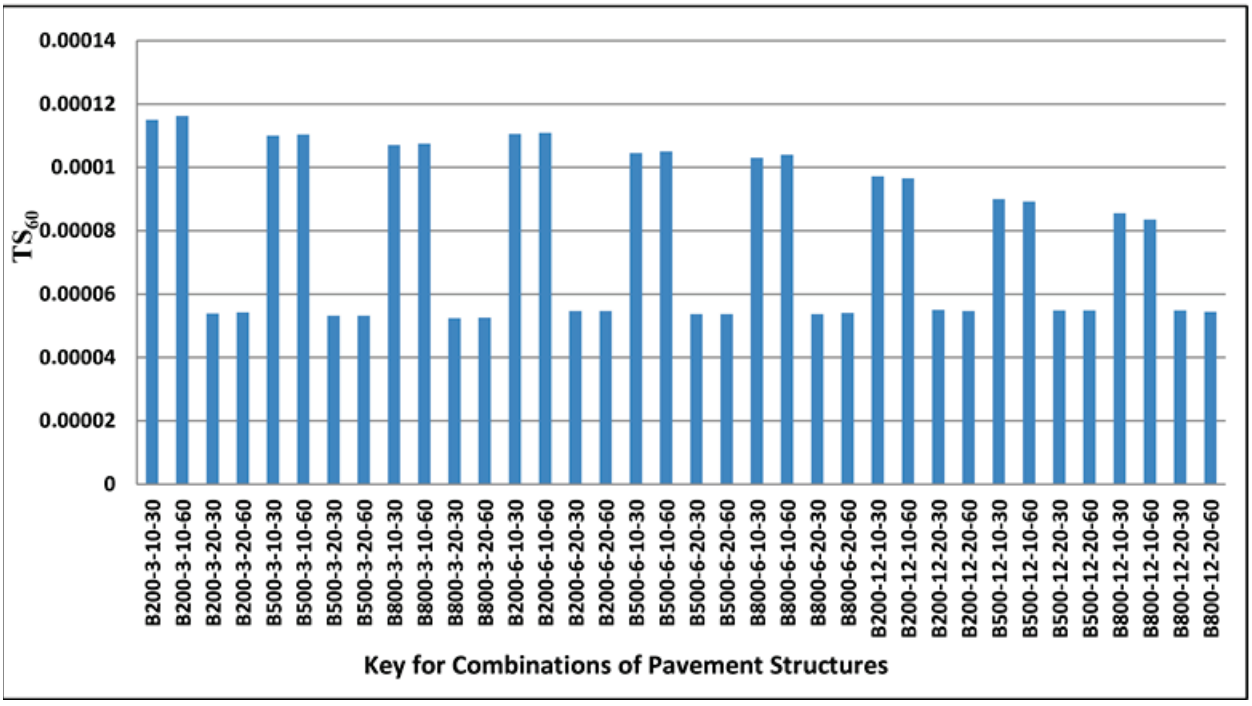

Figure 183. Graph. Variation of TS_{60} calculated with 3D-Move in simulated pavement combinations.

R as defined by Horak was significantly affected by the properties of the surface AC layer and slightly affected by the stiffness of the subgrade.[62,63] Figure 184 shows the variation in R_{60} for the pavement combinations considered.

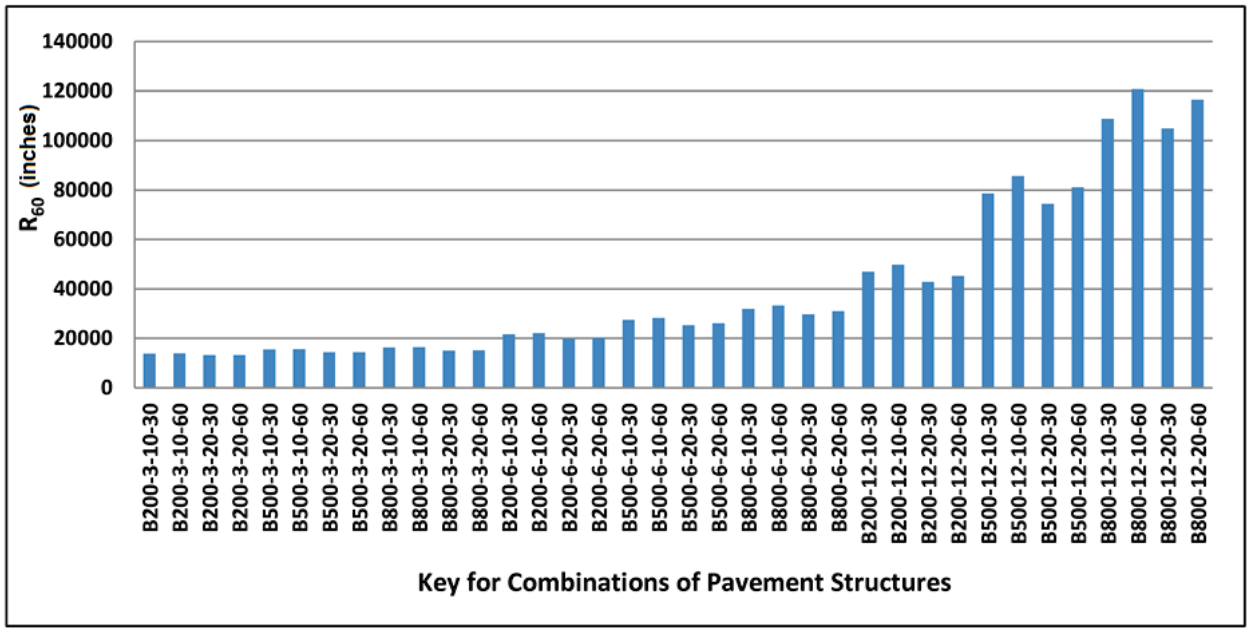

1 inch = 25.4 mm

Figure 184. Graph. Variation of R_{60} calculated with 3D-Move in simulated pavement combinations.

D_{60} seemed to be the most promising parameter for estimating the subgrade modulus, as shown in figure 185. This parameter seemed to be only affected by the subgrade modulus; other material properties did not have a noticeable influence.

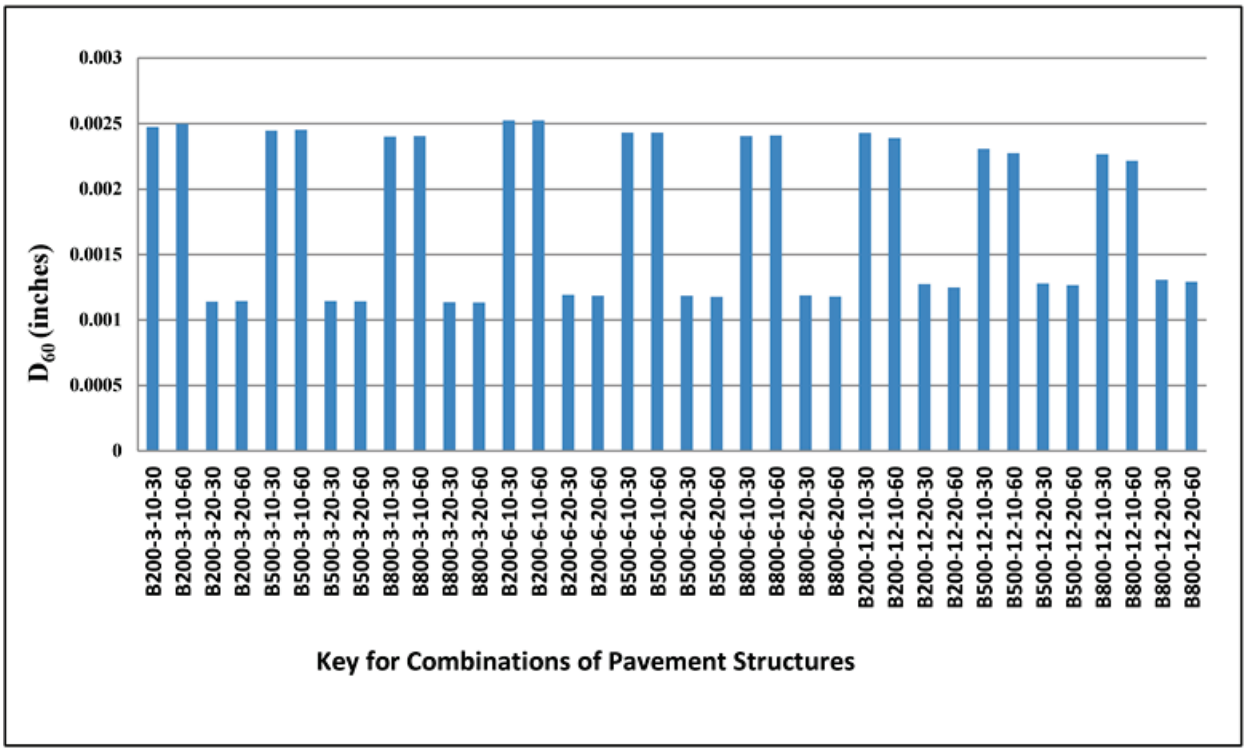

1 inch = 25.4 mm

Figure 185. Graph. Variation of D_{60} calculated with 3D-Move in simulated pavement combinations.

Figure 186 shows the variation in maximum horizontal strain at the bottom of the AC layer for various pavement combinations considered. Table 65 summarizes the response trends as a few of pavement-related parameters are increased one at a time. As shown in the referenced figure and table, increasing subgrade modulus affected the thin and thick pavements differently. For thin pavements, increasing the subgrade stiffness resulted in an increase in the horizontal strains at the bottom of the AC layer, while the opposite trend was observed for thick pavements (i.e., the strains decreased).

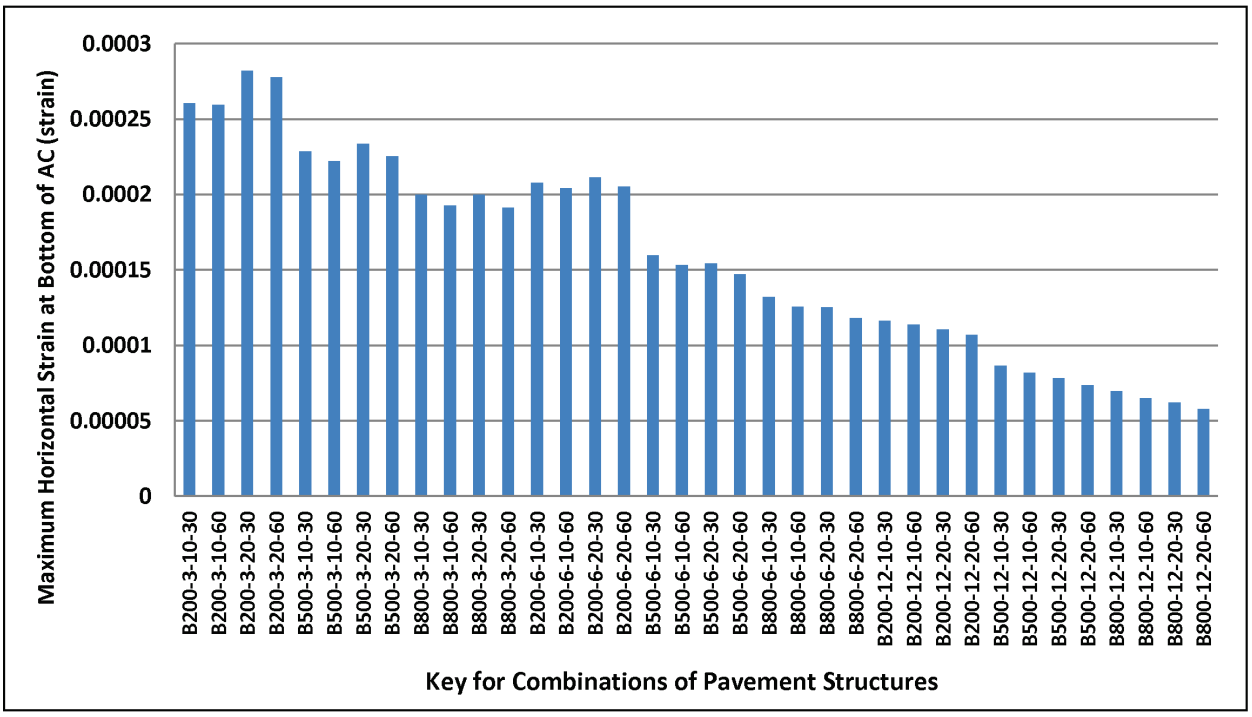

Figure 186. Graph. Variation of maximum horizontal strain at bottom of AC layer in simulated pavement combinations.

Table 65. Effects of an increase in selected pavement parameters on maximum horizontal strain at bottom of AC layer.

Increase in Parameter	Maximum Horizontal Strain at Bottom of AC Layer
AC modulus	Decreased
AC thickness	Decreased
Speed	Decreased
Subgrade modulus	Thin AC (3 inches) increased; thick AC (12 inches) decreased

1 inch = 25.4 mm

Figure 187 through figure 206 show the variability of the correlations of some of the indices to the maximum horizontal strain at the bottom of the AC layer. In all figures, the numbers within parentheses in the legends indicate the number of data points. One of the important interpretations from these figures is that the AC thickness impacted the strengths of the relationships as judged by the R^2 values. Many indices did not consistently relate well with the maximum horizontal strain for thin (3 inches (76.2 mm)) AC pavements. Other material properties, such as the subgrade and AC moduli, also influenced the strengths of the relationships for thin pavements. Conversely, thick (12 inches (304.8 mm)) AC pavements were less sensitive to those parameters.

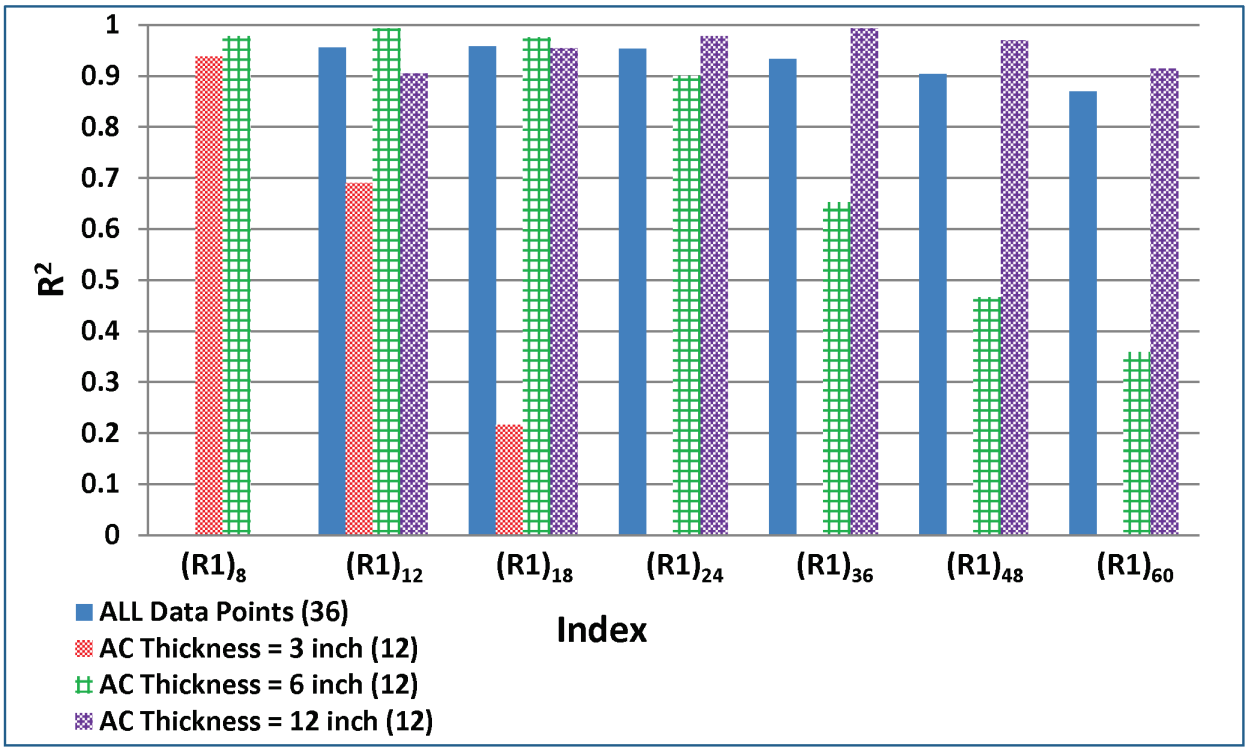

1 inch = 25.4 mm

Figure 187. Graph. Variability of relationships of *R*1 with maximum horizontal strain at bottom of AC layer for various AC thicknesses.

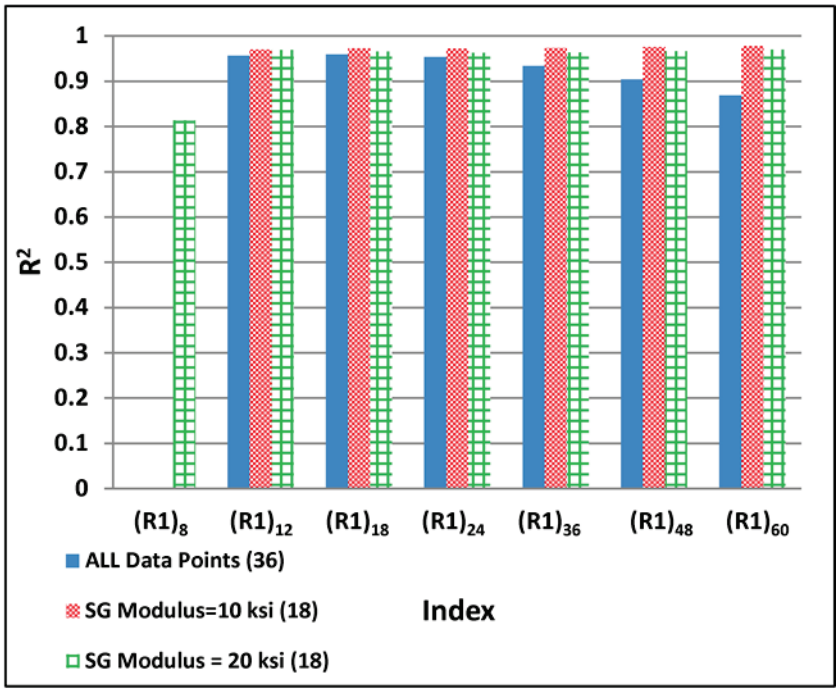

1 ksi = 6.89 MPa

Figure 188. Graph. Variability of relationships of *R*1 with maximum horizontal strain at bottom of AC layer for various subgrade moduli.

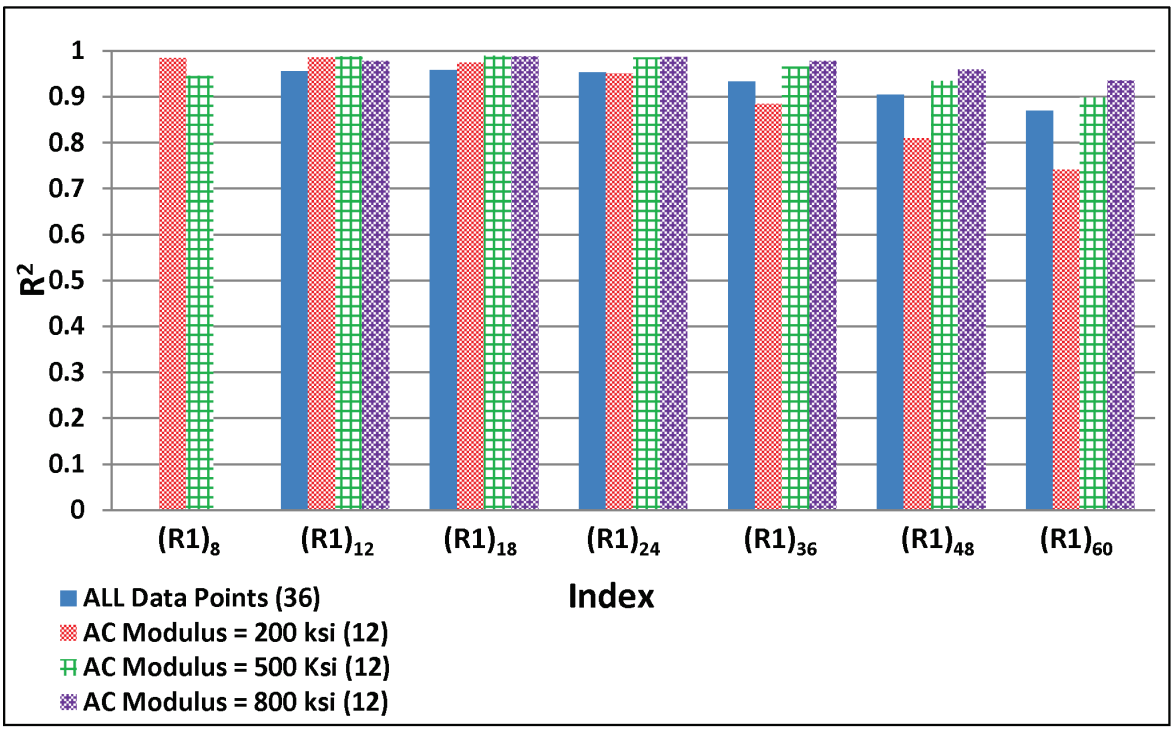

1 ksi = 6.89 MPa

Figure 189. Graph. Variability of relationships of *R*1 with maximum horizontal strain at bottom of AC layer for various AC moduli.

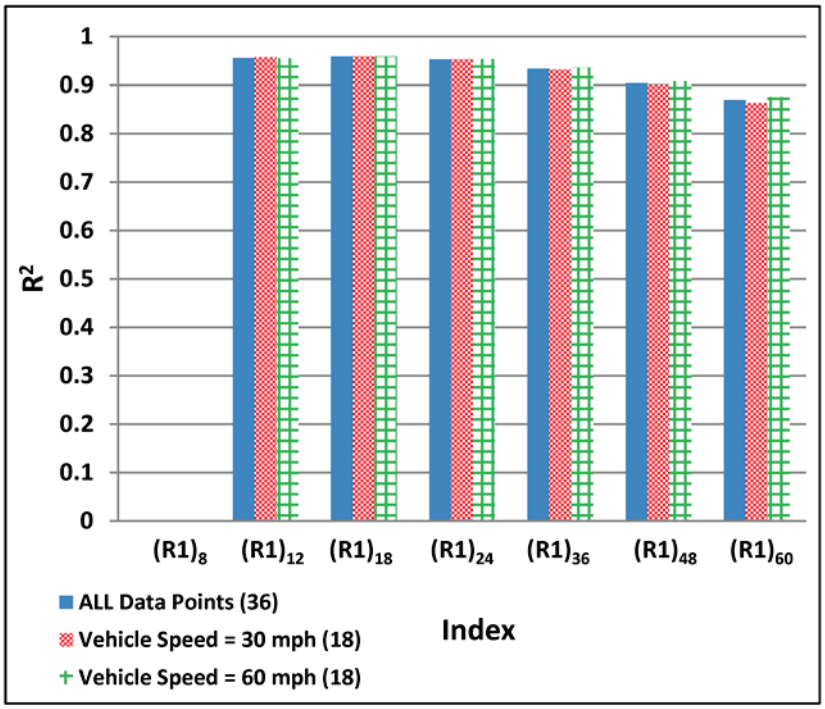

1 mi/h = 1.61 km/h

Figure 190. Graph. Variability of relationships of *R*1 with maximum horizontal strain at bottom of AC layer for various vehicle speeds.

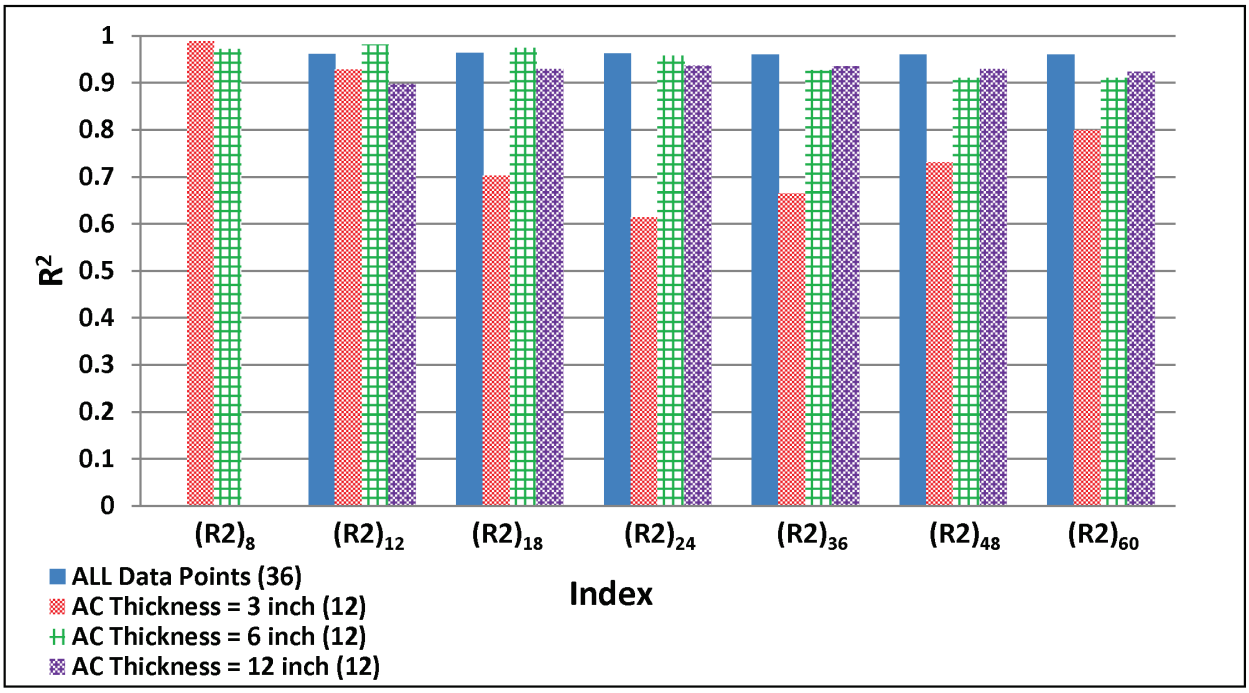

1 inch = 25.4 mm

Figure 191. Graph. Variability of relationships of *R*2 with maximum horizontal strain at bottom of AC layer for various AC thicknesses.

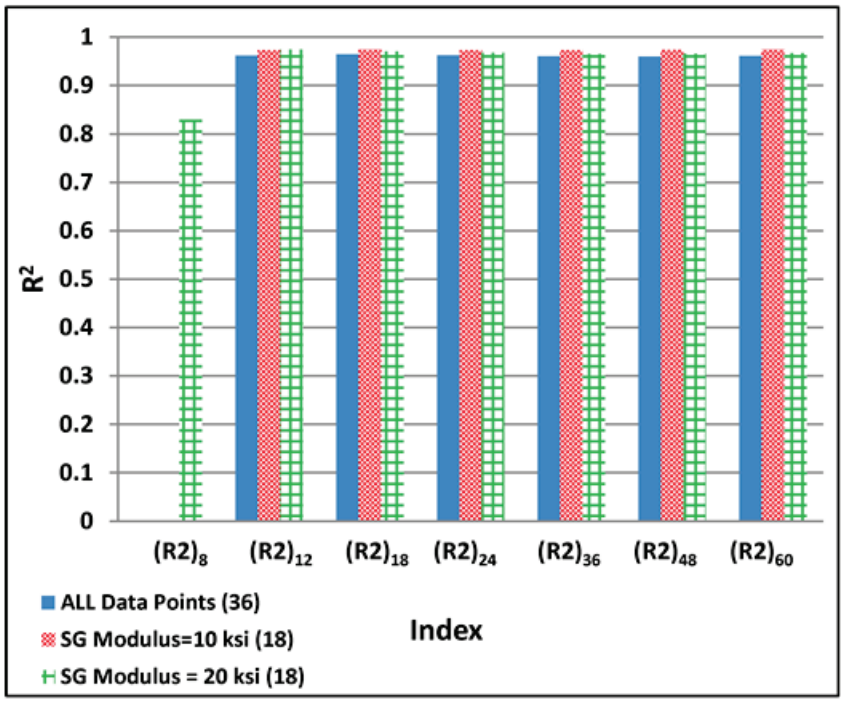

1 ksi = 6.89 MPa

Figure 192. Graph. Variability of relationships of *R*2 with maximum horizontal strain at bottom of AC layer for various subgrade moduli.

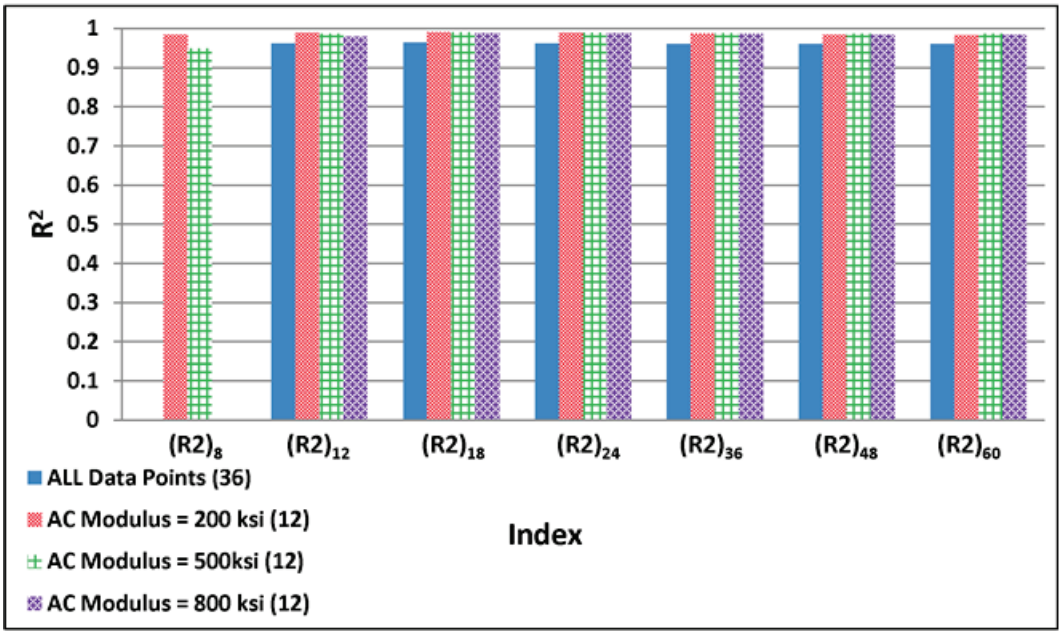

1 ksi = 6.89 MPa

Figure 193. Graph. Variability of relationships of *R*2 with maximum horizontal strain at bottom of AC layer for various AC moduli.

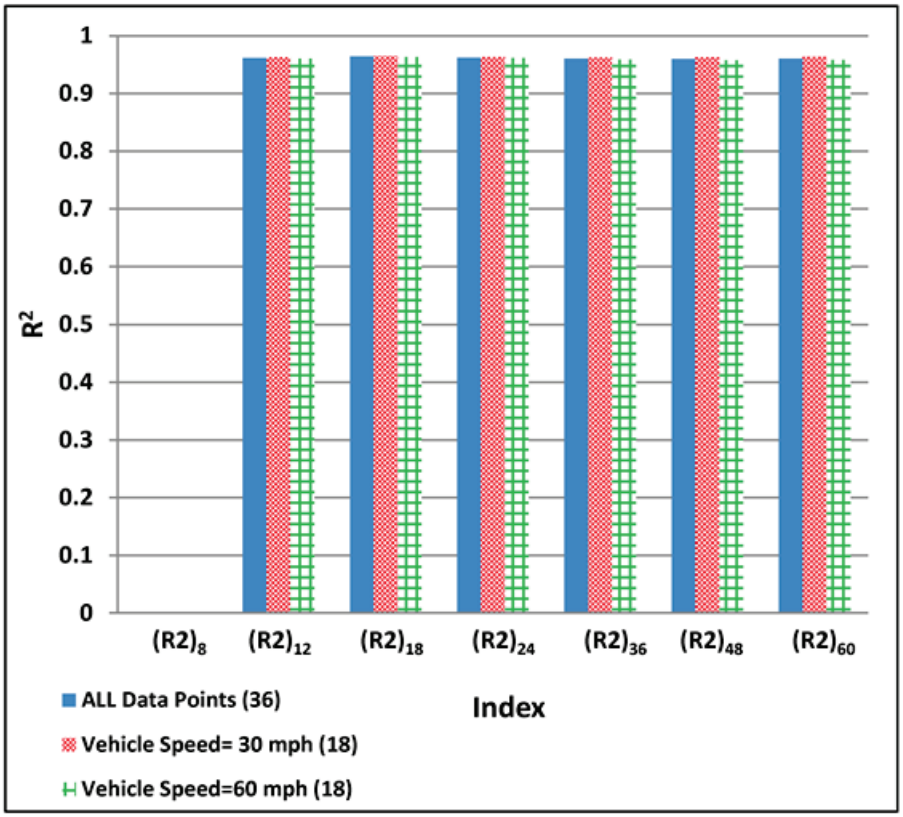

1 mi/h = 1.61 km/h

Figure 194. Graph. Variability of relationships of *R*2 with maximum horizontal strain at bottom of AC layer for various vehicle speeds.

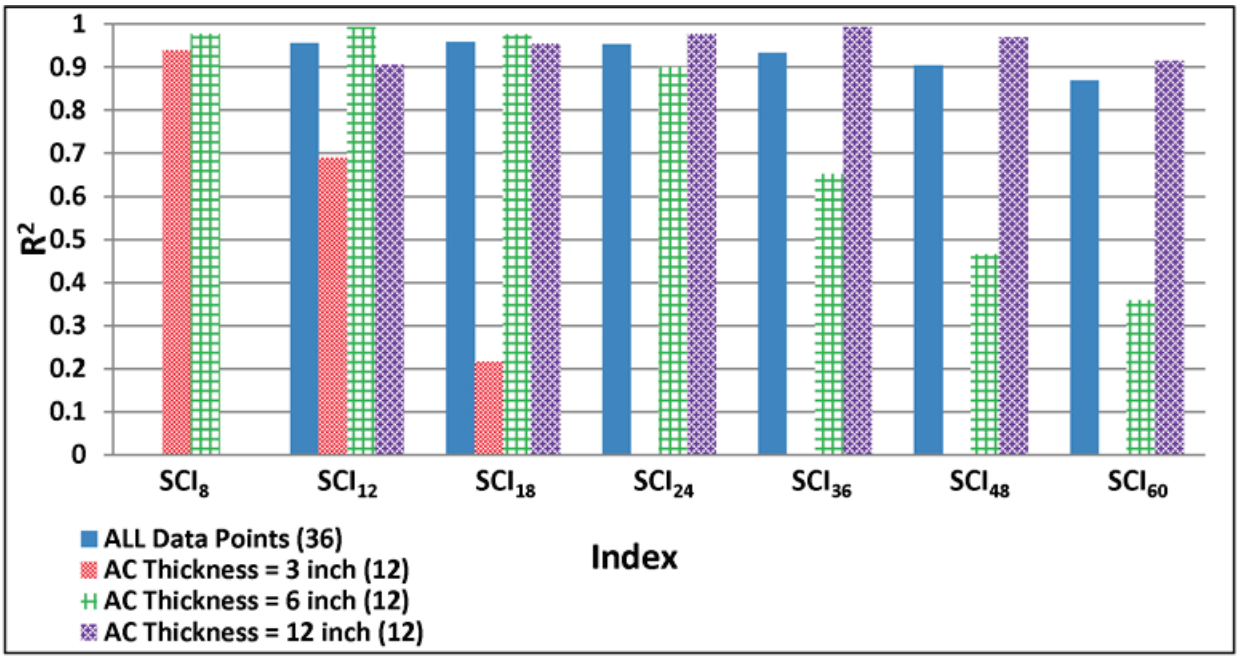

1 inch = 25.4 mm

Figure 195. Graph. Variability of relationships of *SCI* with maximum horizontal strain at bottom of AC layer for various AC thicknesses.

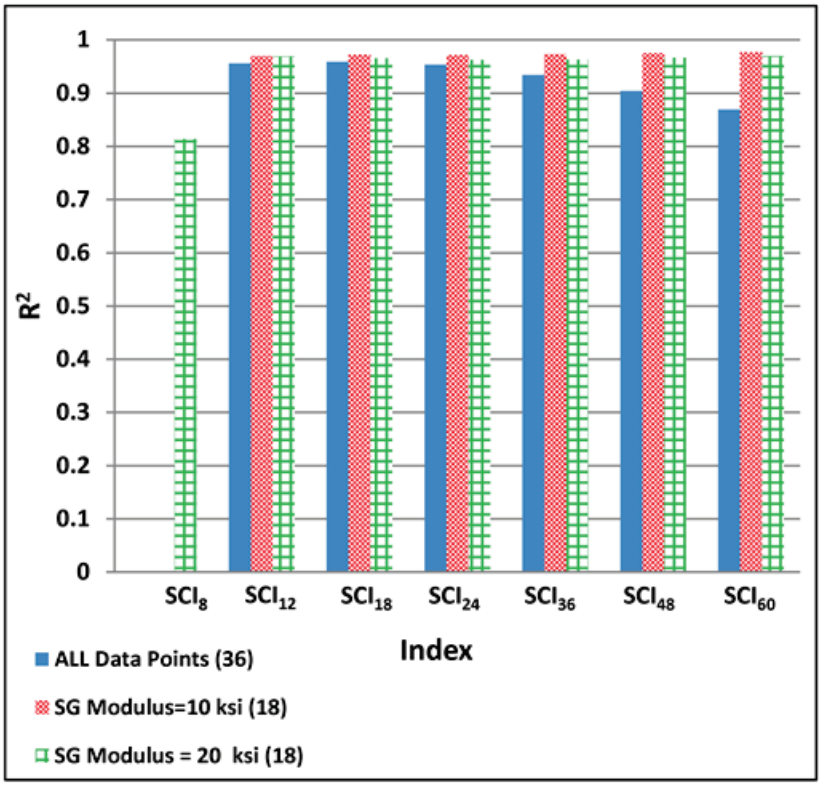

1 ksi = 6.89 MPa

Figure 196. Graph. Variability of relationships of *SCI* with maximum horizontal strain at bottom of AC layer for various subgrade moduli.

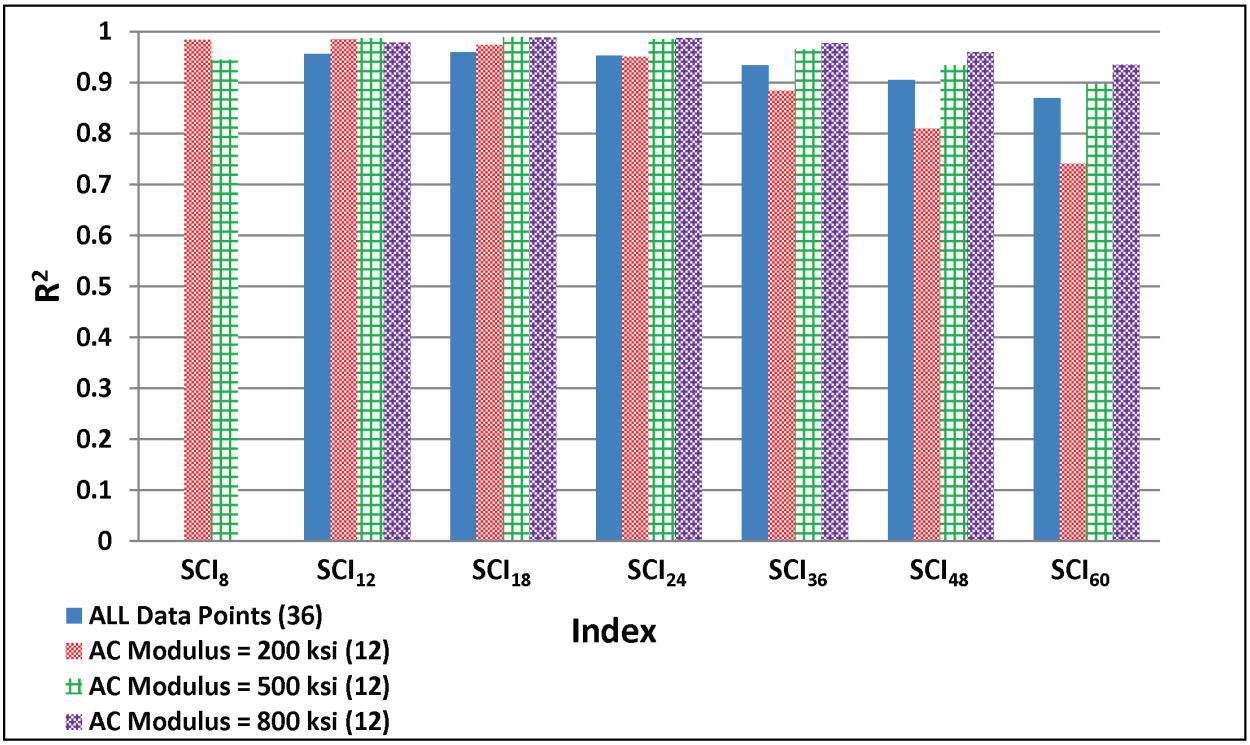

1 ksi = 6.89 MPa

Figure 197. Graph. Variability of relationships of *SCI* with maximum horizontal strain at bottom of AC layer for various AC moduli.

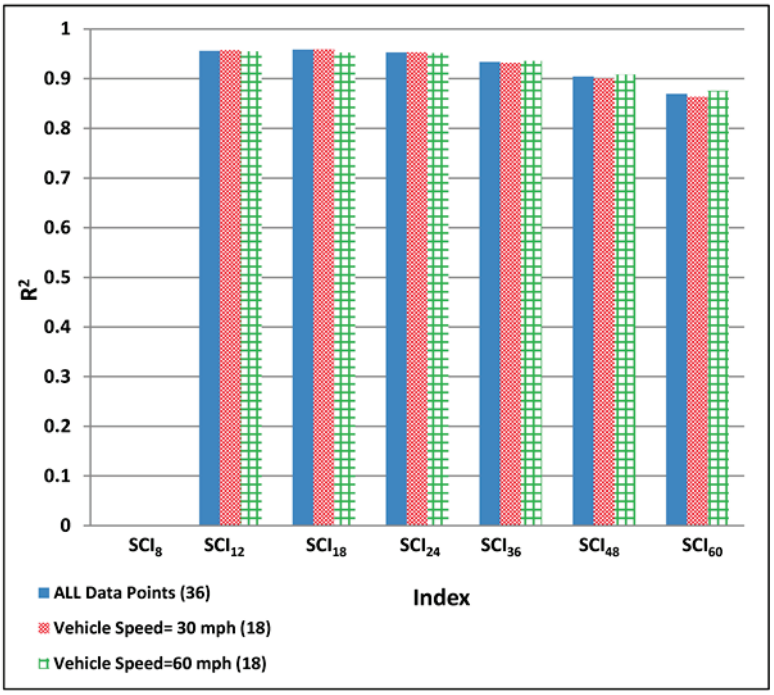

1 mi/h = 1.61 km/h

Figure 198. Graph. Variability of relationships of *SCI* with maximum horizontal strain at bottom of AC layer for various vehicle speeds.

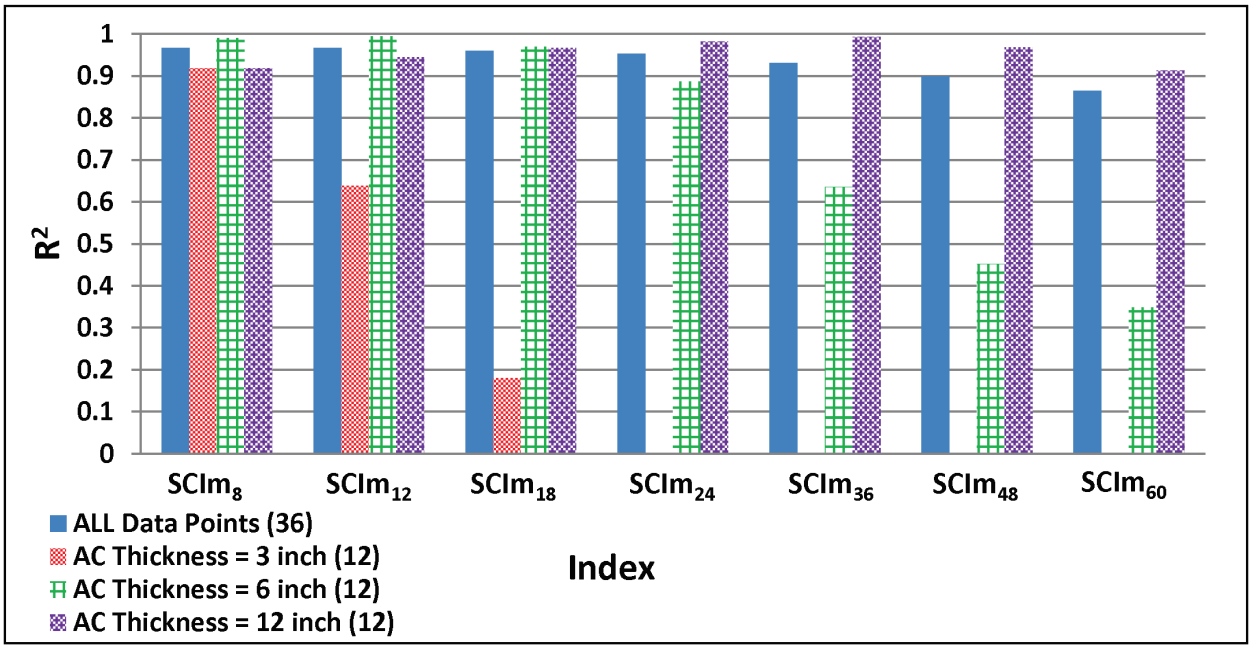

1 inch = 25.4 mm

Figure 199. Graph. Variability of relationships of *SCIm* with maximum horizontal strain at bottom of AC layer for various AC thicknesses.

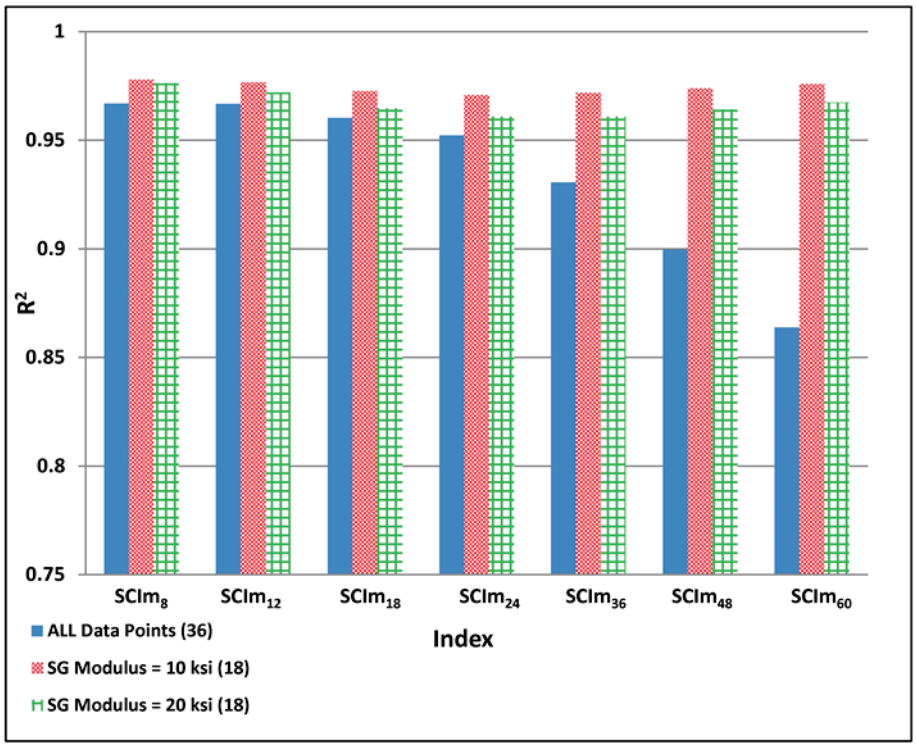

1 ksi = 6.89 MPa

Figure 200. Graph. Variability of relationships of *SCIm* with maximum horizontal strain at bottom of AC layer for various subgrade moduli.

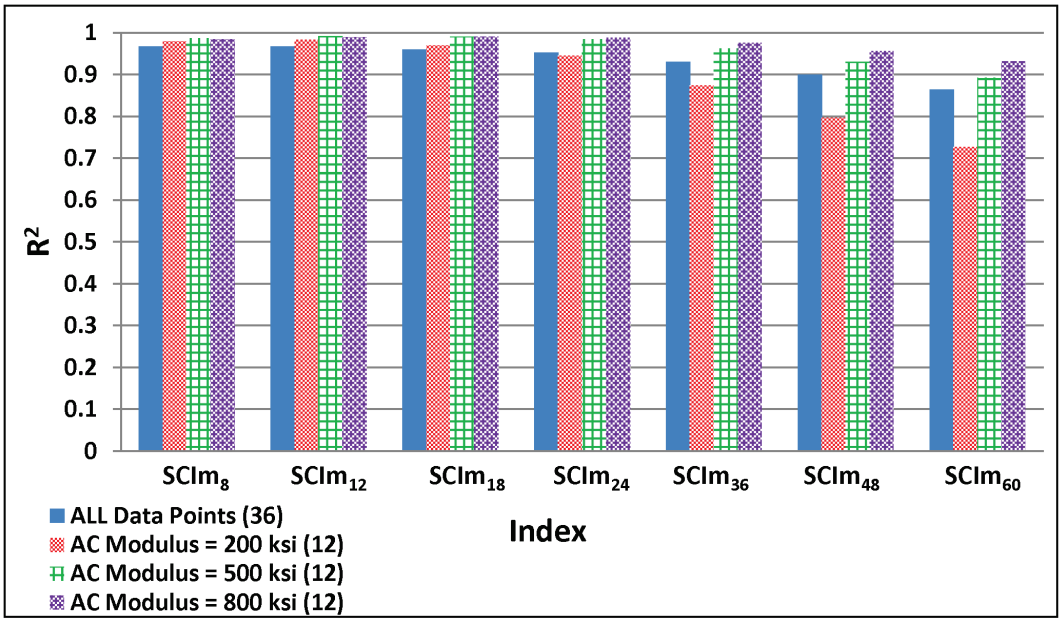

1 ksi = 6.89 MPa

Figure 201. Graph. Variability of relationships of *SCIm* with maximum horizontal strain at bottom of AC layer for various AC moduli.

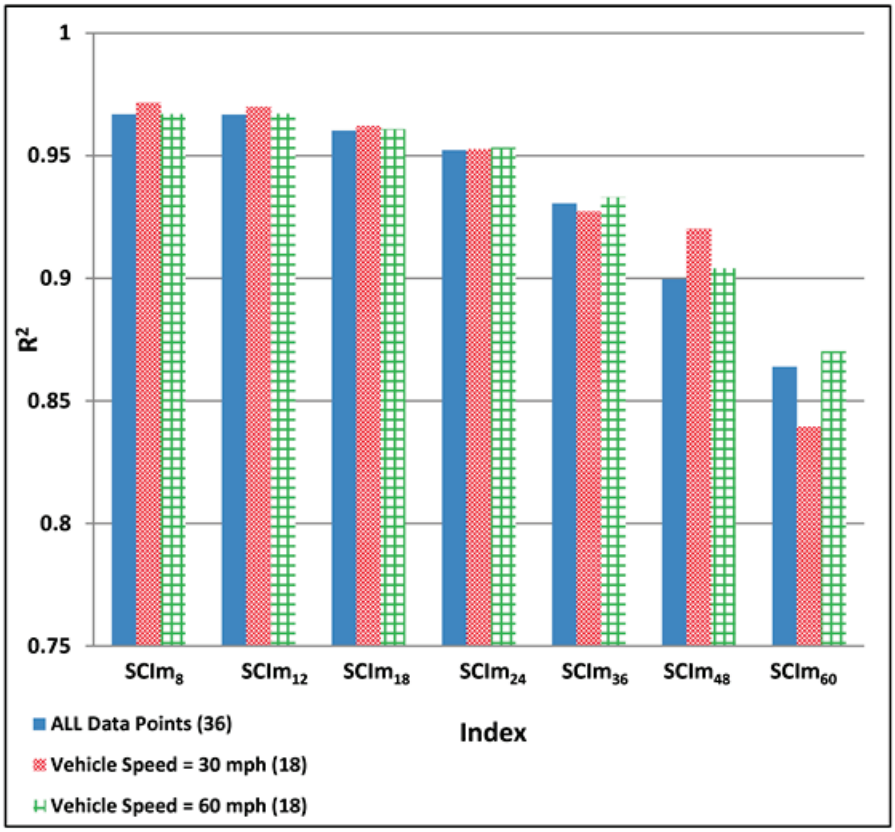

1 mi/h = 1.61 km/h

Figure 202. Graph. Variability of relationships of *SCIm* with maximum horizontal strain at bottom of AC layer for various vehicle speeds.

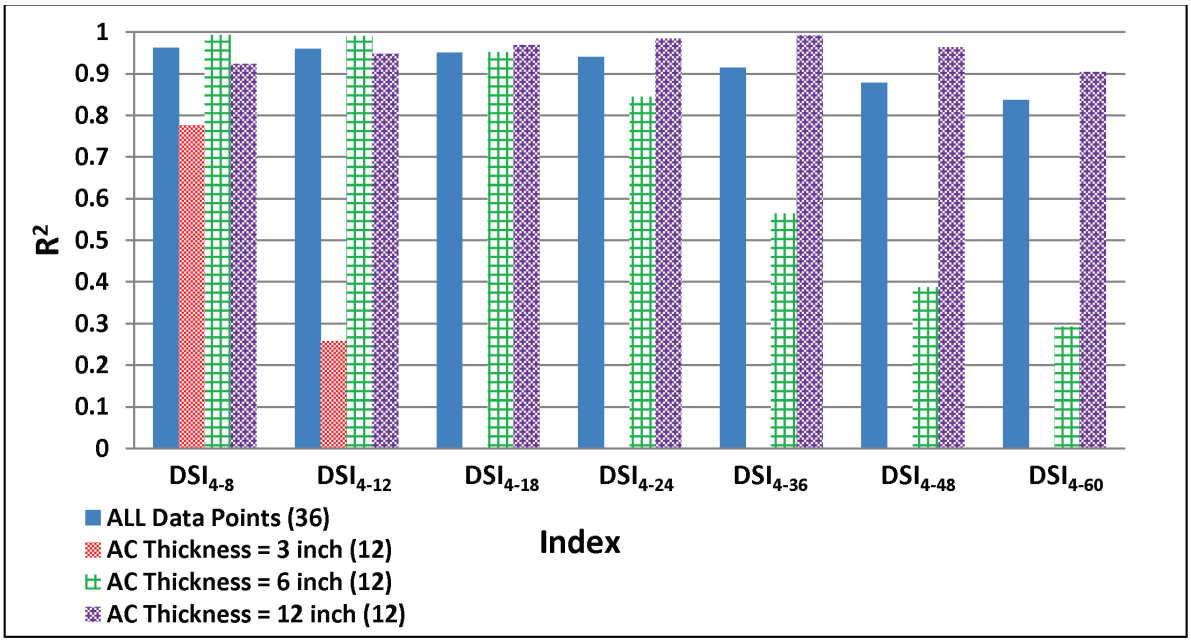

1 inch = 25.4 mm

Figure 203. Graph. Variability of relationships of DSI_{4-r} with maximum horizontal strain at bottom of AC layer for various AC thicknesses.

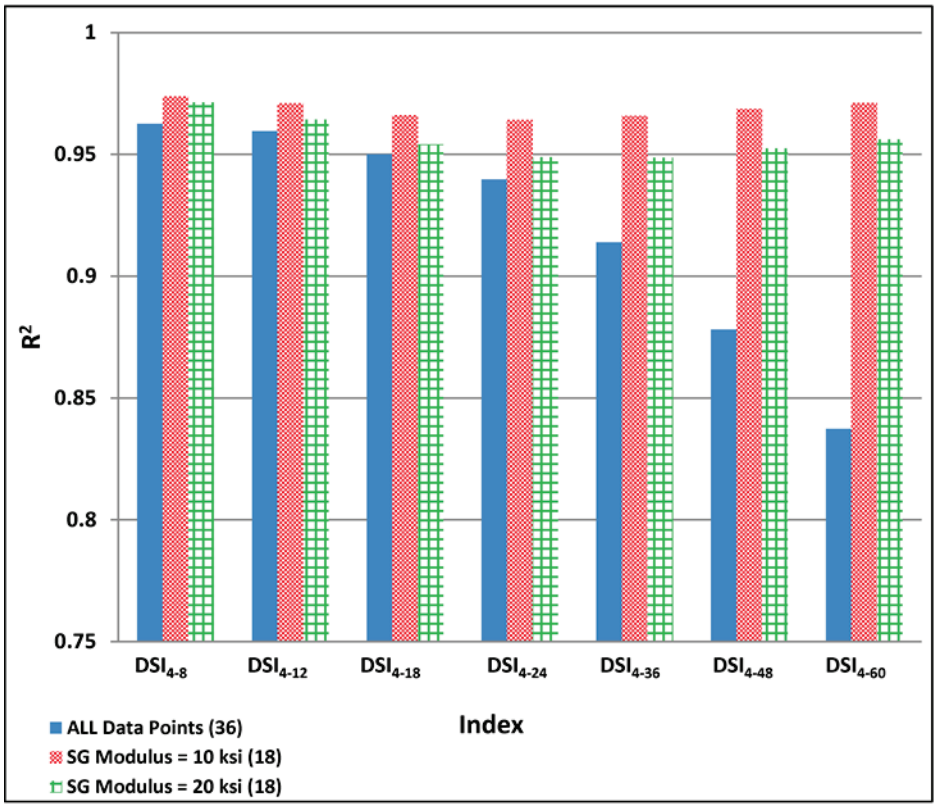

1 ksi = 6.89 MPa

Figure 204. Graph. Variability of relationships of DSI_{4-r} with maximum horizontal strain at bottom of AC layer for various subgrade moduli.

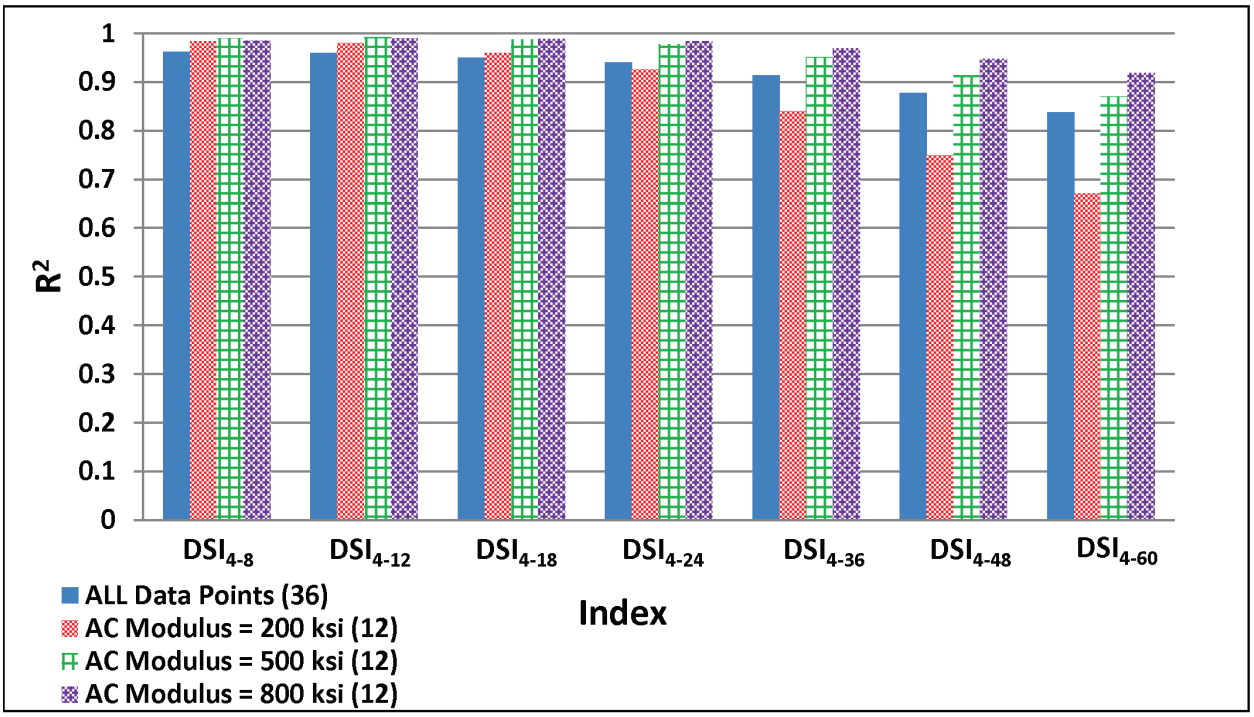

1 ksi = 6.89 MPa

Figure 205. Graph. Variability of relationships of DSI_{4-r} with maximum horizontal strain at bottom of AC layer for various AC moduli.

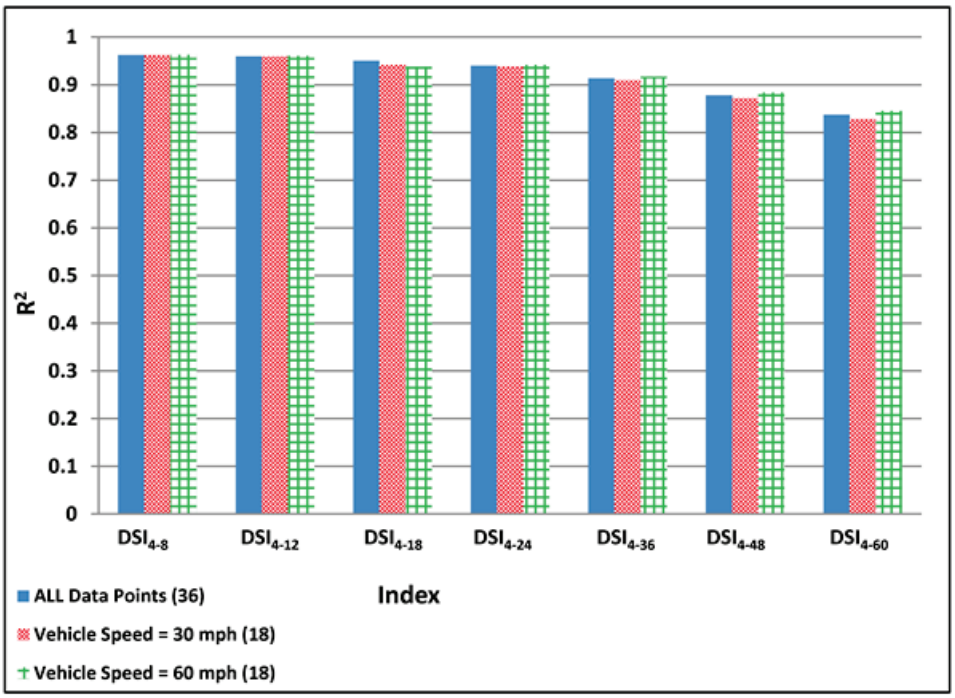

1 mi/h = 1.61 km/h

Figure 206. Graph. Variability of relationships of DSI_{4-r} with maximum horizontal strain at bottom of AC layer for various vehicle speeds.

Table 66 summarizes the goodness of fit for the relationships between each of the indices considered with the maximum horizontal strain at the bottom of the AC layer using a number of subsets. The subsets considered were AC thickness, subgrade modulus, AC modulus, and vehicle speed. Again, AC thickness was the most influential parameter. Subgrade modulus, AC modulus, and loading speed seemed to affect the most appropriate indices only marginally. However, further classifying the pavements based on subgrade modulus could improve the R^2 of thin pavements.

Table 66. Variability of the relationships of the indices with maximum horizontal strain at bottom of AC with respect to AC thickness, subgrade modulus, AC modulus, and vehicle speed.

Relationship with Maximum Horizontal Strain	Index	R^2 (All Data) (36 Cases)	Sensitivity Analysis with Respect to AC Thickness			Sensitivity Analysis with Respect to Subgrade Modulus		Sensitivity Analysis with Respect to AC Modulus			Sensitivity Analysis with Respect to Vehicle Speed	
			3 inches (12 Cases)	6 inches (12 Cases)	12 inches (12 Cases)	10 ksi (18 Cases)	20 ksi (18 Cases)	200 ksi (12 Cases)	500 ksi (12 Cases)	800 ksi (12 Cases)	30 mi/h (18 Cases)	60 mi/h (18 Cases)
*R*1	$R1_8$	N/A	0.9384	0.9777	N/A	N/A	0.8131	0.9841	0.9453	N/A	N/A	N/A
	$R1_{12}$	0.9556	0.6898	0.9931	0.9052	0.9686	0.9681	0.9853	0.9878	0.9784	0.9569	0.9548
	$R1_{18}$	0.9584	0.2165	0.9757	0.9547	0.971	0.9642	0.9741	0.9896	0.988	0.9586	0.9586
	$R1_{24}$	0.9528	Poor	0.9001	0.9775	0.9704	0.9612	0.9507	0.985	0.9871	0.9525	0.9535
	$R1_{36}$	0.9334	Poor	0.6526	0.993	0.9719	0.962	0.8842	0.9654	0.9772	0.9316	0.9354
	$R1_{48}$	0.904	Poor	0.4656	0.9692	0.9741	0.9653	0.8099	0.9343	0.9591	0.8999	0.9079
	$R1_{60}$	0.8691	Poor	0.3587	0.9139	0.9761	0.9684	0.7411	0.8974	0.9348	0.8628	0.875
*R*2	$R2_8$	N/A	0.989	0.9724	N/A	N/A	0.8301	0.9846	0.9492	N/A	N/A	N/A
	$R2_{12}$	0.9614	0.9287	0.9815	0.8977	0.9731	0.9741	0.9898	0.9874	0.9795	0.9628	0.9603
	$R2_{18}$	0.9641	0.7018	0.9741	0.9299	0.9742	0.9703	0.9912	0.9903	0.9876	0.9651	0.9634
	$R2_{24}$	0.9622	0.6138	0.9581	0.9361	0.9729	0.9672	0.9898	0.9896	0.9881	0.9633	0.9614
	$R2_{36}$	0.9602	0.6642	0.9268	0.9348	0.9725	0.9651	0.9866	0.9877	0.9863	0.9622	0.9587
	$R2_{48}$	0.9599	0.7308	0.9103	0.9288	0.9732	0.9654	0.9844	0.9867	0.9848	0.9626	0.9578
	$R2_{60}$	0.9606	0.7989	0.9108	0.9229	0.974	0.9667	0.9834	0.9863	0.9842	0.9638	0.9581
SCI	SCI_8	N/A	0.9384	0.9777	N/A	N/A	0.8131	0.9841	0.9453	N/A	N/A	N/A
	SCI_{12}	0.9556	0.6898	0.9931	0.9052	0.9686	0.9681	0.9853	0.9878	0.9784	0.9569	0.9548
	SCI_{18}	0.9584	0.2165	0.9757	0.9547	0.971	0.9642	0.9741	0.9896	0.988	0.9586	0.9523
	SCI_{24}	0.9528	Poor	0.9001	0.9775	0.9704	0.9612	0.9507	0.985	0.9871	0.9525	0.951
	SCI_{36}	0.9334	Poor	0.6526	0.993	0.9719	0.962	0.8842	0.9654	0.9772	0.9316	0.9354
	SCI_{48}	0.904	Poor	0.4656	0.9692	0.9741	0.9653	0.8099	0.9343	0.9591	0.8999	0.9079
	SCI_{60}	0.8691	Poor	0.3587	0.9139	0.9761	0.9684	0.7411	0.8974	0.9348	0.8628	0.875
	$SCIm_8$	0.9668	0.9187	0.9904	0.9179	0.9778	0.9763	0.9804	0.9875	0.9845	0.9715	0.9669
	$SCIm_{12}$	0.9667	0.6377	0.994	0.9447	0.9766	0.972	0.9832	0.9921	0.9903	0.9699	0.967
	$SCIm_{18}$	0.9602	0.1804	0.9692	0.9666	0.9726	0.9647	0.9706	0.9908	0.9913	0.9621	0.9608
	$SCIm_{24}$	0.9522	Poor	0.8868	0.9825	0.9708	0.9608	0.945	0.9846	0.9882	0.9526	0.9533
	$SCIm_{36}$	0.9305	Poor	0.6355	0.9929	0.9717	0.9609	0.8746	0.9631	0.9762	0.9273	0.9329
	$SCIm_{48}$	0.8997	Poor	0.4518	0.9677	0.9738	0.9642	0.7975	0.9305	0.9568	0.9201	0.9041
	$SCIm_{60}$	0.8639	Poor	0.3479	0.913	0.9758	0.9673	0.727	0.8926	0.9317	0.8395	0.8703

DSI	DSI_{4-8}	0.9625	0.7765	0.9933	0.9238	0.9737	0.9713	0.9836	0.9898	0.9852	0.9622	0.9629
	DSI_{4-12}	0.9595	0.2574	0.991	0.9484	0.971	0.9642	0.9806	0.9918	0.9898	0.959	0.9604
	DSI_{4-18}	0.95	Poor	0.9518	0.969	0.966	0.954	0.9594	0.9872	0.9891	0.9417	0.9382
	DSI_{4-24}	0.9397	Poor	0.8447	0.984	0.9641	0.9488	0.9256	0.9781	0.9843	0.938	0.9417
	DSI_{4-36}	0.9138	Poor	0.5643	0.992	0.9658	0.9486	0.8397	0.9514	0.9694	0.9102	0.9174
	DSI_{4-48}	0.8781	Poor	0.3864	0.9632	0.9687	0.9524	0.7501	0.9134	0.9471	0.8719	0.884
	DSI_{4-60}	0.8374	Poor	0.2929	0.9046	0.9711	0.9561	0.6711	0.8702	0.919	0.8285	0.8457
	DSI_{8-12}	0.9446	Poor	0.9717	0.9629	0.9605	0.9463	0.9614	0.9876	0.9893	0.9432	0.9464
	DSI_{8-18}	0.9256	Poor	0.871	0.9788	0.9522	0.9285	0.9163	0.9731	0.9823	0.9256	0.9285
	DSI_{8-24}	0.9075	Poor	0.6725	0.9897	0.9502	0.9199	0.86	0.9543	0.971	0.9036	0.9117
	DSI_{8-36}	0.8655	Poor	0.3484	0.9848	0.9535	0.9186	0.7354	0.9091	0.9441	0.8584	0.8724
	DSI_{8-48}	0.812	Poor	0.2171	0.9358	0.9577	0.923	0.6203	0.8512	0.9092	0.6676	0.8222
	DSI_{8-60}	0.7544	Poor	Poor	0.8565	0.961	0.9275	0.5277	0.7894	0.868	0.7399	0.7677
	DSI_{12-18}	0.8922	Poor	0.6672	0.9866	0.9387	0.8974	0.8412	0.9432	0.966	0.8872	0.8974
	DSI_{12-24} (BDI)	0.8628	Poor	0.3825	0.9919	0.938	0.8861	0.7578	0.909	0.9438	0.8552	0.8703
	DSI_{12-36}	0.7951	Poor	0.147	0.9644	0.9439	0.8845	0.5987	0.8343	0.8961	0.7826	0.8068
	DSI_{12-48}	0.7153	Poor	Poor	0.8829	0.9495	0.8896	0.4716	0.7465	0.8392	0.6979	0.5487
	DSI_{12-60}	0.636	Poor	Poor	0.7749	0.9534	0.8945	0.3786	0.6604	0.7762	0.6153	0.5881
	DSI_{18-24}	0.7944	Poor	Poor	0.9822	0.9324	0.8543	0.6157	0.8302	0.8887	0.7805	0.788
	DSI_{18-36}	0.6846	Poor	Poor	0.9042	0.9409	0.8542	0.4414	0.7098	0.8048	0.6483	0.6895
	DSI_{18-48}	0.57	Poor	Poor	0.766	0.9476	0.8603	0.3214	0.5832	0.7103	0.5463	0.5796
	DSI_{18-60}	0.4695	Poor	Poor	0.6235	0.9519	0.8651	0.241	0.4749	0.6146	0.4447	0.4808
	DSI_{24-36} (BCI)	0.5723	Poor	Poor	0.7995	0.9448	0.8455	0.3289	0.5857	0.7055	0.2316	0.5947
	DSI_{24-48}	0.4356	Poor	Poor	0.6131	0.9516	0.853	0.2232	0.4353	0.5747	0.4115	0.4587
	DSI_{24-60}	0.3295	Poor	Poor	0.461	0.9558	0.857	0.1565	0.3238	0.4559	0.2184	0.3512
TS	TS_4	0.8724	0.9471	0.9807	0.6903	0.8938	0.9635	0.9787	0.9774	0.8763	0.9053	0.8624
	TS_8	0.9573	0.1228	0.9911	0.9484	0.9692	0.9612	0.9804	0.9918	0.99	0.9564	0.8925
	TS_{12}	0.9236	0.143	0.9096	0.9741	0.9486	0.9236	0.9199	0.9748	0.9836	0.9209	0.9264
	TS_{18}	0.8431	Poor	0.2844	0.991	0.931	0.8665	0.7226	0.8857	0.929	0.8335	0.8782
	TS_{24}	0.7211	Poor	Poor	0.9486	0.9351	0.8423	0.4949	0.7499	0.8275	0.4878	0.7333
	TS_{36}	0.3756	Poor	Poor	0.5418	0.9545	0.8559	0.1879	0.3685	0.5086	0.354	0.3894
	TS_{48}	0.121	Poor	Poor	0.2052	0.9657	0.8309	Poor	0.1103	0.1754	0.1007	0.1268
	TS_{60}	Poor	Poor	Poor	Poor	0.9631	0.2868	Poor	Poor	Poor	Poor	Poor
SD	SD_8	N/A	0.9384	0.9777	N/A	N/A	0.8131	0.9841	0.9453	N/A	N/A	0.9323
	SD_{12}	0.9556	0.6898	0.9931	0.9052	0.9686	0.9681	0.9853	0.9878	0.9784	0.9569	0.9548
	SD_{18}	0.9584	0.2165	0.9757	0.9547	0.971	0.9642	0.9741	0.9896	0.988	0.9586	0.9368
	SD_{24}	0.9528	Poor	0.9001	0.9775	0.9704	0.9612	0.9507	0.985	0.9871	0.9525	0.9558
	SD_{36}	0.9334	Poor	0.6526	0.993	0.9719	0.962	0.8842	0.9654	0.9772	0.93	0.9354
	SD_{48}	0.904	Poor	0.4656	0.9692	0.9741	0.9653	0.8099	0.9343	0.9591	0.8999	0.8665
	SD_{60}	0.8691	Poor	0.3587	0.9139	0.9761	0.9684	0.7411	0.8974	0.9348	0.8628	0.875

Shape factors	$F1$	0.8367	Poor	0.3641	0.5875	0.9689	0.918	0.7359	0.8497	0.8789	0.793	0.7538
	$F2$	0.6588	Poor	Poor	0.4127	0.9193	0.885	0.4727	0.6782	0.7676	0.6447	0.1206
Area	A	0.8063	Poor	0.3538	0.5841	0.9669	0.8978	0.7148	0.8219	0.8478	0.7462	0.7591
AUPP	A_m	0.9588	Poor	0.9075	0.9805	0.9745	0.926	0.9544	0.9879	0.9899	0.9354	0.9081
Midline surface deflection	D_0	0.7719	Poor	0.2321	0.7194	0.9797	0.9302	0.5954	0.7963	0.8559	0.7894	0.7605

1 inch = 25.4 mm
1 ksi = 6.89 MPa
N/A = No correlation exists.

A close examination of the correlations for pavements with AC thicknesses of 3 and 6 inches (76.2 and 152.4 mm) reveals that indices $R1_8$, $R2_8$, SCI_8, $SCIm_8$, TS_4, and SD_8 were best related with the maximum horizontal strain with insignificant influence from the AC layer thickness or modulus. Overall, $R2_{12}$ and $SCIm_8$ appeared to be the most appropriate indices that were only minimally affected by the AC thickness and other factors studied.

It can also be concluded that increases in AC modulus resulted in an improvement in R^2 for almost all indices. As explained earlier, TS, which is a direct TSD measurement, is an important index. As shown in table 66, TS_4 had the highest correlations for pavements with AC layer thicknesses of 3 and 6 inches (76.2 and 127 mm), and TS_8 was one of the most appropriate indices for thicker (AC of 12 inches (304.8 mm)) pavements.

Based on the results presented so far in this chapter, it was recommended that the pavements be divided into the following three groups for selecting indices that most appropriate correlate with the maximum horizontal strain at the bottom of the AC surface layer:

- AC surface layer less than 3 inches (76.2 mm).
- AC surface layer between 3 and 6 inches (76.2 and 152.4 mm).
- AC surface layer greater than 6 inches (152.4 mm).

For pavements with AC surface layer thicknesses greater than 12 inches (304.8 mm), other pavement layer properties (moduli and thicknesses) did not play an important role. Alternatively, for thinner pavements, the most appropriate indices were affected by the subgrade and base moduli.

Most Appropriate Indices for Correlations with Maximum AC Horizontal Strain Using Available Data

In this subsection, the most appropriate indices using all available runs (43 from step 1 and 36 from step 2, as defined in section 8.1) were explored. The pavement sections for the MnROAD accuracy cells represented pavements that were relatively thin with AC thicknesses varying between 3 and 5 inches (76.2 and 127 mm). Conversely, the pavement combinations considered in step 2 included pavements with AC thicknesses between 6 and 12 inches (152.4 and 304.8 mm). Table 67 shows the reasonable indices ($R^2 > 0.9$) when using the combined (steps 1 and 2) database. The total number of reasonable indices with the total database (79 cases) is greater than the number of reasonable indices in step 1 (MnROAD accuracy cells).

Table 67. Most appropriate correlated indices with maximum horizontal AC strain with total database (79 cases).

Best Indices (with Respect to Maximum Horizontal Strain)	Index	R^2
*R*1	$R1_{12}$	0.94
	$R1_{18}$	0.97
	$R1_{24}$	0.95
*R*2	$R2_{12}$	0.92
	$R2_{18}$	0.96
	$R2_{24}$	0.97
	$R2_{36}$	0.94
	$R2_{48}$	0.90
SCI	SCI_{12}	0.94
	SCI_{18}	0.97
	SCI_{24}	0.95
	$SCIm_{8}$	0.92
	$SCIm_{12}$	0.96
	$SCIm_{18}$	0.97
	$SCIm_{24}$	0.94
DSI	DSI_{4-8}	0.94
	DSI_{4-12}	0.97
	DSI_{4-18}	0.95
	DSI_{4-24}	0.92
	DSI_{8-12}	0.96
	DSI_{8-18}	0.91
TS	TS_8	0.97
SD	SD_{12}	0.94
	SD_{18}	0.97
	SD_{24}	0.95
AUPP	A_m	0.95

Summary and Conclusions from 3D-Move Analyses

There are three datasets of 3D-Move runs: (1) MnROAD accuracy cell field trials (step 1); (2) sensitivity analyses with 36 simulated pavement combinations (step 2); and (3) combined data from steps 1 and 2, giving a total of 79 pavement combinations. Table 68 through table 70 presents the reasonable indices with R^2 greater than 0.9 from step 1 as well as the 20 indices with the highest R^2 from step 2 and for the combined database. The number of the reasonable indices ($R^2 > 0.9$) from step 2 and from the combined database was greater than the reasonable indices from step 1. However, it is important to note that the step 1 pavements only considered AC thicknesses that varied between 3 and 5 inches (76.2 and 127 mm).

Table 68. Most appropriate indices for MnROAD accuracy runs (43 cases) with respect to maximum horizontal strain at bottom of AC.

Best Indices (with Respect to Maximum Horizontal Strain)	Index	R^2
*R*1	$R1_{12}$	0.95
	$R1_{18}$	0.93
*R*2	$R2_{18}$	0.95
	$R2_{24}$	0.94
SCI	SCI_{12}	0.95
	SCI_{18}	0.93
	$SCIm_{8}$	0.91
	$SCIm_{12}$	0.95
	$SCIm_{18}$	0.93
DSI	DSI_{4-8}	0.93
	DSI_{4-12}	0.94
	DSI_{4-18}	0.91
	DSI_{8-12}	0.92
SD	SD_{12}	0.95
	SD_{18}	0.93
TS	TS_{8}	0.94
AUPP	A_m	0.91

Table 69. Most appropriate indices for sensitivity analyses (36 cases) with respect to maximum horizontal strain at bottom of AC.

Best Indices (with Respect to Maximum Horizontal Strain)	Index	R^2
*R*1	$R1_{12}$	0.96
	$R1_{18}$	0.96
	$R1_{24}$	0.95
*R*2	$R2_{12}$	0.96
	$R2_{18}$	0.96
	$R2_{24}$	0.96
	$R2_{36}$	0.96
	$R2_{48}$	0.96
	$R2_{60}$	0.96
SCI	SCI_{12}	0.96
	SCI_{18}	0.96
	$SCIm_{8}$	0.97
	$SCIm_{12}$	0.97
	$SCIm_{18}$	0.96
DSI	DSI_{4-8}	0.96
	DSI_{4-12}	0.96
SD	SD_{12}	0.96
	SD_{18}	0.96
TS	TS_{8}	0.96
AUPP	A_m	0.96

Table 70. Most appropriate indices for combined MnROAD accuracy and sensitivity analysis data (79 cases) with respect to maximum horizontal strain at bottom of AC.

Best Indices (with Respect to Maximum Horizontal Strain)	Index	R^2
*R*1	$R1_{12}$	0.94
	$R1_{18}$	0.97
	$R1_{24}$	0.95
*R*2	$R2_{18}$	0.96
	$R2_{24}$	0.97
	$R2_{36}$	0.94
SCI	SCI_{12}	0.94
	SCI_{18}	0.97
	SCI_{24}	0.95
	$SCIm_{12}$	0.96
	$SCIm_{18}$	0.97
DSI	DSI_{4-8}	0.94
	DSI_{4-12}	0.97
	DSI_{4-18}	0.95
	DSI_{8-12}	0.96
SD	SD_{12}	0.94
	SD_{18}	0.97
	SD_{24}	0.94
TS	TS_8	0.97
AUPP	A_m	0.95

Based on the results from step 1, the following observations and conclusions were made (see table 44 for definitions of indices):

- The influences of TSDD load characteristics (tire spacing, tire load, and inflation pressure) on the indices were investigated, and it was determined that the proposed indices were not sensitive to load characteristics.

- The indices that best related to the maximum horizontal strain at the bottom of the AC layer in step 1 (higher R^2 values) are $R1_{12}$, $R2_{18}$, SCI_{12}, or SD_{12}. All these indices are based on deflections close to the center of the load.

- Using D_{max} instead of D_0 to calculate SCI did not significantly improve the correlation (i.e., similar R^2 values); however, the use of *SCIm* did yield slightly better correlations.

- It appears that using D_4 instead of D_0 to calculate SCI also gave correlations with high R^2 values. Therefore, if D_4 in TSD measurements is more precise and accurate than D_0, it should be used in the calculation of the indices.

- Indices based on deflections measured farther away from the load appeared to have better correlations with the vertical subgrade strain. BCI best reflected the role of the lower

portion of the pavement system (i.e., the subgrade), and it related better with vertical strains at the top of the subgrade.

- The most appropriate indices for subgrade vertical strain ($R^2 > 0.95$) were as follows:
  - $DSI_{12-r} = D_{12} - D_r$.
  - $DSI_{18-r} = D_{18} - D_r$.
  - $DSI_{24-r} = D_{24} - D_r$.
- While SCI_{12} was one of the best correlated indices for horizontal strains at bottom of the AC layers ($R^2 = 0.95$), it was not a good index, as indicated by a lower R^2 value, for subgrade vertical strains ($R^2 = 0.62$).

In looking at the combined results from steps 1 and 2, the following observations and conclusions were made:

- D_{60} seemed to be the most promising parameter to estimate subgrade modulus because it was only affected by the subgrade modulus, while other material properties did not noticeably influence this parameter.
- TS is the ratio between the vertical particle velocity and the vehicle speed. Since vertical particle velocity is measured directly by TSD, this index is important since no algorithm is required, thus avoiding potential errors in the estimation of D_0 from the direct TSD measurements. TS_{48} and TS_{60} were affected only by the subgrade modulus. In general, TS_8 showed high sensitivity to changes in the pavement structural properties. Although TS_8 was overall one of the most appropriate indices from steps 1 and 2 and the combined database, sensitivity analyses showed that TS_4 (for AC thicknesses between 3 and 6 inches (76.2 and 152.5 mm)) and TS_8 (for AC thickness greater than 6 inches (152.4 mm)) provided the best correlations with the maximum horizontal AC strains.
- The comparison of maximum horizontal AC strains for various pavement combinations revealed the role of the subgrade modulus. Increases in subgrade modulus resulted in increases in horizontal AC strain in thin pavements (AC thickness of 3 inches (76.2 mm)), while the opposite occurred for thicker pavements (AC thickness of 12 inches (304.8 mm)) (i.e., the horizontal AC strains decreased).
- AC thickness is a critical parameter that should be used to categorize pavements into groups. Subgrade modulus, AC modulus, and loading speed only marginally affected the appropriate indices.
- An increase in AC modulus increased the R^2 values for almost all indices.
- $R2_{12}$ (Horak's equation) was the overall best index, especially since it was only minimally affected by the AC thickness. $SCIm_8$ also provided better correlation with maximum horizontal strains for all pavement and speed combinations regardless of AC thickness.

Ultimately, it was recommended that pavements be divided into the following groupings when comparing indices for estimating maximum horizontal strains in the AC surface layer:

- AC surface layer thickness less than 3 inches (76.2 mm).
- AC surface layer thickness between 3 and 6 inches (76.2 and 152.4 mm).
- AC surface layer thickness greater than 6 inches (152.4 mm).

For AC thicknesses greater than 12 inches (304.8 mm), other pavement layer properties (e.g., moduli and thicknesses) did not play an important role, while for thinner pavements, the appropriate indices were affected by subgrade and base modulus.

8.4 STEP 3: DETERMINING RELATIONSHIP BETWEEN INDEX AND CRITICAL RESPONSES FROM JULEA ANALYSIS

In the previous sections, the 3D-Move analyses identified deflection indices that correlated well with maximum horizontal (or fatigue) strain at the bottom of the asphalt layer. These analyses showed that the correlation between the indices and fatigue strain was most sensitive to the AC thickness; pavements with AC thicknesses less than 3 inches (76.2 mm) were not considered. Also, the analyses identified the best index across the board in situations in which the AC thickness is unknown. Based on these results, the indices summarized in table 71 were considered for further evaluation and development of a deflection index-fatigue strain relationship.

Table 71. Best indices correlating maximum fatigue strain chosen from 3D-Move analyses.

AC Thickness of Pavement Section	Chosen Index from 3D-Move Analysis
Between 3 and 6 inches	$R1_8$, $R2_{12}$, $R2_{18}$, SCI_8, SCI_{12}, DSI_{4-8}, DSI_{4-12}, and TS_4
Greater than 6 inches	$R2_{12}$, $R2_{18}$, SCI_{12}, SCI_{18}, DSI_{4-8}, DSI_{4-12}, DSI_{4-18}, DSI_{8-12}, DSI_{8-18}, TS_4, TS_8, TS_{12}, and AUPP (A_m)
Unknown	$R2_{12}$, $R2_{18}$, SCI_{12}, and DSI_{4-12}

1 inch = 25.4 mm

As part of the evaluation, a wider range of pavement structures were analyzed using JULEA.[26] A database of 15,000 pavement structures was developed using a Monte Carlo simulation, considering a uniform distribution for the modulus and thickness ranges reported in table 72. The corresponding pavement responses (strain and deflections) were computed for each simulated pavement section using JULEA.[26] Additionally, a procedure similar to the one used in the 3D-Move analyses (see figure 168) was used to compute the maximum fatigue strain also using JULEA. Similarly, surface deflections at locations detailed in figure 166 were computed. A configuration consisting of 116-psi (799.24-kPa) tire pressure, 13.5-inch (342.9-mm) tire spacing, and 9,000-lb (4,086-kg) load dual tire typically used in TSDDs was used.

Table 72. Pavement property range used in generating database.

Pavement Parameter	Minimum/ Maximum	AC Layer	Base Layer	Subgrade Layer	Stiff Layer
Modulus (psi)	Minimum	100,000	20,000	5,000	2,000,000
	Maximum	1,000,000	80,000	20,000	
Thickness (inches)	Minimum	2	4	24	Infinite
	Maximum	16	20	240	

1 psi = 6.89 kPa
1 inch = 25.4 mm

Sensitivity Analysis

An effective sensitivity analysis involves a simulation technique that can sample the input variables collectively based on their potential variability and evaluate their effect on a specific distress of a pavement structure. In section 8.3, the computation time involved in 3D-Move analysis limited its utility as a simulation-based sensitivity analysis. Accordingly, the comprehensive JULEA database referenced in the previous section was used to verify the results from 3D-Move sensitivity analyses.[26] The JULEA database was first used to identify the most sensitive pavement properties that affected the critical pavement responses. The identified properties were then used to limit the number of 3D-Move sensitivity analysis. The JULEA database was subsequently used to identify the most sensitive deflection indices, which correlated well with fatigue strains.

The Tornado plot was used to visualize the pavement properties (layer stiffness and thickness) that most significantly affected the fatigue strains.[65] The degree of correlation between fatigue strain and pavement properties was calculated using a rank order correlation coefficient, which is a non-parametric technique for quantifying the relationship between two parameters. The rank order correlation coefficient, *r*, is independent of the relationship between the input and output. As such, it is well suited for studies that involve analytical models to predict fatigue strain (as is the case here). Rank order correlation uses the position (rank) of a data point in an ordered list to compute its correlation coefficient. The rank order correlation coefficient known as Karl Spearman's *r* is calculated between the output and each dependent variable as follows:[65]

$$r = 1 - \left(\frac{6\sum (\Delta R)^2}{n\left(n^2 - 1\right)} \right)$$

Figure 207. Equation. Rank order correlation coefficient.

Where:

r = Rank order correlation coefficient.
ΔR = Difference in the ranks between the input and the output values in the same data pair.
n = Number of simulations.

The magnitude of *r* identifies the extent of correlation between the input and output. The effect of the variable on the predicted response is high when the absolute value of *r* is close to 1. When *r* is close to 0, the effect of the variable on the predicted distress is minimal. A positive correlation value indicates that a low value from the input will lead to a low value in the output,

and a negative correlation indicates a low value from the input will lead to a high value in the output.

Sensitivity of Pavement Properties on Fatigue Strain

Figure 208 shows the sensitivity of fatigue strain to various pavement properties using the rank-ordered correlation coefficient as determined from the JULEA database of 15,000 pavement structures.[26] As shown, AC layer thickness is the most sensitive parameter. Also, the negative correlation for all pavement properties indicates that the increase in each of the simulated pavement properties reduces the maximum fatigue strain. The subgrade stiffness and thickness, for example, had a negligible effect on the maximum fatigue strain.

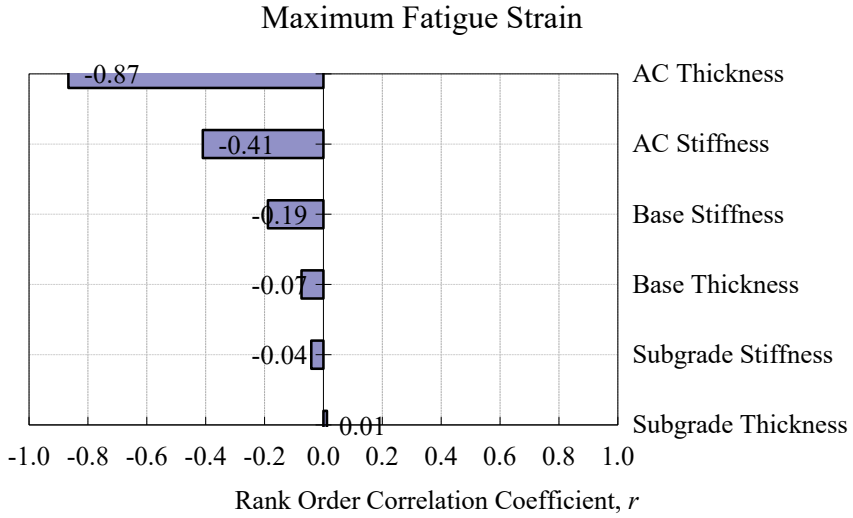

Figure 208. Graph. Sensitivity of pavement properties on maximum fatigue strain.

Sensitivity of Indices to Critical Pavement Design Responses

In section 8.3, it was recommended that pavements be divided into the following AC thickness groupings when comparing indices for estimating fatigue strain:

- AC surface layer thickness less than 3 inches (76.2 mm).
- AC surface layer thickness between 3 and 6 inches (76.2 and 152.4 mm).
- AC surface layer thickness greater than 6 inches (152.4 mm).

In this section, the JULEA database of 15,000 pavement structures was grouped based on AC thickness to verify the sensitivity between deflection indices and fatigue strain.[26]

Pavement Structures with AC Layer Less Than 3 Inches (76.2 mm) Thick

For pavement structures with an AC layer less than 3 inches (76.2 mm) thick, the stiffness of the base, AC, and subgrade layers as well as the thickness of the base layer significantly influenced the fatigue strain. Accordingly, a weak correlation between the deflection indices and fatigue

strains was observed only when the AC thickness was considered. Similar trends were observed in the 3D-Move analyses.

It is hypothesized that the contribution of thin AC layers to the measured deflections is limited, and hence other factors must be taken into consideration to establish deflection index-fatigue strain correlations with a high degree of correlation. However, for network-level PMS applications, a relation involving multiple material properties is not practical, and hence such a relation was not pursued further.

Pavement Structures with AC Layer Between 3 and 6 Inches (76.2 and 152.4 mm) Thick

Figure 209 shows the relative sensitivity of maximum fatigue strain to selected deflection indices for pavement structures with an AC layer thickness between 3 and 6 inches (76.2 and 152.4 mm). As shown, all the indices presented in table 71 have relatively good correlation with maximum fatigue strain.

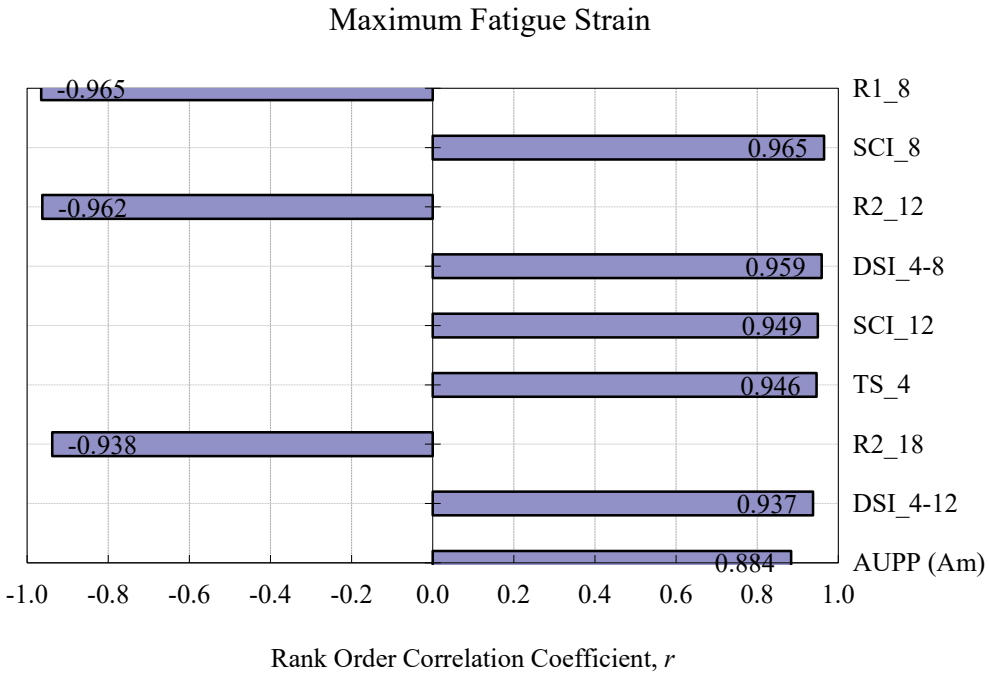

Figure 209. Graph. Sensitivity of curvature index on maximum fatigue strain in thin pavements.

Pavement Structures with AC Layer Between 6 and 16 Inches (152.4 and 406.4 mm) Thick

Figure 210 shows the relative sensitivity of maximum fatigue strain to selected deflection indices for pavement structures with an AC layer thickness between 6 and 16 inches (152.4 and 406.4 mm). As shown, all the indices presented in table 71 had relatively good correlation with maximum fatigue strain.

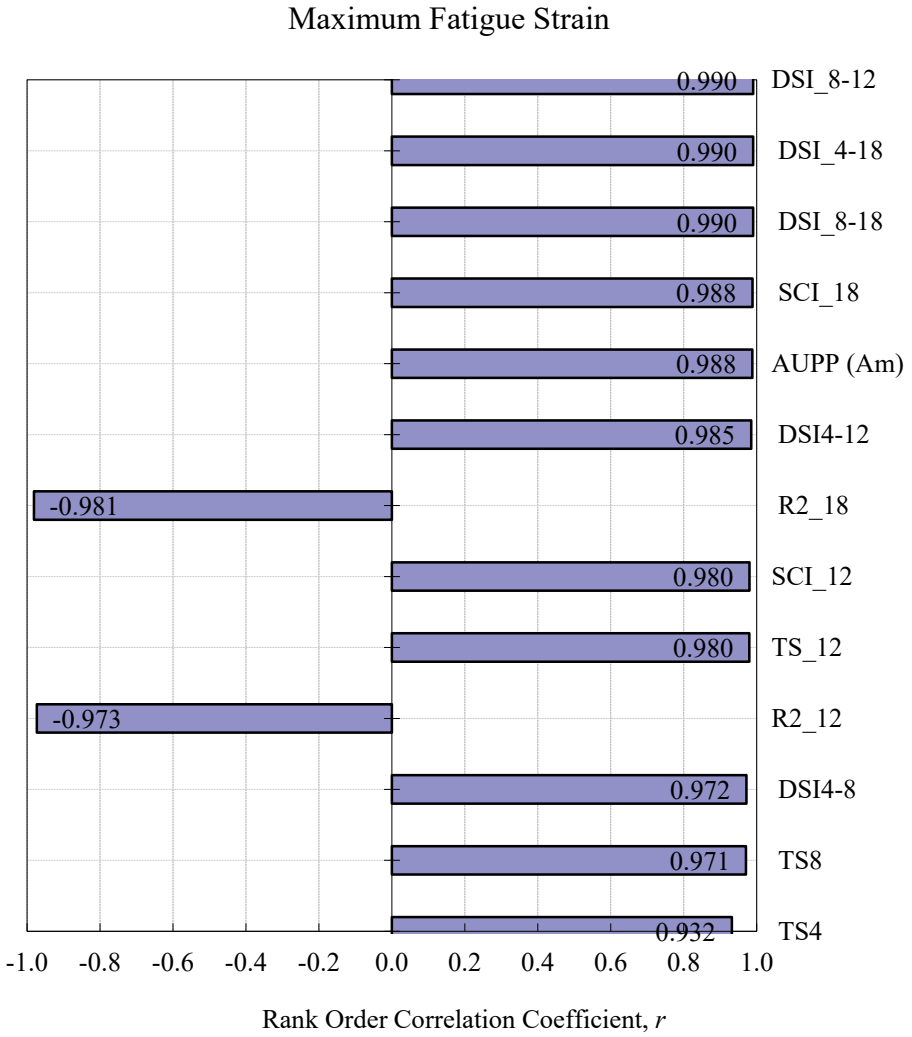

Figure 210. Graph. Sensitivity of curvature index on maximum fatigue strain in thick pavements.

Pavement Structures with Unknown AC Layer Thickness

Figure 209 and figure 210 show that, unlike other indices, the $R2_{12}$ index appears to be a reasonable predictor of maximum fatigue strain for pavements with both thin and thick AC layers. Accordingly, when the AC thickness is not known, the $R2_{12}$ index can be used to estimate maximum fatigue strains based on measured TSDD deflections, as suggested by the 3D-Move sensitivity analyses.

Relationship between Indices and Critical Response

Incorporating TSDD measurements into network-level PMS applications requires an established relationship between the computed or measured indices and fatigue strain. In this section, the fatigue strain was related to the indices deemed sensitive in the previous section and also from the 3D-Move analysis. Table 73 presents the relationships developed for pavement structures with thin (3 to 6 inches (76.2 to 152.4 mm)) and thick (6 to 16 inches ((152.4 to 406.4 mm))

AC layers. The correlation coefficient associated with each relationship is also presented in the table. For thin AC layers, separate relationships were developed for those cases where the AC layer thickness (H1) is greater than the base layer thickness (H2) (i.e., H1/H2 > 1).

Table 73. Relationship between curvature indices and maximum fatigue strain.

AC Layer Thickness	Pavement Sections	Chosen Best Indices	Relation	R^2
Thin (3 to 6 inches)	All	SCI_8 (mil)	$98.754 \times SCI_8^{0.8915}$	0.93
	(H1/H2) > 1		$100.79 \times SCI_8^{0.8958}$	0.96
Thick (6 to 16 inches)	All	SCI_{18} (mil)	$40.224 \times SCI_{18}^{0.9257}$	0.98
Unknown	All	$R2_{12}$ (inches)	$337974 \times R2_{12}^{-0.779}$	0.97

1 inch = 25.4 mm

Because the relations between the deflection indices and maximum fatigue strain can be sensitive to AC layer thickness, better predictions of the maximum fatigue strains are possible when the AC thickness is known or measured during the TSDD testing. The JULEA database was used to categorize the pavement structures according to AC layer thickness in 1-inch (25.4-mm) intervals.[26] Each group contained about 1,000 pavement structures within the pavement properties presented in table 72. Table 74 summarizes the relationships between the most sensitive deflection indices and the fatigue strain for each group. The correlation coefficient for each relationship is also presented in table 74.

Table 74. Relationship between curvature indices and critical pavement responses with known AC thickness.

AC Layer Thickness (inches)	Unbound Layer Properties	Chosen Index	Range of Indices Value (mil)	Maximum Fatigue Strain (microstrain)	R^2
3–4	Base 20–80 ksi and 4–12 inches; subgrade 5–20 ksi and 24–240 inches	SCI_8	1.59 to 8.55	$83.958 \times SCI_8^{0.9903}$	0.90
4–5			1.23 to 6.65	$90.107 \times SCI_8^{1.0049}$	0.95
5–6			0.96 to 4.83	$98.847 \times SCI_8^{0.9723}$	0.97
6–7	Base 20–80 ksi and 4–20 inches; subgrade 5–20 ksi and 24–240 inches	SCI_{18}	1.87 to 10.22	$36.295 \times SCI_{18}^{1.0096}$	0.92
7–8			1.58 to 11.07	$37.106 \times SCI_{18}^{1.0029}$	0.95
8–9			1.38 to 7.33	$38.252 \times SCI_{18}^{0.986}$	0.97
9–10			1.16 to 7.45	$39.638 \times SCI_{18}^{0.9611}$	0.98
10–11			1.02 to 6.89	$40.933 \times SCI_{18}^{0.9195}$	0.97
11–12			0.87 to 6.07	$41.393 \times SCI_{18}^{0.894}$	0.97
12–13			0.79 to 5.1	$41.505 \times SCI_{18}^{0.8672}$	0.96
13–14			0.69 to 4.68	$41.301 \times SCI_{18}^{0.8283}$	0.95
14–15			0.63 to 4.23	$40.361 \times SCI_{18}^{0.8313}$	0.96
15–16			0.59 to 4.27	$39.278 \times SCI_{18}^{0.7978}$	0.95

1 inch = 25.4 mm
ksi = 6.89 MPa

Effect of TSDD Loading Configuration

The RWD and TSD used in the MnROAD field trials had different loading configurations, as summarized in table 75. To study the effect of loading configuration on the relationship between

deflection index and fatigue strain, a separate database of 50,000 pavement structures, each subjected to the TSD and RWD loading configurations, was simulated within the pavement properties presented in table 72.

Table 75. Loading configuration of TSDD used in the field test.

TSDD Equipment	Dual Tire Load (lb)	Tire Pressure (psi)	Dual Tire Spacing (inches)
TSD	11,150	116	13.5
RWD	9,500	100	14.5

1 lb = 0.454 kg
1 psi = 6.89 kPa
1 inch = 25.4 mm

Figure 211 and figure 212 show the relationships between SCI_{12} and fatigue strain for the RWD and TSD loading configurations, respectively. The similarity between the two confirms that the proposed relationships are not dependent on the loading configuration, as was also found during the 3D-Move analysis.

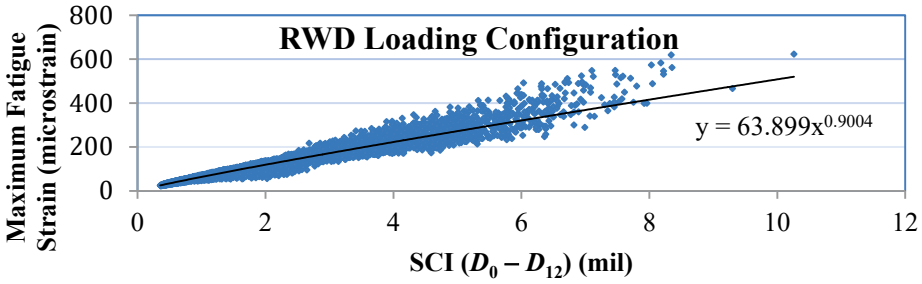

1 mil = 0.0254 mm

Figure 211. Graph. General relationship between maximum fatigue strain and SCI for RWD loading.

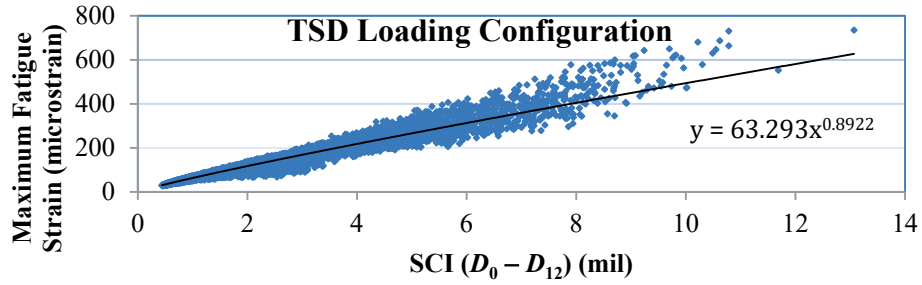

1 mil = 0.0254 mm

Figure 212. Graph. General relationship between maximum fatigue strain and SCI for TSD loading.

8.5 FIELD EVALUATION OF INDICES

So far, the focus of this chapter has been mostly on numerical analyses in order to recommend the most appropriate indices. In this section, the estimated TSD accuracies and precisions reported in chapter 6 were used to estimate the most practical and robust indices among those reported in previous sections. For this evaluation, the TSD new deflection algorithm discussed in chapter 5 was used since the old method did not provide enough data points for the analyses. Since the new TSD algorithm provides deflections at 4-inch (100.6-mm) intervals, including D_0, only indices that conformed to this spacing were addressed. These values, along with the TS directly measured by the TSD, were used to evaluate the precision and accuracy of the most appropriate indices using the data collected during the MnROAD testing. The following subsections describe the process and the results obtained from such evaluation. It should be noted that the trends and recommendations in this section are based on the limited data collected during the MnROAD field testing and are subject to the uncertainties associated with the measurements and analyses enumerated for the accuracy and precision studies outlined in chapters 5 and 6.

Accuracy

For the accuracy evaluation, the selected indices from the TSD were compared with the same indices calculated from the deflection or velocity basins measured with geophone 3 at all cells. The accuracy was evaluated in terms of the percentage of difference as established in chapters 5 and 6 for the deflection slopes irrespective of the AC thickness recommendations for estimating the strains. Figure 213 presents the results from such evaluation. The error bars in the figure correspond to the 25th and 75th percentile ranges of the difference. A 15 percent threshold median difference, which was considered as a reasonable level of difference given the state of the technology, was also added to the plot shown in figure 213. The indices based on the deflection slopes yielded lower difference values as compared to the other indices. The indices based on R seem to be the least accurate.

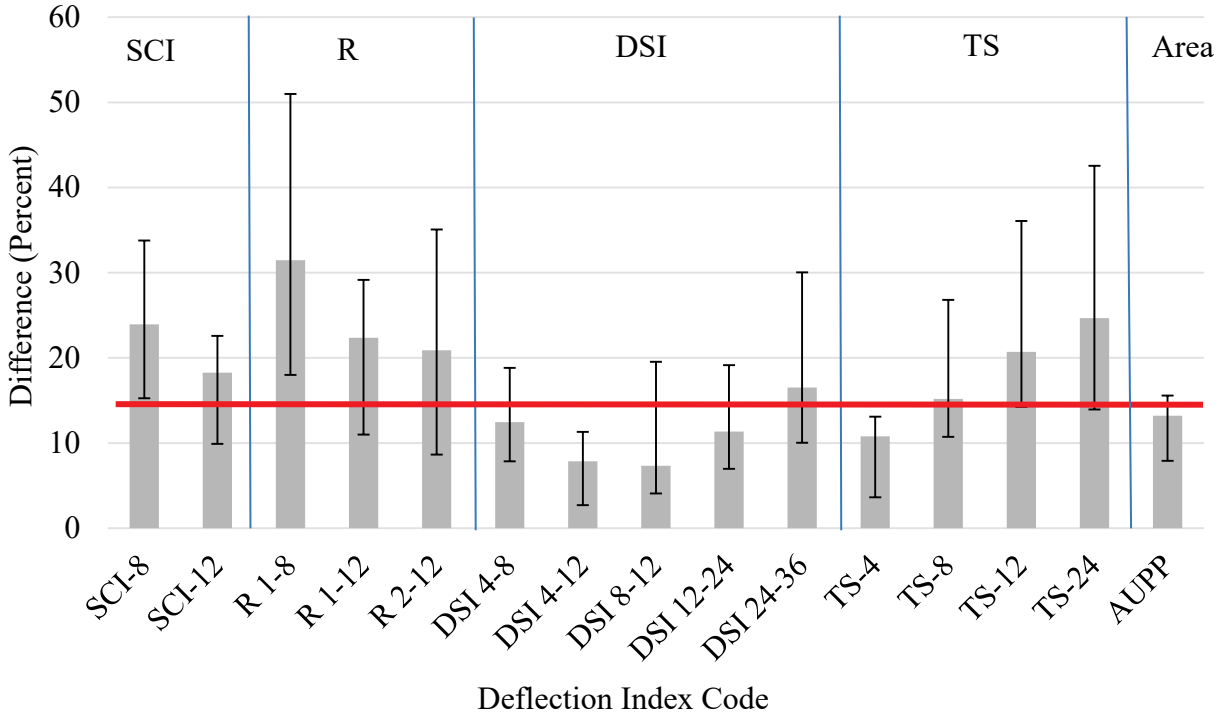

Figure 213. Graph. Accuracy evaluation of indices.

Precision

As presented in section 6.3, the new TSD vertical deflection estimates were found to be less precise than the deflection slope measurements. For this evaluation, precision was incorporated using the same approach but with a slightly different presentation of results. As in chapter 6, the SEE values and ranges were estimated for each index and cell. The median COV, obtained from the ratio between the median SEE and the median range, was used to quantify the precision of each deflection index irrespective of the AC thickness recommendations for estimating the strains. Figure 214 shows the resulting median COVs as well 25th and 75th percentile ranges of the COVs. A 15 percent threshold median COV was also added to the plot as a reasonable precision. Most indices were under this 15 percent threshold COV. As shown, the indices based on the deflection slopes performed better than those based on the TSs by themselves. The three *R* indices performed the worst, with median COVs ranging from 29 to 40 percent.

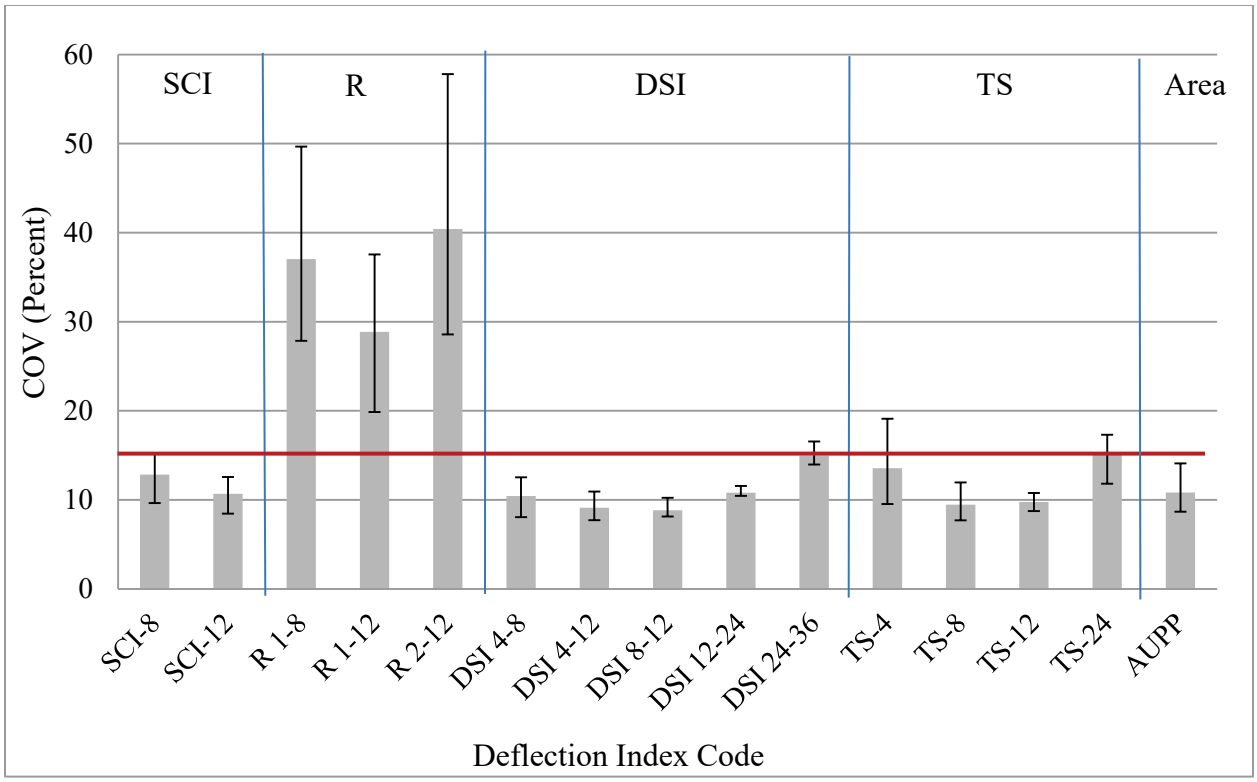

Figure 214. Graph. Precision evaluation of indices.

Overall Field Results

To easily visualize the overall performance of these indices, figure 215 was developed by combining figure 213 and figure 214. This plot, which presents the precision results on the abscissa and the accuracy results on the ordinance, is segmented into four quadrants to further characterize the performance of the indices in question. As shown, the most robust indices are those in the lower left quadrant (marked in green) and include four DSIs, TS_4, and AUPP. The indices in the upper left quadrant (TS and SCI) may also be considered as reasonably precise but not as accurate as those in the lower left quadrant. Based on this study, the three radii of curvature indices under consideration do not seem to yield accurate enough results since they all fall in the upper right-hand quadrant (i.e., quadrant with low accuracy and precision marked in red). DSI_{4-12} was found to be the most robust index based on the TSDD accuracy and precision analyses conducted in this study.

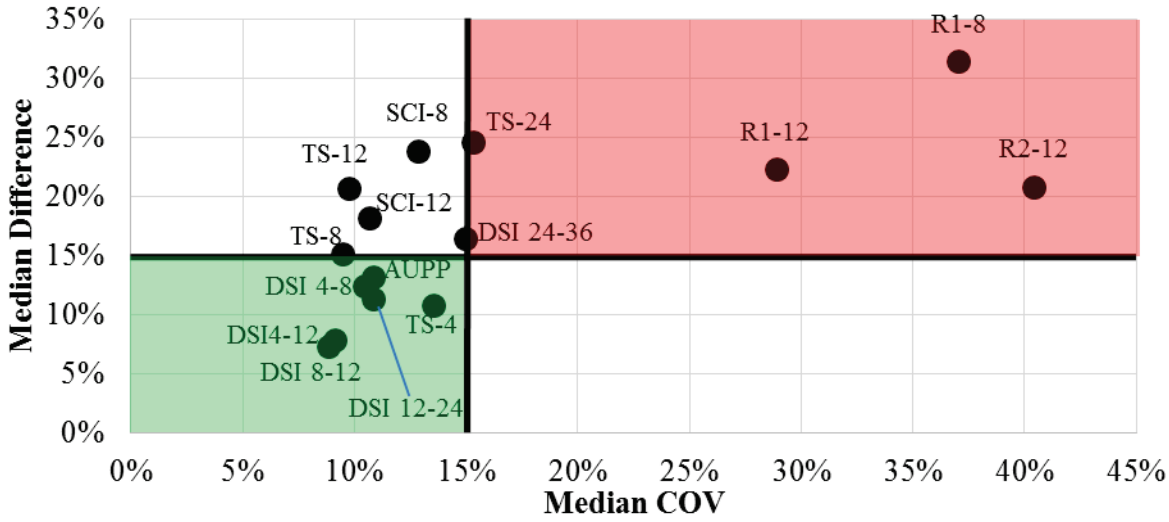

Figure 215. Graph. Overall field performance of indices.

The uncertainties of the modeled indices were evaluated by dividing the SEE in estimating the maximum fatigue strain by the median range of calculated strains for each of the indices for different AC thicknesses as described previously. The results from such analysis are presented in figure 216. This figure depicts the same 15 percent threshold as described in section 8.5. Most of the indices have a median COV below 15 percent except for the ones used to determine the strain for unknown pavement thickness.

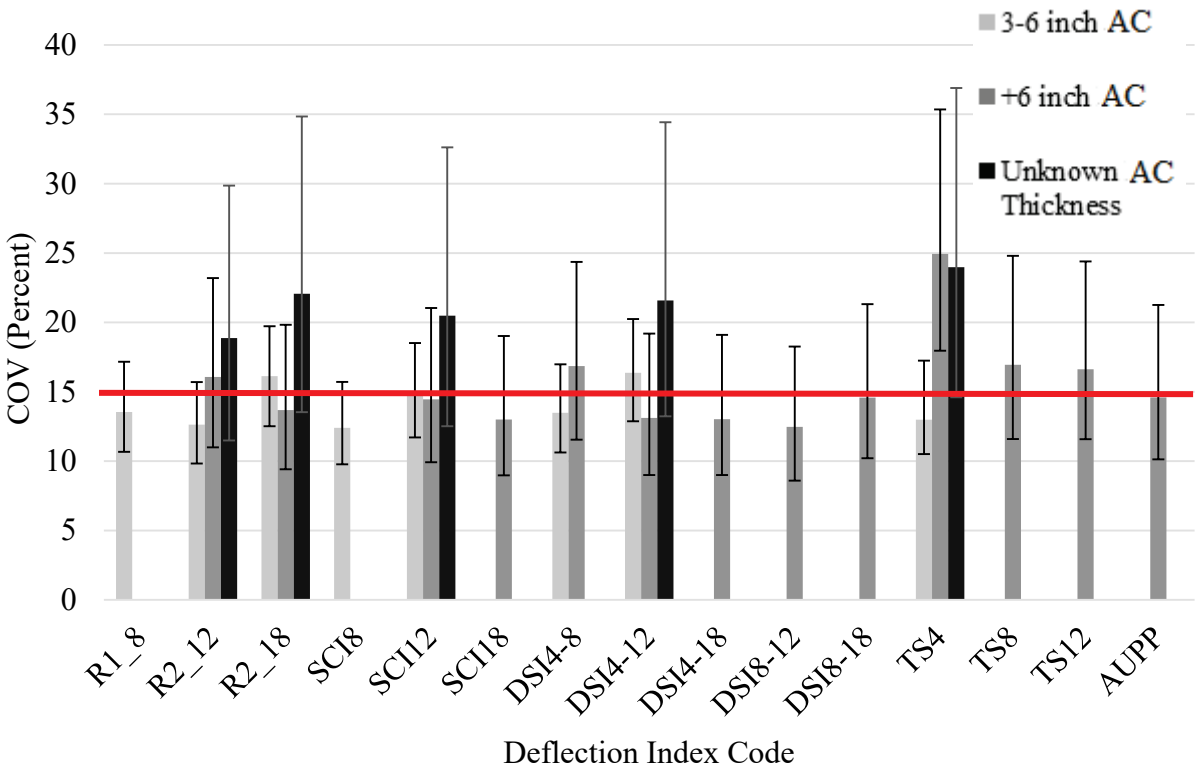

1 inch = 25.4 mm

Figure 216. Graph. Precision of modeled indices in different pavement thicknesses.

8.6 SUMMARY

The overall performance of the selected indices was evaluated by combining the field and JULEA results.[26] The outcomes from figure 214 through figure 216 were combined into table 76. Indices were then ranked within their pavement thickness ranges according to a performance number (see table 77). The device precisions, device accuracies, and model uncertainties were assigned values of 1 (poor) when their COV values were greater than 20 percent, 3 (fair) when their values were between 10 and 20 percent, and 5 (good) for values less than 10 percent. Similarly, the R^2 values were assigned 1 (poor) for values less than 0.90, 3 (fair) for values between 0.90 and 0.95, and 5 (good) for values above 0.95.

Table 76. Summary of performances of different indices.

AC Thickness of Pavement Section	Index	Units	Precision COV (Percent)	Accuracy (Percent Difference)	Model COV (Percent)	Model R^2
Between 3 and 6 inches	DSI_{4-12}	mil	9	8	16	0.88
	SCI_{12}	mil	11	18	15	0.90
	DSI_{4-8}	mil	10	12	13	0.92
	TS_4	mil/inch	14	11	13	0.91
	SCI_8	mil	13	24	12	0.93
	$R1_8$	inches	37	31	14	0.93
	$R2_{12}$	inches	40	21	13	0.93
Greater than 6 inches	DSI_{4-12}	mil	9	8	13	0.97
	DSI_{8-12}	mil	9	7	12	0.98
	SCI_{12}	mil	11	18	14	0.96
	DSI_{4-8}	mil	10	12	17	0.95
	TS_8	mil/inch	9	15	17	0.94
	TS_{12}	mil/inch	10	21	17	0.96
	AUPP	mil	11	13	15	0.97
	$R2_{12}$	inches	40	21	16	0.95
	$TS4$	mil/inch	14	11	25	0.87
Unknown	DSI_{4-12}	mil	9	8	22	0.97
	SCI_{12}	mil	11	18	20	0.97
	$R2_{12}$	inches	40	21	19	0.97
	TS_4	mil/inch	14	11	24	0.93

1 inch = 25.4 mm
1 mil = 0.0254 mm
1 mil/inch = 0.0001 mm/mm

Table 77. Ranking of different indices.

AC Thickness of Pavement Section	Index	Units	Device Precision	Device Accuracy	Model Uncertainty	Model R^2	Overall Performance (1–5)
Between 3 and 6 inches	DSI_{4-12}	mil	5	5	3	1	3.5
	SCI_{12}	mil	3	3	3	3	3.0
	DSI_{4-8}	mil	3	3	3	3	3.0
	TS_4	mil/inch	3	3	3	3	3.0
	SCI_8	mil	3	1	3	3	2.5
	$R1_8$	inches	1	1	3	3	2.0
	$R2_{12}$	inches	1	1	3	3	2.0
Greater than 6 inches	DSI_{4-12}	mil	5	5	3	5	4.5
	DSI_{8-12}	mil	5	5	3	5	4.5
	SCI_{12}	mil	3	3	3	5	3.5
	DSI_{4-8}	mil	3	3	3	5	3.5
	TS_8	mil/inch	5	3	3	3	3.5
	TS_{12}	mil/inch	5	1	3	5	3.5
	AUPP	mil	3	3	3	5	3.5
	$R2_{12}$	inches	1	1	3	5	2.5
	TS_4	mil/inch	3	3	1	1	2.0
Unknown	DSI_{4-12}	mil	5	5	1	5	4.0
	SCI_{12}	mil	3	3	1	5	3.0
	$R2_{12}$	inches	1	1	3	5	2.5
	TS_4	mil/inch	3	3	1	3	2.5

1 inch = 25.4 mm
1 mil = 0.0254 mm
1 mil/inch = 0.0001 mm/mm
Note: A ranking of 1 indicates poor, a ranking of 3 indicates fair, and a ranking of 5 indicates good.

The overall performance was then determined by assigning a 25 percent importance to each of the four parameters (device precision, device accuracy, model uncertainty, and R^2) and obtaining a weighted average of the four parameters. Indices that required a deflection parameter of 18 inches (457.2 mm) were not included in this table since TSD did not report a value at that distance. DSI_{4-12} appears first on the three different AC thicknesses categories. SCI_{12} also performed well in the three AC thickness categories with an overall performance of 3 or higher. It should be noted that device accuracy can be improved if the effectiveness of the deflection algorithm is improved. At a minimum, the TSD old deflection algorithm, which was identified in accuracy analysis (section 6.2) to be better than new deflection algorithm, can be modified to compute the deflections at the locations needed to determine the identified effective indices.

In considering the results and conclusions presented in this chapter, it is important to recognize that a limitation of the analyses is that the device precision and accuracy were obtained for pavements with a AC thickness of 5 inches (127 mm) or less if the full depth reclamation with

engineered emulsion is not considered as AC. The most robust index, DSI_{4-12}, is related to maximum fatigue strain using the JULEA database and is presented in table 78.

Table 78. Relationship between robust TSD index DSI_{4-12} and critical pavement responses with unknown and known AC thickness.

AC Layer Thickness (inches)	Maximum Fatigue Strain (microstrain)	R^2
3–6 (thin AC)	$69.1 \times DSI_{4-12}^{0.9348}$	0.88
6–16 (thick AC)	$76.22 \times DSI_{4-12}^{0.8924}$	0.97
Unknown	$76.24 \times DSI_{4-12}^{0.8969}$	0.97
3–4	$66.96 \times DSI_{4-12}^{0.9351}$	0.77
4–5	$62.567 \times DSI_{4-12}^{1.0174}$	0.88
5–6	$64.66 \times DSI_{4-12}^{1.0379}$	0.94
6–7	$71.646 \times DSI_{4-12}^{1.0005}$	0.96
7–8	$74.381 \times DSI_{4-12}^{0.9757}$	0.97
8–9	$76.458 \times DSI_{4-12}^{0.9427}$	0.98
9–10	$77.802 \times DSI_{4-12}^{0.9107}$	0.97
10–11	$77.868 \times DSI_{4-12}^{0.8674}$	0.96
11–12	$76.861 \times DSI_{4-12}^{0.8395}$	0.95
12–13	$75.154 \times DSI_{4-12}^{0.8149}$	0.95
13–14	$72.194 \times DSI_{4-12}^{0.778}$	0.94
14–15	$70.196 \times DSI_{4-12}^{0.7824}$	0.94
15–16	$66.402 \times DSI_{4-12}^{0.7525}$	0.93

1 inch = 25.4 mm

8.7 TEMPERATURE CORRECTION PROCEDURE

The deflection parameter measured by the TSDD is a function of pavement temperature at the structural evaluation. Consistent evaluation and tracking of the index computed from deflection parameters over the pavement service period requires the maximum fatigue strains computed from the index to be corrected to a standard reference temperature. The recommended approach, developed as part of the project, is as follows:

1. Compute temperature correction factor, T_c, as follows:

$$T_c = 19.791e^{-0.043T_r} - 19.791e^{-0.043T_f} \quad *$$

Figure 217. Equation. Temperature correction factor.

Where:

T_f (°F) = Temperature at time of the TSDD field measurements.
T_r (°F) = Reference temperature, which should be set to 70 °F (21.11°C).

2. Compute dynamic modulus (E_f) based on computed strains and AC layer thickness using relations presented in table 79.

*Modified on November 21, 2016

3. Compute dynamic modulus at reference temperature, E_r of 70 °F (21.11°C) as follows:

$$E_r = \frac{E_f}{(1 - T_c)}$$

Figure 218. Equation. Dynamic modulus at reference temperature.

4. Compute temperature corrected strains using the computed dynamic modulus at reference temperature (E_r) and the inverse of the relations presented in table 79.

While the correlation coefficients for the relations in table 79 are not high, the error in the temperature corrections is expected to be minimal because the same relations are used to compute the AC dynamic modulus from the computed strains and then to re-compute the strains from the temperature corrected AC dynamic modulus.

Table 79. Relationship between maximum fatigue strain (ε) and AC modulus for temperature correction.

AC Layer Thickness (inches)	Relation Between Maximum Fatigue Strain and AC Modulus	R^2
3–4	5.28E+08 x $\varepsilon_{max}^{-1.27}$	0.47
4–5	6.56E+08 x $\varepsilon_{max}^{-1.36}$	0.59
5–6	7.23E+08 x $\varepsilon_{max}^{-1.44}$	0.62
6–7	6.39E+08 x $\varepsilon_{max}^{-1.46}$	0.67
7–8	4.96E+08 x $\varepsilon_{max}^{-1.46}$	0.68
8–9	4.91E+08 x $\varepsilon_{max}^{-1.51}$	0.72
9–10	3.68E+08 x $\varepsilon_{max}^{-1.49}$	0.76
10–11	3.29E+08 x $\varepsilon_{max}^{-1.51}$	0.77
11–12	2.88E+08 x $\varepsilon_{max}^{-1.52}$	0.79
12–13	2.50E+08 x $\varepsilon_{max}^{-1.53}$	0.83
13–14	2.30E+08 x $\varepsilon_{max}^{-1.55}$	0.83
14–15	1.61E+08 x $\varepsilon_{max}^{-1.49}$	0.85
15–16	1.45E+08 x $\varepsilon_{max}^{-1.51}$	0.85

CHAPTER 9. SUMMARY AND CONCLUSIONS

The goal of the project was to establish a reliable measure of the structural condition of bound pavement layers over time based on moving pavement deflection technology measured at posted traffic speeds. The specific project objectives were as follows:

- Assess, evaluate, and validate the capability of traffic speed devices that measure deflection or other pavement responses for pavement structural evaluation at the network level for use in pavement management application and decisionmaking.

- Develop methodologies for enabling the use of the device(s) capable of meeting the first objective in pavement management or alternatively develop recommendations to further develop promising device(s) and/or technologies if the devices do not meet the first objective.

To accomplish the stated goal and objectives, 10 tasks were carried out under 2 phases. The initial phase focused on identifying and assessing capable devices, while the second phase focused on evaluating and validating the field capable devices.

Much of the first phase focused on gathering information related to potentially viable devices. A literature review was performed to investigate and evaluate previous, ongoing, and proposed research projects related to available traffic speed pavement deflection devices that have the potential to meet the project objectives. Based on the literature, an RWD and TSD were found as potentially viable devices that merited further evaluation.

To augment the literature review findings, questionnaires were developed and sent to the device manufacturers as well as owners and users of the devices. Follow-up interviews with specific or clarifying questions were also conducted. These activities further reinforced the RWD and TSD as potential devices capable of meeting the project objectives.

In light of these findings, a work plan (driven by the planned analyses) for the conduct of field trials was developed to perform the following:

- Confirm that the two TSDDs in question met a minimum set of specifications related to the structural evaluation of pavements at the network level, including accuracy and precision requirements.

- Propose processes to incorporate pavement structural information from the TSDDs into network-level PMS applications.

The field trials were performed at the MnROAD facility near Albertville, MN, because it provided a multitude of test sections in one location and readily available information, including environmental and dynamic load response data. Field trial testing was also planned on an 18-mi (29-km) loop located near the MnROAD facility in Wright County, MN.

In addition to the existing sensors, four geophones and one accelerometer were installed to measure deflection velocity and displacement parameters at four MnROAD cells (three flexible

cells covering a range of stiffnesses and one rigid pavement cell). Data from these sensors were used to estimate the accuracy of the TSDDs by statistically comparing the results measured with the newly installed sensors with those reported by the TSDDs at the four cells on three separate repeat passes.

Conversely, the precision analysis included almost all cells of the MnROAD facility as well as the 18-mi (29-km) loop to account for different pavement structures and other factors such as vertical and horizontal curves. To better evaluate the precision of the TSDDs, they were tested at the MnROAD facility at different speeds and at different times of the day. Data were collected up to five times and at two different speeds. Deflection data for the replicate passes at similar speeds and times were statistically compared to estimate precision.

Given the amount of data collected to facilitate the project data analyses, an online database was developed for ease of update and instant access to various data. The raw, reduced, and analyzed data from the accuracy and precision analyses were placed in the database. This database was also populated with other relevant data such as cell and sensor inventory, ambient conditions, pavement structure, and pavement condition (e.g., IRI measurements).

While the performance of the RWD and TSD varied under different field trials and conditions, it was found that both devices were capable of providing reasonably accurate and precise pavement response measurements. The findings from the accuracy and precision analyses were used later in the project to recommend the optimum operational conditions and device limitations. It is important to recognize that the conclusions and recommendations derived from the accuracy and precision analyses were limited by the amount of data available to the project and the precision and accuracy of the sensors used in this study.

Having established that the TSDDs measurements were acceptable, the 3D-Move software, which estimates dynamic pavement responses at any given point within the pavement structure using a continuum-based finite-layer approach, was calibrated using data from the MnROAD facility field trials. The objective of this calibration was to enable the use of the 3D-Move software in the development of methodologies for incorporating TSDD measurements into network-level PMS applications. A key element in the calibration was simulating pavement surface deflections using numerical models with a focus on understanding the parameters that affect the TSDD measurements. Those parameters include changes in TSDD vehicle speed, pavement layer properties (e.g., age and moisture), and vehicle loading (e.g., tire configuration, load, and inflation pressure).

The 3D-Move analyses were calibrated using inputs derived based on the following considerations:

- Existing MnROAD database of pavement layer properties (thicknesses and physical properties) and recent FWD deflection data.
- Representative layer material properties based on backcalculation of FWD deflection data and, subsequently, viscoelastic AC properties as a function of frequency extrapolated for the TSDD field trial temperatures using Witczak's model and AC middepth layer temperatures derived using the BELLS equation.

- Static tire loads measured at the MnROAD facility weighing station.

Numerous 3D-Move analyses were performed to bracket the computed deflection time histories (peak and basin) with the measured ones from the project geophones. The 3D-Move software was further calibrated using strain measurements taken by the MnROAD strain gauges at various interior pavement locations. Since load-induced strains are critical inputs to pavement performance predictions, this effort was considered critical in ascertaining the applicability of the 3D-Move for pavement response predictions to be used in identifying the most promising indices from TSDD measurements that best relate to pavement structure.

The 3D-Move maximum strains correlated well with the MnROAD sensor measurements. Accordingly, it was further concluded that 3D-Move captures the pavement strain responses well, and therefore, can be used to evaluate pavement responses under TSDD loadings.

Pavement structural capacity can be estimated from performance prediction equations, which relate load-induced pavement responses to one or both of the following pavement distresses: AC fatigue cracking and rutting subgrade rutting. The critical load-induced pavement responses that relate to these two distresses are the maximum tensile strain at the bottom of the AC layer and the vertical compressive strain on top of the subgrade, respectively. The focus of this project was on the AC fatigue cracking and therefore maximum tensile strains at the bottom of the AC layer. An analytical investigation was undertaken using a calibrated 3D-Move analysis to explore the relationships between load-induced structural-related responses of a pavement system and the corresponding surface deflection basin-related indices.

A number of previous studies have suggested that deflection-based indices relate reasonably well to the structural capacity of pavements. For the purposes of this project, it was important to identify indices that best correlate with the critical pavement responses. The selection of the best indices was conducted using the following three-step process:

1. The surface deflection indices that correlated well with the critical pavement responses were initially identified using the 3D-Move calibration results (43 datasets), which were based on the TSDD field trials carried out at the MnROAD facility.

2. A sensitivity analysis of the correlations associated with various deflection indices (not limited to those indices identified in step 1) was undertaken using a set of 36 pavement structures (different combinations of layer thicknesses and moduli) at several vehicle speeds as input to 3D-Move.

3. The robustness of the correlations identified in the first two steps was further explored by considering a much larger database of approximately 15,000 pavement structures generated using the layered elastic program JULEA.

Based on the results from the first step, the indices that best relate to the maximum horizontal strains at the bottom of the AC layer were as follows:

- $R1_{12}$ based on the FHWA equation and deflections measured at radial distances of 0 and 12 inches (0 and 304.8 mm) from the load center.

- $R2_{18}$ based on Horak's equation and deflections measured at radial distances of 0 and 18 inches (0 and 457.2 mm) from the load center.

- SCI_{12} based on deflections measured at radial distances of 0 and 12 inches (0 and 304.8 mm) from the load center.

- SD_{12} based on deflections measured at radial distances of 0 and 12 inches (0 and 0.3 m) from the load center.

In addition, the following were determined:

- Using D_0 or D_4 instead of D_{max} to calculate SCI is reasonable.

- The proposed indices (i.e., $R1_{12}$, $R2_{18}$, SCI_{12}, and $SD_{12)}$ were not sensitive to the TSDD load characteristics (i.e., tire spacing, tire load, and inflation pressure).

Similarly, the following major observations and conclusions relating to deflection indices and AC tensile strains (study focus) were made from the combined results from the first two steps:

- SCI_{12} based on deflections measured at radial distances of 0 and 12 inches (0 and 304.8 mm) from the load center best reflects the role of the upper portion of the pavement system, which was significantly influenced by the AC thickness and modulus.

- TS, which is the ratio between the vertical particle velocity and the vehicle speed, is analogous to deflection slope directly reported by the TSD. TS showed high sensitivity to changes in the pavement structural properties while avoiding potential errors in the deflection basin computed from the TSD measurements. Even though TS_8 was one of the most appropriate indices, sensitivity analyses showed that TS_4 correlated well with the horizontal strains for AC thicknesses of 3 to 6 inches (76.2 and 152.4 mm), while TS_8 correlated well for AC thickness greater than 6 inches (152.4 mm).

- AC thickness is a critical parameter that should be used to categorize pavements into groups. Subgrade modulus, AC modulus, and loading speed only marginally affected the indices in table 77. $R2_{18}$, based on Horak's equation and deflections measured at radial distances of 0 and 18 inches (0 and 457.2 mm) from the load center, is a good index only minimally affected by the AC thickness.

Based on the results of the first two steps, it was concluded that for estimating the maximum horizontal strains at the bottom of the AC surface layer, pavements can be grouped into the following categories:

- AC surface layer thickness less than 3 inches (76.2 mm).

- AC surface layer thickness between 3 and 6 inches (76.2 and 152.4 mm).

- AC surface layer thickness greater than 6 inches (152.4 mm).

In the third step, a wider range of pavement structures was analyzed using the layered LE program, JULEA.[26] A database of 15,000 pavement structures over a wide range of layer moduli and thicknesses were simulated using the Monte Carlo technique. The corresponding pavement responses (strains and deflections) were computed for each simulated pavement structure. A procedure similar to the one used in the 3D-Move analyses was used to compute the maximum fatigue strain. Similarly, surface deflections at the same locations used for the first step were computed. The database was used to identify the most sensitive pavement properties that affect the critical responses and the most sensitive indices that correlate well with the critical responses.

The thickness of the AC layer was found to be the most sensitive pavement property that affected the pavement responses in question. The pavement structures in the JULEA database were then grouped based on the AC layer thickness. For pavement structures with a thin (i.e., less than 3 inches (76.2 mm)) AC layer, the stiffness of the base, AC, subgrade, and base thickness significantly influenced the critical pavement responses. A weak correlation between the deflection indices and critical strains was observed only when the AC thickness was considered in the development of correlations. However, for network-level applications, a relationship involving several material properties was not practical and thus was not pursued further.

For pavement structures with AC layer thicknesses between 3 and 6 inches (76.2 and 152.4 mm), it was found that the most sensitive indices for the maximum fatigue strain response were as follows:

- $R1_8$ based on deflections measured at radial distances between 0 and 8 inches (0 and 203.2 mm) from the load center.

- SCI_8 based on deflections measured at radial distances between 0 and 8 inches (0 and 203.2 mm) from the load center.

For pavement structures with an AC layer thickness between 6 and 16 inches (152.4 and 406.4 mm), the indices found to be most sensitive for the maximum fatigue strain response were as follows:

- DSI_{4-18} based on deflections measured at radial distances between 4 and 18 inches (101.6 and 457.2 mm) from the load center.

- SCI_{18} based on deflections measured at radial distances between 0 and 18 inches (0 and 457.2 mm) from the load center.

For pavement structures for which the AC layer thickness was unknown, the $R2_{12}$ index based on Horak's equation and deflections measured at radial distances of 0 and 12 inches (0 and 304.8 mm) from the load center was found to be a reasonable predictor of maximum fatigue strain response for both thin and thick pavements. Accordingly, when the AC thickness information is not available, $R2_{12}$ can be used to estimate the maximum fatigue strain.

Because incorporating TSDD measurements into network-level PMS applications requires establishing a relationship between the computed or measured indices and the critical pavement responses, the critical responses were then related to the corresponding indices deemed sensitive.

For thin AC layers, separate relationships were developed for those cases where the AC layer was thicker and thinner than the base layer.

The final phase of the selection of the indices was to conduct a balance evaluation of the uncertainties associated with the models and relationships developed and the effect of precision and accuracy of the devices on the computed indices. The accuracy of the devices was defined as the median accuracy of the index computed from all tests carried out for that purpose at MnROAD. *Precision* is defined as the ratio of the median of the SEE among replicate runs from all tests carried out in Minnesota divided by the corresponding median deflection index. The uncertainty of the model was assessed by dividing the SEE of the strains for each index divided by the median of the strain estimated. The R^2 values were also used as a second parameter related to the appropriateness of the relationships.

Based on the criteria, the most optimized indices for each pavement thickness range are reported in table 80. The recommended indices include the following:

- DSI_{4-12}, based on deflections at 4 and 12 inches (101.6 and 304.8 mm) from the load center, which was formulated as part of the study, was found to be the most appropriate index regardless of AC thickness (whether known or unknown).

- SCI_{12}, based on deflections at 0 and 12 inches (101.6 and 304.8 mm) from the load center, performed nearly as well as DSI_{4-12}.

Data analyses have shown that indices that can be derived from TSD measurements provide robust assessment of pavement structural condition at the network level. Improvements in the number of sensors and their locations are needed to use the recommended analyses methodologies with the RWD, but these should not be difficult to achieve.

Table 80. Recommended deflection indices.

AC Thickness	Index	Device Precision (Percent)	Device Accuracy (Percent)	Model Uncertainty (Percent)	Model R^2
Between 3 and 6 inches	DSI_{4-12}	9	8	16	0.88
	SCI_{12}	11	18	15	0.90
	DSI_{4-8}	10	12	13	0.92
	TS_4	14	11	13	0.91
Greater than 6 inches	DSI_{4-12}	9	8	13	0.97
	DSI_{8-12}	9	7	12	0.98
	SCI_{12}	11	18	14	0.96
	DSI_{4-8}	10	12	17	0.95
	TS_8	9	15	17	0.94
	TS_{12}	10	21	17	0.96
	AUPP	11	13	15	0.97
Unknown	DSI_{4-12}	9	8	22	0.97
	SCI_{12}	11	18	20	0.97

1 inch = 25.4 mm

Recommendations for incorporating the project findings and conclusions into network-level PMS applications are detailed in the next chapter, including data requirements, selection of indices, computation of strains, temperature correction of strains, and various approaches for relating strains to pavement structural capacity.

CHAPTER 10. RECOMMENDATIONS

The ultimate goal of the project was to establish a reliable measure of the structural condition of all bound pavement layers above the unbound base layer as it deteriorates over time under traffic and environmental loading based on moving pavement deflection technology and measured at posted traffic speeds. Towards achieving this goal, the study focused on the following two activities:

- Evaluating the capabilities of the available TSDDs.
- Developing compatible analysis methodologies for enabling the quantification of pavement deterioration over time under traffic and environmental loading.

A system approach was followed so that the TSDDs could be effectively used as a tool for network-level PMS applications and decisionmaking. The flowchart of an idealized system is shown in figure 219. There are several alternative approaches for implementation. In the suggested approach, the decisions based on the traditional condition metrics are confirmed and/or adjusted based on the pavement structural condition as derived from the TSDD measurements. In this manner, the pavement community has the opportunity to gradually implement the proposed changes while avoiding abrupt changes to their institutional approaches.

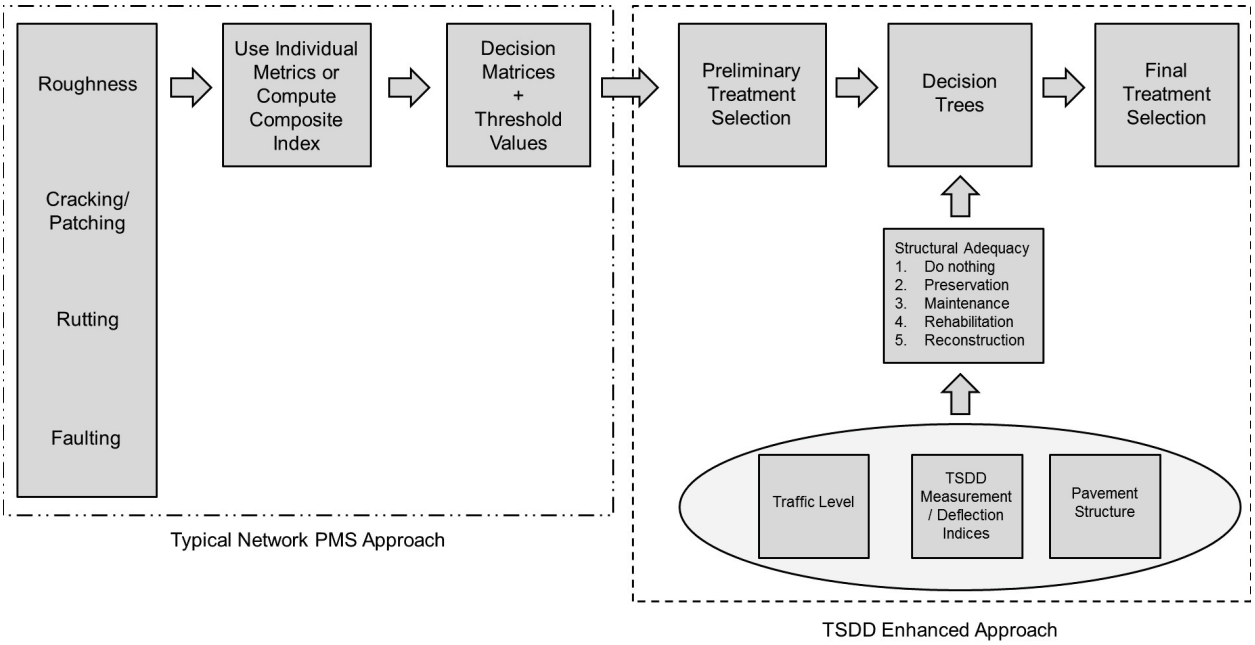

Figure 219. Flowchart. Idealized PMS containing TSDD structural evaluation component.

To deliver a robust system, the level of analysis sophistication should be balanced with the uncertainties of the TSDDs. Since the manufacturers are actively improving the TSDDs, the interpretation and analyses software should also be progressively improved. The following factors were considered in proposing areas of opportunity for improvements to the system in an integrated and balanced manner:

- **Accuracy of measurements** as defined by the closeness of measured deflection parameters to their true values.

- **Precision of measurements** as defined by obtaining similar results on a given section with multiple surveys within a short period.

- **Operational parameters of the devices** such as the speed of the vehicle, the spatial frequency of data reporting by the device, environmental conditions, and road geometry without sacrificing the quality of the data collected.

- **Availability of additional information** such as pavement structure, surface condition of the road, and applied loading (i.e., traffic) to the pavement.

- **Data analyses** in terms of minimum input data necessary to characterize the structural condition of the road, the deflection parameter(s) that best relate to the structural condition, and the optimal algorithm to estimate the structural condition.

- **Data interpretation** in terms of the best use of statistical methods to report a representative structural condition over a representative distance with the spatial variability for each representative distance in addition to the mean value.

Within the context of the above factors, the two devices (TSD and RWD) studied in this project were found to be capable of providing reasonably accurate and precise response measurements for flexible pavements. Since adequate data were not available for proper evaluation, the research team is unable to comment on the applicability of the two devices to rigid pavements.

Based on the system approach discussed so far, practical recommendations are provided in the following subsections in terms of the equipment, data collection, and data analysis to optimize the operation of these devices. Both short- to long-term recommendations for improving the robustness of the system as a network-level PMS tool are provided.

10.1 EQUIPMENT RECOMMENDATIONS

One of the most desirable attributes of the ideal TSDD for use on flexible pavements is for the device to provide deflection parameter basins (i.e., deflection parameters at two or more points). Due to the many years of legacy research with the FWD, the current preference of the pavement community is to use lessons learned from using vertical deflection basins as opposed to other deflection parameters.

Based on the numerical analyses conducted in this study, at least three sensors located between the center and 18 inches (457.2 mm) from the wheels are desirable for quantifying fatigue cracking of the AC layer. Aside from the spot directly between the two wheels, the desirable specific locations for these sensors depend on the pavement structure. For thinner AC layers (less than 6 inches (152.4 mm)), it is desirable for the sensors to be within 8 inches (203.2 mm) from the center of the wheels, while for the thicker pavements, sensors located between 8 and 18 inches (203.2 and 457.2 mm) from the center of the wheels seem best suited for capturing the fatigue cracking potential of the AC layer.

For subgrade rutting, on the other hand, sensors that are 24 inches (609.6 mm) or farther from the center of the wheels are considered appropriate. From the results of the field studies conducted as part of this project, the uncertainty (precision and/or accuracy) associated with the TSD sensors positioned between the wheels and farther than 24 inches (609.6 mm) may require further improvements. It is difficult to comment on the accuracy of the sensors farther than 24 inches (609.6 mm) since the deflections are too small (i.e., less than the sensitivity of the embedded sensors used in the project). Given the available data, it might be reasonable to assume that this statement is also applicable to the TSDD sensors.

In the short term, the two RWD sensors could be repositioned, perhaps at 4 and 12 inches (304.8 mm) in front of the wheel center, to provide deflections that can be used more readily to assess the fatigue cracking of the AC layer. In the medium term, it would be desirable to decrease the uncertainty associated with the reported deflections so that more advanced analyses can be performed. In the long term, the installation of more sensors should be considered.

In the case of the TSD, deflection parameter measurements are provided at multiple locations (up to nine as of the date of this report). Aside from increasing the number of sensors, the best compromise for the TSD evaluated in this project is to place the sensors at distances of 4, 8, 12, and 18 inches (101.6, 203.2, 304.8, and 457.2 mm) from the center of the wheels for evaluating fatigue cracking and 24 and 48 inches (609.6 and 1,219.2 mm) for quantifying subgrade rutting. In addition, a sensor placed behind the rear axle (e.g., -12 inches (-304.8 mm)) would be useful in capturing the viscous lag in the deflection basin due to the moving load.

Aside from repositioning and/or adding sensors, it would also be desirable in the short term to decrease the uncertainty associated with the models for computing the deflection basin from deflection slopes and to improve the precision of the measurements at sensor spacings longer than 24 inches (609.6 mm). In the medium term, and until the pavement community migrates to developing indices based on deflection slope, the algorithm to convert deflection slopes to deflection basin may be improved. The long-term focus of the pavement community should be in implementing an algorithm that can directly use deflection slopes.

It is also helpful to know the load characteristics applied to the pavement during testing, especially as the analyses techniques become more advanced. The load characteristics can change not only due to the vehicle loading and tire pressure, but also due to roughness of the road and strong cross winds during the operation. The reliability of the analysis in the proposed system approached could improve if the load magnitudes are reported along with the deflection parameters. Even though the dynamic load characteristics were not available to the project research team at the time of field testing, the TSD device is currently capable of collecting load information. The RWD developers should consider providing such information.

The issue of the relative and absolute calibrations of the device should also be addressed by the manufacturers. In the short term, it would be useful to have a set of straightforward instructions to document that the sensors are aligned properly, that they collect data correctly, and that other components (e.g., the GPS unit and the temperature sensors) are functioning and collecting data properly. In the medium to long term, a set of measurement protocols should be devised to facilitate the consideration of the impact of the seasonal variations in the analyses as much as possible.

Finally, it would be advantageous to equip the TSDDs with auxiliary devices for measuring the pavement structure (e.g., GPR), pavement smoothness (e.g., IRI), and pavement surface condition (e.g., high-definition cameras). This additional information can not only be used to make the structural analysis more conclusive, but with proper planning, it can be used for other purposes such as asset management, which could make the surveys more affordable.

10.2 DATA COLLECTION RECOMMENDATIONS

The two TSDDs considered in the project collect data densely. However, the data reported are averaged over a certain distance. Theoretically, the shorter the averaging distance, the better the certainty of the analysis will be. However, there is no question that averaging is necessary for State transportation departments to work with a manageable amount of data. In the case of the RWD, averaging is done over 0.1-mi (0.161-km) intervals, while for the TSD, averaging is done over 32.8-ft (10-m) intervals.

Averaging is an effective way of minimizing the amount of random noise in the raw data, but excessive averaging can also mask changes in the signal due to changes in the structural condition of the pavement. The TSDD developers have carefully studied the raw signals from their devices to propose the optimal averaging distances. However, the level of sophistication of the data analysis in the suggested balanced system should be set based on the capabilities of the TSDDs. As such, the uncertainties in the deflection measurements should be delineated from the spatial variation in the measurements due to changes in the pavement structure or condition.

In the short term, manufacturers would report not only the mean deflection parameters but also additional statistical information (such as the standard deviations or coefficients of variation) associated with those mean values and their variability. In that manner, the analyst can judge the level of uncertainties associated with each deflection parameter reported. In the medium term, the level of uncertainties in the measured deflection parameters should be verified through independent research. Such analysis requires access to the raw or spatially averaged data over a short distance (e.g., 3.28 ft (1 m) or less). In the long term, manufacturers would improve their devices to a level that the averaging can be done as part of the analysis and not data collection.

The data collection should ideally be done at the posted speed limit. Based on this study, it seems that the variability in the collected data decreases as the vehicle speed decreases. The best strategy is to collect the data at the lowest practical speed possible without requiring lane closures or causing safety issues. For example, if the maximum posted speed limit is 65 mi/h (104.65 km/h), then data collection at 40 to 45 mi/h (64.4 to 72.45 km/h) may be desirable.

The manufacturer's recommendations concerning calibrations, vehicle warm-up, tire pressure checks, and other vehicle readiness elements should be carefully followed. Also, based on the project findings, the following additional suggestions are provided:

- The impact of the seasonal environmental variations on the TSDD measurements was not evaluated in this project. However, until such study is carried out, the repeat survey of the sites should be carried out during approximately the same time of the year to minimize seasonal effects.

- The short-term variations in ambient temperature were studied at the MnROAD facility as part of this project. Until a formal study is carried out to establish the allowable range of testing temperatures, a conservative operational temperature range of 45 to 85 °F (7.22 to 29.44 °C) is suggested. The lower limit takes into consideration that the uncertainty in the study measurements were lower for less stiff pavement structure. The upper limit is proposed based on the observation that the precision of the devices (at least for the TSD) became worse as the ambient temperature increased.

- Testing is not recommended during precipitation or when the pavement surface is wet due to the current sensors used to measure the pavement responses, which are affected by moisture.

- The impact of the wind was not explicitly studied. However, testing should be carried out with caution in windy conditions, especially when the wind is predominantly perpendicular to the direction of travel. This is especially true if the TSDD-applied load is not being measured on the same side where the deflection measurements are taken.

- The horizontal and vertical curves did not seem to significantly affect the TSD results. Nonetheless, it would be a good practice to carefully review data collected near extreme curves.

- As a quality check, repeat data collection is recommended on a small portion (i.e., 5 to 10 percent) of the network under consideration to ensure consistent data are being collected.

- The frequency of data collection should be further studied by individual State transportation departments by taking into consideration the effective lives of their pavements and their current PMS experiences and practices. Until then, TSDD testing once every 3 to 5 years on average appears reasonable.

- Based on the initial investment, the daily cost of the operation of the TSDDs is significantly greater than testing with the FWD at present. However, based on the daily productively of the two devices, the costs per mile associated with TSDDs are substantially less than the FWDs. The cost associated with the TSDDs may be further reduced as State transportation departments embrace their use, incentivizing more service providers to become available and the analysis algorithms to become more automated.

10.3 RECOMMENDED DATA ANALYSIS FOR NETWORK-LEVEL PMS APPLICATIONS

The suggested TSDD data analysis for incorporation into network-level PMS applications can be summarized in the following four steps:

1. **Calculating representative indices for estimating structural condition of pavement**: Based on this study, the most feasible parameters are DSI or SCI considering the fatigue cracking of the AC layer as the critical parameter.

2. **Estimating horizontal strains at bottom of AC layer using recommended or user selected index**: Based on the available information, the feasible models are recommended in table 80.

3. **Adjusting the estimated strains to a standard temperature**: The strains computed in step 2 need to be corrected to a standard reference temperature for consistent evaluation and tracking of the deflection parameters over time (section 8.7). Assuming a standard reference temperature of 70 °F (21.11 °C), the recommended approach entails the following computations:

    - Compute temperature correction factor based on the temperature at time of the TSDD field measurements and the reference temperature of 70 °F (21.11 °C).

    - Compute the AC dynamic modulus based on the strains computed in step 2 and the AC layer thickness.

    - Compute the AC dynamic modulus at the reference temperature of 70 °F (21.11 °C).

    - Compute the temperature corrected strains using the AC modulus at the reference temperature of 70 °F (21.11 °C).

4. **Establishing structural adequacy of pavements using temperature-corrected strain**: Ideally, it would be desirable for the pavement analyst to be able to determine whether different segments of the pavement network are candidates for preservation, maintenance, rehabilitation, or reconstruction or whether they are adequate as they are. As a minimum, the algorithm associated with this item needs to be able to provide information on whether the pavement is structurally sound for the anticipated traffic and whether a lower level treatment can be used to correct any functional deficiencies or require structural treatment. The initial work toward this goal can be found in Thyagarajan et al. amongst others.[21,66] Abdallah et al. suggests a probabilistic method for this purpose as applied to FWD using artificial neural networks. Similar and/or follow-up work should be pursued by the pavement community.[67]

One of the most critical factors related to data analysis is the spatial averaging of the data. For an effective utilization, spatial statistical analysis and segmentation of the TSDD data are necessary. An effective analysis tool should allow pavement engineers to distinguish the changes in the road segments due to either changes in the pavement structure or the deterioration of the pavement sections. The statistical analysis for segmentation should be done considering the capabilities of the TSDD, and the condition and nature of the pavement structures.

Assuming that the recommendations related to the averaging during data collection presented previously can be addressed, in the short term, a probabilistic structural analysis could be incorporated for a robust segmentation of the roads at the network level. In the medium and long terms, a dynamic and adaptive optimization could be added to assist the decisionmakers.

As stated in the previous two chapters, a single robust universal index that can predict the structural performance of all pavements at the network level could not be identified. For a robust system approach, information about the pavement layer thicknesses and especially the AC layer

is required to use the indices identified. Also, as reflected in the previous section of this chapter, additional data are needed to understand measurement variability and to predict future treatment requirements. These data include the following:

- Surface condition of the pavements, including such parameters as IRI and extent of cracking, to check and/or to help rationalize the results.
- Best estimates of the present traffic and future traffic projection.
- Ambient condition at the time of testing.

It would be highly useful for the manufacturers and/or the owners of the TSDDs to work towards using multi-function survey vehicles by incorporating systems that are currently part of the automated pavement condition survey vehicles.

10.4 RECOMMENDED FUTURE RESEARCH

This report represents the first step toward the eventual implementation of a robust system approach for the structural evaluation of pavements at the network level. The previous sections in this chapter provide several specific technical recommendations to the pavement community to collectively improve the TSDD equipment, data collection, and analyses for network-level applications. The following general items are logical follow-up activities to this study.

The first important follow-on activity should focus on further evaluating the results of this project. The precisions reported for the TSDDs are comparable with those reported by others.[3,19,16] However, the accuracies of the devices have not been reported extensively in the literature. Also, the structural models proposed in this report have not been evaluated using actual field data. The use of data collected by the RWD and TSD for highway agencies throughout the country can be used for this purpose. The data collected by or for international highway agencies (e.g., Denmark, Poland, South Africa, Australia, and Italy) are valuable, too. Of particular interest is the production-level data collected in the United Kingdom for their network-level evaluations over the past few years. In addition to evaluation of the findings, these data will enable the extension of the project results to a broader spectra of conditions, including different pavement structures, environments, and subgrade soils.

Given that the TSDDs have only been commercially available in the recent past, it would be beneficial to monitor the changes in the TSDD deflections seasonally and with the growth of distress over time. For this purpose, the devices should be utilized repeatedly (seasonally) at sites that are being used for LTPP monitoring (similar to or in conjunction with the LTPP program sites). It is acknowledged that this will be a long term project. However, the data collected in that manner, at several diverse sites selected through a careful experimental design, can provide a wealth of information about the frequency of network-level data collection and manner to use the TSDD data. Moreover, making an initial measurement immediately after the completion of the construction of the test sections is not only an efficient way to evaluate the construction quality but also provides a structural capacity datum for the pavement.

Beyond the above recommendations, other potential future research areas under controlled conditions may be necessary to perform the following:

- Confirm the predictive power of the recommended deflection indices through the use of measurements taken by strain gauges at the bottom of the AC layer during TSDD loadings. While the data collected as part of this study served as a first step, there were issues with the functioning of strain gauges, and the data were limited to AC layers of around 5 inches (127 mm) in thickness. Accordingly, additional data for thinner and thicker pavements structures would be preferred.

- Expand and validate the prediction of subgrade compressive strain to complement horizontal tensile strains at the bottom of AC layer.

- Validate the utility of the deflection indices through investigation and implementation of their reasonableness for the network-level PMS application proposed in section 10.3.

- Apply TSDDs to PCC pavements to evaluate their applicability to network-level evaluation of this pavement type, including estimating load transfer and joint condition evaluations.

- Expand the use of the data from TSDDs with multiple sensors for backcalculation of layer moduli and/or assessment of the condition of individual pavement layers as well as overall pavement structure.

- Conduct a more indepth study of the impact of ambient conditions as well as pavement structures/conditions on the deflection measurements for finer adjustments of the operational guidelines as suggested in section 10.2.

- Consider the impact of the non-linear response of the unbound materials in thin pavement structures on the TSDD measured responses.

- Explore methodologies for the development of structural performance curves based on TSDD derived structural indices measured over time for use in conjunction with current performance curves for predicting future condition and programming projects.

Structural capacity is important and the TSDD technology should be in place within the next 5 years. Some institutional issues should also be considered for the smooth transition of the incorporation of TSDDs into network-level PMS applications. Some of the key issues include the following:

- How to gradually incorporate TSDD data into network-level pavement evaluations of the following:

    - Transportation agencies that solely make decisions based on the functional aspects of the pavements (e.g., IRI, cracking, rutting, and faulting) without structural testing.

    - Agencies that utilize FWD for structural testing in addition to functional testing to make decisions.

- Possible incorporation in the near future of TSDD measurements into the pavement rulemaking of the *Moving Ahead for Progress in the 21st Century Act* legislation as a pavement condition metric in addition to IRI, cracking, rutting and faulting, and its use in defining pavement performance measures.(68)

APPENDIX A. DEVICE MANUFACTURERS' QUESTIONNAIRES AND INTERVIEWS

To augment the project literature review findings, questionnaires were developed and sent to the device manufacturers as well as owners and users of the devices. Interviews were also conducted to follow up with specific questions or to pursue clarification. The completed questionnaires as well as highlights from the interviews are contained in this appendix.

Name of moving deflection device: _____

Name of person completing questionnaire: _____

Date questionnaire was completed: _____

I. Device Information for Analysis

1) Please briefly describe the measurement concepts and technology basis of your device. Alternatively, please attach any technical brochure you may have that includes that information.

   _____

2) Please summarize the improvements to the device in the last 3 years.

   _____

3) In terms deformation parameters measured,

   a) How many deformation points are reported for each measurement (loading point) at this time (i.e., can you define a deflection bowl)? _____

   b) What are the offsets from the load to different measurement points? _____

   c) If less than three deformation points are reported, what is the potential of increasing the number of points reported in the near future and how many points will be feasible? _____

4) In terms of loads applied to pavement,

   a) Is it possible to vary the load applied to pavement? Yes ☐ No ☒

      If yes, specify the range _____, and specify how _____.

      If no, do you intend to add this feature? _____ and (if applicable) specify the load range you feel is feasible _____

b) Do you measure and report applied (instantaneous dynamic wheel) load at this time? Yes ☐ No ☒

If no, what is the potential of measuring and reporting applied load in the near future? _____

5) In terms of geospatial information at the time of testing,

a) Do you use a GPS unit? Yes ☒ No ☐

b) What geospatial information is included in the file (can we superimpose on Google® maps, etc.)? _____

6) Is the device equipped with temperature gauge? Yes ☒ No ☐

a) If yes, specify the range _____, and specify how temperature is measured and reported.

b) If no, do you intend to add this feature in the near future? _____

7) Is your device equipped with other measuring technologies (e.g., GPR, video, roughness measurement, etc.)? Yes ☐ No ☒

a) If yes, specify the technology(ies) and parameters reported. _____

b) If no, do you intend to add any auxiliary technologies in the near future? (Please explain.) _____

8) What is the technically feasible range of speeds that your device provides valid measurements (as opposed to safety-related)?

Max. speed (e.g., when data acquisition cannot keep up) _____

Min. speed (e.g., not enough deformation amplitude), if any _____

9) What is the recommended distance between successive readings? _____

Can the user define the distance between successive readings? Yes ☒ No ☐

If yes, specify min. _____ and max. _____

10) What is the recommended spatial averaging distance of the deformation parameters? _____

Can the user define the spatial averaging distance? _____

11) What type of spatial averaging algorithm is used?

_____

12) What types of pavement structures can be tested with confidence using the device (flexible, rigid, or semi-rigid)? If applicable to pavements other than flexible, are there any operational limits (open-ended question)?

_____

II. Device Information for Operation

13) Have you established written test protocols for the device (including pre-testing activities, test protocol during data collection, and post-testing activities)? Yes ☐ No ☒

a) If yes, please attach the document. _____

b) If no, please explain how typically the device is operated. _____

14) Have you established a written calibration process for the device? Yes ☐ No ☒

a) If yes, please attach the document. _____

b) If no, please explain how the accuracy of the measurements is ensured. _____

15) Does pavement texture or other surface characteristics (dark/light/moist pavement) impact your deformation measurement concept/technology? Yes ☒ No ☐ If so, do you account for it in your measurements/analyses?

a) If yes, please explain how:

a) During measurements _____

b) During data analyses _____

b) If no, please explain how the accuracy of the measurements is ensured. _____

16) Do you consider the impact of pavement condition (e.g., roughness, cracking, and rutting) on your measurements/analyses? Yes ☒ No ☐

a) If yes, please explain how:

a) During measurements _____

b) During data analyses _____

b) If no, please explain how the accuracy of the measurements is ensured. _____

III. Device Information for Evaluation

17) The deformation sensors used are _____ manufactured by _____.

a) Under ideal conditions, the stand-alone sensor has the following characteristic:

- Nominal calibration factor is _____ xx/volt
- Precision is _____
- Accuracy is _____
- Effective range is between (min.) _____ and (max.) _____

b) When installed in the system, the sensor has the following characteristic during testing:

- Precision is _____ as determined using the following process _____
- Accuracy is _____ as determined using the following process _____
- Effective range is between (min.) _____ and (max.) _____ as determined using the following process _____.

18) The load sensors used are _____ manufactured by _____.

a) Under ideal conditions, the stand-alone sensor has the following characteristic:

- Precision is _____
- Accuracy is _____
- Effective range is between (min.) _____ and (max.) _____

b) When installed in the system, the sensor has the following characteristic during testing:

- Precision is _____ as determined using the following process _____
- Accuracy is _____ as determined using the following process _____
- Effective range is between (min.) _____ and (max.) _____ as determined using the following process _____

19) The electronics used have the following generic information.

a) A/D board digitizes at _____ (12, 16, or 24) bits.

b) Amplifiers are used to amplify the signals by _____ times for deformation and _____ times for load.

c) Signals are subjected to a (low, high, or band pass) filter(s) with the following characteristics:

- Deformation: _____
- Load: _____

d) The rawest form of data saved by the device are in the form of (raw voltage output, specified processed data at each measurement point, average of __ measurements, etc.):

- Deformation: _____
- Load: _____
- Distance: _____

e) The data that can be shared with the research team are (mark all that apply):

☐ Raw voltage outputs.

☐ Specified processed data at each measurement point.

☐ Average of _____ measurements.

☒ Other (please specify): _____

f) What is the electronic format of the reported data to client? _____ (Please attach an example).

g) Could you please explain what general algorithm used to obtain the data for client report (item f) from the raw data (item d)?

- For Deformation: _____
- For Load: _____
- For Distance: _____

h) Is your device equipped with external ports so that the research team can record the sensor outputs independently?

- For Deformation Sensors: Yes ☐ No ☒
- For Load Sensors: Yes ☐ No ☒

i) If yes, do they allow the research team to collect data with them? _____

People Interviewed: **Doug Steele, David Hein, and William Vavrik**
Date Interviewed: **January 14, 2013**

Interview Conducted by: **Gonzalo Rada, Soheil Nazarian, Nadarajah Sivaneswaran (Siva), and Beth Visintine**

- Individual deflection readings at 0.5-inch intervals.
- Raw data is in binary format.
- No averaging during initial laser processing of measurements.
- RWD has four sensors to collect deflection.
- Second deflection (D_{15}) for diagnostic purposes and is 18 inches apart.
- Vibration of beam not measured; this goes into variability of lasers and aggregating data takes this out.
- Different forms of processing have not [really] been tried (i.e., filtering, moving average, moving standard deviation, etc.).
- Bouncing of truck (sinusoidal cycle) adds noise but this is taken out by average.
- Frequency of texture is main cause of noise in deflection.
- Able to collect data down to 5 mi/h.
- Collect data in temporal domain; based on DMI, use reading every 15 mm regardless of speed to transfer to distance domain.
- Do not measure dynamic load or tire pressure; measure static load and assume constant. Varying dynamic load can add to variability with texture.
- Independent of system, will allow to add tire pressure measuring device.
- Need work plan for field experiment to determine the RWD cost. Will sign a letter of commitment subject to approval of work plan.
- Mentioned Kansas has instrumented sections and to contact Rick Miller.

Name of moving deflection device: _____

Name of person completing questionnaire: _____

Date questionnaire was completed: _____

I. Device Information for Analysis

1) Please briefly describe the measurement concepts and technology basis of your device. Alternatively, please attach any technical brochure you may have that includes that information.

   _____

2) Please summarize the improvements to the device in the last 3 years.

   _____

3) In terms deformation parameters measured:

   a) How many deformation points are reported for each measurement (loading point) at this time (i.e., can you define a deflection bowl)? _____

   b) What are the offsets from the load to different measurement points? _____

   c) If less than three deformation points are reported, what is the potential of increasing the number of points reported in the near future and how many points will be feasible? _____

4) In terms of loads applied to pavement:

   a) Is it possible to vary the load applied to pavement? Yes ☒ No ☐

      If yes, specify the range _____, and specify how _____.

      If no, do you intend to add this feature? _____ and (if applicable) specify the load range you feel is feasible _____

   b) Do you measure and report applied (instantaneous dynamic wheel) load at this time? Yes ☒ No ☐

      If no, what is the potential of measuring and reporting applied load in the near future?

      _____

5) In terms of geospatial information at the time of testing:

   a) Do you use a GPS unit? Yes ☒ No ☐

   b) What geospatial information is included in the file (can we superimpose on Google® maps etc.)? _____

6) Is the device equipped with temperature gauge? Yes ☒ No ☐

   a) If yes, specify the range _____, and specify how temperature is measured and reported.

   b) If no, do you intend to add this feature in the near future? _____

7) Is your device equipped with other measuring technologies (e.g., GPR, video, roughness, measurement, etc.)? Yes ☒ No ☐

   a) If yes, specify the technology(ies) and parameters reported. _____

   b) If no, do you intend to add any auxiliary technologies in the near future? (Please explain.)
   _____

8) What is the technically feasible range of speeds that your device provides valid measurements (as opposed to safety-related)?

   Max. speed (e.g., when data acquisition cannot keep up) _____

   Min. speed (e.g., not enough deformation amplitude), if any _____

9) What is the recommended distance between successive readings? _____

   Can the user define the distance between successive readings? Yes ☐ No ☒

   If yes, specify min. _____ and max. _____

10) What is the recommended spatial averaging distance of the deformation parameters? _____

    Can the user define the spatial averaging distance? _____

11) What type of spatial averaging algorithm is used?

    _____

12) What types of pavement structures can be tested with confidence using the device (flexible, rigid, or semi-rigid)? If applicable to pavements other than flexible, are there any operational limits (open-ended question)?

    _____

II. Device Information for Operation

13) Have you established written test protocols for the device (including pre-testing activities, test protocol during data collection, and post-testing activities)? Yes ☒ No ☐

   a) If yes, please attach the document. _____

   b) If no, please explain how typically the device is operated. _____

14) Have you established a written calibration process for the device? Yes ☒ No ☐

   a) If yes, please attach the document. _____

   b) If no, please explain how the accuracy of the measurements is ensured. _____

15) Does pavement texture or other surface characteristics (dark/light/moist pavement) impact your deformation measurement concept/technology? Yes ☒ No ☐ If so, do you account for it in your measurements/analyses?

   a) If yes, please explain how:

      a) During measurements _____

      b) During data analyses _____

   b) If no, please explain how the accuracy of the measurements is ensured. _____

16) Do you consider the impact of pavement condition (e.g., roughness, cracking, and rutting) on your measurements/analyses? Yes ☐ No ☐

   a) If yes, please explain how:

      a) During measurements _____

      b) During data analyses _____

   b) If no, please explain how the accuracy of the measurements is ensured. _____

III. Device Information for Evaluation

17) The deformation sensors used are _____ manufactured by _____.

   a) Under ideal conditions, the stand-alone sensor has the following characteristic:

      - Nominal calibration factor is _____ xx/volt
      - Precision is _____
      - Accuracy is _____

- Effective range is between (min.) _____ and (max.) _____

b) When installed in the system, the sensor has the following characteristic during testing:

- Precision is _____ as determined using the following process _____
- Accuracy is _____ as determined using the following process _____
- Effective range is between (min.) _____ and (max.) _____ as determined using the following process _____

18) The load sensors used are _____ manufactured by _____

a) Under ideal conditions, the stand-alone sensor has the following characteristic:

- Precision is _____
- Accuracy is _____
- Effective range is between (min.) _____ and (max.) _____

b) When installed in the system, the sensor has the following characteristic during testing:

- Precision is _____ as determined using the following process _____
- Accuracy is _____ as determined using the following process _____
- Effective range is between (min.) _____ and (max.) _____ as determined using the following process _____

19) The electronics used have the following generic information:

a) A/D board digitizes at _____ (12, 16, or 24) bits.

b) Amplifiers are used to amplify the signals by _____ times for deformation and _____ times for load.

c) Signals are subjected to a (low, high, or band pass) filter(s) with the following characteristics:

- Deformation: _____
- Load: _____

d) The rawest form of data saved by the device are in the form of (raw voltage output, specified processed data at each measurement point, average of __ measurements, etc.):

- Deformation: _____
- Load: _____
- Distance: _____

e) The data that can be shared with the research team are (mark all that apply):

☐ Raw voltage outputs.

☒ Specified processed data at each measurement point.

☐ Average of _____ measurements.

☐ Other (please specify): _____

f) What is the electronic format of the reported data to client? _____ (Please attach an example).

g) Could you please explain what general algorithm used to obtain the data for client report (item f) from the raw data (item d)?

- For Deformation: _____
- For Load: _____
- For Distance: _____

h) Is your device equipped with external ports so that the research team can record the sensor outputs independently?

- For Deformation Sensors: Yes ☐ No ☐
- For Load Sensors: Yes ☐ No ☐

i) If yes, do they allow the research team to collect data with them? _____

People Interviewed: **Jørgen Krarup, Leif Grønskov, and Louis Pedersen**

Date Interviewed: **January 15, 2013**

Interview Conducted by: **Gonzalo Rada, Soheil Nazarian, Nadarajah Sivaneswaran (Siva), and Beth Visintine**

- Have fixed data issue with minimum amount of filtering.
- Want us to limit the technical information that we include in the report.
- There is a phase issue within the Doppler sensors.
- The TSD manufacturer is bringing one of their units over to the US at their expense. Project will pay for data collection. FHWA to look into issue with customs and see if there are any workarounds.
- The calibration of the sensor angles is important.
- Measure load within 0.5 kg.
- New Doppler sensors can be moved (unlike TSD version the United Kingdom Transportation Research Library has). Therefore, can place sensors before and after joint to determine load transfer.
- Issue with horizontal curves have been addressed (based on beam movement), but the project team should consider including curves within work plan.
- Willing to provide raw data once they know how the project team will use it. This is not an issue of wanting to hide anything, but want to make sure that it is being used properly (for a specified limited section).
- TSD includes measurement of IRI.
- Speed can be an issue if the sensor height is not properly adjusted. Sensor still works, just less precise. If this happens, the reported data rate drops. This issue has been addressed in the new system.
- Do not recommend measuring below 30 km/h, as this is to avoid the viscoelastic response or minimizes it.
- Agreed to have a letter of commitment by mid-February 2013.

APPENDIX B. SENSOR INSTALLATION AND FIELD TRIALS

Sensor installation and field testing activities in support of the project began on Monday, September 16, 2013, and lasted through Friday, September 27, 2013. A significant amount of data resulted from the field testing activities, which when combined with other relevant data (e.g., pavement structure, pavement condition, climate, etc.) necessitated the development of a project database and Web site to facilitate the planned analyses. A summary of the field activities as well as the project database and Web site development activities is provided in this chapter.

SENSOR INSTALLATION

The installation of geophones and accelerometers at the MnROAD facility took place during the week of September 16, 2013. This section provides a chronological summary account of the activities that took place.

Monday, September 16, 2013

Activities began on Monday morning with a meeting between project team members and MnROAD staff to coordinate the sensor installation and testing activities. The following people were present at the meeting:

- Senthil Thyagarajan (FHWA onsite contractor).
- Carlos Solis (Amec Foster Wheeler Environment & Infrastructure, Inc.).
- Sergio Rocha (University of Texas-El Paso (UTEP)).
- Soheil Nazarian (UTEP).
- Ben Worel (MnROAD/MnDOT).
- Jack Herndon (MnROAD/MnDOT).
- Bob Strommen (MnROAD/MnDOT).
- Len Palek (MnROAD/MnDOT).
- Doug Lindenfelser (MnROAD/MnDOT).

As illustrated in figure 24, 4 geophones and 1 accelerometer were installed at each of MnROAD cells 3, 19, 34, and 72 (for a total of 16 geophones and 4 accelerometers) for accuracy testing. The activities at each cell included the following:

- Marking the locations of the sensors.
- Coring the pavement down to 2.25 from 2.5 inches (57.15 from 63.5 mm) (for sensor containing combined geophone and accelerometer).

- Smoothing the bottom of the holes with an air hammer.
- Grooving the pavement to accommodate the sensor wires.
- Partially grouting the sensors in the core holes.

Tuesday, September 17, 2013

Activities on Tuesday were dedicated to verifying the proper installation and performance of the 20 sensors (16 geophones and 4 accelerometers). The performance of each sensor was verified by comparing the deflection from the MnROAD FWD sensor placed directly on top of the embedded sensor with the corresponding deflection reported by the embedded sensor. Based on the successful verification of the performance of all 20 sensors, the embedded sensors were then fully grouted. The feasibility of aligning the tires of the moving deflection devices with the sensors were also verified using the MnROAD truck.

Wednesday, September 18, 2013

On Wednesday morning, members of the project team went to cell 19 to install and test the pressure tubes, which were the second choice for trigger and timing the DAQ for the embedded sensors. Part of this activity involved figuring out the best way to affix the tubes to the surface of the road so that they would be able to withstand the devices that were being tested and yet be easy to move from cell to cell. The project team set up tubes with asphalt tape and drove with a vehicle at different speeds. It was concluded that asphalt tape would not be strong enough, and nailing the tubes to the road would be time consuming. After discussing the situation with MnROAD personnel, they indicated that they had laser triggers that were no longer being used and that those could possibly work for the planned field testing. Once the circuit and power requirements were inspected, permission was requested from MnROAD to wire one of the triggers to the project team's DAQ system.

Thursday, September 19, 2013

The trigger sensors offered by MnROAD were NX5-RM7B from Panasonic™. They use an infrared LED and a reflector and have a sensing distance of up to 22.96 ft (7 m). The one drawback they have is that they work with 12 Vdc, and the output pulse would have that same amplitude.

Considering that the DAQ system has a limit of ±10 Vdc and the incoming signals from the geophones and accelerometer would have a much lower amplitude, the project team decided to build a small connection box to the MnROAD triggers, which would allow the team to use the signal cables that had been brought to MnROAD and to reduce the pulse amplitude from the trigger. Most of the day was spent building the boxes for the three triggers that were needed. The connection boxes also served to maintain the MnROAD triggers intact; that is, no modification was made to them at all.

The project team had time to set up the triggers at cell 19 and had the MnROAD truck drive at about 40 mi/h (64.4 km/h) to verify their working status.

Friday, September 20, 2013

After analyzing the signals obtained with the MnROAD truck, the project team concluded that the triggering and timing for the field testing could be done with the MnROAD trigger sensors. Two more speeds were performed with the MnROAD truck to ensure everything would work as needed. Markings for the trigger sensor positions were placed on the rest of the cells where accuracy testing was to be done, and some modifications were made to the DAQ system program to include them in the data saving process.

FIELD TRIALS

Sunday, September 22, 2013

Field trial activities began on Sunday morning with a meeting at the MnROAD facility conference room. The objectives of the meeting were as follows:

- Coordinate the upcoming field testing activities between the deflection device manufacturers, MnROAD staff, and the project team.
- Address issues relating to the field testing activities.
- Become familiar with the MnROAD facility.

A list of MnROAD field trials participants includes the following:

- Sergio Luqui (Euroconsult Curviametro).
- Fernando Sanchez (Euroconsult Curviametro).
- Javier Monasterio (Euroconsult Curviametro).
- Rolando Rangosh (Euroconsult Curviametro).
- Mike Sosinski (Euroconsult Curviametro).
- Louis Pederson (Greenwood TSD).
- Jorgen Krarup (Greenwood TSD).
- Wilson Brown (Greenwood TSD).
- David Malmgren-Hansen (Greenwood TSD).
- Doug Steele (ARA RWD).
- Jacob Bennett (ARA RWD).
- Nadarajah Sivaneswaran (FHWA).

- Senthil Thyagarajan (FHWA onsite contractor).
- Gonzalo Rada (Amec Foster Wheeler Environment & Infrastructure, Inc.).
- Sergio Rocha (UTEP).
- Soheil Nazarian (UTEP).
- Ben Worel (MnROAD).
- Jack Herndon (MnROAD).
- Bob Strommen (MnROAD).
- Len Palek (MnROAD).
- Doug Lindenfelser (MnROAD).
- Al Larkin (Federal Aviation Administration).
- Brian Ferne (United Kingdom Transportation Research Laboratory).
- Thomas Van (FHWA).
- Kelvin Wang (Oklahoma State University).
- Kang Sao (South Korea Department of Transportation).

Not all people included in this list participated in the meeting. For example, RWD representatives did not arrive until Sunday evening and hence did not participate in the meeting. A photograph of the devices that participated in the MnROAD field testing activities is provided in figure 220; the RWD, Curviametro, and TSD are shown from left to right. While it participated in the field trials, the Curviametro was not part of this project and hence is not addressed in this report.

Figure 220. Photo. MnROAD field testing devices (September 22 to 27, 2013).

The meeting commenced at 9 a.m. and lasted until around 2 p.m. after a tour of the MnROAD facility with special focus on the MnROAD test cells that were going to be used for accuracy testing in the coming days. The general agenda that was followed at the meeting is as follows:

- 9 to 9:30 a.m.: Introduction.
    - Self-introduction of Participants.
    - Project Goals and Objectives.
    - Project Phase 1 Outcomes and Findings.
    - Project Phase 2 Overview.
- 9:30 to 10:15 a.m.: Field Testing and Other Data Collection Activities.
    - Types of Testing: Accuracy, Precision, and Loop.
    - Testing Locations.
    - Instrumentation: MnROAD and Project Sensors.
    - Testing Schedule: Sequence of Activities.
- 10:15 to 10:30 a.m.: Break.
- 10:30 to 11 a.m.: Group Discussions and Question and Answer.

    - Calibration of Devices.
    - Data Needs and Submittal Requirements.
    - Logistical Issues.
    - Other Issues.
- 11 a.m. to 12 p.m.: Tour of MnROAD Facility.
- 12 to 1p.m.: Group Lunch.

Beyond these items included in the agenda, the most important issue addressed during the meeting was safety, which was covered by MnROAD staff.

Monday, September 23, 2013

Field testing activities on this day focused exclusively on accuracy testing using the ARA RWD and the MnROAD truck. Like the ARA RWD, the Greenwood TSD arrived on Sunday, but it had to be calibrated on Monday prior to testing. Greenwood encountered numerous problems in getting the TSD to the MnROAD facility and hence could not accomplish the calibration in time for the Monday testing. The Euroconsult Curviametro, on the other hand, did not arrive until Monday afternoon due to permit issues encountered when entering Minnesota from Iowa.

From about 7 to 8:30 a.m., members of the project team and ARA RWD staff toured the MnROAD facility, with particular focus on the four accuracy cells (19, 72, 3, and 34). Accuracy testing at cell 19 took place from around 8:30 to 10 a.m. A total of nine passes each were completed by the ARA RWD and MnROAD truck: three passes at ~30 mi/h (48.3 km/h), three passes at ~45 mi/h (72.45 km/h), and three passes at speeds ranging between 50 and 57 mi/h (80.5 and 91.77 km/h). It was not possible to achieve 60 mi/h (96.6 km/h) due to short acceleration distance. The passes were alternated between the two trucks, allowing sufficient time to check results before the next device passed the instrumented cell.

Between 10:30 a.m. and 12 p.m., both the ARA RWD and MnROAD truck completed accuracy testing at cell 72. These two units also completed accuracy testing of cell 3 between 2 and 4 p.m. and of cell 34 between 4 and 5:30 p.m. At cells 72 and 3, a total of nine passes each were completed by the ARA RWD and MnROAD truck: three passes at ~30 mi/h (48.3 km/h), three passes at ~45 mi/h (72.45 km/h), and three passes at 60 mi/h (96.6 km/h). At cell 34, a total of six passes each were completed by the ARA RWD and MnROAD truck: three passes at 30 mi/h (48.3 km/h) and three passes at 45 mi/h (72.45 km/h). It was not possible to complete testing at 60 mi/h (96.6 km/h) on cell 34 due to the short acceleration distance.

During the accuracy testing, data from the geophones and accelerometers installed the week of September 16, 2013, as well as data from the MnROAD working sensors were collected by the combined MnROAD and project team staffs. The MnROAD LVDT rack was also used to collect data at cell 72. Videos were also recorded as each device passed over the embedded geophones/ accelerometer installed at cells where accuracy testing was conducted. All these data were in

addition to those data collected by the ARA RWD as well as other ancillary data available at the MnROAD facility (e.g., weather station data).

The weights of the ARA RWD axles as well as overall vehicle were determined at the end of the day using a static scale owned and operated by MnROAD.

It is important to note that the coordination of field testing activities between personnel from the various devices under consideration, MnROAD staff involved in the field testing, and the project team was accomplished using two-way radios provided by MnROAD. The use of these radios proved invaluable during the course of the week.

Tuesday, September 24, 2013

On Tuesday, all three vehicles were ready for testing (the ARA RWD, Greenwood TSD, and Euroconsult Curviametro). Precision testing, accuracy testing, and testing of the 18-mi (29-km) Wright County loop were carried out.

Between 8:30 and 10 a.m., the initial round (colder temperature) of precision testing of the MnROAD LVR was completed by the ARA RWD and Greenwood TSD. Each device completed five passes at 30 mi/h (48.3 km/h) and then five passes at 45 mi/h (72.45 km/h), one following the other with about a half-loop offset. Precision testing by these two devices at 60 mi/h (96.6 km/h) was not attempted for safety reasons due to geometry of the MnROAD LVR.

From 10 to 11:30 a.m., the Euroconsult Curviametro completed the precision testing of the entire MnROAD LVR. As with the other two devices, they completed five passes, but unlike the other two devices, they only performed the testing at close to 11 mi/h (17.71 km/h), the standard data collection speed for the device.

On completion of the precision testing of the MnROAD LVR by the ARA RWD and Greenwood TSD, these two devices were instructed to conduct the 18-mi (29-km) Wright County loop testing. Three passes of the loop were completed by each device between 10 a.m. and 12 p.m. in accordance with the posted speed limits.

Between 12 and 3:30 p.m., accuracy testing of cell 34 was completed by the Euroconsult Curviametro and the Greenwood TSD. A total of three passes at an approximate speed of 10 mi/h (16.1 km/h) were done by the Euroconsult Curviametro. At this cell, preliminary passes by the Euroconsult Curviametro were required to ensure that the device's geophone coincided as close as possible with the geophone/accelerometer assembly installed the week of September 16, 2013, along the middle of the wheel path at this cell. In the case of the Greenwood TSD, six passes were completed at this cell: three passes at ~30 mi/h (48.3 km/h) and three passes at ~45 mi/h (72.45 km/h). It was not possible to perform accuracy testing of cell 34 with the Greenwood TSD at 60 mi/h (96.6 km/h) due to the short acceleration distance.

From 3:30 to 7 p.m., the second round (warmer temperature) of precision testing of the MnROAD LVR was completed by the three devices. The ARA RWD and Greenwood TSD each completed five passes at 30 mi/h (48.3 km/h) and then five passes at 45 mi/h (72.45 km/h), one following the other with about a half-loop offset. As with the morning round, precision testing by these two devices at 60 mi/h (96.6 km/h) was not attempted for safety reasons. Once these two

devices were done, the Euroconsult Curviametro completed their precision testing of the LVR and completed five passes at approximately 10 mi/h (16.1 km/h).

During precision testing of the MnROAD LVR and accuracy testing at cell 34, data from the cell 34 geophones and accelerometer installed the week of September 16, 2013, as well as data from the functioning MnROAD sensors at cell 34 were collected. It is noted that MnROAD sensor data were collected with computers whose time were set at Central Standard Time, while most other data were recorded using Central Daylight Time. All these data were in addition to those data collected by the ARA RWD, Greenwood TSD, and Euroconsult Curviametro as well as other ancillary data available at the MnROAD facility (e.g., weather station data).

Wednesday, September 25, 2013

On this day, precision and accuracy testing were carried out. Between 8:30 and 10 a.m., the initial round (colder temperature) of precision testing of the MnROAD mainline (from the start of section 20 to the end of section 1) was completed by the ARA RWD and Greenwood TSD. Due to length of the ARA RWD and hence its turning capabilities (it had to go on Interstate 94 and use the closest exits to a complete turnaround), this device was able to do one pass for every two or three passes of the Greenwood TSD. Consequently, ARA RWD and Greenwood TSD completed three and five passes, respectively, each at 30, 45, and 60 mi/h (48.8, 72.45, and 96.6 km/h).

From about 10 a.m. to 12:00 p.m., the Euroconsult Curviametro completed the precision testing of the MnROAD mainline. As with the other two devices, they completed five passes, but unlike the other two devices, they only performed the testing at close to 10 mi/h (16.1 km/h).

From 1 to 4:30 p.m., the second round (warmer temperature) of precision testing of the MnROAD mainline was completed by the three devices. As with the morning round, the Greenwood TSD performed two or three passes per ARA RWD pass due its ability to turn the device without having to leave the MnROAD facility. ARA RWD and Greenwood TSD completed three and five passes, respectively, each at 30, 45, and 60 mi/h (48.8, 72.45, and 96.6 km/h). Once these two devices were done, the Euroconsult Curviametro completed its precision testing of the MnROAD Mainline, completing five passes at approximately 10 mi/h (16.1 km/h).

From 4:30 to 7:30 p.m., accuracy testing of cells 19 and 72 was completed by the Greenwood TSD and Euroconsult Curviametro. The Euroconsult Curviametro was also able to complete accuracy testing of cell 3; the Greenwood TSD encountered hydraulic problems and hence could not complete accuracy testing of cell 3.

For the accuracy testing of cells 19 and 72, the Greenwood TSD completed nine passes at each cell: three passes at 30 mi/h (48.3 km/h), three passes at 45 mi/h (72.45 km/h), and three passes at 60 mi/h (96.6 km/h). The Euroconsult Curviametro completed three passes at each of these two cells as well as at cell 3 at an approximate speed of 10 mi/h (16.1 km/h). At these three cells, one or more preliminary passes by the Euroconsult Curviametro was required in order to ensure that the device's geophone coincided as close as possible with the geophone/accelerometer

assembly installed the week of September 16, 2013, along the middle of the wheel path at these three cells.

During precision testing of the MnROAD mainline, data from the geophones and accelerometers installed the week of September 16, 2013, at cells 19, 72, and 3 were collected. Also, data from functioning MnROAD sensors at cells 19, 20, 72, 4, and 3 were collected. The MnROAD LVDT rack was also used to collect data at cell 72. All these data were in addition to those data collected by the ARA RWD, Greenwood TSD, and Euroconsult Curviametro as well as other ancillary data available at the MnROAD facility (e.g., weather station data).

During accuracy testing of cells 19, 72, and 3 of the MnROAD Mainline, data from the geophones and accelerometers installed the week of September 16, 2013, as well as data from functioning MnROAD sensors were collected. The MnROAD LVDT rack was also used to collect data at cell 72. All these data were in addition to those data collected by the ARA RWD, Greenwood TSD, and Euroconsult Curviametro as well as other ancillary data available at the MnROAD facility (e.g., weather station data).

The weights of the Euroconsult Curviametro axles as well as overall vehicle were determined at the end of the day using a static scale owned and operated by MnROAD.

All required testing activities by the ARA RWD were completed on this day. Prior to their departure from the MnROAD facility, project team staff met with ARA personnel to discuss their data format as well as the data they were going to provide. ARA indicated that the 0.1-mi (0.161-km) ARA RWD data would be provided for the precision testing and 18-mi (29-km) Wright County loop and denser data would be provided for the accuracy testing.

Thursday, September 26, 2013

All required testing activities by the Euroconsult Curviametro were completed on the prior day. Accordingly, prior to their departure from the MnROAD facility, project team personnel met with members of the Euroconsult staff to discuss their data format as well as the data they were going to provide for the precision and accuracy testing at MnROAD. They did not participate in the 18-mi (29-km) Wright County loop testing due to permit and traffic control issues.

Testing on this day was limited to the Greenwood TSD and more specifically to the accuracy testing of cell 3, which Greenwood could not complete the prior day due to problems encountered with the device's hydraulic system. Testing began at around 9 a.m. and was completed by 10:30 a.m. The Greenwood TSD performed nine passes at this cell: three passes at ~30 mi/h (48.8 km/h), three passes at ~45 mi/h (72.45 km/h), and three passes at ~60 mi/h (96.6 km/h).

The weights of the Greenwood TSD RWD axles as well as overall vehicle were determined after completion of the cell 3 accuracy testing day using a static scale owned and operated by MnROAD.

At this point, all required testing activities by the Greenwood TSD were completed. Prior to their departure from the MnROAD facility, project team staff also met with Greenwood staff to discuss their data format as well as the data they were going to provide. Greenwood

representatives indicated they would provide 32.8-ft (10-m) data for the accuracy and precision testing as well as for the 18-mi (29-km) Wright County loop. They also indicated they would provide 3.28-ft (1-m) data for the accuracy testing at cells 34, 19, 72, and 3 but would possibly request a signed data non-disclosure form from the project team prior to providing the data.

Once complete, all planned field activities as detailed in the phase 1 work plan were completed and, in some cases, exceeded in terms of what was accomplished (e.g., it was not anticipated that the ARA RWD was going to do the 18-mi (29-km) Wright County loop testing). Much of the credit for this successful field testing effort goes to the MnROAD staff and their support of the project's field testing activities. The installation of geophones and accelerometers the week of September 16, 2013, was successful, and the same goes for the RWD, TSD, and Curviametro field testing activities the week of September 23, 2013.

The field testing plan that the project team put together seemed reasonable for a 4-day period, but the project team was only able to accomplish it because of (1) the MnROAD staff's instrumentation knowledge/expertise, (2) MnROAD staff's willingness to spend long hours helping the project team, and (3) MnROAD's great facility (layout, instrumentation, etc.), which makes carrying out projects such as this one much easier.

Friday, September 27, 2013

No field testing activities took place on this day. However, project team members videographed the 18-mi (29-km) Wright County loop and met with MnROAD staff to gather the MnROAD sensor and other supporting data collected over the past 4 days as well as to better understand those data.

ACKNOWLEDGEMENTS

The original maps shown in figure 22, figure 60, and figure 117 through figure 121 are the copyright property of Google Maps® and can be accessed from http://maps.google.com. The map in figure 22 contains overlays of nine sections that depict the location of tested routes. The map in figure 60 contains overlays of precision analysis results that depict the structural condition of LVR. The maps in figure 117 through figure 121 contain overlays of COVs of the deflection slopes that depict the precision of the first five TSD sensors in tested routes. The map overlays were developed as a result of this research project.

REFERENCES

1. AASHO. (1962). *The AASHO Road Test: Report 5—Pavement Research*, Special Report 61E, Highway Research Board, American Association of State Highway Officials, Washington, DC.

2. Siddharthan, R.V., Yao, J., and Sebaaly, P.E. (1998). "Pavement Strain from Moving Dynamic 3-D Load Distribution," *Journal of Transportation Engineering, 124*(6), 557–566.

3. Arora, J., Tandon, V., and Nazarian, S. (2006). *Continuous Deflection Testing of Highways at Traffic Speeds*, Report No. FHWA/TX-06/0-4380, Texas Department of Transportation, Austin, TX.

4. Austroads. (2012). *Review of the Traffic Speed Deflectograph—Final Project Report*, AP-R395-12, Austroads, Sydney, New South Wales.

5. Bryce, J., Katicha, S., Flintsch, G., and Ferne, B. (2011). *Analyzing Repeatability of Continuous Deflectometer Measurements*, 90th Meeting of the Transportation Research Board, Washington, DC.

6. Bryce, J.M., Flintsch, G.W., Katicha, S.W., and Diefenderfer, B.K. (2013). *Developing a Network-Level Structural Capacity Index for Structural Evaluation of Pavements*, Report No. VCTIR 13-R9, Virginia Center for Transportation Innovation & Research, Charlottesville, VA.

7. Diefenderfer, B.K. (2010). *Investigation of the Rolling Wheel Deflectometer as a Network-Level Pavement Structural Evaluation Tool*, Report No. FHWA/VTRC 10-R5, Federal Highway Administration, Washington, DC.

8. Dynatest®. (2011 b). *Determination of Subgrade Modulus and Stiffness of Pavement Layers for Measurement Bearing Capacity Under Fast Moving Wheel Load*, World Intellectual Property Organization, Geneva, Switzerland.

9. Dynatest®. (2011 a). *Triangulation of Pavement Deflections Using More Than Four Sensors*, World Intellectual Property Organization, Geneva, Switzerland.

10. Elseifi, M., Abdel-Khalek, A.M., and Dasari, K. (2012). *Implementation of Rolling Wheel Deflectometer (RWD) in PMS and Pavement Preservation*, Report No. FHWA/11.492, Louisiana Department of Transportation and Development, Baton Rouge, LA.

11. Ferne, B.W., Langdale, P., and Fairclough, R. (2012). *Network Implementation of Innovative Structural Condition Assessment at Traffic Speed*, Transport Research Laboratory, Crowthorne, United Kingdom.

12. Flintsch, G., Ferne, B., Diefenderfer, B., Katicha, S., Bryce, J., and Nell, S. (2012). *Evaluation of Traffic Speed Continuous Deflection Devices*, 91st Meeting of the Transportation Research Board, Washington, DC.

13. Flintsch, G., Ferne, B., Diefenderfer, B., Katicha, S., Bryce, J., Nell, S., and Clark, T. (2012). *Assessment of Continuous Pavement Deflection Measuring Technologies*, Draft Final Report, SHRP 2 R06(F), Strategic Highway Research Program, Washington, DC.

14. Gedafa, D.S., Hossain, M., Miller, R., and Steele, D.A. (2008). *Network-Level Pavement Structural Evaluation Using Rolling Wheel Deflectometer*, 87th Meeting of the Transportation Research Board, Washington, DC.

15. Hausman, J.J. and Steele, D.A. (2011). *Using the Rolling Wheel Deflectometer (RWD) to Improve Pavement Management Decisions*, 8th International Conference on Managing Pavement Assets, Santiago, Chile.

16. Katicha, S.W., Flintsch, G.W., and Ferne, B. (2012). *Estimation of Pavement TSD Slope Measurements Repeatability from a Single Measurement Series*, 91st Meeting of the Transportation Research Board, Washington, DC.

17. Martin, T. (2012). *Benefits and Risks of Investing in Network-Level Deflection Data Collection*, AP-T217-12. Austroads Technical Report, Sydney, Australia.

18. Muller, W.B. and Roberts, J. (2013). "Revised Approach to Assessing Traffic Speed Deflectometer Data and Field Validation of Deflection Bowl Predictions," *International Journal of Pavement Engineering*, *14*(4), 388–340.

19. Rada, G.R. and Nazarian, S. (2011). *The State-of-the-Technology of Moving Pavement Deflection Testing*, Report No. FHWA-HIF-11-013, Federal Highway Administration, Washington, DC.

20. Stubstad, R., Carvalho, R., Briggs, R., and Selezneva, O. (2012). *Simplified Techniques for Evaluation and Interpretation of Pavement Deflections for Network-Level Analysis: Guide for Assessment of Pavement Structure Performance for PMS Applications*, Report No. FHWA-HRT-12-025, Federal Highway Administration, Washington, DC.

21. Thyagarajan, S., Sivaneswaran, N., Petros, K., and Muhunthan, B. (2011). *Development of a Simplified Method for Interpreting Surface Deflections for in-Service Flexible Pavement Evaluation*, 8th International Conference on Managing Pavement Assets, Santiago, Chile.

22. Zhang, Z., Manuel, L., Damnjanovic, I., and Li, Z. (2003). *Development of a New Methodology for Characterizing Pavement Structural Condition for Network-Level Applications*, Report No. FHWA/TX-04/0-4322-1, Texas Department of Transportation, Austin, TX.

23. Baltzer, S. (2009). *Three Years of High Speed Deflectograph Measurements of the Danish State Road Network*, 8th International Conference on Bearing Capacity of Roads, Railways and Airfields, Champaign, IL.

24. Van Cauwelaert, F.J., Alexander, D.R., White, T.D., and Baker, W.R. (1989). *Multilayer Elastic Program for Backcalculation Layer Moduli in Pavement Evaluation. Nondestructive*

Testing of Pavements and Backcalculation of Moduli. ASTM International, West Conshohocken, PA.

25. U.S. Army Corps of Engineers. (2015). *Paver^{TM} User Manual Version 7.05*, Washington, DC.

26. Uzan, J. (undated). *JULEA: Jacob Uzan Layered Elastic Analysis*, Technion University, Haifa, Israel.

27. Asphalt Institute. (1982). *Research and Development of the Asphalt Institute's Thickness Design Manual* (MS-1), 9th Edition, Research Report 82-2, Lexington, KY.

28. National Cooperative Highway Research Program. (2004). *Guide for Mechanistic-Empirical Design of New and Rehabilitated Pavement Structures*, Final Report, Transportation Research Board, Washington, DC.

29. Ullidtz, P., Harvey, J., Basheer, I., Jones, D., Wu, R., Lea, J., and Lu, Q. (2010). "CalME: Mechanistic-Empirical Design Program for Flexible Pavement Rehabilitation," T*ransportation Research Record 2153*, 143–152, Transportation Research Board, Washington, DC.

30. Horak, E. and Emery, S. (2009). *Evaluation of Airport Pavements with FWD Deflection Bowl Parameter Benchmarking Methodology*, 2d European Airport Pavement Workshop, Amsterdam, Netherlands.

31. Siddharthan, R.V., El-Mously, M., Krishnamenon, N., and Sebaaly, P.E. (2002b). "Validation of a Pavement Response Model Using Full-Scale Field Tests," *International Journal in Pavement Engineering*, *3*(2), 85–93.

32. Siddharthan, R.V., Krishnamenon, N., and Sebaaly, P.E. (2000). "Pavement Response Evaluation Using Finite-Layer Approach," *Transportation Research Record 1709*, 43–49, Transportation Research Board, Washington, DC.

33. Siddharthan, R.V., Krishnamenon, N., El-Mously, M., and Sebaaly, P.E. (2002a). "Investigation of Tire Contact Stress Distributions on Pavement Response," *Journal of Transportation Engineering*, *128*(2), 136–144.

34. Pennsylvania Transportation Institute. *Test Track Facility*, The Pennsylvania State University, State College, PA. Obtained from: http://www.larson.psu.edu/testTrack. Site last accessed June 14, 2016.

35. Siddharthan, R., Sebaaly, P.E., El-Desouky, M., Strand, D., and Huft, D. (2005). "Heavy Off-Road Vehicle Tire-Pavement Interactions and Response," *Journal of Transportation Engineering, 131*(3), 239–247.

36. Hajj, E.Y., Ulloa, A., Siddharthan, R.V., and Sebaaly, P.E. (2012). "Equivalent Loading Frequencies for Dynamic Analysis of Asphalt Pavements," *Journal of the Materials in Civil Engineering*, *25*(9), 1,162–1,170.

37. Chabot, A., Chupin, O., Deloffre, L., and Duhamel, D. (2010). "ViscoRoute 2.0: A Tool for the Simulation of Moving Load Effects on Asphalt Pavement," *Road Materials and Pavement Design an International Journal*, *11*(2), 227–250.

38. Cebon, D. (1999). *Handbook of Vehicle-Road Interaction*, Taylor & Francis Group, Abingdon, United Kingdom.

39. Wang, Q., McDaniel, J.G., and Wang, M.L. (2012). "Dynamic Tire Pressure Sensor for Measuring Ground Vibration," *Journal of Sensors*, *12*(11), 15,192–15,205.

40. ASTM D7228-06a. (2011). "Standard Test Method for Prediction of Asphalt-Bound Pavement Layer Temperatures," *Book of Standards Volume 04.03*, ASTM International, West Conshohocken, PA.

41. Google Maps®. (2015). *Testing loop in Wright County, MN*. Generated via Google Maps® online. Obtained from: https://www.google.com/maps/@45.1870974,-93.9261044,11.5z. Generated 2015.

42. Dias, K., Gravesen, J., Hjorth, P.G., Larsen, P., Please, C., Radulovic, L., Wang, L., Aagaard, L. (2005). *Beneath the Wheel: Greenwood Engineering*, *54th European Study Group with Industry*, University of Southern Denmark, Odense, Denmark.

43. Hersbøll, J.A. (2008). *Undersøgelse af kørebanedeformationer ved hjælp af en Traffic Speed Deflectometer*, Master's Thesis, Technical University of Denmark, Denmark.

44. Pedersen, L., Hjorth, P.G., and Knudsen, K. (2013). *Viscoelastic Modelling of Road Deflections for Use with the Traffic Speed Deflectometer*, Technical University of Denmark, Lyngby, Demark.

45. Google Maps®. (2015). *Color-coded statistic map*. Generated via Google Maps® online. Obtained from: https://www.google.com/maps/@45.2628913,-93.7123039,1355m/data=!3m1!1e3. Generated 2015.

46. Google Maps®. (2015). *Wright County 18-mi (29-km) loop TSD 36-inch (914.4-mm) sensor COV*. Obtained from: https://www.google.com/maps/@45.1822944,-93.9229026,10744m/data=!3m1!1e3. Generated 2015.

47. Google Maps®. (2015). *Wright County 18-mi (29-km) loop TSD 24-inch (609.6-mm) sensor COV*. Obtained from: https://www.google.com/maps/@45.1822944,-93.9229026,10744m/data=!3m1!1e3. Generated 2015.

48. Google Maps®. (2015). *Wright County 18-mi (29-km) loop TSD 12-inch (304.8-mm) sensor COV*. Obtained from: https://www.google.com/maps/@45.1822944,-93.9229026,10744m/data=!3m1!1e3. Generated 2015.

49. Google Maps®. (2015). *Wright County 18-mi (29-km) loop TSD 8-inch (203.2-mm) sensor COV*. Obtained from: https://www.google.com/maps/@45.1822944,-93.9229026,10744m/data=!3m1!1e3. Generated 2015.

50. Google Maps®. (2015). *Wright County 18-mi (29-km) loop TSD 4-inch (101.6-mm) sensor COV*. Obtained from: https://www.google.com/maps/@45.1822944,-93.9229026,10744m/data=!3m1!1e3. Generated 2015.

51. Huhtala, M. and Pihlajamaki, K. (1992). "New Concepts on Load Equivalency Measurements," *Proceedings of the 7th International Conference of Asphalt Pavements*, 194–208, Nottingham, United Kingdom.

52. Al-Qadi, I.L. and Wang, H. (2009). *Evaluation of Pavement Damage Due to New Tire Designs*, Research Report ICT-09-048, Illinois Center for Transportation, Rantoul, IL.

53. Liu, W. and Scullion, T. (2001). *MODULUS 6.0 for Windows: User's Manual*, Texas Transportation Institute, College Station, TX.

54. Lukanen, E., Stubstad, R., and Briggs, R. (2000). *Temperature Predictions and Adjustment Factors for Asphalt Pavement*, Report No. FHWA-RD-98-085, Federal Highway Administration, Washington, DC.

55. Irwin, L.H., Orr, D.P., and Atkins, D. (2011). *FWD Calibration Center and Operational Improvements: Redevelopment of the Calibration Protocol and Equipment*, Report No. FHWA-HRT-07-040, Federal Highway Administration, Washington, DC.

56. Kim, Y.R., Underwood, B., Sakhaei Far, M., Jackson, N., and Puccinelli, J. (2011). *LTPP Computed Parameter: Dynamic Modulus*, Report No. FHWA-HRT-10-035, Federal Highway Administration, Washington, DC.

57. NCHRP Report 1-37A. (2004). *Guide for Mechanistic-Empirical Design of New and Rehabilitated Structures*, National Cooperative Highway Research Program, Washington, DC.

58. Velasquez, R., Hoegh, K., Yut, I., Funk, N., Cochran, G., Marasteanu, M., and Khazanovich, L. (2009). *Implementation of the MEPDG for New and Rehabilitated Pavement Structures for Design of Concrete and Asphalt Pavements in Minnesota*, MN/RC 2009-06, Minnesota Department of Transportation, Duluth, MN.

59. AASHTO T315-10. (2011c). *Standard Method of Test for Determining the Rheological Properties of Asphalt Binder Using a Dynamic Shear Rheometer (DSR)*, American Association of State Highway and Transportation Officials, Washington, DC.

60. Seo J., Kim Y., Cho J., and Jeong S. (2013). "Estimation of In Situ Dynamic Modulus by Using MEPDG Dynamic Modulus and FWD Data at Different Temperatures," *International Journal of Pavement Engineering*, *14*(4), 343–353.

61. Rabe, R. (2013). *Structural Pavement Monitoring with Non-Destructive Measuring Devices—Experience from a Pilot Project in Germany*, Presentation at the 9th International Conference on Bearing Capacity of Roads, Railways and Airfields, Trondheim, Norway.

62. Horak, E. (1987). “The Use of Surface Deflection Basin Measurements in the Mechanistic Analysis of Flexible Pavements,” *Proceedings of the Sixth International Conference Structural Design of Asphalt Pavements*, *1*, 990–1,001, University of Michigan, Ann Arbor, MI.

63. Horak, E. (1987). *Aspects of Deflection Basin Parameters Used in a Mechanistic Rehabilitation Design Procedure for Flexible Pavements in South Africa*, Doctorate Dissertation, University of Pretoria, Pretoria, South Africa.

64. Carvalho, R., Stubstad, R., Briggs, R., Selezneva, O., Mustafa, E., and Ramachandran, A. (2012). *Simplified Techniques for Evaluation and Interpretation of Pavement Deflections for Network-Level Analysis*, Report No. FHWA-HRT-12-023, Federal Highway Administration, Washington, DC.

65. Vose, D. (1997). *Quantitative Risk Analysis: A Guide to Monte Carlo Simulation Modelling*, John Wiley & Sons, New York, NY.

66. Thyagarajan, S., Sivaneswaran, N., and Petros, K. (2015). “Incorporating Traffic Speed Deflection Devices in Structural Evaluation of Flexible Pavement: Methodologies for Pavement Management Application,” *Transportation Research Record 2523*, 72–79, Transportation Research Board, Washington, DC.

67. Abdallah, I., Ferregut, C., Nazarian, S., and Lucero, O.M. (2000). “Prediction of Remaining Life of Flexible Pavements with Artificial Neural Networks,” *Proceedings of the Symposium on Nondestructive Testing of Pavements and Back Calculation of Moduli*, 484–498, ASTM International, West Conshohocken, PA.

68. Government Printing Office. (2012). *Moving Ahead for Progress in the 21st Century*, Pub. L. 112-141, Government Printing Office, Washington, DC.

HRDI-20/09-16(WEB)E